# Modélisation expérimentale de la précipitation des minéraux carbonatés lors de l'activité bactérienne

Irina Bundeleva

# THÈSE

**En vue de l'obtention du**

## DOCTORAT DE L'UNIVERSITÉ DE TOULOUSE

**Délivré par** *l'Université Toulouse III - Paul Sabatier*

**Discipline ou spécialité :** Biogéochimie

---

**Présentée et soutenue par *Irina A. BUNDELEVA***

**Le** *24 juin 2011*

**Titre :**

*Modélisation expérimentale de la précipitation des minéraux carbonatés lors de l'activité bactérienne.*

---

**JURY**

Professeur Bruno LARTIGES, Université Paul Sabatier, Toulouse, *président*

Professeur Christophe DUPRAZ, professeur assistant, Université du Connecticut, Storrs, *rapporteur*

Docteur Bénédicte MENEZ, chargée de recherche CNRS, IPGP, Paris, *rapporteur*

Docteur Steeve BONNEVILLE, Université de Gree, Bruxelles, *examinateur*

---

**Ecole doctorale :** Sciences de l'Univers, de L'Environnement et de l'Espace (SDU2E)

**Unité de recherche :** *Géosciences Environnement Toulouse (GET)*

**Directeur(s) de Thèse :** *Pascale BENEZETH, directeur de recherche CNRS, GET, Toulouse*
*Oleg POKROVSKY, chargé de recherche CNRS, GET, Toulouse*

# Remerciements

Cette thèse est le résultat de trois ans de recherche au laboratoire Géosciences Environnement Toulouse (GET) (jusqu'à janvier 2011 Laboratoire des Mécanismes et Transferts en Géologie (LMTG)). Ce travail m'a été proposé par Pascale Bénézeth et Oleg Pokrovsky, que je remercie chaleureusement. J'ai pu grâce à eux me perfectionner dans des disciplines qui n'étaient pas – initialement – mes disciplines de prédilection, en particulier la géologie, géochimie, minéralogie. Je suis reconnaissant à mes encadrants de m'avoir guidé dans les moments difficiles, en particulier le début de thèse. Je remercie tout particulièrement Jacques Schott d'avoir veillé sur moi durant cette période d'adaptation.

Je remercie Christophe Dupraz et Bénédicte Menez d'avoir accepté de réaliser le rapport de ce manuscrit. J'adresse également mes remerciements à Steeve Bonneville qui a accepté de participer au Jury de ma soutenance. Je suis reconnaissante à Bruno Lartiges d'avoir présidé ce Jury.

Je tiens également à remercier mon amie Liudmila Shirokova, qui m'a énormément aidé sur la partie microbiologique. Je voudrais dire «Merci» à Vasileios Mavromatis pour son aide précieuse lors des analyses isotopique du magnésium.

Beaucoup de techniciens œuvrent sans relâche dans ce laboratoire et sont un soutien irremplaçable pour nous, doctorants. Je pense à Carole Causserand, Thierry Aigouy, Michel Thibaut, Stéphanie Balor, Sophie Gouy, Manuel Henry, Jérôme Chmeleff, Jonathan Prunier, Stéphanie Mounic, Philippe Besson. Merci pour leur chaleur humaine et leur accueuil.

Un grand merci à tous les doctorant-e-s et post-doctorant-e-s du labo pour avoir égayé mes dures journées par leur sourire, fou-rire, blagues et même avec des discussions scientifiques sérieuses (Thomas et Marianne, Emilie et Fabrice, Julien et Sylvie, Elena et Laurent, Ekaterina, Svetlana, Alisson, Quentin, Nico, Sylvaine, Aude, Jean-Sébastien, Joaquin, ). Merci aux occupants successifs du bureau F161 (Camille Truche, Sophie Demouy, Guilhem Hoareau, Jérémy Masbou, Alexandre Bellefleur, Anh-Tuan Nguyen) d'avoir assuré une ambiance incroyable tout au long de ces trois ans.

Je suis très reconnaissant à ma famille (mes parents Alexandre et Tatiana, mes sœurs Liudmila et Alexandra) et mes amies russes (Anna, Evguenia, Irina, Galina, Natalia, Evgueni, Lusia, Anton) de m'avoir aidé dans toutes les situations. J'adresse également mes remerciements à famille D'Abzac (Louis, Brigitte, François-Xavier, Alexandre) qui m'a aidé à bien m'intégrer dans ma nouvelle vie, à amélioré mon français.

Enfin, ce travail n’aurait pu aboutir sans le soutien et aide de mon cher ami François-Xavier. FX, merci à toi. Merci.

Je vous souhaite à tout(e)s la bonne continuation, bonne chance et bonne courage.

Soyez heureux !

# Abstract

Microbially-induced mineralization is considered as one of the main natural processes controlling $CO_2$ levels in the atmosphere and a major structural and ecological player, in the modern and in the past ecosystems. In this study are presented the data of laboratory experimental work on $CaCO_3$ precipitation with pure cultures of two anoxygenic phototrophs bacteria (APB): haloalcaliphilic *Rhodovulum steppens* A-20s and neutrophilic halophilic *Rhodovulum* sp. S-17-65; and cyanobacteria *Gloeocapsa* sp.. These bacteria represent two important groups of photosynthetic organisms in the past and at present time. APB is the oldest microorganism which could be dominant during the anoxygenic period of Earth's life (approximately 4 billon years ago) whereas the origin of oxygen evolving microorganisms (cyanobacteria) is placed at about 3.5 billion years ago as based on oxidation records of the Earth's crust. In modern ecosystems, cyanobacteria are the dominant primary producers. Nonetheless, the potential of APB are abundant in the modern microbial mats and stromatolites and thus may represent a considerable fraction of the standing biomass. However, biomineralization induce by these bacteria has not been thoroughly studied up to now.

In this context, the aim of this thesis is to characterize the process of biological $CaCO_3$ precipitation and to assess the existence of metabolic processes protecting studied bacteria against carbonate mineralization on their surfaces. For this, kinetic experiments, SEM and TEM imaging, EDX and XRD analyses, zeta-potential measurements and Ca adsorption into bacterial surface were carried out.

The result of this study demonstrates the participation of studied bacteria in $CaCO_3$ precipitation. Zeta-potential measurements suggest the existence of a cells protection mechanism for studied APB, based on the metabolic maintenance of a positive surface charge at alkaline pH, preserving active bacteria against $Ca^{2+}$ adsorption and subsequent carbonate precipitation on their surfaces. The existence of the same mechanism for *Gloeocapsa* sp. was not confirmed.

Overall, the results of this study show two different mechanisms of $CaCO_3$-nucleation: an unspecific supersaturation by APB and a specific nucleation at the cell wall by cyanobacteria *Gloeocapsa* sp..

**Key words:** Anoxygenic phototrophic bacteria, *Rhodovulum* sp., Cyanobacteria, *Gloeocapsa* sp., electrophoresis, zeta potential, calcium, bicarbonate, adsorption, calcite, calcium carbonate, precipitation, kinetics.

# Résumé

La minéralisation induite par l'activité microbienne joue un rôle majeur dans le fonctionnement des écosystèmes passés et présents. Cette étude présente les données expérimentales de précipitation de $CaCO_3$ à partir de cultures pures de deux types de bactéries anoxygéniques phototrophiques (APB) : *Rhodovulum steppens* A-20s haloalcaphilique et *Rhodovulum* sp. S-17-65 neutrophilique halophilique, ainsi que de cyanobactéries *Gloeocapsa* sp.. Ces bactéries représentent deux groupes importants d'organismes photosynthétiques depuis les temps les plus anciens jusqu'à nos jours. Les APB sont des microorganismes dominants durant la période anoxygénique de la Terre (il y a environ 4 milliards d'années) tandis que l'origine des microorganismes évoluant grâce à l'oxygène (cyanobactéries) se situe à environ 3.5 milliards d'années, en se basant sur les enregistrements d'oxydation de la croûte terrestre. Au sein des écosystèmes modernes, les cyanobactéries sont les producteurs primaires dominants. Cependant, le potentiel des APB est important de part leur abondance dans les biolfilms microbiens et les stromatolites modernes, représentant ainsi une fraction considérable de la biomasse effective. La biomineralisation induite par ces bactéries a toutefois été très peu étudiée jusqu'à présent.

Dans ce contexte, cette thèse a pour objectif principal de caractériser les processus biologiques de précipitation de $CaCO_3$ et d'évaluer l'existence d'un processus métabolique protégeant les bactéries étudiées contre la minéralisation de carbonates à leur surface. Pour cela, des expériences cinétiques, des mesures de potentiel zeta et d'adsorption de Ca à la surface bactérienne, couplées à des observations par Microscopie Electronique à Balayage (MEB), en Transmission (MET) et des analyses chimiques par émission et diffraction de rayons X (EDX et XRD) ont été menées.

Les résultats de cette étude démontrent que les bactéries étudiées prennent une part active dans la précipitation de $CaCO_3$. Les mesures de potentiel zeta suggèrent l'existence d'un mécanisme de protection de la cellule pour les APB étudiées, basé sur le maintien métabolique d'une charge de surface positive à pH alcalin, préservant les bactéries actives de

l'adsorption de $Ca^{2+}$ et de la précipitation subséquente de carbonates à leur surface. L'existence d'un tel mécanisme n'est pas confirmée pour *Gloeocapsa* sp..

Ainsi, deux mécanismes différents de nucléation de $CaCO_3$ peuvent être mis en évidence : un premier mettant en jeu une sursaturation non-spécifique pour les bactéries anoxygéniques phototrophiques (APB), et un deuxième par nucléation spécifique au niveau de la membrane cellulaire pour les cyanobactéries *Gloeocapsa* sp..

**Mots-clés** : Bactéries anoxygéniques phototrophique, *Rhodovulum* sp., Cyanobactéries, *Gloeocapsa* sp., électrophorèse, potentiel zeta, calcium, bicarbonate, adsorption, calcite, précipitation, cinétique

.

# Table of contents

# Introduction

# Résumé de l’introduction en français

La biominéralisation est le processus de formation des minéraux au cours de l'activité des organismes vivants. En comparaison avec les minéraux produits de manière inorganique, les biominéraux ont souvent des propriétés spécifiques de forme, de taille et de cristallinité conduisant à la notion de biosignature. D’autre part les compositions isotopiques et en éléments en trace sont différentes de celles des minéraux abiotiques (Lowenstam and Weiner, 1989).

La minéralisation microbienne est un acteur majeur des écosystèmes passés et présents. Les stromatolites ("structures organo-sédimentaire principalement accrétées par le piégeage des sédiments, leur liaison, et/ou la précipitation in situ à la suite de la croissance et de l'activité métabolique des micro-organismes" (Papineau et al., 2005)) sont présents dans les relevés géologiques et sont des bio-signatures importantes de la Terre primitive et pour la recherche de vie extraterrestre. Les plus anciens exemples de fossiles de stromatolites préservés datent d'environ 3,5 milliards d'années et proviennent d’Australie occidentale et d'Afrique du Sud (Lowe, 1980). Les stromatolites se développent par accrétion et par précipitation de minéraux à leur surface, où le développement microbiologique est également le plus remarquable, et se traduit communément par des biofilms finement stratifiés (Reid et al., 2003).

Dans cette étude sont présentées les données des travaux expérimentaux effectués sur des cultures de deux souches de bactéries anoxygéniques phototrophiques (APB) pourpres non-sulfatées et une souche de cyanobactéries *Gloeocapsa* sp .. Ces bactéries ont été choisies pour plusieurs raisons. Elles représentent deux groupes majeurs d'organismes photosynthétiques tout on long de l’histoire de la Terre. Les APB sont les plus anciens micro-organismes probablement dominants au cours de la période anoxygénique de la Terre (il y a environ 4 milliards d’années). Les premiers organismes évoluant avec l’oxygène (cyanobactéries) datent d’environ 3,5 milliards d'années, selon les enregistrements géologiques d'oxydation de la croûte terrestre (Xiong et Bauer, 2002). Dans les écosystèmes modernes ces cyanobactéries sont les principaux producteurs primaires. Néanmoins, les APB sont abondantes dans les biofilms microbiens et les formations de stromatolites modernes et peuvent donc représenter une fraction considérable de la biomasse effective (Papineau et al. 2005). Il existe de grandes différences entre le métabolisme des ABP et celui des cyanobactéries. Une description détaillée de la diversité des bactéries étudiées et leur

métabolisme est développée dans le **Chapitre 1**. Brièvement, les bactéries anoxygéniques phototrophiques sont connues pour utiliser une grande variété de substrats comme donneurs d'électrons dans la photosynthèse, dont l'hydrogène, le soufre, mais aussi de petites molécules organiques (Bosak et al., 2007). Les cyanobactéries quand à elles utilisent les électrons de l'eau pour la production d'oxygène. Cette grande différence entre ces bactéries pourrait expliquer des mécanismes distincts de précipitation des carbonates.

Plusieurs hypothèses ont été avancées pour décrire les mécanismes responsables de la précipitation du carbonate de calcium par des bactéries. Elles peuvent être classées en deux groupes: biologiquement induite et biologiquement contrôlée (Lowenstam, 1989). Dans le premier cas, les minéraux précipitent car les organismes modifient le micro-environnement chimique de la couche d'eau adjacente à la cellule. Dans le second cas, le rôle de l'organisme va au-delà du rôle de la seule augmentation de la sursaturation locale: il contrôle le processus de minéralisation par l'intermédiaire d'une matrice organique constituée de macromolécules qui passent de la membrane externe des cellules à la solution (Dittrich et Obst, 2004). Par exemple, la précipitation de carbonate de calcium sur des substances polymériques extracellulaires (EPS) de bactéries hétérotrophes sulfato-réductrices a été observée par Aloisi et al. (2006).

Par conséquent, mon étude a été orientée autour de trois grandes questions:

1. Quel est le rôle de la surface des bactéries étudiées dans la précipitation de carbonate de calcium ?
2. Quel est le rôle de ces différentes bactéries dans cette précipitation ?
3. Quel est le mécanisme de formation de ces minéraux carbonatés ?

Afin d'apporter des réponses à ces questions, différentes techniques expérimentales ont été utilisées et sont détaillées dans le **Chapitre 2**. Des mesures du potentiel zeta ont été réalisées en fonction du pH, de la force ionique, des concentrations en $Ca^{2+}$ et bicarbonate ($HCO_3^-$), et avec ou sans lumière afin de caractériser la charge surfacique des bactéries dans des environnements différents. A ces mesures s'ajoutent des expériences d'adsorption de calcium. Ces travaux sont réunis sous la forme d'un article sous presse dans *Journal of Colloid and Interface Science* (**Chapitre 3**). Par ailleurs, des expériences cinétiques ont été effectuées afin de quantifier le rôle des bactéries sur les vitesses de précipitation des carbonates. Les mécanismes biologiques actifs ont été étudiés en comparant les cinétiques de précipitation de $CaCO_3$ abiotiques et biotiques. Les résultats obtenus, en particulier le rôle important de l'activité métabolique microbienne (photosynthèse) dans la précipitation de

$CaCO_3$ sont décrits dans les **Chapitres 4 et 5** pour APB et Cyanobactéries *Gloeocapsa* sp., respectivement (sous forme de manuscrits : un soumis à *Chemical Geology* et l'autre qui sera soumis à *Geobiology*, respectivement). La possibilité de précipitation microbienne de $CaCO_3$ sur la surface et les exopolysaccharides (EPS) des cellules bactériennes a été examinée par microscopie électronique à transmission (MET). Cette technique permet de répondre à la troisième question et notamment de comprendre le mécanisme de précipitation déclenché par différents types de bactéries. Les caractéristiques morphologiques des minéraux précipités ont été déterminées par microscopie électronique à balayage (MEB) et diffraction des rayons X (XRD).

L'ensemble des résultats obtenus dans cette étude permet : 1) de mieux comprendre les mécanismes de formation des carbonates aussi bien en contexte paléontologique (passé) que dans les temps présents (séquestration géologique du $CO_2$, cycles biogéochimiques) et 2) d'apporter de précieuses informations sur l'évolution de la vie microbienne dans les premières périodes de l'histoire biologique ainsi que sur la formation des écosystèmes bactériens contemporains (contexte écologique).

# Introduction

Biomineralization is the process of mineral formation during activity of living organisms. Biominerals, in contrast to organominerals, often have their own specific properties of shape, size, crystallinity, isotopic and trace element compositions (Lowenstam and Weiner, 1989), leading to the general notion of biosignature.

Microbially-induced mineralization is considered as one of the main natural processes controlling $CO_2$ levels in the atmosphere and a major structural and ecological player, in the modern and in the past ecosystems (Dupraz et al., 2009). Stromatolites ("organo-sedimentary structure predominantly accreted by sediment trapping, binding, and/or in situ precipitation as a result of the growth and metabolic activity of microorganisms" (Papineau et al., 2005)) are found throughout the geological record and are important biosignatures of the early Earth and in the search for extraterrestrial life. The oldest examples of preserved fossil stromatolites in the geological record are about 3.5 billion years old and have been found in Western Australia and South Africa (Lowe, 1980). Stromatolites grow by accretion and precipitation of material at the outer surface layer, where the most conspicuous microbiology also occurs, commonly as a thinly stratified microbial mat (Reid et al., 2003). In modern natural systems, biological $CaCO_3$ precipitation occurs in different forms, such as (Dupraz et al., 2009):

- $CaCO_3$ precipitation in travertine platforms of specific hotspring mats in Yellowstone (Farmer, 2000; Fouke et al., 2000);
- Dolomite production in saline lagons like Lagoa Vermelha Brazil (Vasconcelos et al., 2006) ;
- Microbialite formation in hypersaline and/or alkaline lakes (Arp et al., 2003; Dupraz et al., 2004) as well as in freshwater rivers and lakes (Freytet and Verrecchia, 1999);
- Open marine stromatolites in the Bahamas (Reid et al., 2003) and in the hypersaline coastal Shark Bay (Ried et al., 2003; Burns et al., 2004).

Numerous works have addressed calcium carbonate formation via cyanobacterial activity (Thompson and Ferris, 1990; Hartley et al., 1995; Douglas and Beveridge, 1998; Obst and Dittrich, 2006; Dittrich and Sibler, 2010; Kranz et al., 2010; Martinez et al., 2010;), algal and coral (Ries, 2010) with a number of studies devoted to mineral precipitation via sulphate-

reducing (Vasconselos et al., 1995; Warthmann et al., 2000; Van Lith et al., 2003; Bontognali et al., 2008), methanogenic archae (Kenward et al., 2009) and heterotrophic ureolitic (Ferris et al., 2004; Mitchell and Ferris, 2005, Dupraz et al., 2009) and aerobic halophilic (Sánchez-Román et al., 2011) bacteria. Whereas these studies are certainly helpful for understanding contemporary settings of microbial calcification, the deciphering of past biocalcification processes is still at the very beginning.

There are several characteristics which make bacteria as ideal nucleating agents for mineral precipitation. Due to their small size, bacteria as a group have the highest surface area-to-volume ratio of any group of living organisms and this, together with the presence of charge chemical groups on their cell surface, is responsible for the potential mineral-nucleating ability of these cells (Douglas and Beveridge, 1998).

The understanding of microbial-mineral interactions is critical for interpretation of the mineral formation mechanism. In modern and historical ecosystems microbiological life is presented in the form of community, i.e. microbial mats. Microbial mats are widely regarded as the Earth's earliest ecosystem (Tice and Lowe, 2006) and have been present on Earth since 3 billion years (Schopf, 2006). The typical arrangement of microbial groups is a vertical organized structure, where the lamination is determined by the light quantity and quality (Dupraz et al., 2009). According to the study of Dupraz et al. (2009), depending on the mat type, five to seven key groups of microorganisms can enter into the microbial mat composition: 1. photolithoautotrophs (i.e. cyanobacteria); 2. aerobic (chemoorgano-) heterotrophs; 3. fermenters; 4. anaerobic heterotrophs (predominantly sulfate-reducing bacteria); 5. sulfide oxidizers. 6. anoxyphototrophs (i.e. purple and green (non) sulfur bacteria)); 7. methanogens.

The typical microbial mat structure and combined metabolic-geochemical reactions leading to carbonate precipitation and dissolution are presented in Figure 1.

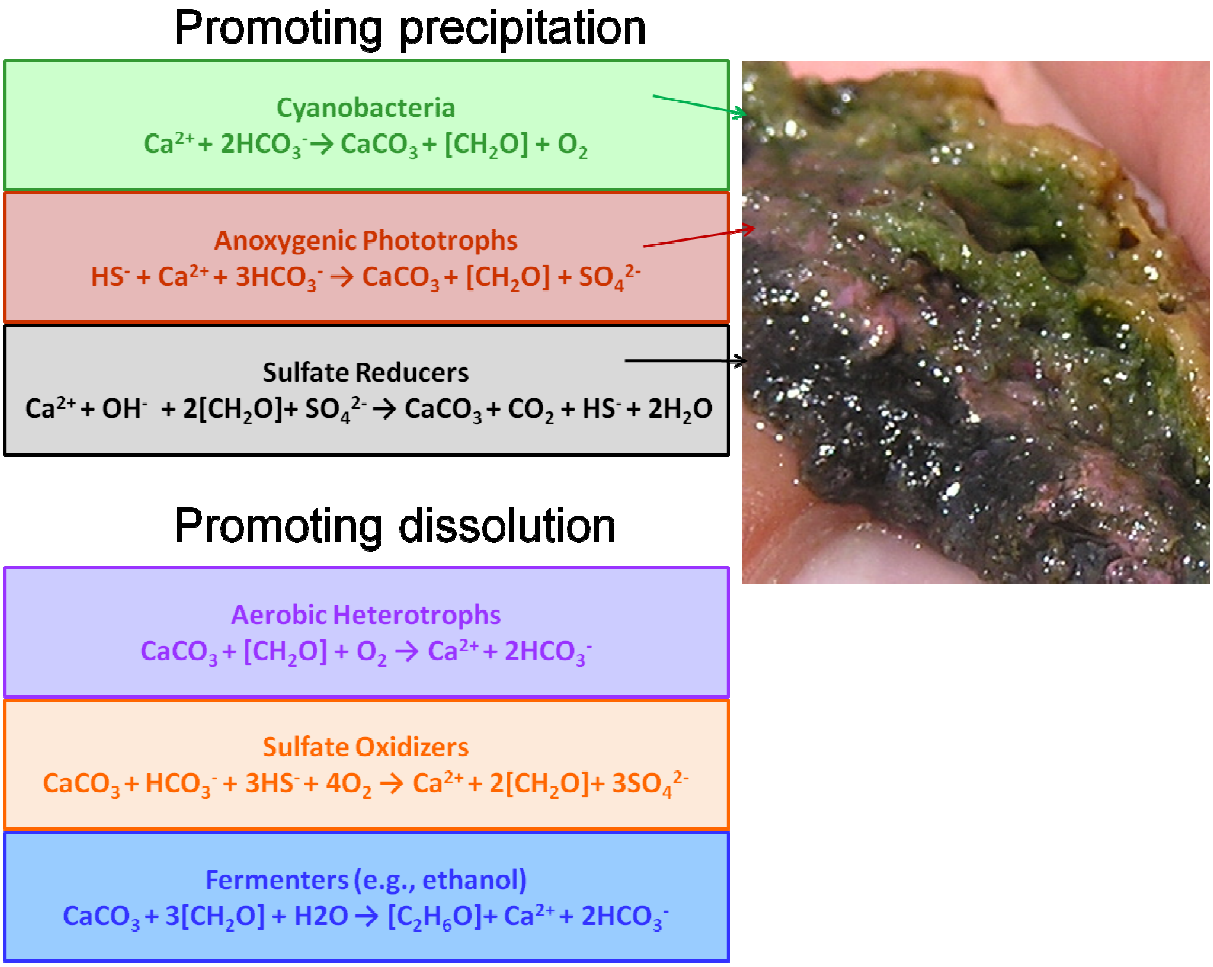


**Fig. 1. Metabolic-geochemical reactions in a microbial mat leading to carbonate precipitation and dissolution (modified from Dupraz et al., 2009).**

In this figure the six major guilds of microorganisms that compose a typical microbial mat are arranged by their respective effects on the precipitation process. Associated equations combine metabolic and geochemical reactions (Dupraz et al., 2009). All these processes are detailed in the study of Visscher and Stolz (2005). Photosynthesis and sulfate reduction are known to increase alkalinity (promoting carbonate precipitation), whereas aerobic respiration, sulfide oxidation and fermentation are more likely to induce dissolution. When oxygen-depending metabolisms stop during the night, anaerobic heterotrophy such as sulfate reduction prevails. The net carbonate precipitation depends on the balance between the different metabolic activities as well as their temporal and spatial variations (Dupraz et al., 2009).

From the early Proterozoic and certainly since Precambrian-Cambrian boundary until the end of the Cretaceous, calcifying cyanobacteria frequently occur in normal marine

environments (Ries, 2010). After the end of the Cretaceous, however, they seem to be restricted to non-marine settings. At the present time, calcification by cyanobacteria occurs almost exclusively in freshwater, alkaline and hypersaline or brackish water (Merz, 1992). Although anoxygenic photosynthesis does not dominate primary production in the modern stromatolites, this metabolism may have been crucial for the growth of Archean and some Palaeoproterozoic stromatolites (Bosak et al., 2007). It has been suggested that anoxygenic photosynthesis could determine primary productivity in shallow marine environments before the rise of oxygenic photosynthesis and the widespread atmospheric oxygenation (Olson and Blankenship, 2004). Thus, biofilms formed by anoxygenic photosynthetic microorganisms would have helped building stromatolites even before cyanobacteria became the dominant primary producers in Precambrian reefs (Bosak et al., 2007).

In order to better understand the role of each group of bacteria in carbonate precipitation, the individual metabolic reactions of the guilds outlined above must be considered (Dupraz et al., 2009). Then, individual laboratory experimental study of each group must be conducted in the context of carbonate precipitation.

The aim of this thesis is to characterize the process of biological $CaCO_3$ precipitation and to assess the existence of metabolic processes protecting studied bacteria against carbonate mineralization on their surfaces. More precisely, this study focused on three important questions:

- What is the role of surface of studied bacterial in calcium carbonate precipitation?
- What is the role of these different bacteria in this precipitation?
- What is the mechanism of the biological carbonates mineral formation?

To address these questions, two types of bacteria were used: pure cultures of two strain of purple non-sulfur anoxygenic phototrophs bacteria (APB) and one strain of cyanobacteria *Gloeocapsa* sp..These bacteria were chosen for the following reasons. They represent two important groups of photosynthetic organisms in the past and at present time. APB is the oldest microorganism which could be dominant during the anoxygenic period of Earth's life (approximately 4 billon years ago). The origin of oxygen evolving microorganisms (cyanobacteria) is placed at about 3.5 billion years ago as based on oxidation records of the Earth's crust (Xiong and Bauer, 2002). In modern ecosystems cyanobacteria are the dominant primary producers. Nonetheless, the potential of APB are abundant in the modern microbial

mats and stromatolites and thus may represent a considerable fraction of the standing biomass (Papineau et al. 2005). However, biomineralization induce by these bacteria has not been thoroughly studied up to now.

As there are great differences between the metabolism and diversity of APB and cyanobacteria, a detailed description of these bacteria is presented in the **Chapter 1**. Briefly APB are known to use a wide variety of substrates as electron donors in photosynthesis, including hydrogen, sulfide, and small organic molecules (Bosak et al., 2007). Cyanobacteria use electrons from $H_2O$ with $O_2$ production. This great difference between these bacteria could be the reason for different mechanisms of carbonate precipitation.

A large variety of mechanisms were proposed to explain calcium carbonate precipitation by bacteria. They can be classified onto two groups: biologically induced and biologically controlled (Lowenstam, 1989). In the first case, the mineral precipitates because the organisms change the chemical microenvironment of the water layer adjacent to the cell. In the biologically controlled process, the role of organism goes beyond the role of merely increasing local oversaturation: the organism control the processes of mineralization via an organic matrix consisting of macromolecules that reach out from the outer cell membrane into the solution (Dittrich and Obst, 2004). As an example of the second mechanism, calcium carbonate precipitation on extracellular polymeric substances (EPS) of heterotrophic sulphur reducing bacteria was observed by Aloisi et al. (2006).

Microbial cell surface and excreted extracellular polymeric substances (EPS), which carry a net negative electric charge and have the capacity to bind $Ca^{2+}$ ions, are frequently cited as being the sites of carbonate nucleation (Aloisi et al., 2006). The architecture of membranes differs for various cell types and with that also the specificity of the interaction between lipids and peptides\proteins. Membrane of Gram-positive as well as of Gram-negative bacteria express a high amount of negative charged lipids at the outer leaflet of the membrane which is in direct contact with the extracellular environment (Hagge et al., 2006) thus capable of adsorbing $Ca^{2+}$ ions.

Different experimental techniques were used as detailed in **Chapter 2**. Zeta-potential measurements were performed under different conditions (pH, ionic strength, various $[Ca^{2+}]$ and $[HCO_3^-]$ concentrations, with/without light) to characterize the bacterial cell surface charge in different solution environments and to determine the degree to which bacteria metabolically control their surface potential equilibria. These measurements were reinforced by Ca adsorption experiments as presented in **Chapter 3**. Moreover, kinetic experiments were

performed to quantify the role of bacteria on the rate of carbonate precipitation. The active biological processes were investigated by comparing kinetics of microbiological and chemical (abiotic) $CaCO_3$ precipitation. In **chapters 4 and 5** are presented the physical and biochemical evidences of bacterial mineral precipitation, in which microbial metabolic activities (photosynthesis) plays an important role. Sanning Electron Microscopy and X-ray diffraction have been used to characterize the nature and the forms of the precipitated minerals, whereas Transmission Electron Microscopy (TEM) has been used to localize the microbial precipitation of carbonates on/or near the surface of bacterial cells. This technique helps to answer the third question and understands the mechanism of precipitation driven by different type of bacteria. The results and interpretation are presented in **Chapter 4 and 5**.

Overall, the results of this study can help to answer important questions about i) carbonate formations in past (paleontological context) and present time (context of $CO_2$ storage and biogeochemical cycle); ii) evolution of microbial life in the earliest periods of biological history (biological context); and iii) bacterial ecosystems formations under contemporary land surface conditions (ecological context).

# Chapter I

# Description of Anoxygenic phototrophic bacteria and Cyanobacteria

Plants, algae, and cyanobacteria are known as oxygenic photoautotrophs because they synthesize organic molecules from inorganic materials, convert light energy into chemical energy, use water as an electron source, and generate oxygen as an end product of photosynthesis. Unlike the oxygenic plants, algae, and cyanobacteria, anoxygenic phototrophs do not use water as an electron source and, therefore, do not produce oxygen during photosynthesis. The electrons come from compounds such as hydrogen gas, hydrogen sulfide, and reduced organic molecules. This chapter will give a short introduction into the diversity of anoxygenic phototrophic bacteria (APB) and of cyanobacteria, list some important properties of the species, and indicate important physiological features. Two strains of anoxygenic phototrophs (purple nonsulfur anoxygenic phototrophic bacteria) and oxygenic phototrophs cyanobacteria *Gloeocapsa* sp. were studied in this work.

# 1. Anoxygenic phototrophic bacteria (APB)

Anoxygenic phototrophic bacteria have always attracted scientists because of their position at the beginning of life evolution and their ability to perform photosynthesis in the absence of air and without producing oxygen. Despite the common feature of these bacteria, there are significant variations in their morphological, physiological and molecular properties, including molecular structures of the photosynthetic pigments and the photosynthetic apparatus (Blankenship et al, 2004).

The literature contains significant information on the geochemical activity, physiology and distribution of APB in earth surface environments. Places of mass dwelling of APB usually divide into three types: thermal sources, shallow water reservoirs (salty and fresh), the stratified water body such as lakes reservoirs. However, in small amounts APB are also present in practically all aquatic systems and flooded soils (Gorlenko, 1977).

## 1.1. Anoxygenic photosynthesis

Anoxygenic photosynthetic bacteria differ from oxygenic organisms in that each species has only one type of reaction center (photosynthetic reaction center is a complex of several proteins, pigments and other co-factors assembled together to execute the primary energy conversion reactions of photosynthesis) (Blankenship et al., 1995). In some photosynthetic bacteria the reaction center is similar to photosystem II and in others it is similar to photosystem I (Fig. 1). However, neither of these two types of bacterial reaction center is capable of extracting electrons from water, so they do not evolve $O_2$. Many species can only survive in environments that have a low concentration of $O_2$. To provide electrons for the reduction of $CO_2$, anoxygenic photosynthetic bacteria must oxidize inorganic or organic molecules available in their environment. For example, the purple bacterium *Rhodobacter sphaeroides* can use succinate to reduce $NAD^+$ by a membrane-linked reverse electron transfer that is driven by a transmembrane electrochemical potential. Although many photosynthetic bacteria depend on Rubisco and the Calvin cycle for the reduction of $CO_2$, some are able to fix atmospheric $CO_2$ by other biochemical pathways (Huzisige and Ke, 1993).

Despite these differences, the general principles of energy transduction are the same in anoxygenic and oxygenic photosynthesis. Anoxygenic photosynthetic bacteria contain bacteriochlorophyll, a family of molecules that are similar to the chlorophyll, that absorb strongly in the infrared region between 700 and 1000 nm. The antenna system consists of bacteriochlorophyll and carotenoids that serve as reaction center where primary charge separation occurs (Blankenship et al., 1994). The electron carriers include quinone (e.g., ubiquinone, menaquinone) and the cytochrome *bc* complex, which is similar to the cytochrome *bf* complex of oxygenic photosynthetic apparatus. As in oxygenic photosynthesis, electron transfer is coupled to the generation of an electrochemical potential that drives phosphorylation by ATP synthase and the energy required for the reduction of $CO_2$ is provided by ATP and NADH, a molecule similar to NADPH (Briggs, 1989).

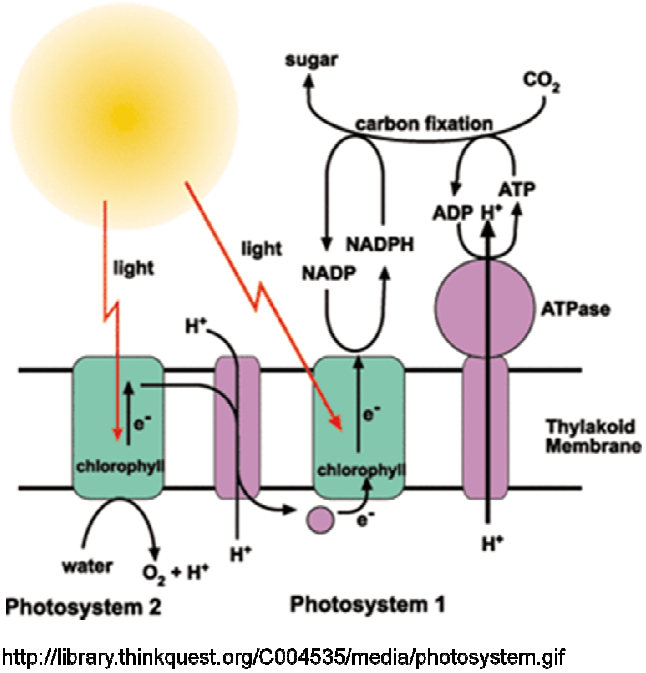


**Fig. I. 1. Schematic of photosystems I and II.**

## 1.2. Diversity of Anoxygenic Phototrophic Bacteria

There are 7 groups of APB: filamentous anoxygenic phototrophs (Fig. 2A), phototrophic purple nonsulfur bacteria (Fig. 2B), green sulfur bacteria (Fig. 2C), phototrophic sulfur bacteria, heliobacteria (Fig. 2D), thermophilic anoxygenic phototrophs, aerobic anoxygenic phototrophs (Blankenship et al, 2004). To illustrate the diversity of APB we will consider some the most interesting examples.

Filamentous anoxygenic phototrophs are a diverse group of photosynthetic bacteria that are of particular evolutionary significance. The best known species is the thermophilic *Chloroflexus aurantiacus* (Fig. 2A). This organism is a prominent member of hot spring microbial mat communities. Because it has an interesting combination of characteristics found in very different and diverse groups of phototrophic prokaryotes, it is of particular significance in addressing questions of evolutionary importance (Frigaard and Bryant, 2004).

There are several other strains of filamentous photosynthetic bacteria from a wide range of environments that are substantially different from *Cf. aurantiacus*, yet have enough similarity in fundamental photosynthetic features to be likely relatives. Sequence data (16S rRNA) are needed to define the phylogenetic range of the family Chloroflexaceae.


http://www.chm.bris.ac.uk/motm/oec/images/PhotoGrps.jpg

**Fig. I. 2. Anoxygenic phototrophic bacteria: A. *Chloroflexus* (green non-sulfur bacteria, Chloroflexaceae), B. *Rhodospirillum* (purple non-sulfur bacteria, Rhodospirillaceae), C. *Chlorobium* (green sulfur bacteria, Chlorobiaceae), D. *Heliobacterium* (Gram-positive, Heliobacteriaceae).**

The physiology of *Cf. aurantiacus* is intriguing in several aspects. The recently described autotrophic $CO_2$ fixation pathway involving 3-hydroxypropionate is unlike any other known autotrophic mechanism. *C. aurantiacus* is also unique among all groups of phototrophs in lacking the capacity for nitrogen fixation. The regulation of pigment synthesis in response to changing growth conditions is particularly interesting due to the presence of two different photosynthetic pigments located in different sub-cellular environments. The fact that *Cf. aurantiacus* is a thermophile provides another dimension of complexity to its physiology. It is also quite resistant to UV radiation. Some of its characteristics may be relicts from Precambrian ancestors (Blankenship et al, 2004).

Other interesting example of APB is heliobacteria (Fig. 2D). Heliobacteria are anoxygenic phototrophs that contain bacteriochlorophyll *g* as their sole chlorophyll pigment. These organisms are primarily soil residents and are phylogenetically related to Gram-positive bacteria, in particular to the endospore-forming *Bacillus/Clostridium* line. Some species of heliobacteria produce heat resistant endospores containing dipicolinic acid and elevated $Ca^{2+}$ levels. Heliobacteria can grow photoheterotrophically on a limited group of organic substrates and chemotrophically (anaerobically) in darkness by pyruvate or lactate fermentation. They are also active nitrogen-fixers. Their photosynthetic system resembles that of photosystem I of green plants but is simpler, containing a small antenna closely associated with the reaction center located in the cytoplasmic membrane; no chlorosomes; typical of the green sulfur bacteria; or differentiated internal membranes, typical of purple bacteria, are found in the heliobacteria. These bacteria are apparently widely distributed in rice soils and occasionally

found in other soils. The ecology of heliobacteria may be tightly linked to that of rice plants, and the ability of heliobacteria to produce endospores probably has significant survival value in the highly variable habitat of rice soils. The unique assemblage of properties shown by the heliobacteria has necessitated creation of a new taxonomic family of anoxygenic phototrophic bacteria, the Heliobacteriaceae, to accommodate organisms of this type (Madigan and Ormerod, 1995)

It is apparent that very few species of anoxygenic phototrophs occur or grow at high temperatures, particularly when compared to species numbers for thermophilic Archaea and non-photosynthetic Bacteria. *Chloroflexus* spp. are the most thermotolerant (up to ~70 °C) (Fig. 3), but none of the APB are in the hyperthermophilic category. Recognizing that there may be some endemic populations of anoxygenic phototrophic bacteria that have not been dispersed among geographically disparate geothermal sites, the major factors affecting the distribution of these bacteria are temperature, pH, and concentration of sulfide. Oxygen may have an effect on the vertical distribution and the diel vertical migration of some species within mats. Facultative aerobic metabolism appears to be a property of many of the anoxygenic phototrophs (but not *Chlorobium or Heliobacillus*) in these dynamic habitats. Light quantity and quality are affected by the diversity of pigmentation within the vertically stratified communities and adaptation to low photon fluence rates is a necessity for many species (Castenholz and Pierson, 2004).

Phototrophic sulfur bacteria are characterized by oxidizing various inorganic sulfur compounds for use as electron donors in carbon dioxide fixation during anoxygenic photosynthetic growth. These bacteria are divided into the purple sulfur bacteria (PSB) and the green sulfur bacteria (GSB). They utilize various combinations of sulfide, elemental sulfur, and thiosulfate and sometimes also ferrous iron and hydrogen as electron donors (Frigaard and Dahl, 2009). Phototrophic sulfur bacteria often form mass developments in aquatic environments, either planktonic or benthic, where anoxic layers containing reduced sulfur compounds are exposed to light. From the point of view of population dynamics, the abundance of these organisms is the consequence of a certain balance between growth and losses. Both specific growth rates and specific rates of loss through several processes are analyzed in several environments, in an attempt to generalize on the growth status of blooms of phototrophic sulfur bacteria. The available information indicates the existence of an upper limit for the production of these bacteria in nature, and seems to suggest the existence of an upper limit for biomass based in the balance between growth and losses (Hell et al., 2008)

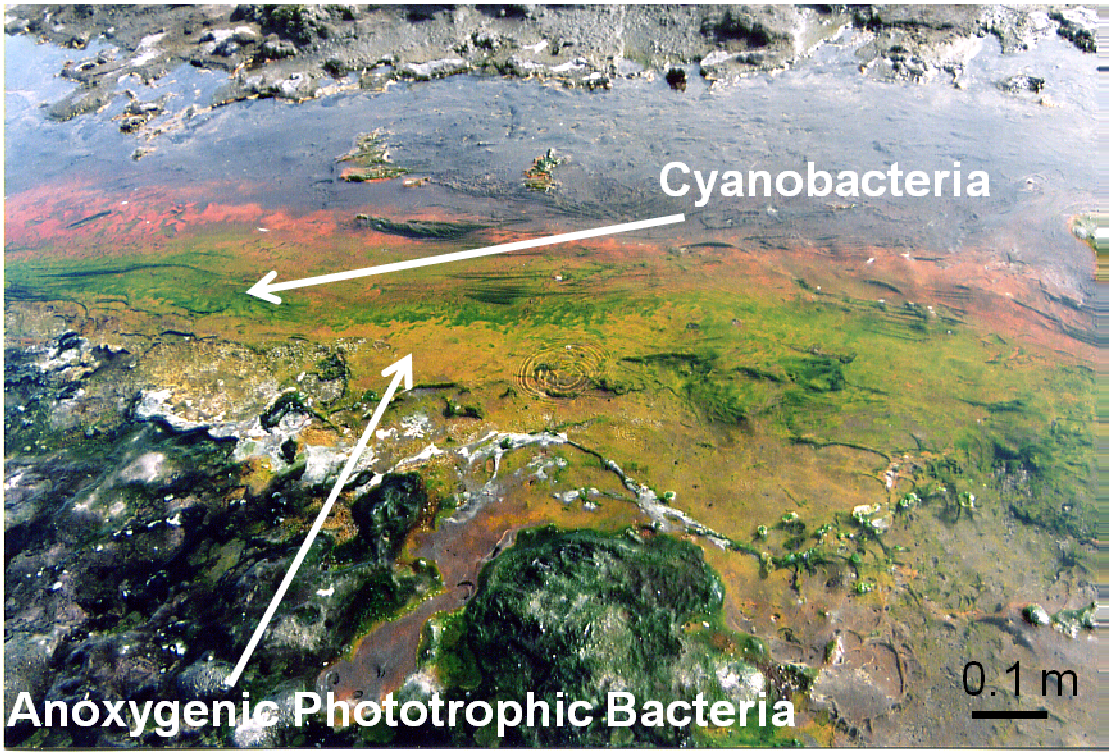


**Fig. I. 3. APB and cyanobacteria in the hot spring (40-60°C), Kamchatka, Russia.**

During the last 15 years, more than 20 new strains of aerobic anoxygenic phototrophs bacteria which possess bacteriochlorophyll (BChl) *a* have been identified (Blankenship et al, 2004). They are distinguished from typical anaerobic (anoxygenic) phototrophs in that they synthesize BChl only under aerobic conditions and cannot grow without $O_2$ or other oxidants, even under light. In some species, photosynthetic activities have been demonstrated. Reaction centers and light-harvesting complexes isolated from some species were shown to be similar to those of typical purple photosynthetic bacteria. The regulatory mechanism of synthesis of pigments and proteins of the photosynthetic apparatus are apparently opposite with respect to $O_2$ pressure compare to that of typical anoxygenic phototrophs. The low content of BChl, unique composition of carotenoids and presence of non-photosynthetic carotenoids in most strains are other marked characteristics of these aerobic bacteria. Phylogenetically, they are not classified into single group. Species so far described are distributed rather widely within the *α*-subclass of Proteobacteria (purple bacteria) in which most of the purple nonsulfur bacteria as well as many non-photosynthetic bacteria are included. Apparently, these aerobic BChl-containing bacteria represent an evolutionary transient phase from anaerobic phototrophs to aerobic non-phototrophs. However, some characteristic features distinct from

anaerobic phototrophs suggest that most of them are in an evolutionary stable state **(**Yurkov and Beatty, 1998)**.**

Our experimental study of calcium carbonate biomineralization during bacterial activity deal with two strain of purple nonsulfur APB: *Rhodovulum steppense* sp. nov. A-20s and *Rhodovulum sp.* S-17-65.

### 1.2.1. Rhodovulum steppense sp. nov. A-20s

*Rhodovulum steppense* (step.pen'se, N.L. n. *steppum* steppe; L. neut. suff. *-ense* suffix used with the sense of pertaining to; N.L. neut. adj. *steppense* pertaining to the steppe, widespread in steppe soda lakes). The type strain, A-20s$^T$ (=VKM B-2489$^T$ =DSM 21153$^T$). The 16S rRNA gene sequences of A-20s strain were deposited in GenBank under the following accession numbers: EU741680–EU741684, EU918391, FJ895099 (Kompantseva *et al.*, 2009).

Strains of purple nonsulfur bacteria *Rhodovulum steppense* sp. nov. A-20s were isolated from the shallow-water steppe soda lake Khilganta (Zabaikal'skii Krai, southern Siberia, Russia) (Fig. 4A) in the cryoarid zone of Central Asia (Kompantseva *et al.*, 2010).

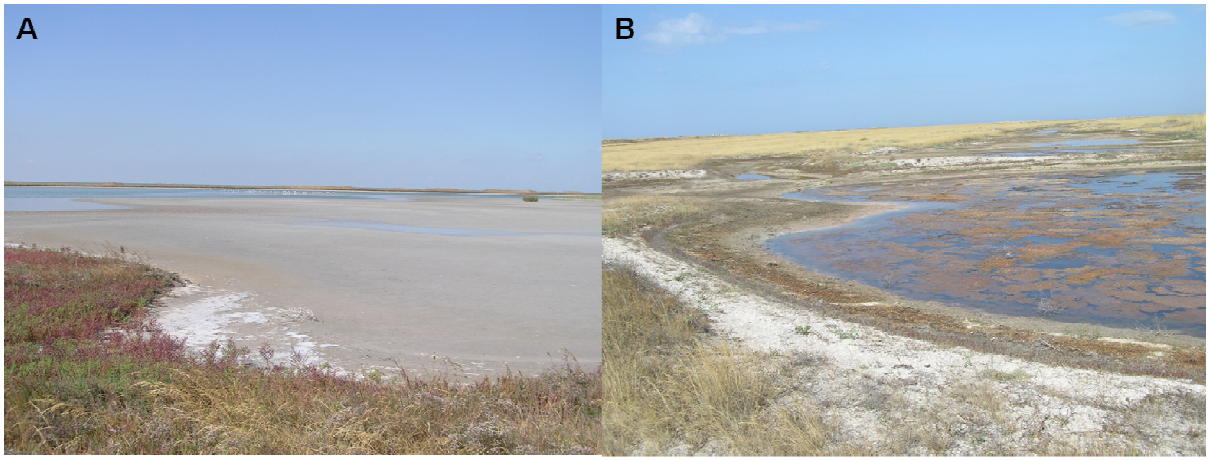


**Fig. I. 4. (A) Lake Khilganta, Zabaikal'skii Krai, southern Siberia, Russia; (B) Hypersaline water body in Crimea steppe.**

Cells are ovoid to rod-shaped, 0.3–0.8 µm wide and 1.0–2.5 µm long (Fig. 5A), mobile by means of polar flagella, multiply by binary fission, and contain vesicular internal photosynthetic membranes. Ultrathin sections of cells of strain A-20s showed a Gram-negative type of cell wall. The internal photosynthetic membranes formed multiple vesicles (Fig. 5B).

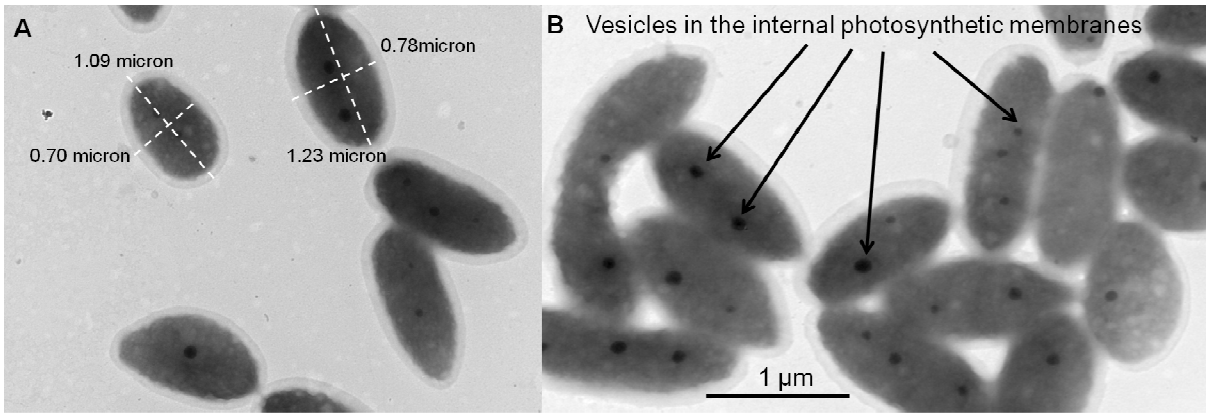


**Fig. I. 5. (A,B) TEM images of APB A-20s. Nutrient solution. 10 days old culture. (B) Vesicles in the internal photosynthetic membranes of APB A-20s.**

Cell suspensions are yellow to brown in anoxic conditions (Fig. 6A) and red in the presence of $O_2$ when grown aerobically (Fig. 6B).

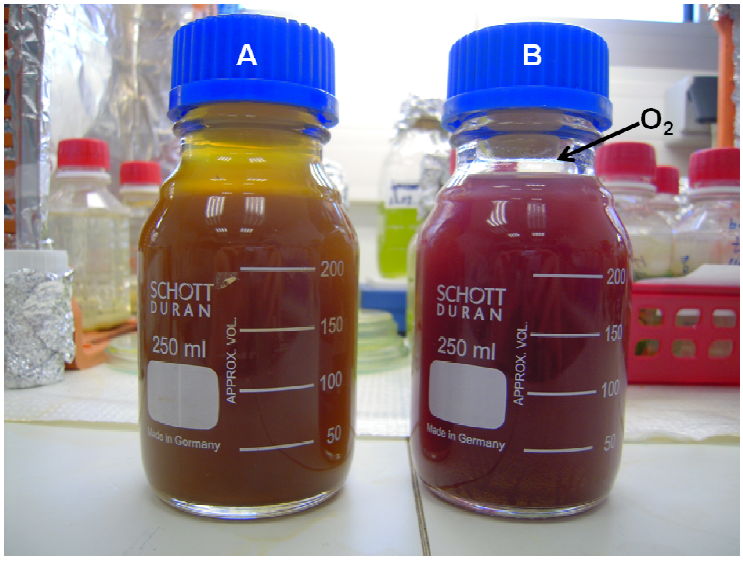


**Fig. I. 6. Bacterial suspensions of A-20s cultivated in anoxic conditions (brown color) (A) and in the presents of oxygen (red color) (B).**

The photosynthetic pigments of this APB strain are bacteriochlorophyll a and carotenoids of the spheroidene series (Kompantseva et al., 2009). In vivo absorption spectra show maxima at 461, 483, 515, 592, 803 and 861 nm. Growth occurs anaerobically in the light (photoheterotrophically) or aerobically in the dark (chemoheterotrophically). Growth is

best with propionate, butyrate, valerate, pyruvate, lactate and glycerol. Asparagine, acetate, caprylate, malate, succinate, formate, fumarate, glutamate, mannose, ethanol, casein hydrolysate and yeast extract are also used. Alanine, arginine, aspartate, ornithine, proline, threonine, valine, citrate, benzoate, tartrate, arabinose, glucose, maltose and fructose support slow growth. No growth occurs with sucrose, sorbitol, mannitol or methanol. No anaerobic respiration takes place with nitrite, nitrate or fumarate. Growth at the expense of fermentation does not occur. Sulfide, sulfur and thiosulfate support photolithoautotrophic and chemolithoautotrophic growth, in the course of which they are oxidized to sulfate. Sulfide as electron donor is oxidized via temporary deposition of extracellular elemental sulfur. No growth occurs with hydrogen as electron donor. Ammonium salts are used as the nitrogen source. Sulfate, thiosulfate, elemental sulfur and cysteine are used as the sulfur source. Three vitamins (biotin, thiamine, niacin) are needed as growth factors. Obligately haloalkaliphilic: growth occurs within a wide range of salinity (0.3–10 %, w/v) and pH (7.5–10) (Kompantseva et al., 2010). Growth optima are at 1–5 % NaCl, pH 8.5 and 25–35 °C. No growth occurs in the absence of NaCl and/or at pH 7. The major quinone is ubiquinone Q-10. This APB strain is resistant to amikacin, ampicillin, chlortetracycline, bacitracin, vancomycin, gentamicin, nystatin, nalidixic acid, novobiocin, penicillin, rifampicin, kanamycin, lincomycin, neomycin and streptomycin, but sensitive to tetracycline, benzylpenicillin and polymixin B.

Anaerobically in the light and in the presence of organic compounds, the strain A-20s reduced selenite and tellurite (at initial concentrations of up to 10 mM) to elemental selenium and tellurium, respectively (Kompantseva et al., 2010).

### 1.2.2. Rhodovulum sp. S-17-65

Bacteria *Rhodovulum sp.* S-17-65 were isolated a long time ago and originally described as *Rhodobacter euryhalinus*, renamed later in *Rhodovulum euryhalinum*. In light of new data this species includes only typical strain, but not *Rhodovulum sp.* S-17-65. Thereby, Rhodovulum sp. S-17-65 is likely to be another species, which have been not described yet. In this subsection we provide the old description of bacteria S-17-65.

*Rhodobacter euryhalinus* (Gr. adj. *eurus*, wide, broad; Gr. n. *hals halos*, salt; L. suff. *-inus -a -um*, suffix used with the sense of belonging to; N.L. neut. adj. *euryhalinum*, living in a wide range of salinity). Type strain: strain Kompantseva KA-65 = KA-65 = DSM 4868. GenBank/EMBL/DDBJ accession number for the 16S rRNA gene sequence of the type strain: D16426 (Kompantseva, 1989).

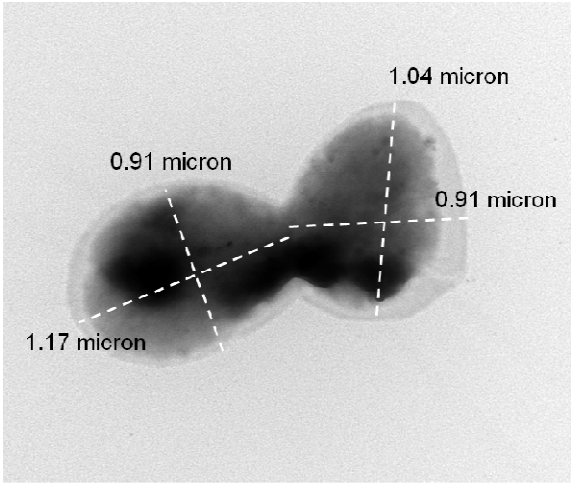


**Fig. I. 7. TEM images of cells S-17-65. Nutrient solution. 10 days old culture.**

Strains of purple nonsulfur bacteria *Rhodovulum* sp. S-17-65 isolated from the hypersaline water body in Crimea steppe (Fig. 4B). It was shown that the main factors determining efficiency of growth were: increase salt content, sulphide content in silt deposits, unstable character of anaerobic conditions in bottom water (Gorlenko et al., 1983).

The form of cells is coccus or short rod-shaped, the size is 0.7-0.1.0 µm wide and 1.0–3.0 µm long (Fig. 7), the cells are mobile by means of polar flagella, multiply by binary fission. Cell suspensions are brown as shown in Fig. 8.

**Fig. I. 8. Cells suspension of APB S-17-65.**

The photosynthetic pigments are bacteriochlorophyll *a* and carotenoids of the spheroidene series. The growth occurs anaerobically in the light (photoorganoheterotroph) or

microaerophilically in the dark on organic substrate. The cultures can growth photoototrophicaly with sulphide. S-17-65 is obligately halophilic with growth optima of 12 % NaCl, pH 7-8 and 25–35 °C. The source of nitrogen is ammonium, source of sulfur are sulfide, cysteine. These bacteria need four vitamins: $B_1$, $B_5$, biotin, n-aminobenzoate (Kompantceva, 1985).

# 2. Cyanobacteria

A cyanobacterium (also known as blue-green algae, blue-green bacteria, and Cyanophyta) is a phylum of bacteria that obtain their energy through photosynthesis. The name "cyanobacteria" comes from the color of the bacteria (Greek: κυανός (kyanós) = blue).

The ability of cyanobacteria to perform oxygenic photosynthesis is thought to have converted the early reducing atmosphere into an oxidizing one, which dramatically changed the composition of life forms on Earth by stimulating biodiversity and leading to the near-extinction of oxygen-intolerant organisms (Smith, 1982).

Cyanobacteria can be found in almost every conceivable environment, from oceans and fresh water to bare rock and soil. They can occur as planktonic cells or form phototrophic biofilms in fresh water and marine environments. They occur in damp soil or even on temporarily moistened rocks in deserts. A few are endosymbionts in lichens, plants, various protists, or sponges and provide energy for the host. Some live in the fur of sloths, providing a form of camouflage (Madigan et al., 2000).

Aquatic cyanobacteria are probably best known for the extensive and highly visible blooms that can form in both freshwater and the marine environment and can have the appearance of blue-green paint or scum (Fig. 9). The association of toxicity with such blooms has frequently led to the closure of recreational waters when blooms are observed. Marine bacteriophages are a significant parasite of unicellular marine cyanobacteria. When they infect cells, they lyse them, releasing more phages into the water (Rippka et al., 1979).

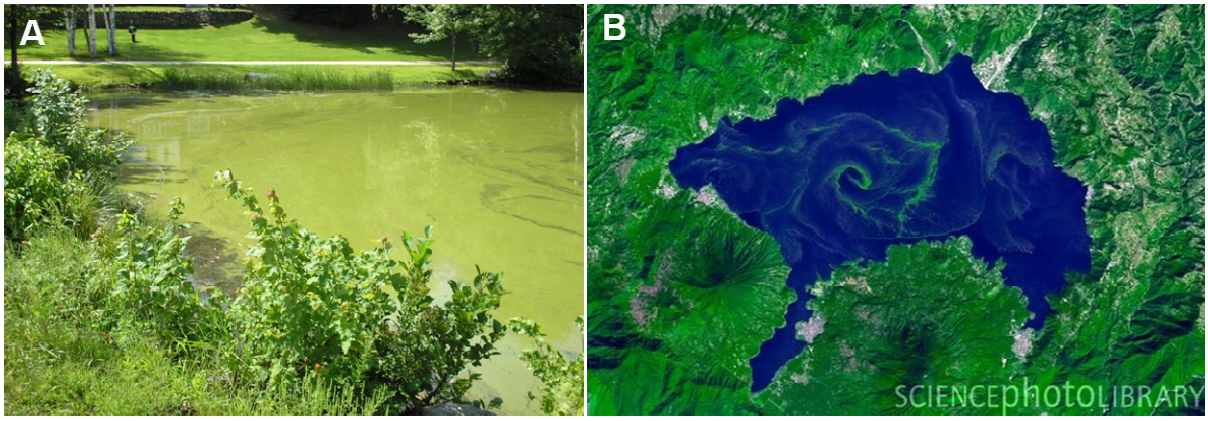


**Fig. I. 9. Blooms of cyanobacteria. (A) Lake in New England; (B) Lake Atitlán, Guatamala highlands, satellite image, November 22, 2009.**

## 2.1. Oxygenic Photosynthesis of Bacteria

The photosynthetic process in all plants and algae as well as in certain types of photosynthetic bacteria involves the reduction of $CO_2$ to carbohydrate and removal of electrons from $H_2O$, which results in the release of $O_2$. In this process, known as oxygenic photosynthesis, water is oxidized by the photosystem II reaction center, a multisubunit protein located in the photosynthetic membrane. Years of research have shown that the structure and function of photosystem II is similar in plants, algae and certain bacteria, so that knowledge gained in one species can be applied to others. This homology is a common feature of proteins that perform the same reaction in different species. This homology at the molecular level is important because there are estimated to be 300,000-500,000 species of plants (Huzisige and Ke, 1993).

Cyanobacteria are photosynthetic prokaryotic organisms that evolve $O_2$ (Bryant, 1994). Fossil evidence indicates that cyanobacteria existed over 3 billion years ago and it is thought that they were the first oxygen evolving organisms on earth (Wilmotte, 1994). Cyanobacteria are presumed to have evolved in water in an atmosphere that lacked $O_2$. Initially, the $O_2$ released by cyanobacteria reacted with ferrous iron in the oceans and was not released into the atmosphere. Geological evidence indicates that the ferrous Fe was depleted around 2 billion years ago, and earth's atmosphere became aerobic. The release of $O_2$ into the atmosphere by cyanobacteria has had a profound affect on the evolution of life.

The photosynthetic apparatus of cyanobacteria is similar to that of chloroplasts. The main difference is in the antenna system. Cyanobacteria depend on chlorophyll a and specialized protein complexes (phycobilisomes) to gather light energy (Sidler, 1994). They do not contain chlorophyll b. As in chloroplasts, the chlorophyll a is located in membrane bound proteins. The phycobilisomes are bound to the outer side of the photosynthetic membrane and act to funnel exciton energy to the photosystem II reaction center. They are composed of phycobiliproteins, protein subunits that contain covalently attached open ring structures known as bilins that are the light absorbing pigments. Primary photochemistry, electron transport, phosphorylation and carbon reduction occur much as they do in chloroplasts. Cyanobacteria have a simpler genetic system than plants and algae that enable them to be easily modified genetically. Because of this, cyanobacteria have been used as a model to understand photosynthesis in plants. By genetically altering photosynthetic proteins, researchers can investigate the relationship between molecular structure and mechanism (Barry et al., 1994).

Over the past three decades several types of oxygenic bacteria known as prochlorophytes (or oxychlorobacteria) have been discovered that have light harvesting protein complexes that contain chlorophyll a and b, but do not contain phycobilisomes (Palenik and Haselkorn 1992, Urbach et al., 1992; Matthijs et al., 1994). Because prochlorophytes have Chlorophyll a/b light harvesting proteins like chloroplasts, they are being investigated as models for plant photosynthesis.

## 2.2. Diversity of cyanobacteria

The cyanobacteria were traditionally classified by morphology into five sections, referred to by the numerals I-V. The first three - Chroococcales, Pleurocapsales, and Oscillatoriales - are not supported by phylogenetic studies. However, the latter two - Nostocales and Stigonematales - are monophyletic, and make up the heterocystous cyanobacteria. The members of Chroococales are unicellular and usually aggregate in colonies. The classic taxonomic criterion has been the cell morphology and the plane of cell division. In Pleurocapsales, the cells have the ability to form internal spores (baeocytes). The rest of the sections include filamentous species. In Oscillatoriales, the cells are uniseriately arranged and do not form specialized cells (akinetes and heterocysts). In Nostocales and

Stigonematales the cells have the ability to develop heterocysts in certain conditions. Stigonematales, unlike Nostocales, includes species with truly branched trichomes (Smith, 1982).

Cyanobacteria include unicellular and colonial species. Colonies may form filaments, sheets or even hollow balls. Some filamentous colonies show the ability to differentiate into several different cell types: vegetative cells, the normal, photosynthetic cells that are formed under favorable growing conditions; akinetes, the climate-resistant spores that may form when environmental conditions become harsh; and thick-walled heterocysts, which contain the enzyme nitrogenase, vital for nitrogen fixation. Heterocysts may also form under the appropriate environmental conditions (anoxic) when fixed nitrogen is scarce. Heterocyst-forming species are specialized for nitrogen fixation and are able to fix nitrogen gas into ammonia ($NH_3$), nitrites ($NO_2^-$) or nitrates ($NO_3^-$) which can be absorbed by plants and converted to protein and nucleic acids (atmospheric nitrogen cannot be used by plants directly). Rice crops utilize healthy populations of nitrogen-fixing cyanobacteria in some rice paddy fertilizers (Scanlan and Nyree, 2002). Rippka (Rippka et al., 1979) divides the cyanobacteria into five sections. She describes first two sections, I and II, as "Unicellular; cells single or forming colonial aggregates held together by additional outer cell wall layers". Her other three sections, III to V, she describes as "Filamentous; a trichome (chain of cells) which grows by intercalary cell division". The paper by Rippka et al. (1979) contains many micrographs of cell morphologies typical of these genera.

*Anabaena* (Fig. 10) is a genus of filamentous cyanobacteria, found as plankton. It is known for its nitrogen fixing abilities, and they form symbiotic relationships with certain plants, such as the mosquito fern. They are one of four genera of cyanobacteria that produce neurotoxins, which are harmful to local wildlife, as well as farm animals and pets. Production of these neurotoxins is assumed to be an input into its symbiotic relationships, protecting the plant from grazing pressure (Mishra et al. 2009).

*Oscillatoria* (Fig.11) is another genus of filamentous cyanobacterium which is named for the oscillation in its movement. Filaments in the colonies can slide back and forth against each other until the whole mass is reoriented to its light source. It is commonly found in watering-troughs waters, and is mainly blue-green or brown-green. *Oscillatoria* is an organism that reproduces by fragmentation. *Oscillatoria* forms long filaments of cells which can break into fragments called hormogonia. The hormogonia can grow into a new, longer filament. Breaks in the filament usually occur where dead cells (necridia) are present. Each

filament of oscillatoria consists of trichome which is made up of rows of cells. The tip of the trichome oscillates like a pendulum (Madigan et al. 2000).


**Fig. I. 10. Cyanobacteria *Anabaena* (Scientific classification: Kingdom: Bacteria, Phylum: Cyanobacteria, Order: Nostocales, Family: Nostocaceae, Genus: Anabaena).**

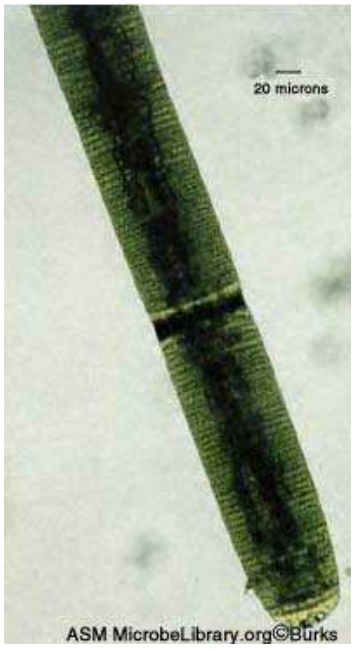


**Fig. I. 11. Cyanobacteria *Oscillatoria* (Scientific classification: Kingdom: Bacteria, Phylum: Cyanobacteria, Class: Cyanophyceae, Order: Oscillatoriales, Family: Oscillatoriaceae, Genus: Oscillatoria).**

Some of cyanobacterial organisms contribute significantly to global ecology and the oxygen cycle. Although *Prochlorococcus* (Fig.12) is the smallest known phototroph it contributes 30-80% of primary production in the world's oligotrophic oceans, and is consequently plays a significant role in the global carbon cycle and the Earth's climate. This tiny marine unicellular cyanobacterium was discovered in 1986 and accounts for more than half of the photosynthesis of the open ocean (Scanlan et al. 2002).

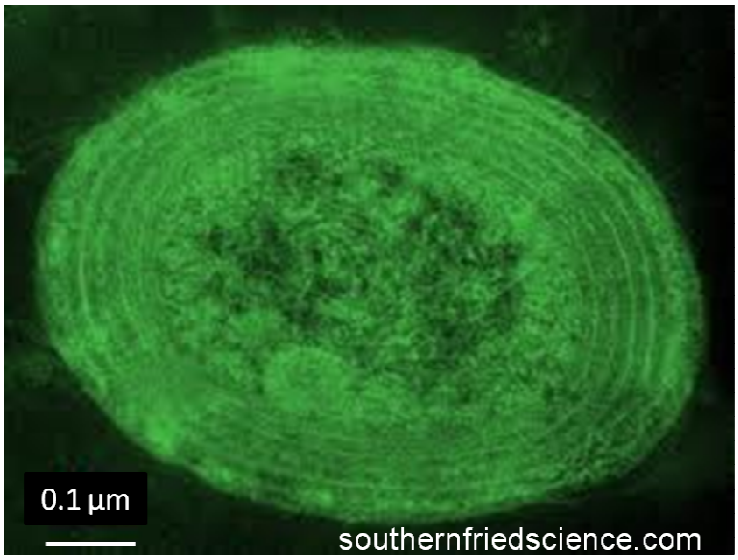


**Fig. I. 12. Cynobacteria *Prochlorococcus* (Scientific classification: Kingdom: Bacteria, Phylum: Cyanobacteria, Order: Synechococcales, Family: Synechococcaceae, Genus: Prochlorococcus)**

Each individual cell of a cyanobacterium typically has a thick, gelatinous cell wall. They lack flagella, but some species may move by gliding along surfaces. Many of the multi-cellular filamentous forms of *Oscillatoria* are capable of a waving motion; the filament oscillates back and forth. In water columns some cyanobacteria float by forming gas vesicles, like in archaea. These vesicles are not organelles as such. They are not bounded by lipid membranes but by a protein sheath (Smith, 1982).

In our experimental study of calcium carbonate biomineralization cyanobacteria *Gloeocapsa sp.* was studied in details for determinate its role in precipitation and the mechanism of this precipitation.

### 2.2.1. Cyanobacteria Gloeocapsa sp.

Scientific classification: Kingdom: Bacteria, Class/Phylum: Cyanobacteria, Order: Chroococcales, Family: Chroococcaceae.

*Gloeocapsa* (from the Greek *gloia* (glue) and the Latin *capsa* (box)) may be unicellular or made up of small groups of cells grouped together within concentric mucilage envelopes (Fig. 13). The individual colonies are usually spherical, microscopic, and enclosed within larger masses of mucilage. The cells are oval-shaped or ellipsoidal, and hemispherical after dividing. Each cell has a rounded, firm, inner mucilaginous sheath surrounded by older sheath material from the parent cell, revealing the pattern of cell division. The sheaths are colorless or vivid shades of yellow, brown, red, orange, blue, or violet, and may be affected by changes in pH. The cells are usually bright blue-green or olive green and do not have distinct gas vesicles (Smith, 1982).

*Gloeocapsa* cells divide along three perpendicular planes during successive generations. Each daughter cell grows to the size and shape of the parent cell before dividing again. The parent colonies disintegrate to form new daughter colonies (Madigan, 2000).

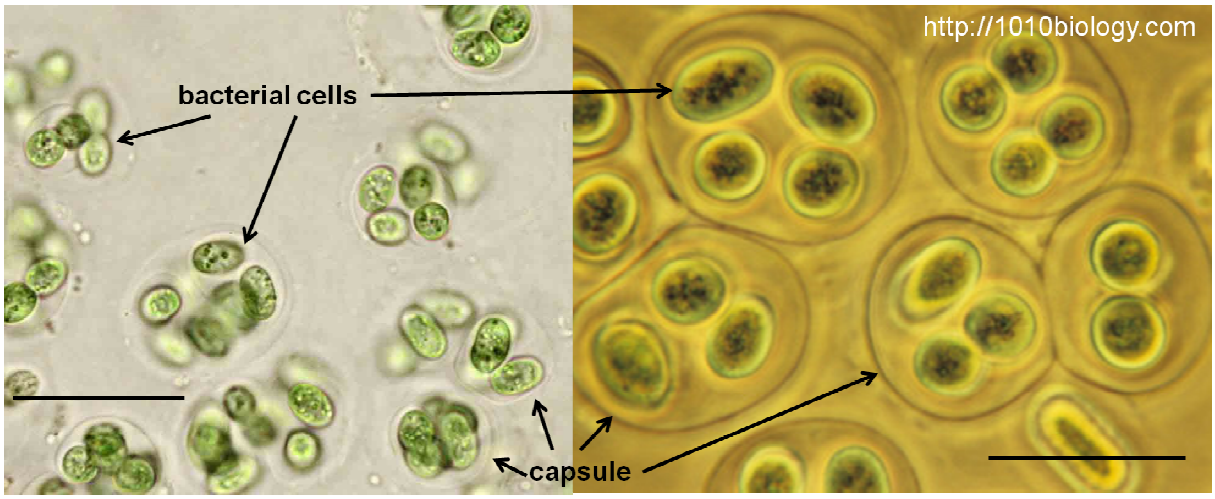


**Fig. I. 13. Cyanobacteria *Gloeocapsa* (cells surrounded by a capsule). The black scale bars are 10 µm.**

Most species of *Gloeocapsa* live in freshwater lakes, on wet stony substrates, on tree bark, or in terrestrial environments such as moist soils. Many grow on wet rocks or mountain walls, while some species are restricted to calcareous or acidic rocky surfaces. Some live

within porous rocks in hot desert regions or can be seen as black bands on high intertidal seacoast rocks. Some species of *Gloeocapsa* are symbiotic with fungi, forming lichens (Smith, 1982).

Cyanobacterium *Gloeocapsa* sp. used in this study is usually made up of small number of cells grouped within concentric mucilage envelopes. The individual colonies are spherical, microscopic, and enclosed within larger masses of mucilage. Gloeocapsa sp. f-6gl was provided from the culture collection of the Institute of Microbiology RAS (Moscow), isolated from a hot spring (30-40°C) in Kamchatka (Pokrovsky et al., 2008).

### 2.2.2. Cyanobacteria Synecochoccus sp.

Scientific classification: Kingdom: Bacteria, Phylum: Cyanobacteria, Order: Synechococcales, Family: Synechococcaceae, Genus: Synechococcus.

*Synechococcus* (from the Greek *synechos* (in succession) and the Greek *kokkos* (berry)) is a unicellular cyanobacterium that is very widespread in the marine environment. Many freshwater species of *Synechococcus* have also been described (Madigan et al., 2000).

A Synechococcus cyanobacterium was isolated from the surface of coastal stromatolites sampled in February 2008 from the depth of 1 m at 50 m from the shoreline of the Salda Lake, SW Turkey (Fig. 14).

**Fig. I. 14. Salda Lake, SW Turkey.**

The cultures of *Synechococcus* sp. were purified on the agar BG-11 or Pratt media and individual colonies was grown in synthetic, cyanobacteria BG-11 Freshwater Solution for 3 weeks until the stationary growth phase was reached. Continuous illumination at 2000 lx was provided from fluorescent lamps. Cyanobacteria *Synechococcus* typically consists of isolated elongated cells, without significant amount of mucilage. Its size varies from 0.8 µm to 1.5 µm (Fig. 15). They are gram negative cells with highly structured cell walls that may contain projections on their surface. Electron microscopy frequently reveals the presence of phosphate inclusions, glycogen granules and more importantly highly structured carboxysomes (Smith, 1982) (Fig.15).

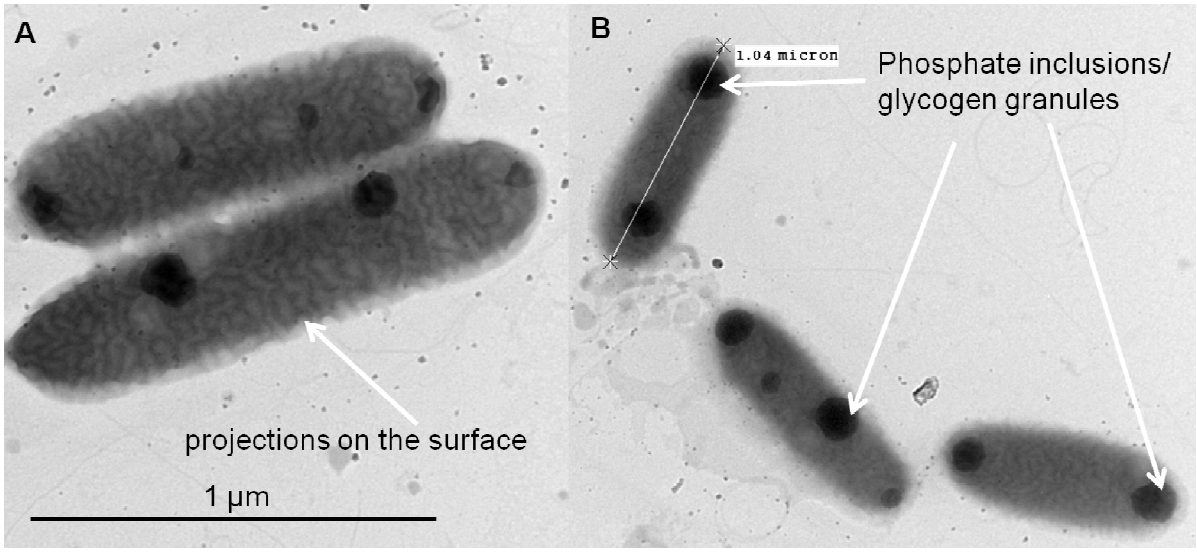


**Fig. I. 15. TEM images of cyanobacteria Synechococcus sp. (A) Projections on their surface; (B) Phosphate inclusions / glycogen granules.**

Laboratory modeling experiments with cyanobacteria *Synechococcus* sp. were performed in order to characterize hydrous magnesium carbonate precipitation in alkaline lake (stromatolites formation) and to assess the range and characterize the mechanisms of Mg isotope fractionation in lacustrine environment. The results of this study are described in the articles Mavromatis et al. (2011) and Shirokova et al. (2011). These works are presented in Appendices 1 and 2.

# Chapter II

# Materials and methods

# 1. Bacterial growth and cultivation

## 1.1. Bacterial growth

Bacterial growth is the division of one bacterium into two daughter cells in a process called binary fission. Providing no mutational event occurs, the resulting daughter cells are genetically identical to the original cell. Hence, "local doubling" of the bacterial population occurs. Both daughter cells from the division do not necessarily survive. However, if the number surviving exceeds unity on average, the bacterial population undergoes exponential growth. The measurement of an exponential bacterial growth curve in batch culture was traditionally a part of the training of all microbiologists; the basic means requires bacterial enumeration (cell counting) by direct and individual (microscopic, flow cytometry (Skarstad et al, 1983)), direct and bulk (biomass), indirect and individual (colony counting), or indirect and bulk (most probable number, turbidity, nutrient uptake) methods (Zwietering et al., 1990).

Bacterial growth can be modeled with four different phases as shown in a typical curve of bacterial growth in Fig. 1 below: lag (latent, A) phase, exponential or log phase (B), stationary phase (C), and death phase (D).

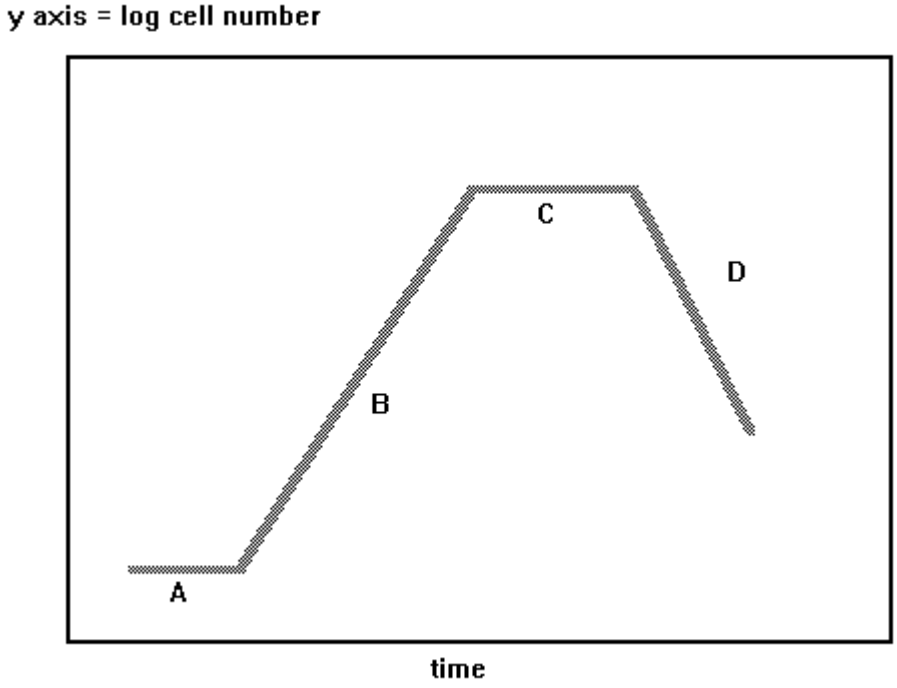


**Fig. II. 1. Typical curve of bacterial growth.**

During *lag phase* (A), bacteria adapt themselves to growth conditions. It is the period where the individual bacteria are maturing and not yet able to divide. During the lag phase of the bacterial growth cycle, synthesis of RNA, enzymes and other molecules occurs. Note that in this phase the microorganisms are not dormant (Hett and Rubin, 2008).

*Exponential phase* (B) (sometimes called the log phase or the logarithmic phase) is a period characterized by cell doubling. The number of new bacteria appearing per unit time is proportional to the present population. If growth is not limited, doubling will continue at a constant rate so both the number of cells and the rate of population increase doubles with each consecutive time period. For this type of exponential growth, plotting the natural logarithm of cell number against time produces a straight line. The slope of this line is the specific growth rate of the organism, which is a measure of the number of divisions per cell per unit time (Novick, 1955). The actual rate of this growth (i.e. the slope of the line in the figure) depends upon the growth conditions, which affect the frequency of cell division events and the probability of both daughter cells surviving. Under controlled conditions, cyanobacteria can double their population four times a day. Exponential growth cannot continue indefinitely, however, because the medium becomes depleted of nutrients and enriched with wastes.

During *stationary phase* (C), the growth rate slows down as a result of nutrient depletion and accumulation of toxic products. This phase is reached as the bacteria begin to exhaust the resources that are available to them. This phase is characterized by a constant biomass value as the rate of bacterial growth is equal to the rate of bacterial death.

At *death phase* (D), bacteria run out of nutrients and die (Zwietering et al., 1990).

This basic batch culture growth model draws out and emphasizes aspects of bacterial growth which may differ from the growth of impure culture or microbial consortia. It emphasizes clonality, asexual binary division, the short development time relative to replication itself, the seemingly low death rate, the need to move from a dormant state to a reproductive state or to condition the media, and finally, the tendency of lab adapted strains to exhaust their nutrients (Novick, 1955).

In reality, even in batch culture, the four phases are not well defined. The cells do not reproduce in synchrony without explicit and continual prompting and their exponential phase growth is often not ever a constant rate, but instead a slowly decaying rate, a constant stochastic response to pressures both to reproduce and to go dormant in the phase of declining nutrient concentrations and increasing waste concentrations (Hett and Rubin, 2008).

Liquid is not the only laboratory environment for bacterial growth. Spatially structured environments such as biofilms or agar surfaces present additional complex growth models

(Madigan et al. 2000). In contrast to experiments in biomineralization on agar media, we used only liquid culture in the present study. The main reason of this is the inability of researcher to control and monitor solute parameters (pH, $pCO_2$, Alk, [Ca], [Mg], nutrients) in the agar media which does not allow quantifying the rates and identifying the governing factors of the microbial mineral precipitation processes.

## 1.2. Anoxygenic phototrophic bacterial (APB) growth and cultivation

### 1.2.1. Bacteria growth medium preparation and conditions of cultivation

Both APB, A20-S and S-1765 (which are presented in chapter 1), were cultured in Pfenning's growth medium of the following composition (Pfenning and Lippert, 1966) : $KH_2PO_4$ (330 mg/L), $MgCl_2*6H_2O$ (330 mg/L), $NH_4Cl$ (330 mg/L), KCl (330 mg/L), $Na_2SO_4$ (330 mg/L), $CaCl_2$ (50 mg/L), $NaHCO_3$ (5 g/L for A-20s, 0.5 g/L for S-17-65), NaCl (25 g/L for A-20s , 120 g/L for S-17-65), sodium acetate (1 g/L), casamino acids (0.1 g/L), yeast extract (0.1 g/L), $B_{12}$ (20 μg/L), and Trace metal solution (1 ml/L (composition see paragraph 1.3.1)). For S-17-65, $Na_2S$ (0.1 g/L) and cysteine (0.3 g/L) were added as a source of sulphur.

Culture (growth) medium is prepared in 2 stages. At the first stage, inorganic components (in the form of salts) were added in the distilled (MQ) water. After that, solution was sterilised in autoclave (121°C, 2050 mBar, 25 min). The sterile solution is transferred to a laminar hood box. At the second stage (in laminar hood box), other components (in the form of 10% sterile solution) are added in a solution. Finally, the suspension of living bacterial cells is added in this solution.

Stock cultures of bacteria were kept in sealed glass bottles in oxygen-free conditions at 23-30°C, under constant 2000 lx light (Kompantseva at al. 2009), and placed on a rotator shaker at 10 rpm to grow until the stationary stage is reached (5 to 7 days).

### 1.2.2. Characterization of APB bacterial growth

The overall growth rate was very similar between the two cultures in a wide range of pH and Dissolved Inorganic Carbon (DIC] concentrations (see Chapter 4). The curves of both APB's growth in the nutrient solution are presented in the Fig. 2. As it can be seen from this figure, lag phase's duration for A-20s and S-17-65 is 70-80 and 100-120 hrs, respectively.

The exponential phase for bacteria A-20s is short and characterized by fast biomass development during the first 40 hrs. The duration this phase for S-17-65 is longer than that for A-20s (160 hrs) and is characterized by slower bacterial biomass evolution. Stationary phase time is achieved after 200 and 100 hrs for A-20s and S-17-65, respectively. Finally, death phase starts at the same moment for both bacteria, within 320-340 hrs after the beginning of the experiments.

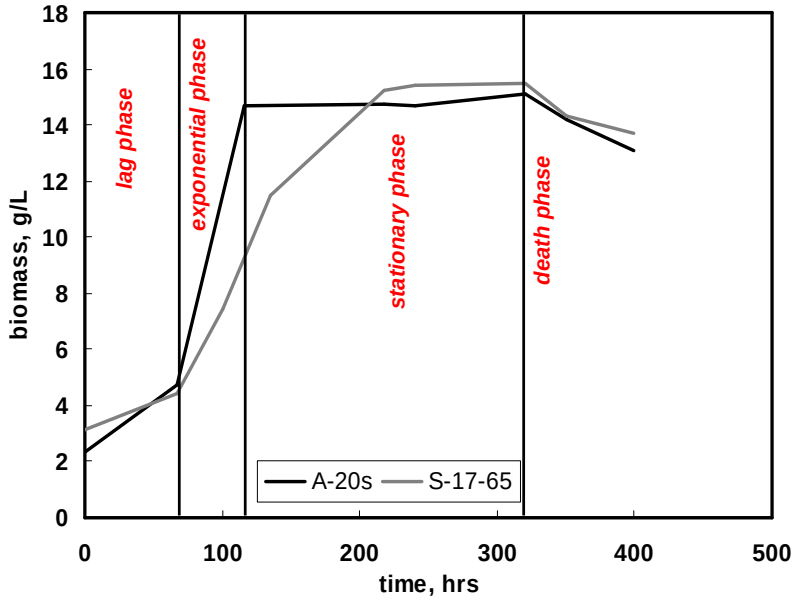


**Fig. II. 2. Curves of APBs A-20s and S-17-65 growth in the nutrient solution.**

Experiments with both APB culture in nutrient medium with Mg additions (1-100 mM) have shown that this metal, at concentration higher that 10 mM, inhibits bacterial biomass growth. This result suggests that Mg, at high concentrations, becomes a toxic metal for this APB.

The possibility of bacterial growth in dilute nutrient medium was tested. The experiments in dilute medium (factor of 2 and 10 times) demonstrated the absence of bacterial growth in these conditions.

## 1.3. Cyanobacteria growth and cultivation

### 1.3.1. Bacterial growth medium, preparation and conditions of cultivation

*Gloeocapsa sp.* were grown in Cyanobacteria BG-11 Fresh-water Solution Medium (Sigma-Aldrich C3061) of the following composition (Rippka at al., 1979): $NaNO_3$ (150 g/L), $K_2HPO_4*3H_2O$ or $K_2HPO_4$ (40 g/L or 30 g/L), $MgSO_4*7H_2O$ (75 g/L), $CaCl_2*2H_2O$ (36 g/L), Citric Acid (6 g/L, Ammonium Citrate (6 g/L), $Na_2CO_3$ (20 g/L), Trace metal solution (composition see below, 1 ml/L). This medium is traditionally used for most cyanobacteria.

Trace metal solution: $H_3BO_3$ (2.86 g/L), $MnCl_2*4H_2O$ (1.81 g/L), $ZnSO_4*7\ H_2O$ (0.222 g/L), $NaMoO_4*5H_2O$ (0.39 g/L), $CuSO_4*5H_2O$ (0.079 g/L), $Co(NO_3)_2*6H_2O$ (0.0494 g/L) (Rippka at al., 1979).

All components are added in the distilled (MQ) water. After that, solution is sterilised in autoclave (121°C, 2050 mBar, 20 min). Obtained sterile solution is transferred to a laminar hood box. Finally, suspension of living bacterial cells is added in this solution.

Stock culture of Gloeocapsa sp. were kept at room temperature (23±1°C) under constant cool white fluorescent light illumination (4700 lx) on a rotator shaker at 250 rpm.

### 1.3.2. Characterization of Gloeocapsa sp. growth

The curves Gloeocapsa sp. growth in the nutrient solution are presented in Fig. 3. As it can be seen from this figure, lag phase's duration is 70-80 hrs (3 days). The exponential phases for Gloeocapsa sp. are longer than APB and characterized by slow biomass development during the 50-55 days. Stationary phase time is achieved after 55 days. Finally, death phase starts after 80 days of experiments.

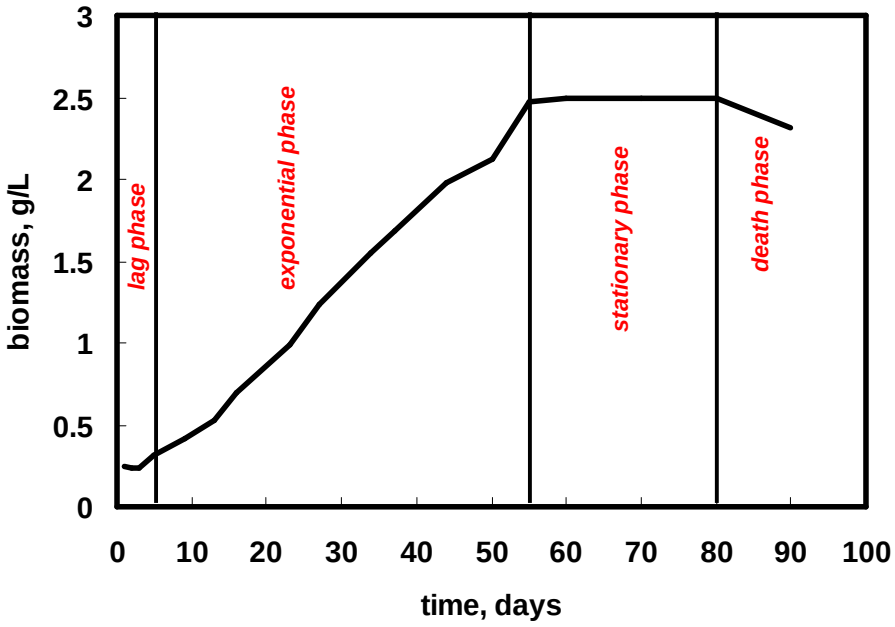


**Fig. II. 3. Curves Gloeocapsa's of growth in the nutrient solution.**

## 2. Electrophoretic Measurements

The composition and structure of bacterial surface is responsible for important processes such as biomineralization, bacterial adhesion, and biofilm formation (Borrok & Fein, 2004). In order to better understand the mechanisms of all these processes, it is necessary to know bacterial surface charge depending upon environmental conditions (pH, presence of different organic/inorganic charged/non charged particles, temperature etc.). Electrophoretic (named also electrokinetic) measurement is very useful for cells it surface characteristic. Microelectrophoresis is a powerful technique for characterizing the electric double layer of microbial cell surfaces (van der Wal et al., 1997; Gelabert at al., 2004).

This subchapter is undertaken to explain the physical theories of electrical double layer's (EDL) structure; structural's features of bacterial EDL and method to characterise it (electrophoretic measurements).

## 2.1. Electrical double layer (EDL)

In contact with a polar medium (water) the solid surface (e.g. majority of minerals and cells) show a definite surface charge as the consequence of ionization, ionic adsorption and ionic desorption. This surface charge influences the arrangement of neighbouring ions of the polar medium. Ions of the opposite charge (counter-ions) will be attracted to the particle surface while ions of like charge (co-ions) will be repulsed from the surface (Zembala, 2004). The formation of an interfacial charge causes a rearrangement of the local free ions in the solution to produce a thin region of nonzero net charge density near the interface. The arrangement of the charges at the solid-liquid interface formed the electrical double layer (EDL) (Lyklema, 1993).

There are two part of EDL as depicted in Fig. 4. The thin layer of counter-ions immediately next to the charged solid surface or surface of cells, called the *compact layer*. The counter-ions in the compact layer are immobile due to the strong electrostatic attraction. Counter-ions outside the compact layer are mobile. This part of the EDL is called the *diffuse layer*. In diffuse layer the ions are arranged under the influence of electrical forces and thermal movements (Lyklema, 1993).

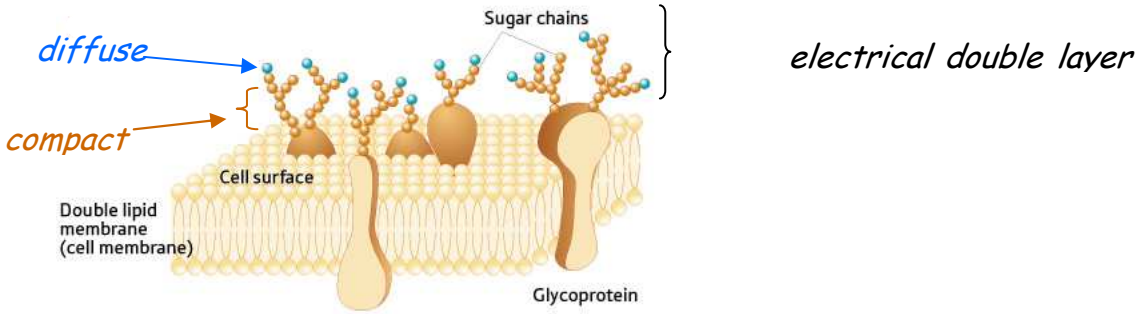


**Fig. II. 4. Electrical double layer of bacterial cells (modified from http://www.rikenresearch.riken.jp).**

There are several theories to describe the structure of the EDL (theories of Helmholtz Double Layer (1879) and Gouy-Chapman Double Layer (1910 and 1913)). In this work we briefly described Stern theory of EDL structure.

## 2.2. Stern theory of the Diffuse Double Layer

The Gouy-Chapman theory provides a better approximation of reality than does the Helmholtz theory, but it still has limited quantitative application. It assumes that ions behave as point charges (which they cannot) and that there is no physical limits for the ions in their approach to the surface (which is not true). Stern, therefore, modified the Gouy-Chapman theory by assuming that ions do have finite size, so that they cannot approach the surface closer than a few nm. In other words, the first ions of the Gouy-Chapman Diffuse Double Layer are not at the surface, but at some distance $\delta$ away from the surface. This distance will usually be taken as the radius of the ion. As a result, the potential and concentration of the diffuse part of the layer is low enough to justify treating the ions as point charges.

Stern also assumed that it is possible that some of the ions are specifically adsorbed by the surface in the plane $\delta$, and this layer has been named the Stern Layer. Therefore, the potential will drop by $\Psi_o - \Psi_\delta$ over the "molecular condenser" (i.e. the Helmholtz Plane) and by $\Psi_\delta$ over the diffuse layer. $\Psi_\delta$ has been names the zeta ($\zeta$) potential (Alekseev et al., 1988).

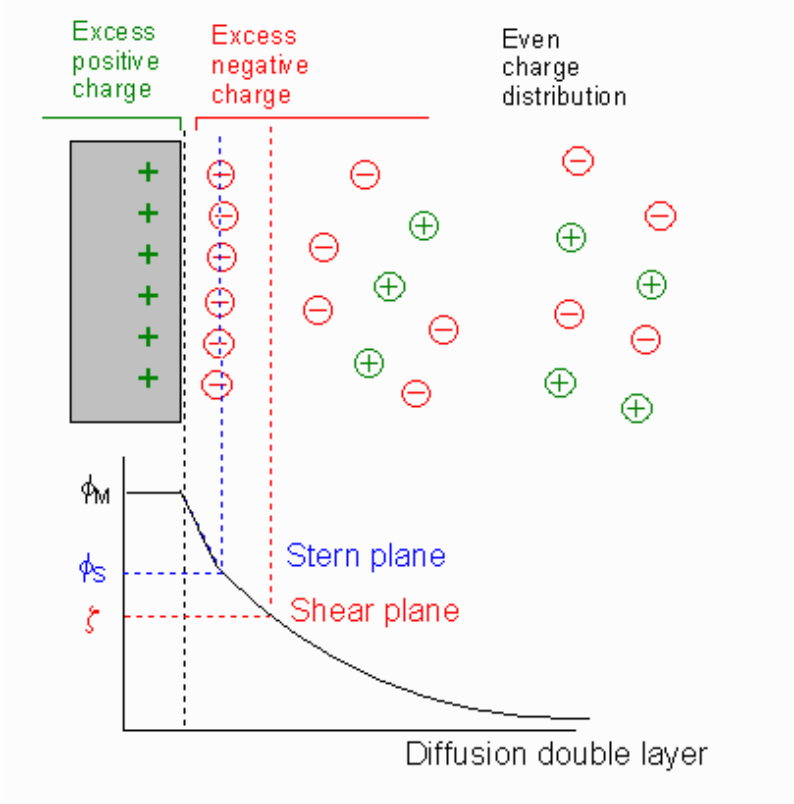


**Fig. II. 5. This diagram serves as a visual comparison of the amount of counter-ions in each the Stern Layer and the Diffuse Layer of smectite when saturated with the three alkali earth ions.**

The double layer is formed in order to neutralize the charged surface and, in turn, causes an electrokinetic potential between the surface and any point in the mass of the suspending liquid. This voltage difference is on the order of millivolts and is referred to as the surface potential. The magnitude of the surface potential is related to the surface charge and the thickness of the double layer. As we leave the surface, the potential drops off roughly linearly in the Stern layer and then exponentially through the diffuse layer, approaching zero at the imaginary boundary of the double layer. The potential curve is useful because it indicates the strength of the electrical force between particles and the distance at which this force comes into play. A charged particle will move with a fixed velocity in a voltage field. This phenomenon is called electrophoresis. The particle's mobility is related to the dielectric constant and viscosity of the suspending liquid and to the electrical potential at the boundary between the moving particle and the liquid. This boundary is called the slip plane and is usually defined as the point where the Stern layer and the diffuse layer meet. The relationship between zeta potential and surface potential depends on the level of ions in the solution. The figure above (Fig. 5) represents the change in charge density through the diffuse layer. The electrical potential at this junction is related to the mobility of the particle (and is called the zeta potential). Although zeta potential is an intermediate value, it is sometimes considered to be more significant than surface potential as far as electrostatic repulsion is concerned (Valleau, 1982).

## 2.3. Zeta (ξ) potential of bacterial cells

As it was defined in previous section, the zeta potential is the electrostatic potential at the boundary dividing the compact layer and the diffuse layer. Zeta potential is influenced by pH, ionic strength (the concentration and type of ions present) and the concentration of any charged molecules. The effect of the pH, or ionic strength of the medium or the concentration of an additive on the zeta potential can give information about the EDL of cells (Hunter, 1981).

Biological amphoteric molecules such as amino acid and proteins contain both acidic and basic functional groups. Amino acids which make up proteins may be positive, negative, neutral or polar in nature, and together give a protein its overall charge (Harden and Harris, 1952). Bacterial surface contain a lot of different proteins and as result their charges

depending on the functional groups present in the surface. The net charge on the surface is affected by pH of their surrounding environment and can become more positively or negatively charged due to the loss or gain of protons ($H^+$) (Dittrich et al. 2009). Net cell surface charge can be assessed on the basis of zeta potential which is the electrical potential of the interfacial region between the bacterial surface and the aqueous environment (Saito et el, 1997). Zeta potential can be estimated by measuring cellular electrophoretic mobility in an electric field (Mozes and Rouxhet, 1990).

Bacterial cells possess a net negative electrostatic potential surface charge when cultivated at physiological pH values (Mozes and Rouxhet, 1990). Competition between counter ion neutralization and molecular motion results in the establishment of an interfacial EDL. The inner region is referred to as the Stern layer and consists of the surface proper, as well as the ions with which it is electrostatically bound. The outer region protrudes into the aqueous environment and consists of more diffuse distribution of anions and cations which participate in electrostatic interactions between the cell and other charged surfaces. The zeta potential approximates the potential of the inner portion of the diffuse layer (Wilson et al., 2001).

Molecules comprising the outer cell envelope which contribute to the net electronegativity of the overall bacterial cell surface are structurally disparate and differ somewhat as a function of Gram reactivity. The peptidoglycan cell wall of gram-positive bacteria influences surface electronegativity by virtue of phosphoryl groups located in the substituent teichoic and teichuronic acid residues, as well as unsubstituted carboxylate groups (Beveridge, 1988). In contrast, the peptidoglycan of gram-negative bacteria is sequestered within the periplasmic space by virtue of the outer membrane and is therefore not exposed to the extracellular environment. Negative electrostatic surface charge in these organisms is conferred by the phosphoryl and 2-keto-3-deoxyoctonate carboxylate groups of lipopolysaccharide located in the outer leaflet of the outer membrane (Wilson et al., 2001).

Taking together, the complexity of bacterial surface makes predictions relative to biophysical parameters, such as surface charges, rather difficult. Polymers composing bacterial surface contain dissociable groups. Since most cell surfaces contain both basic and acidic groups, the surface is amphoteric, with a more negative net charge at high pH and more positive charge at low pH (Bayer and Sloyer, 1990).

## 2.4. Isoelectric point (IEP)

The point where the plot passes through zero zeta potential is defined as *isoelectric point (IEP)*. The pH of IEP ($pH_{IEP}$) is the pH at which a particular molecule or surface carries no net electrical charge (c.a., negative and positive charges are equal) (Kosmulski and Saneluta, 2004). At a pH below their IEP, particles carry a net positive charge; above their IEP they carry a net negative charge (Michen and Graule, 2010).

Within recent years a number of workers have referred to differences in the isoelectric point of bacteria. And the general tendency is that the isoelectric point in the gram positive bacteria varied from pH 1.75 to 4.15 and in the gram negative group from 2.07 to 3.65. These results indicate that the IEP values for gram negative cells do not vary over as wide a range as for gram positive cells. It is apparent, however, that the isoelectric point of the gram negative group does not occur at more alkaline reactions than of the gram positive bacteria. This feature is due to the protoplasm of the gram positive cells with high ribonucleic acid content which would exhibit greater acidic properties than that of gram negative cells (Bayer and Sloyer, 1990).

## 2.5. Electrophoresis method

A variety of methods has been used in the past to characterize bacterial cell surfaces with regard to overall electrostatic properties (Wilson et al., 2001). Microelectrophoresis is one such method and involves the placement of cell suspension in an electrophoresis cell, application of voltage across the cell, and direct microscopic observation of the movement of individual bacteria over a given distance, the velocity of which is then used to calculate electrophoretic mobility (Brinton and Lauffer, 1959). Electrophoretic mobility can be used to ascertain zeta potential values from which cell surface charge can be estimated by calculation. The direction and rate of the movement is dependent on a variety of factors such as ionic strength, temperature, pH of the medium, as well as electric field strength and the net surface charge of the bacterium (Wilson et al., 2001). Figure 6 shows an example of the movement of bacterial cells in electrostatic field (experiment with APB A-20s).

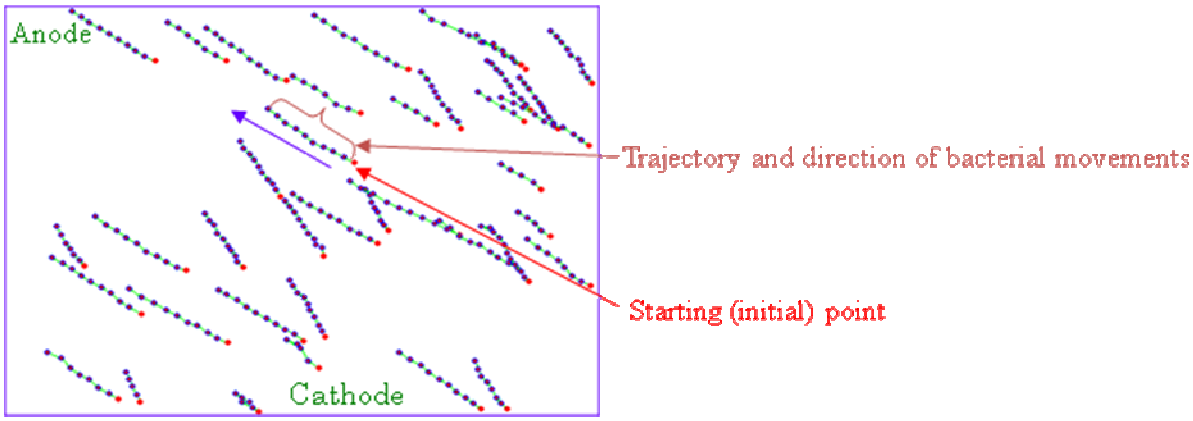


**Fig. II. 6. Movement of bacterial cells in electrostatic field (experiment with APB A-20s).**

## 2.6. Zeta potential measurements

The measurement of zeta potential is based on one of the three electrokinetic effects: electrophoresis, electroosmosis, and the streaming potential. In the electrophoresis method, the ξ –potential is determined by placing fine particles in an electric field and measuring their mobility, $\upsilon_E$, using a suitable microscopic technique. The mobility is then related to the ξ – potential at the interface using the Smoluchowski equation:

$$\upsilon_E = 4\pi\varepsilon_0\varepsilon_r\zeta(1+\kappa r)/6\pi\mu \quad ,$$

where $\varepsilon_0$ and $\varepsilon_r$ are the relative dielectric constant and the electrical permittivity of a vacuum respectively; μ is the solution viscosity; r is the particle radius and κ is Debye-Hückel parameter (Chesworth and Zasoski, 2008).

In this study, zeta potentials of APB cells were measured using a CAD Instrumentation “Zetaphoremeter IV” Z 4000, microelectrophoremeter (Fig. 7).

**Fig. II. 7. Microelectrophoremeter CAD Instrumentation "Zetaphoremeter IV" Z 4000**

### 2.6.1. Preparation of the cells for zeta potential measurements

For zeta potential measurements, cell suspensions of metabolically active, inactive ($NaN_3$-treated), and dead (autoclaved) A-20s or S-17-65 were prepared in 0.01, 0.1 and 0.5 mol/L aqueous NaCl solutions, with typical cell concentrations of 10 $mg_{wet}$/L. Note that the conversion factors of wet to dry (lyophilized) weight applied for studied microorganisms and for adsorption measurements were equal to 11.7 and 16.1 for A-20s and S-17-65, respectively. The cultures were harvested at the late exponential – stationary growth stage by centrifugation at 10,000 rpm (7000 g) for 10 min at 20°C. The cells were rinsed in 0.1 mol/L NaCl corresponding to optimal physiological conditions and centrifuged twice at 10,000 rpm for 10 minutes. Finally, bacterial suspension was washed in appropriate electrolyte solution and centrifuged. Resulting bacterial suspension was equilibrated for 1-1.5 hours in the specific electrolyte solution (0.01, 0.1 or 0.5 mol/L NaCl) at pH 7-8 prior to zeta potential measurements at variable pHs. Average equilibration time of bacterial suspension at a given pH was between 3 and 5 minutes, and no pH drift was observed during electrophoretic measurements. The cell integrity was maintained during experiments in acidic (pH < 4) and alkaline (pH > 10) solutions, as verified by optical microscopic examination. Additional zeta potentials were recorded for active bacterial cells after they were equilibrated for 1 h in the presence of 1.0 and 10 mmol/L $NaHCO_3$ or 1.0 and 10 mmol/L $CaCl_2$. Electrophoretic measurements were also performed in the dark using bacteria that were previously kept for 24 hours in complete darkness. Keeping the bacteria in the dark during 24 hrs, comparable with

cell division time, and maintaining the full darkness condition during the measurement were intended to insure that the light phase of photosynthesis is completely absent.

Dead (heat-killed) cells were prepared by autoclaving part of the fresh stock of biomass at 121°C for 20 minutes and performing the rinsing procedure as described above for live cells. Inactivated cells were prepared by rinsing part of the fresh (live) biomass in 0.1 mol/L $NaN_3$ during 1-2 hrs. Inactivated cells were prepared by rinsing part of the fresh (live) biomass in 0.01 mol/L $NaN_3$ during 1-2 hrs. Sodium azide suppresses bacterial activity by inhibiting cytochrome oxidase and is widely used for inactivating cells while keeping the surfaces physically and chemically intact (Urrutia Mera et al., 1992; Johnson et al., 2007).

### 2.6.2. Procedure of zeta potential measurements

The electrophoretic measurements were performed at 20 to 25°C in a quartz cell connecting two Pd electrode chambers. The cells were illuminated by a 2 mW He/Ne laser. During the measurements an electric field of 80 V $cm^{-1}$ was applied in each direction for 20 s and the images of moving cells were transmitted to a computer via a CCD camera. The zeta potentials of the cells were measured by timed image analysis. Measurements were performed at pH ranging from 2.5 to 11.0 with a pH resolution of 0.4 units. The pH of these suspensions was increased manually by adding 2–10 μL aliquots of 0.01–1 M NaOH or 0.01-1 M HCl. Three replicates were carried out and each was performed with a renewed bacteria suspension. The uncertainty of zeta potential measurements ranged from 5% to 20%. Electrophoretic mobilities were converted to zeta potentials using the Smoluchowski equation (Bazant, 2009):

$$\zeta = \frac{(\varepsilon \times \mu_E)}{\eta}$$

where $\zeta$ stands for the zeta potential (mV) and $\varepsilon$, $\eta$ and $\mu_E$ represent the dielectric constant of the solution, the viscosity and the electrophoretic mobility, respectively ($\mu_E = V_E/E$ with $V_E$ = electrophoretic rate ($s^{-1}$) and $E$ = electric field ($V.m^{-1}$)).

Results and discussions of zeta potential measurements with APB are presented in **Chapter 3.**

# 3. Calcium adsorption

Bacterial cell walls display a strong affinity for a wide variety of aqueous metal cations. Adsorption of aqueous metal cations onto bacterial cell walls is likely to be an abiotic process, controlled only by the acid/base properties of the exposed cell wall surface functional groups, and by affinity of each type of functional group for specific aqueous metals (Fein at el., 1997). Previous experiments indicate that isolated cell walls and whole bacteria exhibit similar affinities for aqueous metals (Mullen at al., 1989), reflecting the abiotic nature of at least the initial metal-bacteria interaction at the cell wall surface (Fein at al., 1997).

## 3.1. Isotherm of adsorption

Adsorption is the adhesion of atoms, ions, biomolecules or molecules of gas, liquid, or dissolved solids to a surface. This process creates a film of the *adsorbate* (the molecules or atoms being accumulated) on the surface of the *adsorbent*. Adsorption process is generally classified as physisorption (characteristic of weak van der Waals forces) or chemisorption (characteristic of covalent bonding). It may also occur due to electrostatic attraction (Lyklema, 1993). Adsorption is usually described through isotherms. In this study we used two types of isotherm: isotherm of calcium adsorption as a function of pH (pH-dependent adsorption edge) and isotherm of calcium adsorption at constant pH as a function of metal concentration in solution (adsorption isotherm).

## 3.2. Metal adsorption onto bacterial surfaces

Bacterial cell walls contain a variety of surface organic functional groups. The dominant groups of the bacterial surface are carboxyl, amino, hydroxyl and phosphate sites (Beveridge, 1991; Dittrich and Sibler, 2006). To characterize metal adsorption onto the bacterial cells, several parameters can be determined:

- The relative and absolute concentrations of these types of organic functional groups on the cell wall.

- The total surface area of bacterial walls in contact with the aqueous phase.
- Deprotonation constant for each of the important functional groups.
- Metal-organic stability constant for each metal and organic functional group of interest.

Because different functional groups become active under different pH conditions the different adsorption reactions occur. The negative charge of the cell wall results predominantly from deprotonation of carboxyl, phosphate, and hydroxyl functional groups exposed on the outer surface of the cell wall. Deprotonation reactions for theses three dominant functional group types are, respectively (Fein, 1997):

$$R\text{-}COOH \leftrightarrow R\text{-}COO^- + H^+$$

$$R\text{-}POH \leftrightarrow R\text{-}PO^- + H^+$$

$$R\text{-}OH \leftrightarrow R\text{-}O^- + H^+$$

Note that phosphate groups in bacteria can exist in several different forms: inorganic forms of phosphate such as orthophosphate and its oligomers, and organic species in the form of phosphate mono- and diesters (Dittrich, 2006). In the study of Dittrich and Sibler (2005) it was shown that three distinct sites exist on the bacterial surfaces of two *Synechococcus*-type unicellular autotrophic picocyanobacteria strain: carboxyl, phosphate and amino groups with pK values of 4.8-5.0; 6.6-6.7; 8.8-8.7, respectively.

Interactions between aqueous metal cations (M) and deprotonated surface sites on the bacterial cell wall can be represented by the following association reactions:

$$M^{m+} + R\text{-}COO^- \leftrightarrow R\text{-}COO(M)^{(m-1)+}$$

$$M^{m+} + R\text{-}PO^- \leftrightarrow R\text{-}PO(M)^{(m-1)+}$$

$$M^{m+} + R\text{-}O^- \leftrightarrow R\text{-}O(M)^{(m-1)+}$$

Three cell surface sites known to attract $Ca^{2+}$ are carboxyl ($> COO^-$), phosphodiester ($> PO_4^-$), and phosphoryl ($>PO_4^{2-}$) sites. Reactions forming $Ca^{2+}$ complexes with these sites can be written as:

$$Ca^{2+} + > COOH \rightarrow (> COO - Ca)^{+} + H^{+}$$

$$Ca^{2+} + > PO_4H \rightarrow (> PO_4 - Ca)^{+} + H^{+}$$

$$Ca^{2+} + > PO_4H_2 \rightarrow (> PO_4 - Ca)^{0} + 2H^{+}$$

Like mineral surfaces, bacterial surfaces are charged and create an electric field. The resulting electrostatic interaction between this electric field and aqueous ions must be accounted for when expressing the equilibrium constant of a reaction involving surface sites. These interactions may be quantified using the following relationship:

$$K=K_{Intrinsic} \exp(-F\Psi/RT)$$

Where F and R are Faraday's constant and gas constant, respectively, T is absolute temperature, $K_{Intrinsic}$ represents the equilibrium constant referenced to zero surface charge and zero surface coverage, and Ψ is the electric potential of the bacterial surface (Feid, 1997). The interaction between aqueous metal cations and surface functional groups of bacterial cell wall is represented schematically in Figure 8.

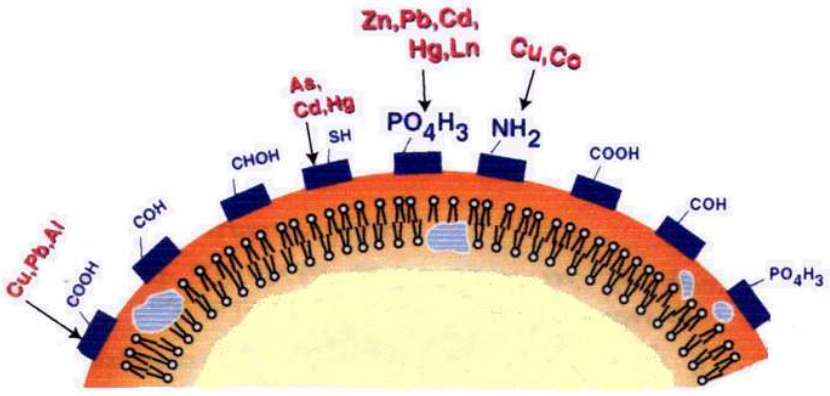


**Fig. II. 8. Interaction between aqueous metal cations and surface functional groups of bacterial cell wall.**

### 3.3. Experimental procedure of Ca adsorption on cell surfaces

The calcium adsorption experiments were designed to provide a quantitative characterization of metal binding by bacterial cells in a wide range of pH and $Ca^{2+}$ concentrations in solution. For this, two types of experiments were carried out:

- adsorption at constant initial calcium concentration in solution as a function of pH (pH-dependent adsorption edge) and
- adsorption at constant pH as a function of metal concentration in solution (adsorption isotherm).

All experiments were performed in undersaturated solutions with respect to any calcium carbonate phase as verified by speciation calculations with the MINTEQA2 computer code and corresponding database (Allison et al., 1991; Martell et al., 1997).

Live, freshly harvested (stationary stage) cells, sodium azide-inactivated and heat-killed (autoclaved) bacteria were used in the adsorption experiments. The cells were rinsed in 0.1 mol/L NaCl and 0.01 mol/L EDTA solutions for 15 minutes and again in 0.1 mol/L NaCl solution prior the experiments. This procedure allowed desorption of all possible $Mg^{2+}$, $Ca^{2+}$ ions from the cell's surfaces that might occurred during the APB culture.

The initial calcium concentration in experiments with APB was 17 µmol/L at variable pH and varied between 0.1 and 800 µmol/L at constant pH. In experiments with *Gloeocapsa sp.* initial calcium concentration at variable pH was 2.3-17 µmol/L and at constant pH between 4.2 and 25 µM/L. The pH was adjusted by adding aliquots of NaOH (0.1 and 0.01 mol/L) or HCl (1.0, 0.1 and 0.01 mol/L), whereas, constant pH of 5.5 to 6.7 was maintained by adding 0.005 mol/L MES (2-morpholinoethanesulfonic acid monohydrate) buffer. Adsorption experiments were conducted in 8 mL sterile polypropylene vials during 3 and 24 hr at 25 ± 0.2°C, in continuously agitated bacteria suspension with an ionic strength of 0.1 mol/L NaCl. The biomass concentration was kept constant at 10 $g_{humid}$/L.

The adsorption of calcium on cell surfaces was quantified by subtracting, at each solution pH, the concentration of calcium remaining in bacterial suspension from the concentration of added calcium in the supernatant (control experiments without biomass). The adsorption of calcium on reactor walls and cellular Ca release from the biomass in the full range of studied pH was negligible (<10%) compared to the initial amount of Ca added. This was routinely verified by Ca analyses in the blank (supernatant) and in the zero-added-Ca cell suspension experiments. Nonetheless, the measured Ca concentrations in these blank

experiments (to the limit of detection) were explicitly taken into account to calculate the adsorption isotherm.

All filtered solutions (0.22 µm filter) were analyzed for aqueous Ca concentration using flame atomic absorption spectroscopy (Perkin Elmer AAnalyst 400) with an uncertainty of ±2% and a detection limit of 0.5 µmol/L.

Results and discussion of adsorption experiments with APB and cyanobacteria are presented in **Chapters 3 and 5**, respectively.

# 4. Kinetics experiments

To characterise the link between the rate of bacterial growth (biomass production) and the rate of $CaCO_3$ precipitation as well as between other parameters (Omega ($\Omega$), pH, [Ca], [DIC], [Alk]), batch kinetic experiments were performed. There are fundamental differences between kinetic experiments with APB and cyanobacteria because of the essential difference between these bacteria. This section is devoted to the description of these kinetics experiments, of sampling and sample preparation for the analysis. In the end of the section are presented the short descriptions of all analytical methods used in this study for liquid samples analysis.

## 4.1. Kinetics experiments conditions with anoxygenic phototrophic bacteria

Kinetic experiments were carried out with initial concentration of calcium chloride and sodium bicarbonate ranging from 1 to 10 and 5 to 20 mM, respectively. All biotic experiments were performed with initial biomass concentration between 1.6 and 3.5 $g_{wet}$/L. Experiments were carried out over a range of initial saturation index ($\Omega_{init.}$) with respect to calcite varying between 8 and 230 for A-20s, and between 2 and 60 for S-17-65. The biomass of cells, pH, [$Ca^{2+}$] and [DIC] (or [Alk] in the car of inert electrolyte) were measured as a function of time. Blank experiments (without cell or with inactivated cells) were always carried out.

Kinetic experiments were performed at 25 ± 1°C in a climate chamber in nutrient (phosphate-free culture medium solution) and in nutrient-free inert electrolyte (0.1 M NaCl) with live, dead and $NaN_3$-inactivated cells. Composition of culture medium solutions was constants (see above) for all experiments. For each kinetic experiment (in nutritive or in inert electrolyte) only [$Ca^{2+}$] and [$HCO_3^-$] was changed and 0.1 M solution of $NaN_3$ (sodium azide) was used for cells inactivation.

Experiments were conducted using discontinuous batch mode in two to three replicates. Mother suspension of cells in nutrient or inert electrolyte solution was mixed homogeneously and separated into 5-10 sealed 25-mL sterile glass bottles without headspace. 10 ml of homogeny solution (first sampling) is collected to measure the initial conditions of experiment (biomass, pH, [$Ca^{2+}$], DIC). Time zero is the time of this first sampling.

The bottles were placed in a rotator mixer at 24 rpm and under continuous light 2000 lx (Fig. 9). Periodically, one whole bottle was sampled to monitor the chemical and microbiological evolution of the system. About 30% of experiments were performed in duplicates and triplicates; typical experimental reproducibility was 10-20%.

The initial conditions as well as the variation of all experimental parameters in each individual kinetic experiment are presented in the Table 1 in the Chapter 4 and in the Appendix 3, respectively.

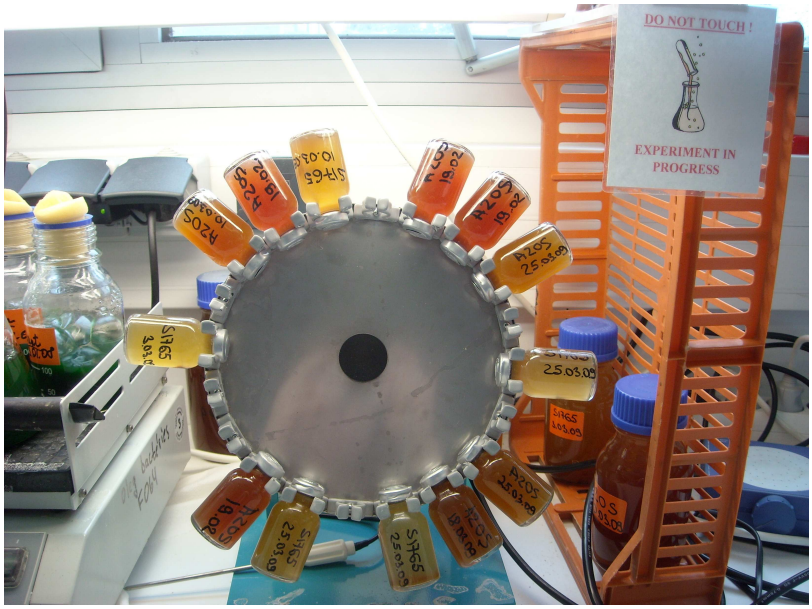


**Fig. II. 9 . Rotator with the bottles in the kinetic experiment with APB A-20s and S-17-65.**

### 4.2. Kinetics experiments conditions with cyanobacteria *Gloeocapsa* sp.

Kinetic experiments were performed at 25±1°C in closed Schott® 1L glass bottle reactors containing 800 ml of the initial solution (bacterial growth medium with $CaCl_2$ and $NaHCO_3$ addition) (Fig. 10). Experiments were carried out with initial concentration of calcium chloride and sodium bicarbonate ranging from 1 to 50 and 5 to 10 mM, respectively. All biotic experiments were performed with initial biomass concentration between 0.04-0.66 (in nutrient solution) and 1.5-1.7 $g_{wet}$/L (in inert electrolite). Precipitation experiments were carried out over a range of initial saturation index ($\Omega_{init.}$) with respect to calcite varying between 15.1 and 147.9 (in nutrient solution) 66.1 and 83.2 (in inert electrolite). The 30 % of experiments were conducted in duplicates.

The initial conditions as well as the variation of all experimental parameters in each individual kinetic experiment are presented in Table 2 of **Chapter 5** and in the **Appendix 4**, respectively.


**Fig. II. 10. Closed batch kinetic reactor used in the kinetic experiment with cyanobacteria *Gloeocapsa* sp.**

## 4.3. Liquid samples preparation and analysis

One bottle from rotator (in the case of APB) or 10 ml of bacterial suspension (in the case of *Gloeocapsa sp.*) were taken every 2-3 days for monitoring the chemical and microbiological evolution of the system. Approximately 2 ml of solution were used to estimate the concentration of bacterial cells by measuring optical density and pH. The remaining 5 mL were filtered through a 0.22 µm acetate cellulose membrane filter to remove active or dead bacterial cells from the suspension. The filtrate was analyzed for [Ca], [DIC]/ [Alk] (Fig.11).

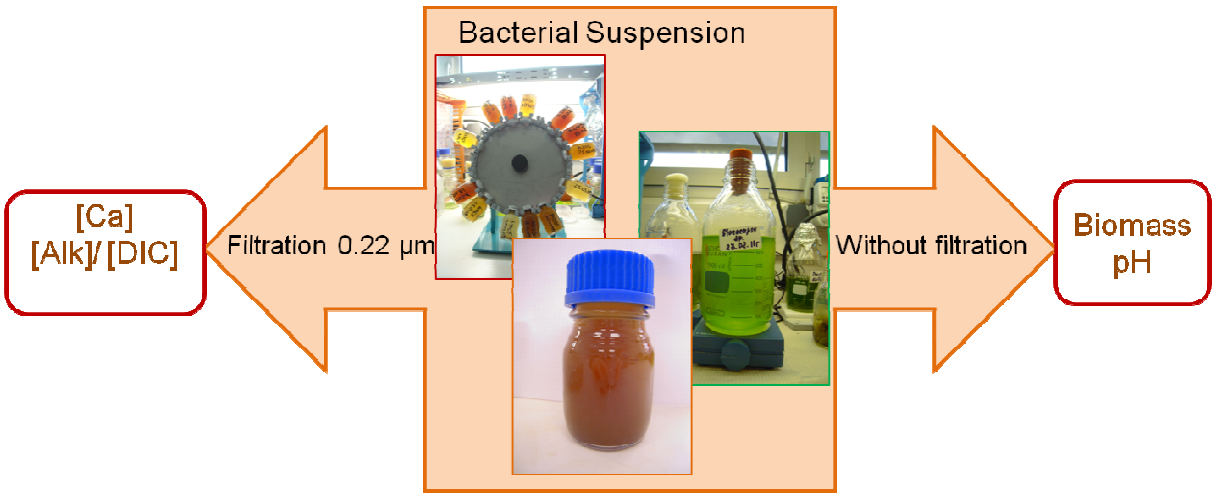


**Fig. II. 11. Schematic of liquid simple preparation for analysis.**

### 4.3.1. pH and cells biomass mesurements

The pH in each sample was measured using a Fisher pH combined electrode, with an uncertainty of 0.01 units, previously calibrated using pH 4.01, 6.86, 9.18 buffer solutions at 25°C.

For unicellular organisms such as the bacteria, growth can be measured in terms of two different parameters: changes in cell mass and changes in cell numbers. There are a lot of methods of bacterial biomass measurements. Methods for measurement of the cell mass involve both direct and indirect techniques.

Direct *physical measurement* of dry weight, wet weight, or volume of cells after centrifugation.

Direct *chemical measurement* of some chemical component of the cells such as total N, total protein content.

Indirect *measurement of chemical activity* such as rate of $O_2$ production or consumption, $CO_2$ production or consumption, etc.

*Haemocytometry* is a total count method where every cell (dead or alive) is counted. It works by introducing a standard amount of bacteria solution in to the haemocytometer - a glass slide with lots of grid lines. This is placed under a microscope and the number of cells counted using a standard method.

In *dilution plating,* $1cm^3$ of original bacterial solution is taken and diluted with $9cm^3$ of water. The same is done with this diluted solution and so on. A sample from each dilution is cultured; once individual colonies can be seen, it means each of those represents a single bacterium that was in the solution. The number is multiplied by the dilution factor.

*Turbidity measurements* employ a variety of instruments to determine the amount of light scattered by a suspension of cells. Particulate objects such as bacteria scatter light in proportion to their numbers. The turbidity or optical density of a suspension of cells is directly related to cell mass or cell number, after construction and calibration of a standard curve. The method is simple and nondestructive, but the sensitivity is limited to about $10^7$ cells per ml for most bacteria (Madigan et al., 2000).

In our study we used combination of two methods: direct physical measurement of dry/wet biomass after centrifugation and turbidity measurement. Firstly, concentration of bacterial cells was estimated by measuring optical density (turbidmetry) at a 650 nm wavelength for APB (Kompanceva et al., 2009) and at 750 nm for cyanobacteria *Gloeocapsa sp.* (Hu et al., 2000; Sarcina and Mullineaux, 2000). Secondly, known volume of the same bacterial suspension was taken for centrifugation. Bacterial mass after centrifugation was weighed and freeze-dried. The mass of bacterial cells (in $g_{biomass\ dry}/L$ and $g_{biomass\ wet}/L$) with corresponding measured optical density had been calculated. Conversion factor from optical density (D) to $g_{biomass\ wet}/L$ is 3.3 for A-20s and 4.2 for S-17-65 and 2.0 for *Gloeocapsa sp.* Conversion factors from biomass wet to biomass dry are 0.54 and 1.01 for A-20s and S-17-65, respectively.

### 4.3.2. Ca, Alkalinity and DIC analyses

Calcium concentration was determined using flame atomic absorption spectroscopy via a Perkin Elmer AAnalyst 400 Spectrophotometer with an uncertainty of ±2% and a detection limit of 0.5 µmol/L. The series of standard solution were prepared by addition of a precise amount of $CaCl_2$ into MilliQ water with $HNO_3$ and $La^{3+}$ addition.

In organic-free solutions (experiments in the inert electrolyte), alkalinity was determined following a standard HCl titration procedure using automatic titration cell TitroLine alpha TA10 plus (Schott Instruments®) with an uncertainty of ±2% and a detection limit of $5\times10^{-5}$ M.

In organic-rich nutrient solutions, dissolved inorganic carbon (DIC) was measured using Shimadzu SCN Analyzer after calibration of the instrument in a series of standard solution (10, 50, 100 ppm). All samples before analysis were diluted 20 times by MilliQ water. This yielded an uncertainty of ±10% and a detection limit of $4\times10^{-5}$ M.

# 5. Solid phase analyses

For better understanding of the spatial organisation/interaction between bacteria cell and precipitated minerals, different microscopic and spectroscopic techniques were used.

Scanning electron microscope (SEM) and X-ray powder diffraction (XRD) analyses were used for crystals characterisation (form, size, and chemical compositions) and for identifying the mineralogy of precipitates during bacterial activity. Moreover, Transmission Electron Microscope (TEM) analysis was used for bacterial cells characterisations (form, size, organisations, and the surface chemical compositions) as well as for better understanding bacteria-mineral relationship during the precipitation process.

## 5.1. Precipitation experiments

Precipitation experiments with APB were carried out in the 0.5 L bottles to collect sufficient quantity of solid phase at the end of experiment. Precipitation experiments with

cyanobacteria *Gloeocapsa sp.* were conducted in the same reactors than kinetic experiments. Preparation, condition and duration of precipitation experiment were the same as in kinetic experiments described previously. During and at the end of experiments visual precipitates were formed on the glass walls of reactors and in the bacterial suspension (Fig. 12 A and B, respectively).

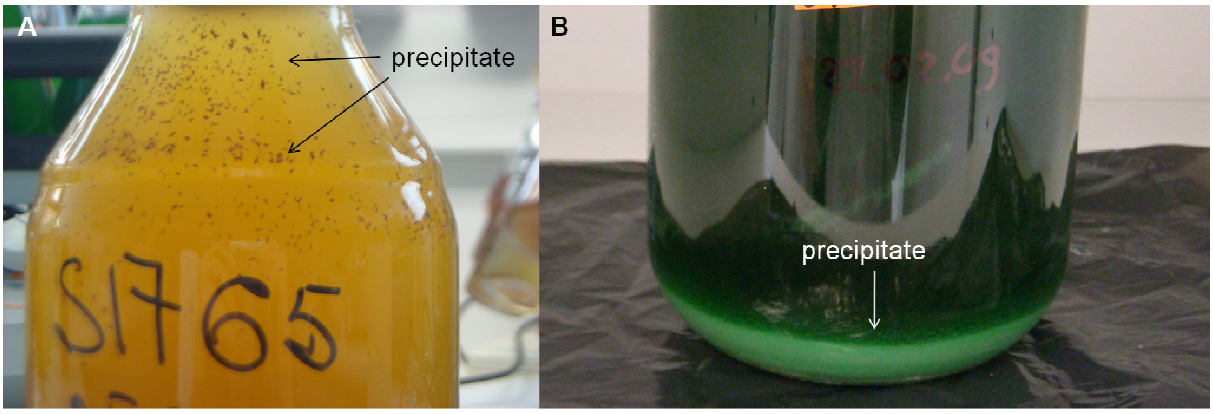


**Fig. II. 12. Precipitate formation on the glass walls of reactor during the experiment with APB (S-17-65) (A) and with cyanobacterial suspension experiment with Gloeocapsa sp. (B)**

## 5.2. SEM and XRD analyses

Bacterial suspensions from the reactor, containing live bacteria and crystalline precipitates were collected at the end of the precipitation experiment. Suspension were centrifuged at 10 000 rpm for 10 min, and washed twice with a MilliQ water. A part of bacterial biomass + mineral (mixtures of APB cells and precipitated mineral phase) was treated in 10% $H_2O_2$ at the same solution pH as in the experimental samples in order to remove organic matter. Resulted solid phases were rinsed in MilliQ water, frozen at -80°C and freeze-dried. Selected samples were studied by SEM and X-ray diffraction for mineral characterization.

Microscopic examination of crystals was performed using a JEOL JSM840a scanning electron microscope (SEM) equipped with a Princeton Gamma Technology (PGT) EDX detector, operating at 20kV. Examinations were carried out after carbon film coating

deposition on the sample surface. Shown in Figure 13 are some examples of SEM images, collected during this study.

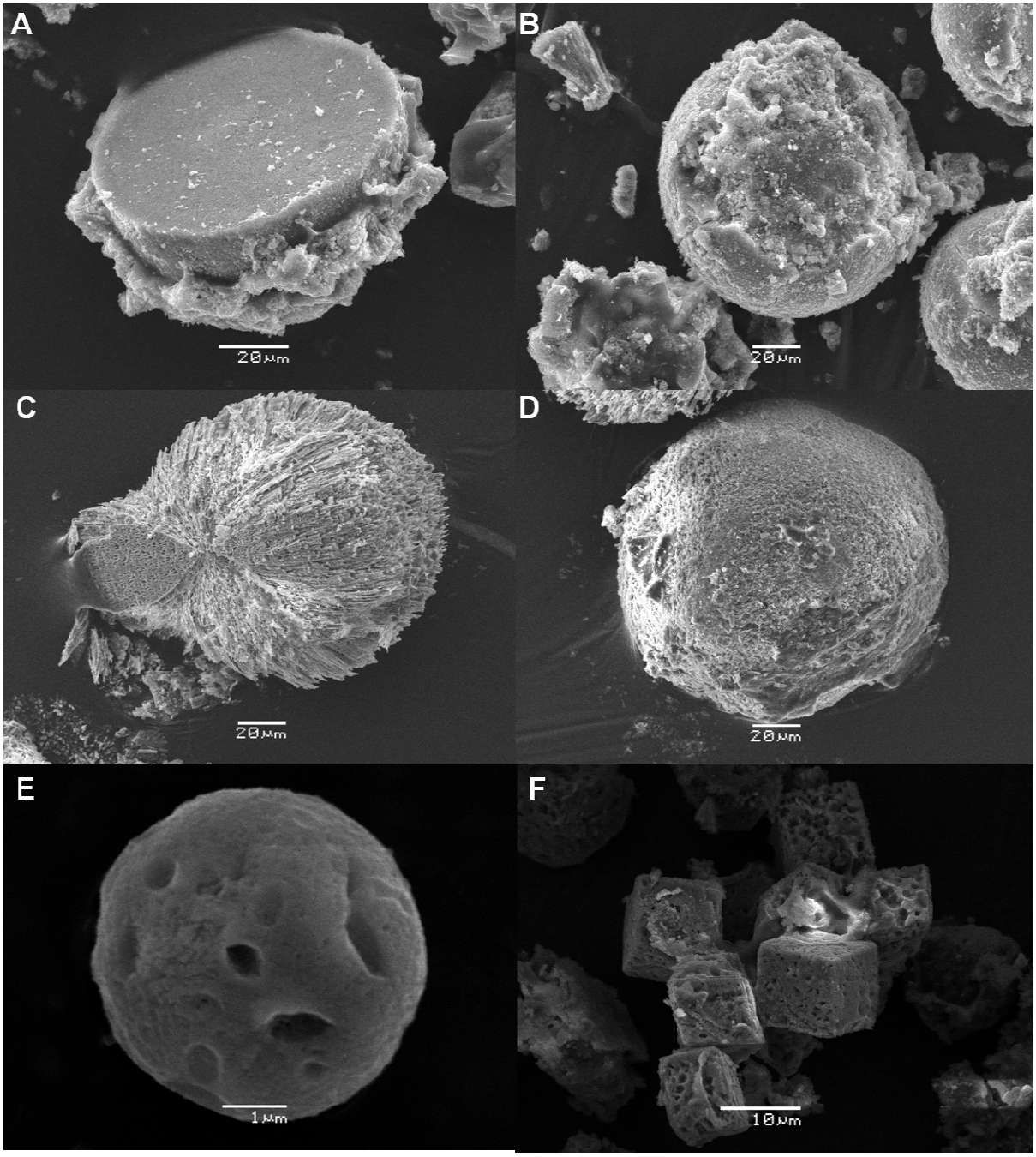


**Fig. II. 13. SEM images of calcite formed in nutrient solution in the experiment with bacteria A-20s (A, B), S-17-65 (C, D). Initial experimental conditions: 10 mM $CaCl_2$ and 10 mM $NaHCO_3$ (A-D); inert electrolyte with A-20s (E, F); 7 mM $CaCl_2$ and 5 mM $NaHCO_3$ (E); 10 mM $CaCl_2$ and 5 mM $NaHCO_3$ (F).**

X-ray powder diffraction analysis was performed with a INEL CPS 120 powder diffractometer on finely powdered samples using $Co_{K\alpha}$ radiation (40 kV and 30 mA), scanning speed of $0.02^{o}s^{-1}$. The time constant was set at 2 s. The XRD analysis of biotic precipitates formed in nutrient-free inert electrolyte yielded calcite and vaterite formation with both APB species. In the experiments carried out in nutrient solutions the XRD analysis showed the presence of calcite and monohydrocalcite. XRD analysis of precipitates formed in experiments with Gloeocapsa sp. showed the formation of calcite. As an example, a XRD spectrum is presented in Fig. 14, indicating the detection of calcite in this sample.

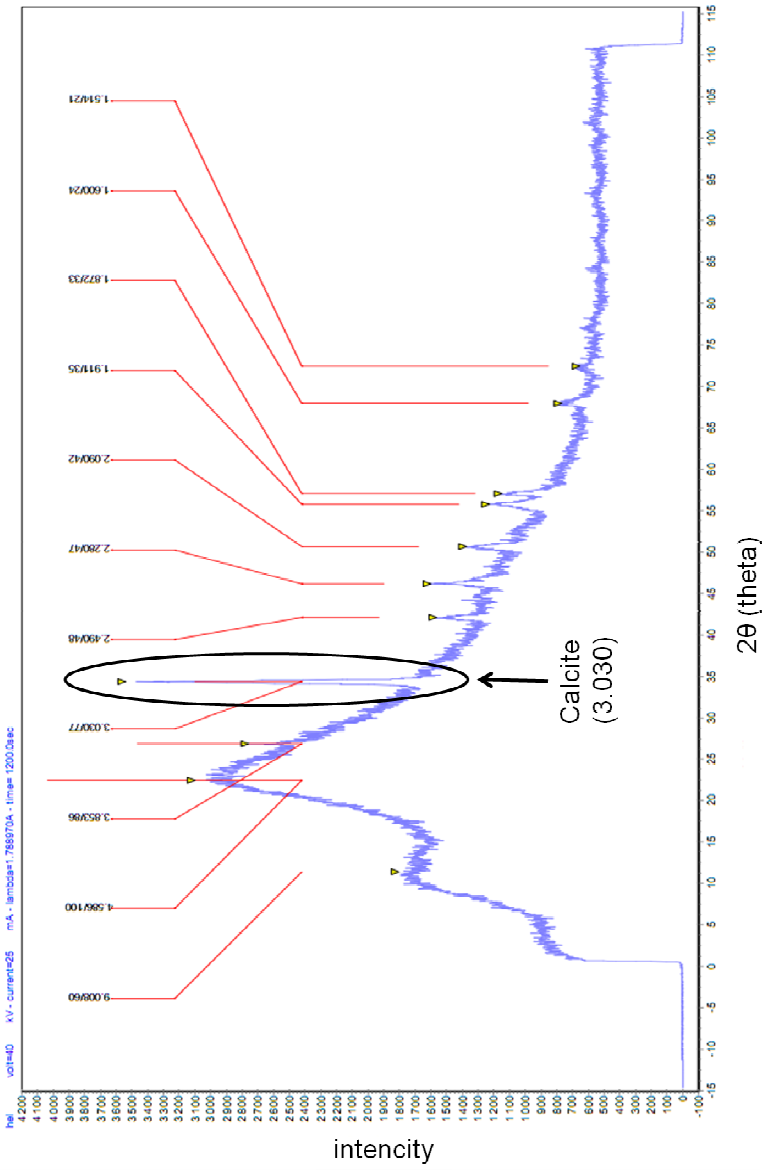


**Fig. II. 14 .XRD spectra of precipitate for experiment with APB A-20s (initial conditions 10 mM $CaCl_2$, 10 mM $NaHCO_3$) with the standard peaks for calcite (3.030) (black outlining and arrows), indicating the detection of calcite in this sample.**

### 5.3. Transmission Electron Microscope (TEM)

Materials for TEM must be specially prepared to thicknesses which allow electrons to transmit through the sample, much like light is transmitted through materials in conventional optical microscopy (Graef, 2003). Because the wavelength of electrons is much smaller than that of light, the optimal resolution attainable for TEM images is many orders of magnitude better than that from a light microscope. Thus, TEM can reveal the finest details of internal structure - in some cases as small as individual atoms. Magnifications of 350 000 times can be routinely obtained for many materials, whilst in special circumstances; atoms can be imaged at magnifications greater than 15 million times. For biological samples, cell structure and morphology is commonly determined whilst the localization of antigens or other specific components within cells is readily undertaken using specialized preparative techniques. The energy of the electrons in the TEM determines the relative degree of penetration of electrons in a specific sample, or alternatively, influence the thickness of material from which useful information may be obtained. Thus, for the physical and biological sciences, TEM is a complementary technique to conventional crystallographic methods such as X-ray diffraction (Williams and Carter, 2009).

Mineral-free cells and cell biomass with precipitated $CaCO_3$ were examined using Transmission Electron Microscopy (TEM) with a JEOL JEM 12000 EX and JEOL JEM 2100F (equipped with a field emission gum (FEG) and PGT EDX detector) at 80 kV. Cell suspension was rinsed using sterile nutrient solution (without sodium chloride addition) or MilliQ water, centrifuged 2 min at 10 000 rpm. TEM samples for analyses were prepared by immersing 200 mesh copper grids coated with a carbon film (Fig. 15) for 10 s in prepared bacterial suspension. Dried grids were used for TEM analysis.

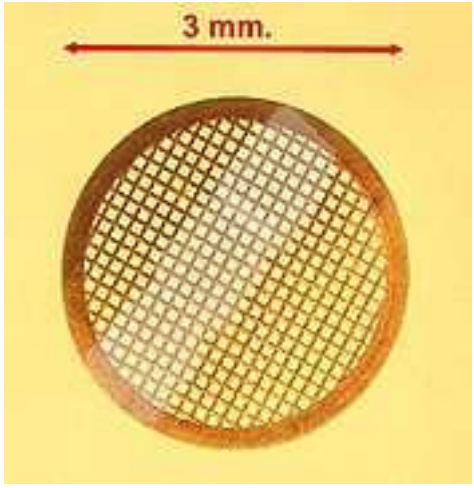


**Fig. II. 15. TEM sample support mesh "grid", with ultramicrotomy sections.**

In Figures 16 and 17 below are shown the few examples of TEM images, which were obtained during this study. It can be seen from these figures that there are no significant differences between APB cells in nutrient medium (Fig. 16 A,C) and in precipitation experiment (Fig. 16 B,D) since no calcium carbonate is observed on the cell surfaces and around the cells. In contrast, for the precipitation experiments involving the cyanobacteria *Gloeocapsa sp.* we observed crystals of $CaCO_3$ located around bacterial cells (Fig. 16 F and Fig. 17).

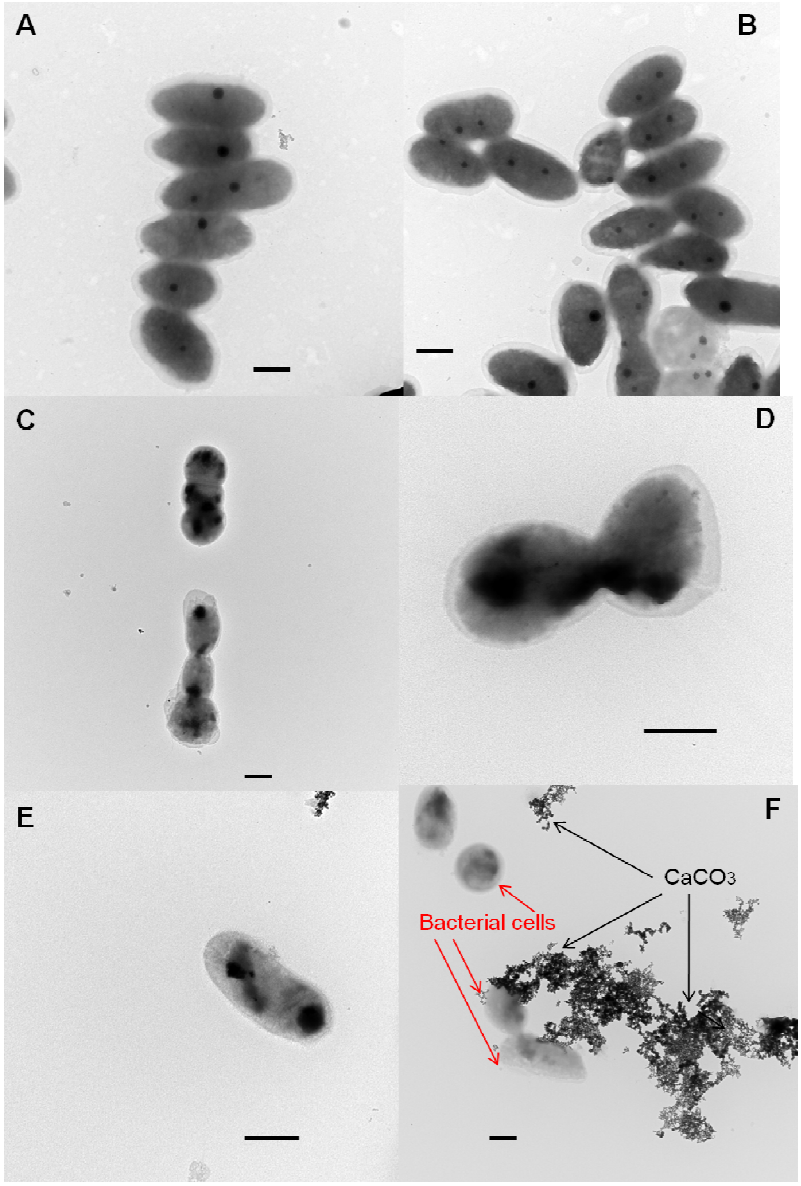


**Fig. II. 16. TEM images (microscope JEOL JEM 12000 EX) of active A-20s (A,B), S-17-65 (C,D) and *Gloeocapsa* sp. (E,F) in nutrient ($CaCO_3$-free) solution (A,C,E) and media supersaturated with respect to calcite (B,D,F). Initial experimental conditions: experiments with APB (B, D) 10 mM $CaCl_2$, 10 mM $NaHCO_3$; experiment with *Gloeocapsa* sp. (F): 1 mM $CaCl_2$, 10 mM $NaHCO_3$). The black scale bars are 500 nm.**

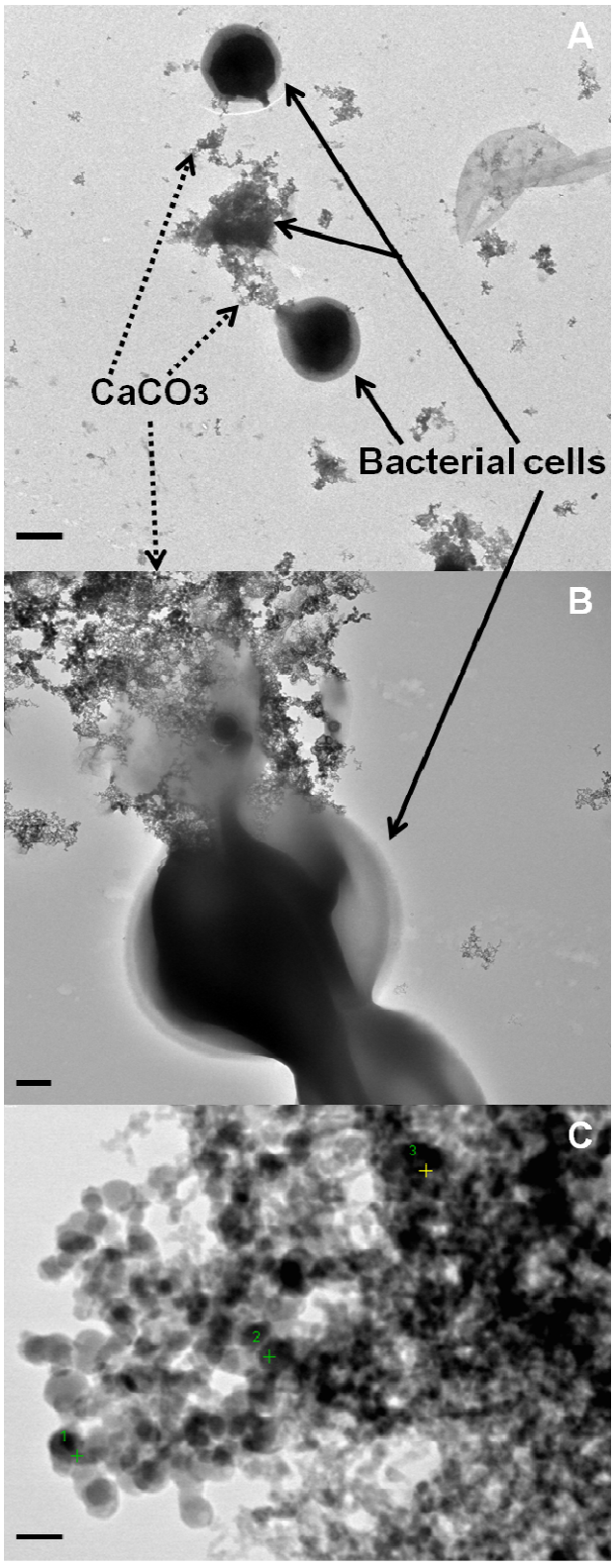


**Fig. II. 17. TEM images (microscope JEOL JEM 2100F) of active Gloeocapsa sp. with $CaCO_3$ around the cells (A,B) and the crystals of calcite formed around bacterial cells (C) in nutrient media supersaturated with respect to calcite (initial experimental conditions: 1 mM $CaCl_2$, 10 mM $NaHCO_3$). The black scale bars are (A) 2 µm; (B) 0.5 µm; (C) 0.1 µm.**

# Chapter III

# Zeta-potential of anoxygenic phototrophic bacteria and Ca adsorption at the cell surface

# Résumé en français

Des mesures de mobilité électrophorétiques et d'adsorption de Ca ont été réalisées sur la surface des cellules de bactéries anoxygéniques phototrophiques (A-20S et S-17-65) vivantes, inactivées et mortes afin de déterminer la manière dont ces bactéries contrôlent leur potentiel de surface. Le potentiel Zeta de ces deux bactéries a été mesuré en fonction du pH, de la force ionique, et des concentrations en calcium et bicarbonate.

Pour des APB vivantes dans une solution de NaCl à 0.1mol.$L^{-1}$, le potentiel Zeta est proche de 0 pour des pH de 2.5 à 3 et diminue jusqu'à -30mV à -40mV dans une gamme de pH comprise entre 5 et 8. En milieu alcalin, on note une augmentation inhabituelle du potentiel Zeta avec des valeurs maximales de -10mV à -20mV pour des pH de 9 à 10.5. Cette augmentation est cependant atténuée lors de l'ajout de $NaHCO_3$ (jusqu'à 10 mmol.$L^{-1}$) mais très peu affectée par l'addition d'une quantité équivalente de Ca. A l'inverse, pour les cellules de bactéries inactivées (exposées à $NaN_3$, un inhibiteur métabolique) et mortes (par le biais d'une forte chaleur), le potentiel Zeta reste stable (-30mV à -60mV en fonction de la force ionique) entre pH 5 et 11, et aucune augmentation n'est rapportée dans des solutions alcalines. L'adsorption de Ca à la surface des cellules A-20s est plus significative qu'à la surface de S-17-65, et démarre à pH plus acide, ce qui est en accord avec les mesures de potentiel Zeta en présence de 0.001 à 0.01 mol.$L^{-1}$ de $CaCl_2$. D'une manière générale, ces résultats indiquent que les APB peuvent contrôler, par le biais de leur métabolisme, leur potentiel Zeta afin d'attirer de manière électrostatique les nutriments à pH alcalin tout en rejetant/évitant les ions Ca qui sont susceptibles d'entrainer la précipitation de $CaCO_3$ au sein de la cellule et à sa surface, causant des phénomènes d'incrustation.

Par analogie avec d'autres bactéries, deux mécanismes peuvent être suggérés pour expliquer cette augmentation inhabituelle du potentiel Zeta (moins négatif) des bactéries anoxygéniques phototrophiques dans les solutions alcalines: *i)* augmentation de la consommation de micronutriments sous la forme d'anions et *ii)* refoulement des ions $Ca^{2+}$ de la surface des cellules dans le but de les protéger d'une incrustation de précipités de $CaCO_3$. Ce dernier mécanisme est en accord avec les résultats d'adsorption du Ca à la surface des cellules obtenus dans la gamme des compositions physiologiques de la solution. Une légère différence du degré d'augmentation du potentiel Zeta et d'adsorption du Ca entre les deux souches de bactéries étudiées est compatible avec les différences de tailles des surfaces et les gammes physiologiquement optimales de la solution.

Les détails et résultats de cette étude sont présentés dans la section suivante sous forme d'un article sous presse dans *Journal of Colloid and Interface Science*.

Journal of Colloid and Interface Science xxx (2011) xxx–xxx

Contents lists available at ScienceDirect

Journal of Colloid and Interface Science

www.elsevier.com/locate/jcis

# Zeta potential of anoxygenic phototrophic bacteria and Ca adsorption at the cell surface: Possible implications for cell protection from $CaCO_3$ precipitation in alkaline solutions

Irina A. Bundeleva [a], Liudmila S. Shirokova [a,b], Pascale Bénézeth [a], Oleg S. Pokrovsky [a,*], Elena I. Kompantseva [c], Stephanie Balor [d]

[a] Géosciences Environnement Toulouse, GET, Université de Toulouse, CNRS-IRD-OMP, 14 Avenue Edouard Belin, 31400 Toulouse, France
[b] Institute of Ecological Problems of the Northern Regions, Russian Academy of Science, 29 Naberezhnaja Sev. Dviny, Arkhangelsk, Russia
[c] Winogradsky Institute of Microbiology, Russian Academy of Sciences, Moscow, Russia
[d] Plateau de Microscopie électronique, FRBT CNRS FR3451, Bat. IBCG, 118 Route de Narbonne, F-31062 Toulouse, France

ARTICLE INFO

*Article history:*
Received 7 February 2011
Accepted 9 April 2011
Available online xxxx

*Keywords:*
Anoxygenic phototrophic bacteria
*Rhodovulum* sp.
Electrophoresis
Zeta potential
Calcium
Bicarbonate
Adsorption
Calcite

ABSTRACT

Electrophoretic mobility measurements and surface adsorption of Ca on living, inactivated, and heat-killed haloalkaliphilic *Rhodovulum steppense*, A-20s, and halophilic *Rhodovulum* sp., S-17-65 anoxygenic phototrophic bacteria (APB) cell surfaces were performed to determine the degree to which these bacteria metabolically control their surface potential equilibria. Zeta potential of both species was measured as a function of pH and ionic strength, calcium and bicarbonate concentrations. For both live APB in 0.1 M NaCl, the zeta potential is close to zero at pH from 2.5 to 3 and decreases to −30 to −40 mV at pH of 5–8. In alkaline solutions, there is an unusual increase of zeta potential with a maximum value of −10 to −20 mV at a pH of 9–10.5. This increase of zeta potential in alkaline solutions is reduced by the presence of $NaHCO_3$ (up to 10 mM) and only slightly affected by the addition of equivalent amount of Ca. At the same time, for inactivated (exposure to $NaN_3$, a metabolic inhibitor) and heat-killed bacteria cells, the zeta potential was found to be stable (−30 to −60 mV, depending upon the ionic strength) between pH 5 and 11 without any increase in alkaline solutions. Adsorption of Ca ions on A-20s cells surface was more significant than that on S-17-65 cells and started at more acidic pHs, consistent with zeta potential measurements in the presence of 0.001–0.01 mol/L $CaCl_2$. Overall, these results indicate that APB can metabolically control their surface potential to electrostatically attract nutrients at alkaline pH, while rejecting/avoiding Ca ions to prevent $CaCO_3$ precipitation in the vicinity of cell surface and thus, cell incrustation.



## 1. Introduction

The composition and structure of bacterial surface are responsible for important processes such as biomineralization, bacterial adhesion, and biofilm formation [1]. The cell surface contains various functional groups such as carboxylate, phosphate, hydroxylate and amino moieties, which are deprotonized as a function of environmental pH [2,3], thereby conferring negative electrostatic charge to the cell periphery [4], notably at physiological pH values.

Microelectrophoresis is a powerful technique for characterizing the electric double layer of microbial cell surfaces [4–19]. The main advantages of this technique, compared to more commonly used surface titrations, is that (1) it provides straightforward information about the sign and the magnitude of cell surface electrostatic potential at the shear plane without specific assumptions and postulates; (2) it is almost instantaneous, capable of measuring zeta potential within several minutes after the preparation of suspension and without requiring specific stability criteria, unlike the surface titration [20]; (3) it can probe surface potential in extreme solution conditions (pH < 3 and >9, high carbonate concentration where the surface titration is not possible) and (4) principles of measurements are very similar among different apparatus so that the results of various studies are directly comparable [21–23].

Among various groups of microorganisms, heterotrophic bacteria, algae and cyanobacteria were extensively studied using microelectrophoresis techniques in the context of metal adsorption, biomineralization, and biofilm formation [11,14,16–19,24–26]. These observations allowed comprehensive understanding of surface electrokinetic properties of most bacterial groups in a wide range of pH and ionic strength [27].

* Corresponding author.
*E-mail address:* oleg@get.obs-mip.fr (O.S. Pokrovsky).

0021-9797/$ - see front matter © 2011 Elsevier Inc. All rights reserved.
doi:10.1016/j.jcis.2011.04.033

YJCIS 16813
25 April 2011
ARTICLE IN PRESS
No. of Pages 11, Model 5G



Most microorganisms exhibit negative electrophoretic mobilities (zeta potential) at pH > 2 [13,28], which is most likely linked to the dominance of negatively charged carboxylate groups of the cell wall and sulfate of the extracellular polysaccharides attached to the cells surface in the form of compact capsules or diffuse slime layers. Because at pH above the $pK_a$ of most organic acids the cell surface functional groups are fully or partially deprotonated, it is very unlikely that cell surface potential becomes less negative with pH increase. Recently, however, an unusual phenomenon of less negative or even positive zeta potential of cyanobacteria in alkaline solutions (pH ~9–10) has been reported [16]. It was tentatively related to the physiological status of cyanobacterial cells that need to acquire bicarbonate ions ($HCO_3^-$) for photosynthesis. At the same time, active cyanobacteria apparently protect themselves from Ca carbonate precipitation and Ca adsorption at the surface by creating a positive surface potential at the pH of photosynthesis [29]. The acidification of cell surface environment and the generation of net positive charge in the course of carbonate precipitation and photosynthesis were also suggested in earlier studies [30,31].

However a question remains, in particular how far these mechanisms can be extended to other non-oxygenic photosynthesizing microorganisms notably those that use organic carbon sources but not $CO_2$/$HCO_3^-$ yet precipitating $CaCO_3$ in the vicinity of the cells. In this regard, anoxygenic phototrophic bacteria (APB) are especially interesting because, at the conditions of our experiments they use acetate and other organic substances for organic matter production during photosynthesis [32,33]. At the same time, these bacteria do participate in $CaCO_3$ precipitation in alkaline lakes and are often considered to be linked to Archean and Palaeoproterozoic carbonate stromatolite formation [34]. As such, they should also be able to protect their surfaces against incrustation by $CaCO_3$.

Therefore, we measured the zeta potential and Ca ion adsorption onto active, inactivated, and dead cells surfaces of two typical but contrasting species of anoxygenic phototrophic bacteria (APB): haloalkaliphilic *Rhodovulum steppense*, A-20s and neutrophilic halophilic *Rhodovulum sp.*, S-17-65 in order to check the existence of positive surface potential in alkaline solutions and try to link it to Ca and bicarbonate adsorption as a function of pH and ionic strength.

## 2. Materials and methods

### 2.1. Anoxygenic phototrophic bacteria (APB) cultures

Two distinct anoxygenic phototrophic bacteria (APB) were used in this study: recently described species *R. steppense* A-20s (hereafter referred to as A-20s) and strain *Rhodovulum sp.* S-17–65 (hereafter referred to as S-17–65), which, according to genotypic and phenotypic characteristics, must be assigned to a new species of the genus *Rhodovulum*. Obligatory haloalcaliphilic A-20s (optimal growth conditions are 1–5% NaCl and pH of 8.5) was isolated from steppe soda lake (Transbaikal region, Russia) in southern Siberia [33]. The halophilic (growth range 5–25% NaCl with optimum at 12%) neutrophilic S-17-65 was extracted from hypersaline water body in the Crimea steppe [35]. Natural environment of these APB is as follow: pH = 9.5, Dissolved Inorganic Carbon (DIC) = 0.1 - mol/L, salinity = 4%, $T$ = 23–30 °C for A-20s [36] and pH = 7–8, DIC = 0.01 mol/L, salinity = 20 % and $T$ = 25–35 °C for S-17-65 [35]. The optimal environmental conditions (salinity, $HCO_3^-$ and $O_2$-concentration) for alkaliphilic *R. steppense* A-20s and halophilic *Rhodovulum* sp. S-17-65 are quite different.

Both APB were cultured in Pfenning's growth medium of the following composition [37] : $KH_2PO_4$ (330 mg/L), $MgCl_2{\cdot}6H_2O$ (330 mg/L), $NH_4Cl$ (330 mg/L), KCl (330 mg/L), $Na_2SO_4$ (330 mg/L), $CaCl_2$ (50 mg/L), $NaHCO_3$ (5 g/L for A-20s, 0.5 g/L for S-17-65), NaCl (25 g/L for A-20s , 120 g/L for S-17-65), sodium acetate (1 g/L), casamino acids (0.1 g/L), yeast extract (0.1 g/L), $B_{12}$ (20 μg/L), and trace elements solution (1 ml/L [37]). For S-17-65, $Na_2S$ (0.1 g/L) and cysteine (0.3 g/L) were added as a source of sulfur. Stock cultures of bacteria were kept in sealed glass bottles in oxygen-free conditions at 23–30 °C, under constant 2000 lx light [33], and placed on a rotator shaker at 11 rpm to grow till the stationary stage (5–7 days). The overall growth rate was very similar between two cultures in a wide range of pH and [DIC]. Studied anoxygenic phototrophic bacteria do not use dissolved $CO_2$ and $HCO_3^-$ during photosynthesis in the presence of organic substrate. This was proven by quite stable (±10%) DIC concentration during bacterial growth experiments which produced 15–20 $g_{wet}$/L biomass. However, photolithoautotrophic growth of both strains is possible with sulfide as electron donor on organic-free media.

### 2.2. Preparation of cells

For zeta potential measurements, cell suspensions of metabolically active, inactive ($NaN_3$-treated), and dead (autoclaved) A-20s or S-17-65 were prepared in 0.01, 0.1 and 0.5 mol/L aqueous NaCl solutions, with typical cell concentrations of 10 $mg_{wet}$/L. Note that the conversion factors of wet to dry (lyophilized) weight applied for studied microorganisms and for adsorption measurements were equal to 11.7 and 16.1 for A-20s and S-17-65, respectively. The cultures were harvested at the late exponential – stationary growth stage by centrifugation at 10,000 rpm (7000 g) for 10 min at 20 °C. The cells were rinsed in 0.1 mol/L NaCl corresponding to optimal physiological conditions and centrifuged twice at 10,000 rpm for 10 min. Finally, bacterial suspension was washed in appropriate electrolyte solution and centrifuged. Resulting bacterial suspension was equilibrated for 1–1.5 h in the specific electrolyte solution (0.01, 0.1 or 0.5 mol/L NaCl) at pH 7–8 prior to zeta potential measurements at variable pHs. Average equilibration time of bacterial suspension at a given pH was between 3 and 5 min, and no pH drift was observed during electrophoretic measurements. The cell integrity was maintained during experiments in acidic (pH < 4) and alkaline (pH > 10) solutions, as verified by optical microscopic examination. Additional zeta potentials were recorded for active bacterial cells after they were equilibrated for 1 h in the presence of 1.0 and 10 mmol/L $NaHCO_3$ or 1.0 and 10 mmol/L $CaCl_2$. Electrophoretic measurements were also performed in the dark using bacteria that were previously kept for 24 h in complete darkness. Keeping the bacteria in the dark during 24 h, comparable with cell division time, and maintaining the full darkness condition during the measurement were intended to insure that the light phase of photosynthesis is completely absent.

Dead (heat-killed) cells were prepared by autoclaving part of the fresh stock of biomass at 121 °C for 20 min and performing the rinsing procedure as described above for live cells. Although the heat-killing procedure can significantly modify the cell surface structure, it still remains a widely used method for producing control alive material [16,17,38,39]. Moreover, optical microscopic examination showed that heat-killed cells maintained their integrity and shape after heat treatment.

Inactivated cells were prepared by rinsing part of the fresh (live) biomass in 0.01 mol/L $NaN_3$ during 1–2 h. Sodium azide suppresses bacterial activity by inhibiting cytochrome oxidase and is widely used for inactivating cells while keeping the surfaces physically and chemically intact [40–42]. Cell growth of both cultures in the presence of 0.01 M $NaN_3$ in nutrient solution was completely suppressed as proven in separate series of experiments.



Please cite this article in press as: I.A. Bundeleva et al., J. Colloid Interface Sci. (2011), doi:10.1016/j.jcis.2011.04.033

### 2.3. Microelectrophoresis

Zeta potentials of APB cells were measured in a quartz cell placed between two Pd electrode chambers, using a CAD Instrument "Zetaphoremeter IV" Z 4000. The cells were illuminated by a 2 mW He/Ne laser. During the measurements an electric field of 80 V $cm^{-1}$ was applied in each direction for 20 s and the images of moving cells were transmitted to a computer via a CCD camera. Measurements were performed at pH ranging from 2.5 to 11.0 with a pH resolution of 0.4 units. To avoid atmospheric $CO_2$ consumption and $CaCO_3$ supersaturation in $CaCl_2$ solutions at pH above 8.0, $N_2$ gas was bubbled through cell suspension prior and during the measurements.

The pH of these suspensions was increased manually by adding 2–10 μL aliquots of 0.01–1 mol/L NaOH or 0.01–1 mol/L HCl. Three replicates were carried out and each was performed with a renewed bacteria suspension in the measurement chamber. The uncertainty of zeta potential measurements was around 10%. Electrophoretic mobilities were converted to zeta potentials using the Smoluchowski–Helmholtz equation [43]:

$$\zeta = \frac{(\varepsilon \times \mu_E)}{\eta}$$

where $\zeta$ stands for the zeta potential (mV) and $\varepsilon$, $\eta$ and $\mu_E$ represent the dielectric constant of the solution, the viscosity and the electrophoretic mobility, respectively ($\mu_E = V_E/E$ with $V_E$ = electrophoretic rate ($s^{-1}$) and $E$ = electric field (V $m^{-1}$)). In the CAD Instrument of IV-th generation, ionic strength (I) is approximated from the conductivity which is routinely recorded. The change of viscosity originated from other than I source is very unlikely, given quite low concentration of DOC during in bacterial suspensions (less than 10 ppm, see Section 4). Despite its simplicity, Smoluchowski's equation is widely used for calculating zeta potentials from the electrophoretic mobilities of quartz [21], silica [44] diatoms [14] and cyanobacteria [17] and biological materials [4,10].

### 2.4. Ca adsorption on cell surfaces

The calcium adsorption experiments were designed to provide a quantitative characterization of metal binding by bacterial cells in a wide range of pH and $Ca^{2+}$ concentrations in solution. For this, two types of experiments were carried out: (i) adsorption at constant initial calcium concentration in solution as a function of pH (pH-dependent adsorption edge) and (ii) adsorption at constant pH as a function of metal concentration in solution (adsorption isotherm). All experiments were performed in undersaturated solutions with respect to any calcium carbonate phase as verified by speciation calculations with the MINTEQA2 computer code and corresponding database [45,46].

The initial calcium concentration was 17 μmol/L at variable pH and varied between 0.1 and 800 μmol/L at constant pH. The pH was adjusted by adding aliquots of NaOH (0.1 and 0.01 mol/L) or HCl (1.0, 0.1 and 0.01 mol/L), whereas, constant pH of 5.5 and 6.7 was maintained by adding 0.005 mol/L MES (2-morpholinoethanesulfonic acid monohydrate) buffer. Adsorption experiments were conducted in 8 mL sterile polypropylene vials during 3 and 24 h at 25 ± 0.2 °C, in continuously agitated bacteria suspension with an ionic strength of 0.1 mol/L NaCl. The biomass concentration was kept constant at 10 $g_{wet}$/L. Live, freshly harvested (stationary stage) cells, sodium azide-inactivated and heat-killed (autoclaved) bacteria were used in the adsorption experiments. The cells were rinsed in 0.1 mol/L NaCl and 0.01 mol/L EDTA solutions for 15 min and again in 0.1 mol/L NaCl solution prior the experiments. This procedure allowed desorption of all possible $Mg^{2+}$, $Ca^{2+}$ ions from the cell's surfaces that might occurred during the APB culture.

The adsorption of calcium on cell surfaces was quantified by subtracting, at each solution pH, the concentration of calcium remaining in bacterial suspension from the concentration of calcium added in the supernatant. The adsorption of calcium on reactor walls and cellular Ca release from the biomass in the full range of studied pH was negligible (<10%) compared to the initial amount of Ca added. This was routinely verified by Ca analyses in the supernatant and in the zero-added-Ca cell suspension experiments. Nonetheless, the measured Ca concentrations in these blank experiments (to the limit of detection) were explicitly taken into account to calculate the adsorption isotherm.

All filtered solutions were analyzed for aqueous Ca concentration using flame atomic absorption spectroscopy (Perkin Elmer AAnalyst 400) with an uncertainty of ±2% and a detection limit of 0.5 μmol/L. Dissolved organic carbon (DOC) was analyzed using a Carbon Total Analyzer (Shimadzu SCN) with an uncertainty of 3% and a detection limit of 0.1 mg/L. The DOC concentration during adsorption and electrophoretic measurements remained quite low, between 5 and 10 mg/L and did not vary with pH and ionic strength in any systematic manner, suggesting negligible cell lysis and degradation in the full range of studied solution conditions.

### 2.5. Transmission Electron Microscopy (TEM) analysis

Aliquots of suspensions containing live bacterial cultures were examined using Transmission Electron Microscopy (TEM) with a JEOL JEM 12000 EX and JEOL JEM 2100F (equipped with a field emission gum (FEG) and PGT EDX detector) at 80 kV. The shift of C and O peaks towards low energies due to the non-linearity of the EDX detector of low energy. Cell suspension was rinsed using sterile nutrient solution (without sodium chloride addition) or MilliQ water, centrifuged 2 min at 10 000 rpm. TEM samples for analyses were taken by immersing grids coated with a carbon film for 10 s in prepared bacterial suspension. Dried grids were used for TEM analysis.

## 3. Results

### 3.1. Electrophoresis

The zeta potential of live, $NaN_3$-inactivated and dead (heat-killed) cells of the two APB bacteria was measured as a function of pH and ionic strength, whereas zeta potential of live cells was also measured as a function of calcium and bicarbonate ion concentrations, with and without light. Note that experiments with calcium and bicarbonate addition and experiments in the darkness were not performed for inactivated/heat-treated cells because in contrast to live cultures, dead and inactivated APB cells do not display any maxima of zeta potential in alkaline solutions (see below). The condition of electrophoretic experiments are presented in Table 1.

#### 3.1.1. Effect of pH and ionic strength

The zeta potentials of live A-20s and S-17-65 cultures in 0.5, 0.1, 0.01 mol/L NaCl are shown as a function of pH in Fig. 1a and b.

It can be seen from these figures that the magnitude of zeta potential decreases yielding less negative values with increasing ionic strength, from pH 4 to 10. The pH of isoelectric point ($pH_{IEP}$) is close or below 3 for A-20s and below 2 for S-17–65. However, it cannot be determined precisely because there is no common intersection point of zeta potential curves obtained at various ionic strengths. Moreover, it can be observed for both species, and specifically in physiologically favorable 0.1 mol/L NaCl, a decrease in zeta potential between pH 2 and 5, a rather constant value for 5 < pH < 8 and an increase for pH above 8–9. This pattern is also

Please cite this article in press as: I.A. Bundeleva et al., J. Colloid Interface Sci. (2011), doi:10.1016/j.jcis.2011.04.033

YJCIS 16813
25 April 2011
ARTICLE IN PRESS
No. of Pages 11, Model 5G



**Table 1**
Experimental conditions of zeta potential measurements. All experiments performed under light unless indicated ([*]).

| Bacteria | State of bacteria | Composition of solution | pH range |
|---|---|---|---|
| A-20s | Live | 0.5 M NaCl | 3.0–11.0 |
| A-20s | Azide-treated | 0.5 M NaCl | 3.1–11.0 |
| A-20s | Dead | 0.5 M NaCl | 3.0–11.0 |
| A-20s | Live | 0.1 M NaCl | 2.8–11.0 |
| A-20s | Azide-treated | 0.1 M NaCl | 2.8–11.1 |
| A-20s | Dead | 0.1 M NaCl | 3.0–10.9 |
| A-20s | Live | 0.01 M NaCl | 2.8–10.8 |
| A-20s | Azide-treated | 0.01 M NaCl | 3.1–11.0 |
| A-20s | Dead | 0.01 M NaCl | 2.9–11.4 |
| A-20s | Live | 0.1 M NaCl + 0.001 M $NaHCO_3$ | 7.0–11.0 |
| A-20s | Live | 0.1 M NaCl + 0.01 M $NaHCO_3$ | 7.1–11.0 |
| A-20s | Live | 0.1 M NaCl + 0.001 M $CaCl_2$ | 3.1–10.9 |
| A-20s | Live | 0.1 M NaCl + 0.01 M $CaCl_2$ | 2.9–11.0 |
| A-20s* | Live | 0.1 M NaCl | 3.8–11.1 |
| S-17-65 | Live | 0.5 M NaCl | 2.4–10.8 |
| S-17-65 | Azide-treated | 0.5 M NaCl | 3.1–11.1 |
| S-17-65 | Dead | 0.5 M NaCl | 2.8–11.0 |
| S-17-65 | Live | 0.1 M NaCl | 3.1–11.0 |
| S-17-65 | Azide-treated | 0.1 M NaCl | 3.2–11.3 |
| S-17-65 | Dead | 0.1 M NaCl | 3.2–10.8 |
| S-17-65 | Live | 0.01 M NaCl | 3.1–10.9 |
| S-17-65 | Azide-treated | 0.01 M NaCl | 2.7–11.1 |
| S-17-65 | Dead | 0.01 M NaCl | 2.8–11.1 |
| S-17-65 | Live | 0.1 M NaCl + 0.001 M $NaHCO_3$ | 7.5–11.0 |
| S-17-65 | Live | 0.1 M NaCl + 0.01 M $NaHCO_3$ | 7.3–11.0 |
| S-17-65 | Live | 0.1 M NaCl + 0.001 M $CaCl_2$ | 3.0–11.0 |
| S-17-65 | Live | 0.1 M NaCl + 0.01 M $CaCl_2$ | 2.8–11.0 |

[*] Experiment and measurements were performed in complete darkness.

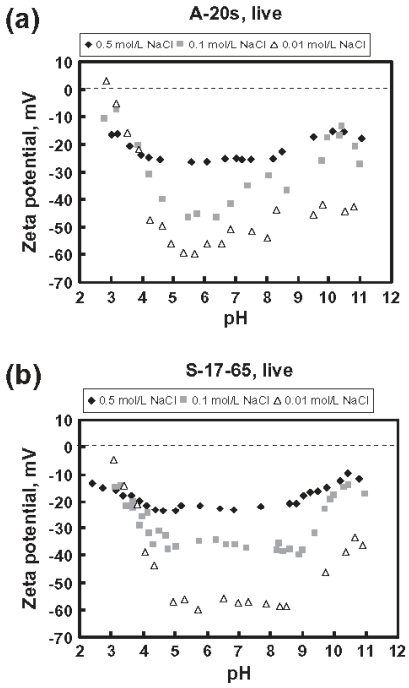


**Fig. 1.** Measured zeta potential of live A-20s (a) and S-17-65 (b) as a function of pH (2–11) and ionic strength at 10 $mg_{wet}$ biomass/L. The error bars are within the symbol size.

maintained in 0.01 M NaCl but becomes less pronounced at higher ionic strength. Indeed, in 0.5 M NaCl zeta potential of both species is similar for active, $NaN_3$-inactivated and heat-killed cells, as shown in Fig. 2a and b. In this solution, there is a slight increase

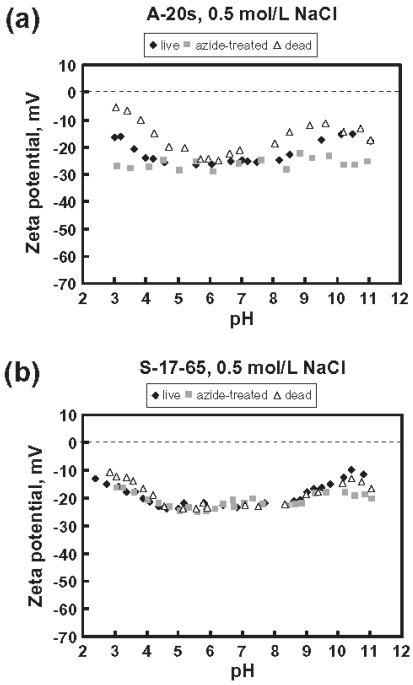


**Fig. 2.** Measured zeta potential of A-20s (a) and S-17-65 (b) as a function of pH (2–11) and 0.5 M NaCl at 10 $mg_{wet}$ biomass/L. The error bars are within the symbol size.

of zeta potential at pH > 8.5–9, especially pronounced for live S-17-65.

The effect of cell status (live, heat-killed and $NaN_3$-inactivated) on zeta potential in 0.1 M NaCl is shown in Fig. 3.

At lower ionic strength, the zeta potential of both living cells increases at pH > 9–10 exhibiting a local maximum at around ~[−10; −20] mV in these alkaline solutions, especially pronounced in 0.1 mol/L NaCl (Fig. 3a and c). This maximum is also visible in 0.01 mol/L NaCl, although the magnitude of zeta potential is lower than that at $I = 0.1$, i.e., ~[−30; −40] mV (Fig. 3b and d). On the other hand, dead (heat-killed) and $NaN_3$-inactivated cells show a decrease of the zeta potential till pH 4.5 and almost constant value above that pH (Fig. 3a–d). More importantly and in contrast to live cultures, dead and inactivated APB cells do not display any increase of zeta potential at pH around 10 both in 0.01 and 0.1 mol/L NaCl solutions (Fig. 3a–d). Note also that dead bacteria exhibit approximately 10–20 mV less negative zeta potential values in neutral solutions and a clear $pH_{IEP}$ of 3.5 ± 0.1 at 0.01 mol/L NaCl for both bacterial cultures (Fig. 3b and d).

### 3.1.2. Effect of Ca and bicarbonate ions

Zeta potential of live A-20s and S-17-65 were measured in the presence or absence of $CaCl_2$ and $NaHCO_3$ at fixed total ionic strength which was achieved by varying the concentration of NaCl added in the solution. The values of zeta potential for both bacteria with and without $CaCl_2$ at most environmentally relevant $I = 0.1$ mol/L are reported in Fig. 4. For A-20s (Fig. 4a), the decrease of zeta potential at pH 5–7 is much smaller in the presence of 0.001 and 0.01 mol/L $CaCl_2$ compared to Ca-free solutions, with almost 20 mV difference at pH around 6. It can be also seen that the addition of $Ca^{2+}$ ions only slightly modifies the position of zeta potential maximum occurring at pH around 10.

Please cite this article in press as: I.A. Bundeleva et al., J. Colloid Interface Sci. (2011), doi:10.1016/j.jcis.2011.04.033

YJCIS 16813
25 April 2011
ARTICLE IN PRESS
No. of Pages 11, Model 5G



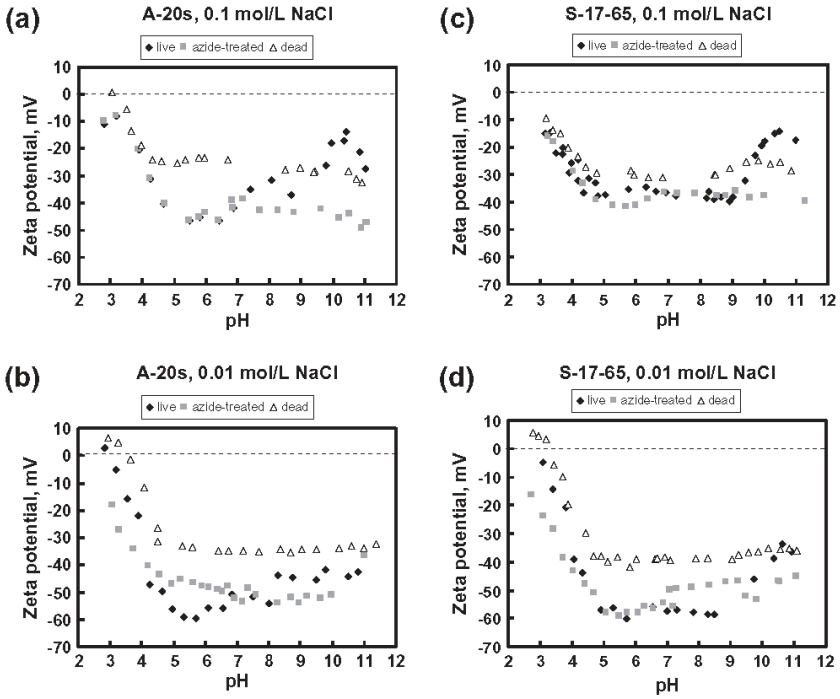


**Fig. 3.** Measured zeta potential of A-20s and S-17-65 in 0.1 M (a and c) and 0.01 M (b and d) NaCl, respectively, and as a function of pH (2–11) at 10 $mg_{wet}$ biomass/L. The error bars are within the symbol size.

In contrast, for S-17-65 (Fig. 4b), the presence of 0.01 mol/L $CaCl_2$ does not modify zeta potential compared to Ca-free solutions up to pH of 7.5, whereas addition of lower concentrations (c.a., 0.001 mol/L $CaCl_2$) decrease zeta potential in the pH range 4–7 as well as above pH 10. At pH between 8 and 10 the zeta potential increases in the presence of $Ca^{2+}$ ions. Noteworthy that, in contrast to Ca-free solutions, there is no clear decrease of zeta potential at pH above 10.5–11 in the presence of 0.01 mol/L $CaCl_2$. Overall, the modification of zeta potential in the presence of $CaCl_2$ suggests the adsorption of Ca ions on APB surface which occur at different pH and in different degree for two studied cultures.

The addition of 0.001–0.01 mol/L sodium bicarbonate ($NaHCO_3$) decreases significantly the zeta potential values of living A-20s and S-17-65 cells, as illustrated in Fig. 5a and b, respectively. Two important features can be observed from these two figures. First, at pH of 7–9, there is a ~20 and ~10 mV potential decrease for A-20s and S-17-65, respectively. Second, at pH above 9, there is a net decrease of zeta potential in the presence of both $NaHCO_3$ concentrations and for both bacteria. However, for A-20s there is no complete suppression of zeta potential increase in alkaline solutions (pH 9–11) in the presence of added bicarbonate (Fig. 5a). In contrast, there is a full suppression of zeta potential increase in the presence of 0.01 M $NaHCO_3$ for S-17-65 (Fig. 5b).

### 3.1.3. Effect of light

The results of zeta potential measurements for live bacteria under the light and in complete darkness are shown in Fig. 6, with lower values in darkness compared to values obtained under light at $6 \leqslant pH \leqslant 9$. Concurrently, the shape and magnitude of zeta potential at pH above 9 do not depend on the cell environment: both experiments demonstrate a maximum of zeta potential (−15 mV) at pH around 10–10.5. We interpret the less negative potential in circum-neutral solutions ($6 \leqslant pH < 9$) as due to the generation of protons similar to what is reported for cyanobacteria during the oxygenic stage of the photosynthesis [31]. In contrast, the zeta potential increase to less negative values at pH above 9 observed with and without light apparently represents an intrinsic property of live APB cultures in alkaline solutions, not necessarily linked to the photosynthesis.

## 3.2. Ca adsorption

The pH-dependent adsorption edge for both APB cells, performed in 0.1 mol/L NaCl and with a biomass of 10 $g_{wet}$/L exposed for 3 h in the dark, is illustrated in Fig. 7.

At the same pH and initial Ca concentration ($[Ca^{2+}]_o$ = 17 μmol/L), the percentage of adsorbed Ca was always higher in experiments with A-20s compared to S-17-65. For the latter, the adsorption edge starts at pH around 5, whereas A-20s demonstrated significant Ca adsorption at pH 3 with a maximum of adsorption edge attained at pH = 7–8. Kinetic factors are unlikely to control the adsorption yield as demonstrated by the use of Fig. 8. Reported in this figure is the adsorption edge for S-17-65 (as an example) measured at different exposure time. It can be clearly seen that there is no significant difference in the percentage of adsorbed Ca for 3 and 24 h of exposure time.

"Langmuirian" adsorption isotherms recorded for both live APB species at three constant pHs (5.5, 5.9 and 6.7) and Ca concentrations from 1 to 800 μmol/L are illustrated in Fig. 9.

Similar to pH-dependent adsorption edge, the adsorption of calcium at constant pH and $[Ca^{2+}]_{aq} \leqslant 100$ μmol/L is higher for the A-20s culture compared to the S-17-65 one. At higher aqueous Ca concentrations, from 200 to 800 μmol/L, there is no significant difference between two cultures in the adsorption maximum (~20–30 μmol $Ca/g_{wet}$). The slopes of dependence between $[Ca^{2+}]_{ads}$ and $[Ca^{2+}]_{aq}$ in 0.1 mol/L NaCl deduced from this figure

Please cite this article in press as: I.A. Bundeleva et al., J. Colloid Interface Sci. (2011), doi:10.1016/j.jcis.2011.04.033

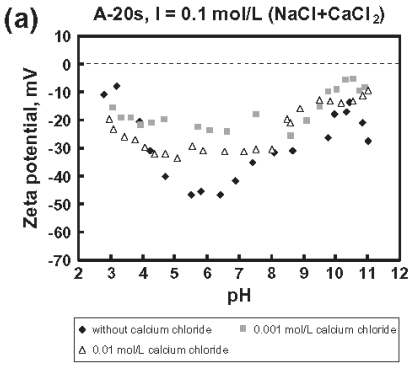


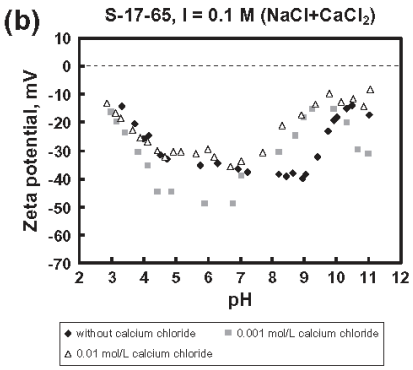


**Fig. 4.** Measured zeta potential of live A-20s (a) and S-17-65 (b) at $I = 0.1$ M in the presence of $CaCl_2$ at 10 $mg_{wet}$ biomass/L. The error bars are within the symbol size.

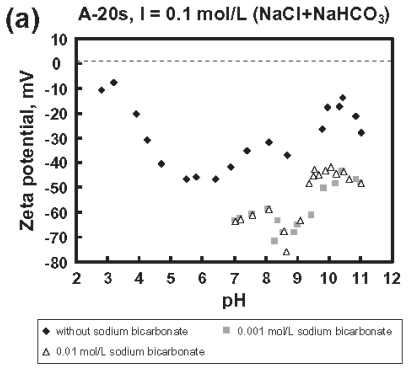


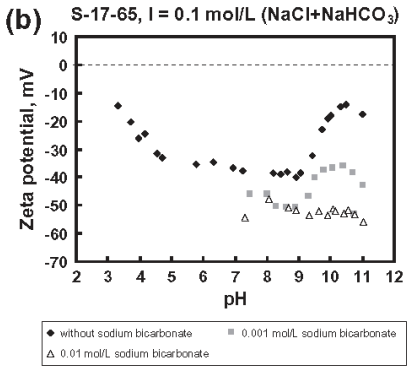


**Fig. 5.** Measured zeta potential of live A-20s (a) and S-17-65 (b) at $I = 0.1$ M in the presence of $NaHCO_3$ at 10 $mg_{wet}$ biomass/L. The error bars are within the symbol size.

is close to 1 for both cultures, indicating a stoichiometric ratio of surface site to aqueous calcium ion. However, at lower $[Ca^{2+}]_{aq}$ (<10–20 μmol/L) the slope of this dependence for A-20s culture is close to 0.7 suggesting some change in the stoichiometry of surface adsorption reaction. Note the similarity of "Langmuirian" adsorption isotherms for A-20s strain at pH 6.70 and 5.55. This may stem from the fact that above pH 5.5, from 70% to 80% of Ca are already adsorbed at the cell wall (Fig. 7). As such the effect of pH at these conditions is of second order importance in controlling the overall adsorption yield.

Comparison of Ca adsorption by live and $NaN_3$-inactivated A-20s cells was performed at pH around 7 in 0.1 mol/L NaCl (Fig. 10). In both types of cells, continuous illumination was provided and the exposure time was around 20 h. It can be seen from Fig. 10 that there is no major difference in the concentration of adsorbed Ca between live and inactivated cultures at high surface loading, whereas at low surface loading, in the environmentally-relevant Ca concentration range, at $[Ca^{2+}]_{aq} < 100$ μM and $[Ca^{2+}]_{ads} < 5$ μmol/$g_{wet}$, there is a systematically higher adsorption of Ca on the inactivated cells compared to the live cultures.

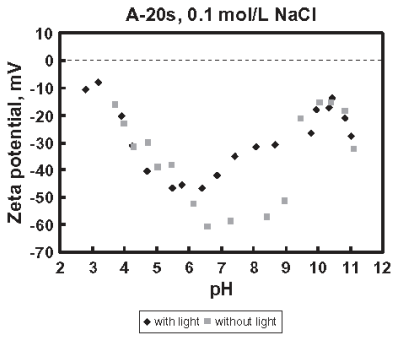


**Fig. 6.** Measured zeta potential of live A-20s in 0.1 M NaCl in the presence of light and in the darkness at 10 $mg_{wet}$ biomass/L. Results for measurements in the darkness were obtained on cultures that were kept without light during 24 h prior the experiments. The error bars are within the symbol size.

## 4. Discussion

### 4.1. Effect of ionic strength and pH on zeta potential

Both APB species demonstrate classical zeta potential dependence on ionic strength: a decrease of the magnitude of negative zeta potential with increasing ionic strength (Fig. 1), which suggests the existence of negative spatial charge distribution around their outer region. Microbial extracellular polymeric substances (EPS) have a strong potential to exchange protons, regulate the surface charge and even precipitate carbonate minerals [47]. The presence of EPS around bacterial cells surface is known to significantly modify the cell electrophoretic properties notably the electrostatic effect of the ionic strength [13]. For example, weak effect of ionic strength on electrophoretic mobility of EPS-rich *Bacillus licheniformis* observed in the range of 0.1–0.001 mol/L has been explained by the contraction of the EPS layer with ionic strength [19] and the change in charge density associated with swelling of the EPS envelope at low ionic strength, which would compensate

Please cite this article in press as: I.A. Bundeleva et al., J. Colloid Interface Sci. (2011), doi:10.1016/j.jcis.2011.04.033

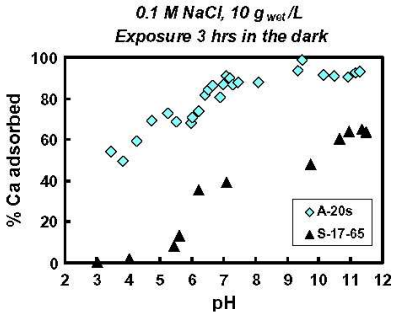


**Fig. 7.** Percentage of adsorbed calcium as a function of pH for live *Rhodovulum steppense A-20s* (open diamonds) and *Rhodovulum sp.* (solid triangles) *S-17-65*. Experimental conditions: 25 °C, $[Ca]_o$ = 17 μmol/L, 10 $g_{wet}$ biomass/L in 0.1 M NaCl and 3 h of exposure time under darkness. The error bars are within the symbol size.

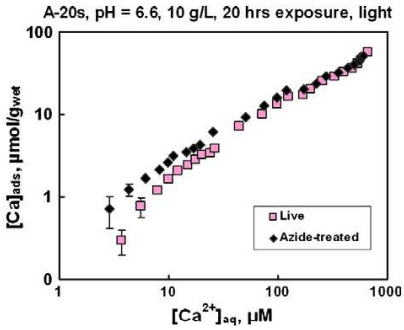


**Fig. 10.** Concentration of adsorbed calcium (μmol/$g_{wet}$) as a function of calcium concentration in solution (μmol/L) for live and azide-treated (0.01 M $NaN_3$) A-20s. Experimental conditions: 25 °C, pH = 6.6, 10 $g_{wet}$ biomass/L in 0.1 M NaCl and 20 h of exposure under light. The error bars are within the symbol size unless indicated.

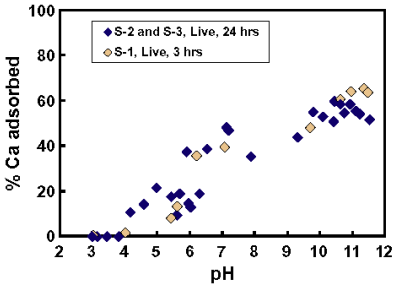


**Fig. 8.** Percentage of adsorbed Ca as a function of solution pH for Rhodovulum sp. S-17-65 culture after 3 and 24 h exposure time. Experimental conditions: 25 °C, $[Ca]_o$ = 17 μmol/L, 10 $g_{wet}$ biomass/L in 0.1 M NaCl under darkness. The error bars are within the symbol size.

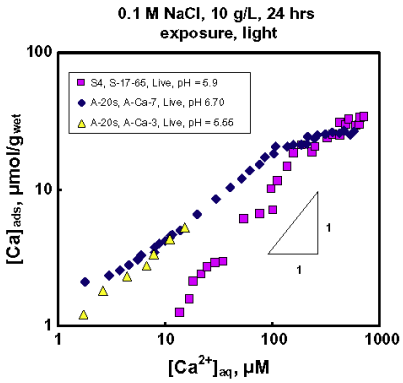


**Fig. 9.** Concentration of adsorbed calcium as a function of calcium concentration in solution (constant-pH adsorption isotherm) for live *Rhodovulum steppense* A-20s and *Rhodovulum sp. S-17-65*. Experimental conditions: 25 °C, pH 5.5-6.7, 10 $g_{wet}$ biomass/L in 0.1 M NaCl and 24 h of exposure time under light. The error bars are within the symbol size.

for charge-shielding [10]. A similar mechanism was invoked in a recent study of gram negative EPS-rich *Pseudomonas aureofaciens* [18]. In the absence of information on the EPS of studied APB, we can use only indirect methods of evaluation of their role in controlling cell electrostatic properties. In contrast to the above-mentioned heterotrophic bacteria, the effect of ionic strength on APB zeta potential is clearly pronounced, so we do not expect any significant impact of cell surface EPS of live anoxygenic phototrophic bacteria on their electrophoretic properties. This is further confirmed by zeta potential measurement in A-20s cultures subjected to multiple rinsing procedure which is capable of removing significant part of loosely bound cell surface EPS [17,18], while capsule EPS may remain attached Comparison (not shown) of zeta potential values of rinsed and non-rinsed cells at pH = 5, 8, and 10 in 0.1 mol/L NaCl demonstrate an insignificant and non-systematic difference of ±3 mV.

The pH of isoelectric point ($pH_{IEP}$) of live and inactivated APB species lays between 2 and 3, which are similar to the values reported for most microorganisms [23,48,49]. At these pH's the concentration of negatively charged surface sites such as carboxylate, phosphoryl, hydroxyl, sulfate is equal to that of the positively charged surface groups, such as amine, of the cell interface proteins. The less negative potential of autoclaved bacteria and clearly pronounced $pH_{IEP}$ of 3.5 in 0.1 mol/L NaCl (Fig. 3b and d) are most likely linked to partial physical removal of negatively charged moieties of most surface carboxylate layers after autoclaving and extensive rinsing. The partial degradation of the membrane and leaching of the surface capsule EPS layers due to autoclaving may also occur, even though the cell integrity was proved by microscopic observations. In contrast, the $pH_{IEP}$ of live and inactivated APB are similar (Fig. 3a–d) suggesting that the zeta potential of live APB in acidic solutions are mostly controlled by chemical properties of the cell surface and weakly influenced by metabolic activity. In fact, investigated halophilic bacteria may not be completely viable in acidic solutions which explains the similarity of $pH_{IEP}$ between untreated and $NaN_3$-inactivated cells.

### 4.2. Effect of bicarbonate ions and comparison with cyanobacteria

Similar to previous results on *Synechococcus* sp. and *Planktothrix* sp. Cyanobacteria [16] , there is a net increase of live cell zeta potential towards more positive values at pH ~ 10. It is important to note that the zeta potential increase at pH ~ 10 is mostly pronounced in 0.1 mol/L NaCl, solution similar to typical environment of cell growth in natural setting and in laboratory culture. Because this increase of zeta potential is observed only for active cells, it certainly indicates a metabolically-controlled mechanism.

Indeed, the systematic shift of zeta potential towards more negative values in the presence of added $NaHCO_3$ at pH of 7–11 suggests that the adsorption of bicarbonate/carbonate ions (at pH of 7–9) and physiological (metabolic) processes (at pH of 9–11) are responsible for the observed shape of zeta potential dependence on pH. A suppression of increasing trend of zeta potential

Please cite this article in press as: I.A. Bundeleva et al., J. Colloid Interface Sci. (2011), doi:10.1016/j.jcis.2011.04.033

YJCIS 16813
25 April 2011
ARTICLE IN PRESS
No. of Pages 11, Model 5G



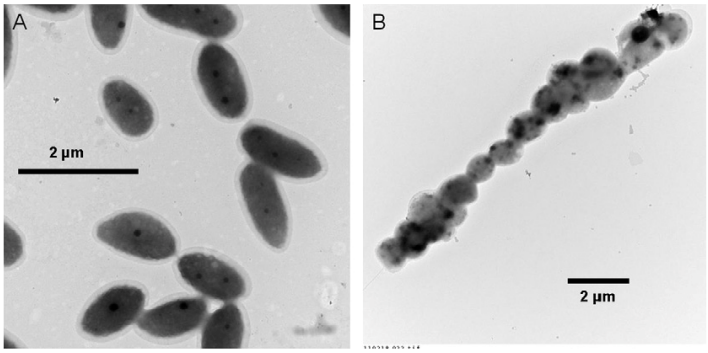


**Fig. 11.** TEM images of live A-20s (A) and S-17-65 (B) in nutrient solution. The scale bar is 2 μm and the magnification is 25,000× (A) and 12,000× (B).

for S-17-65 bacteria in the presence of 0.01 mol/L $NaHCO_3$ at $9 \leqslant pH \leqslant 11$ is apparently linked to active cellular response which ceases the positive potential creation at these concentrations of added bicarbonate/carbonate ions.

Bacterial cells imaging by TEM showed that the cells of A-20s culture are 0.5–0.6 μm wide and 1–1.5 μm long (Fig. 11a) whereas the cells of S-17-65 are 0.8–1.0 μm wide and 1.2–1.5 μm long (Fig. 11b). The cells of A-20s are isolated whereas the cells of S-17-65 are linked together forming long chains. Therefore, both slightly larger size of S-17-65 and their spatial organization lead to less amount of potentially reactive surface sites per g weight compared to A-20s because the former produce smaller surface area available for adsorption.

The smaller quantity of positively (as well as negatively) charged functional groups on S-17-65 compared to A-20s led to full saturation (screening) of these surface moieties in the presence of 0.01 mol/L sodium bicarbonate. Although our experimental setup did not allow quantifying the $HCO_3^-/CO_3^{2-}$ binding on viable cells, this explanation is consistent with lower surface site density for Ca ions on S-17-65 compared to A-20s revealed by adsorption experiments (Fig. 7) as discussed below (Section 4.3).

Overall, results of APB zeta potential dependence on pH in the presence of added sodium bicarbonate are slightly different from those obtained on cyanobacteria *Planktothrix* sp. and *Synechococcus* sp. [16]. The zeta potential of both APB species decreases from -10 mV in $NaHCO_3$–free solutions to −40 mV in the presence of 1 mmol/L $NaHCO_3$ at pH 9.5–10.5 (Fig. 5). As opposed to APB, the addition of 1 mmol/L of $NaHCO_3$ to active cyanobacteria enhances the positive potential at alkaline pH (9–10) [16]. Indeed, $HCO_3^-$ diffusion usually limits photosynthesis of cyanobacteria at concentration below about 1 mM [50] which is typical for many freshwater environments. Recently studied *Planktothrix* sp. and *Synechococcus* sp. cyanobacteria are probably unique as they are capable of developing a positive zeta potential at alkaline pH conditions, which allows then to attract $HCO_3^-$ anion, required for photosynthetic activity [16,29].

In contrast to freshwater and marine cyanobacteria, the APB A-20s live in alkaline soda lakes with typical bicarbonate concentration of 5–130 mmol/L (0.3–7.8 g/L) and pH ranging from 8.5 to 10.5 [51]. As a result, *Rhodovulum* sp. A-20s require almost 10 times higher concentration of added bicarbonate (10 mM compared to 1 mM for cyanobacteria) to suppress the zeta potential increase in alkaline solutions (Fig. 5b).

The reason for zeta potential increase in alkaline solution observed for both APB species is certainly different from active $HCO_3^-$-acquisition mechanism proposed for cyanobacteria [16]. Unlike cyanobacteria, both species of *Rhodovulum* do not require bicarbonate ions for their photosynthesis in the presence of organic compounds as carbon source [32,33,36,51,52]. Note that, despite the reported photolithoautotrophic nature of *Rhodovulum* species [33], in the present work, the cell growth in mineral media could not be achieved. As such, bicarbonate and carbonate ion adsorption on less negatively charged surface maintained by the cell in alkaline solution is the most likely mechanism of observed zeta potential pattern in the presence of $NaHCO_3$ (Fig. 5a and b). Even if photosynthetic $HCO_3^-$ uptake was partially pronounced, it could not interfere in cell surface potential regulation in alkaline solutions as confirmed by electrophoretic measurements with live cells under the light and in the full darkness. Experiments without light when the photosynthesis is absent also demonstrated zeta potential increase at pH ~ 10 (Fig. 6). Therefore, metabolically-created less negative zeta potential in alkaline solutions for APB is probably not linked to $HCO_3^-/CO_3^{2-}$ uptake. Note that the suppression of zeta potential increase in the presence of $NaHCO_3$ cannot be explained by extrusion of protons due to more active respiration under alkaline conditions required to keep the proton gradient stable, as it is known for heterotrophic bacteria [42]. Indeed, the zeta potential drop in the presence of $NaHCO_3$ is observed exactly at the same pH as that in $NaHCO_3$ free solutions, both for photosynthesizing (on the light) and respiring (in the dark) cells.

Possible reasons for less negative surface potential in alkaline solutions may be (i) active protection of cell from $CaCO_3$ incrustation [29] and/or (ii) physiological requirements for micronutrients [31]. At present, distinguishing between these two mechanisms is not possible. The first mechanism will be discussed in the next section. The second mechanism is supported by the environmental conditions of APB habitats. Indeed, anoxygenic alkaliphilic bacteria live in highly saline soda environment (up to 5 g/L $NaHCO_3/Na_2CO_3$ and 100 g/L NaCl) at pH around 9–10 which may locally rise to 11 in the diurnal cycle of photosynthesis [32]. At these conditions, most micronutrients (anions B, Si, V, Mo, and trace metals Cu, Zn, Fe, Mn, Ni and Co) are present in the form of negatively charged or neutral ions and hydroxyl, chloride, carbonate, sulfide and hydrosulfide complexes. Electrostatic attraction of these complexes to the cell surface will certainly be facilitated by decreasing the negative surface potential as revealed by electrophoretic measurements in this study.

### 4.3. Effect of calcium ions and cell protection from $CaCO_3$ incrustation

Another possible explanation for zeta potential increase in alkaline solutions, linked to the metabolic maintenance of a positive surface charge at alkaline pH, is protecting active cell against Ca adsorption and subsequent calcite formation at their surfaces [29]. Similarly, spectroscopic and microscopic observations suggested that precipitation of an amorphous $CaCO_3$ layer within the

Please cite this article in press as: L.A. Bundeleva et al., J. Colloid Interface Sci. (2011), doi:10.1016/j.jcis.2011.04.033

external EPS sheaths of cyanobacteria could serve as a protection mechanism against uncontrolled precipitation of a thermodynamically stable phase calcite on their surface [53]. For APB live in lakes of high pH and bicarbonate concentration, where $CaCO_3$ precipitation is a common phenomenon, a permanently acting protection mechanism may be as important as metabolic requirements for nutrient uptake. The ability of studied APB to precipitate $CaCO_3$ during their metabolism is demonstrated in laboratory kinetic experiments, yielding calcite and vaterite precipitation in the vicinity of live A-20s and S-17-65 cells [54–57]. Experiments of Ca adsorption allow quantification of the concentration of surface centers capable of participating in this "protection" mechanism. Indeed, "langmuirian" Ca adsorption isotherm at pH ~ 7 exhibits up to 1.5–2 times lower surface Ca adsorption for live cells compared to $NaN_3$-inactivated cultures (Fig. 10). Concurrently, at high surface loading (5–50 μmol $Ca/g_{wet}$) and Ca concentration in solution above 20 μmol/L, the adsorption density was very similar between live and $NaN_3$-inactivated cells (Fig. 10). Therefore, the number of surface sites participating in positive potential creation that is capable to significantly affect Ca binding at the live cell surfaces is less than 3 $\mu mol/g_{wet}$ biomass. In neutral solutions, this is much smaller than the typical concentration of adsorbed Ca at the conditions of our experiments (e.g., 10–50 $\mu mol/g_{wet}$, see Figs. 9 and 10). As such, the active metabolic effect on Ca adsorption is pronounced only in alkaline solutions and at very low Ca concentrations which were not extensively investigated in this study.

Taken together, results of the present study suggest clear metabolic control on less negative cell surface charge and zeta potential of anoxygenic phototrophic bacteria in alkaline solutions which appears to be an intrinsic property of these microorganisms. This feature may be tentatively linked to both physiological demand of nutrients and cell protection from Ca adsorption and $CaCO_3$ incrustation. The cell response to the change of solution conditions could be $Ca^{2+}$, $HCO_3^-$ concentration - induced or solution saturation index ($\Omega_{CaCO_3}$) – induced phenomenon, but also permanently operating reaction helping the cell to maintain less negative surface potential. Molecular and physiological mechanisms responsible for developments of this surface potential on APB in alkaline solutions, by analogy with other gram-negative bacteria, may be: (1) conformational changes in the S-layer protein arrangement [9] producing positive electric potential (the APB are reported to possess a regular S-layer on the outer surface [58]), (2) lysine-rich protein production within the cytoplasmic membrane [11] bringing about an excess of positive sites within the surface layers, (3) proton secretion by the APB cell wall via proton-pumping [31] and (4) enhanced respiration under alkaline conditions required to keep the proton gradient stable [42]. Further culture growth, Ca adsorption and surface complexation modeling and Ca carbonate precipitation experiments with APB are necessary to better distinguish between these mechanism in order to understand their role in nutrient acquisition and carbonate biomineralization.

How unique are phototrophic bacteria in developing this positive (less negative) surface potential in basic solutions? Note that we have not observed any significant zeta potential increase in alkaline solution for live cyanobacteria *Gloeocapsa* sp. [17]. Unlike unicellular APB or *Synechococcus* sp., *Gloeocapsa* sp. possess significant capsular envelope around several adjacent cells which probably precludes the active metabolic process of individual cells to be recognized at the macroscopic scale of cell aggregates. It is also possible that the zeta potential increase in alkaline solution will not necessarily be detectable for all type of photosynthesizing organisms because many bacteria possess a thick EPS layer bearing significant amount of negatively-charged groups. The thick EPS coating may prevent the detection of positive potential created by metabolic process. This is confirmed by observations of marine and freshwater diatoms. The freshwater peryphytic diatom *Navicula minima* demonstrates a slight increase of electrophoretic mobilities at pH around 9–10 in 0.1 mol/L NaCl where as marine planktonic diatom *Thalassiosira weisflogii*, having much higher proportion of organic coating on the cell surface, do not exhibit an increase of electrophoretic mobilities at pH between 5 and 13 [14]. A recent compilation of isoelectric points of viruses, although demonstrate the wide variety of $pH_{IEP}$, from 1.9 to 8.4, does not indicate the existence of less negative or positive zeta potentials in alkaline solutions [59]. Therefore, this property may be intrinsic to microorganisms having distinct cell wall.

## 5. Conclusions

We demonstrate, in a suite of electrophoretic and macroscopic batch adsorption experiments, that anoxygenic phototrophic bacteria (APB) are capable of regulating their electric surface potential in alkaline solutions (pH ~ 10–10.5). This produces an unusual, less negative zeta potential at these conditions, previously non-reported for most bacteria except cyanobacteria. This effect is absent for heat-killed and $NaN_3$-inactivated cells and it is significantly suppressed in the presence of 1–10 mM added bicarbonate ions. The presence or not of light does not affect the zeta potential increase in alkaline solutions.

Based on analogy with other bacteria, two parallel mechanisms can be suggested to explain this novel feature of zeta potential increase of APB in alkaline solutions linked to the appearance of less negative zeta-potential: (i) enhancement of uptake of the micronutrients in the form of anions and (ii) $Ca^{2+}$ ions repelling from the cell surface in order to protect the cells from $CaCO_3$ incrustation. The latter mechanism is consistent with the results of Ca adsorption on the cell surface in the physiological range of solution composition. A slight difference between two studied bacterial strains in the degree of zeta potential increase and Ca adsorption is compatible with difference in surface areas and optimal physiological range of solution parameters.

## Acknowledgments

We thank two anonymous reviewers for their insightful comments. This work was supported by the GRASP project (MRTN-CT-2006-035868), INSU program "INTERVIE" and partially by RFBR (Project No. 07-04-00651a) and the program "Origin and Evolution of the Biosphere" (Russian Academy of Sciences).

This work benefited of the assistance of the electron microscopy facility of the FRBT and of the TRI Imaging platform of Toulouse.

## References

[1] D. Borrok, J.B. Fein, Geochim. Cosmochim. Acta 68 (2004) 3043–3052.
[2] J.B. Fein, C.J. Daughney, N. Yee, T.A. Davis, Geochim. Cosmochim. Acta 61 (1997) 3319–3328.
[3] J.B. Fein, A.M. Martin, P.G. Wightman, Geochim. Cosmochim. Acta 65 (2001) 4267–4273.
[4] W.W. Wilson, M.M. Wade, S.C. Holman, F.R. Champlin, J. Microbiol, Methods 43 (2001) 153–164.
[5] V.P. Harden, J.O. Harris, Biochim. Biophys. Acta 65 (1952) 198–202.
[6] E.C. Reynolds, A. Wong, Infect. Immun. 39 (1983) 1285–1290.
[7] M.E. Bayer, J.L. Sloyer, J. General, Microbiology 136 (1990) 867–874.
[8] T.J. Beveridge, P.H. Pouwels, M. Sára, A. Kotiranta, K. Lounatmaa, K. Kari, E. Kerosuo, M. Haapasalo, E.M. Egelseer, I. Schocher, U.B. Sleytr, L. Morelli, M.-L. Callegari, J.F. Nomellini, W.H. Bingle, J. Smit, E. Leibovitz, M. Lemaire, I. Miras, S. Salamitou, P. Béguin, H. Ohayon, P. Gounon, M. Matuschek, K. Sahm, H. Bahl, R. Grogono-Thomas, J. Dworkin, M.J. Blaser, R.M. Woodland, D.G. Newell, M. Kessel, S.F. Koval, FEMS Microbiol. Rev. 20 (1997) 99–149.
[9] R. Rachel, D. Pum, J. Marda, D. Majs, J. Komrska, V. Krzyzánek, G. Rieger, K.O. Stetter, FEMS Microbiol. Rev. 20 (1997) 13–23.
[10] A. Van Der Wal, W. Norde, A.J.B. Zehnder, J. Lyklema, Colloids Surf., B 9 (1997) 81–100.
[11] M. Zinovieva, C. Fresneau, B. Arrio, Bioelectrochem. Bioenergy 46 (1998) 55.
[12] U.B. Sleytr, T.J. Beveridge, Trends Microbiol. 7 (1999) 253–260.

Please cite this article in press as: I.A. Bundeleva et al., J. Colloid Interface Sci. (2011), doi:10.1016/j.jcis.2011.04.033

[13] H. Hayashi, S. Tsuneda, A. Hirata, H. Sasaki, J. Colloid Interface Sci. 22 (2001) 149–157.
[14] A. Gélabert, O.S. Pokrovsky, J. Schott, A. Boudou, A. Feurtet-Mazel, J. Mielczarski, E. Mielczarski, N. Mesmer-Dudons, O. Spalla, Geochim. Cosmochim. Acta 68 (2004) 4039–4058.
[15] M. Dittrich, S. Sibler, J. Coll, J. Colloid Interface Sci. 286 (2005) 487–495.
[16] R.E. Martinez, O.S. Pokrovsky, J. Schott, E.H. Oelkers, J. Colloid Interface Sci. 323 (2008) 317–325.
[17] O.S. Pokrovsky, R.E. Martinez, S.V. Golubev, E.I. Kompantseva, L.S. Shirokova, Appl. Geochem. 23 (2008) 2574–2588.
[18] A.G. González, L.S. Shirokova, O.S. Pokrovsky, E.E. Emnova, R.E. Martínez, J.M. Santana-Casiano, M. González-Dávila, G.S. Pokrovski, J. Colloid Interface Sci. 350 (2010) 305–314.
[19] J. Tourney, B.T. Ngwenya, J. Colloid Interface Sci. 348 (2010) 348.
[20] L. Kapetas, B.T. Ngwenya, A.M. Macdonald, S.C. Elphick, J. Colloid Interface Sci., submitted for publication.
[21] M. Kosmulski, E. Maczka, W. Janusz, J.B. Rosenholm, J. Colloid Interface Sci. 250 (2002) 99–103.
[22] M. Kosmulski, A.S. Dukhin, T. Priester, B. Jarl, J.B. Rosenholm, J. Colloid Interface Sci. 263 (2003) 152–155.
[23] M. Kosmulski, J. Colloid Interface Sci. 337 (2009) 439–448.
[24] O.S. Pokrovsky, G.S. Pokrovsky, A. Gelabert, J. Schott, A. Boudou, Environ. Sci. Technol. 39 (2005) 4039–4058.
[25] M. Dittrich, S. Sibler, Langmuir 22 (2006) 5435–5442.
[26] M. Obst, M. Dittrich, Gechem. Geophys. Geosystem. 7 (2006) 15.
[27] J.F.L. Duval, F. Gaboriaud, Colloid Interface Sci. 15 (2010) 184–195.
[28] D.V. Richmond, D.J. Fisher, A.H. Rose, D.W. Tempest, Advances in Microbial Physiology, Academic Press, 1973, pp. 1–29.
[29] R.E. Martinez, E. Gardês, O.S. Pokrovsky, J. Schott, E.H. Oelkers, Geochim. Cosmochim. Acta 74 (2010) 1329–1337.
[30] M.U.E. Merz, W.R. Schlue, H. Zankl, Facies 26 (1992) 81–102.
[31] T.A. McConnaughey, J.F. Whelan, Earth Sci. Rev. 42 (1997) 95–117.
[32] B. Jagannathan, J.H. Golbeck, S. Moselio, Photosynthesis: microbial, in: Encyclopedia of Microbiology, Academic Press, Oxford, 2009, pp. 325–341.
[33] E.I. Kompantseva, A.V. Komova, N.A. Kostrikina, Int. J. Syst. Evol. Microbiol. 60 (2010) 1210–1214.
[34] T. Bosak, S.E. Greene, D.K. Newman, Geobiology 5 (2007) 119–126.
[35] V.M. Gorlenko, E.I. Kompantseva, S.A. Korotkov, N.N. Pouchkova, A.S. Savvichev Izvestiya, AN SSSR, Seriya biol. 3 (1984) 362–374.
[36] E.I. Kompantseva, A.V. Komova, A.V. Krauzova, T.V. Kolganova, A.N. Panteleeva, Microbiology 78 (2009) 246–253.
[37] N. Pfenning, K.D. Lippert, Arch. Mikrobiol. 55 (1966) 245–256.
[38] B.T. Ngwenya, Chemosphere 67 (2007) 1982–1992.
[39] P.A. Kenward, R.H. Goldstein, L.A. Gonzalez, J.A. Roberts, Geobiology 7 (2009) 556–565.
[40] M. Urrutia Mera, M. Kemper, R. Doyle, T.J. Beveridge, Environ. Microbiol. 58 (1992) 3837–3844.
[41] K.J. Johnson, D.A. Ams, A.N. Wedel, J.E.S. Szymanowski, D.L. Weber, M.A. Schneegurt, J.B. Fein, Geobiology 5 (2007) 211–218.
[42] R.C. Hunter, V.R. Phoenix, A. Saxena, T.J. Beveridge, Can. J. Microbiol. 56 (2010) 527–538.
[43] M.Z. Bazant, M.S. Kilic, B.D. Storey, A. Ajdari, Adv. Colloid Interface Sci. 152 (2009) 48–88.
[44] V.M. Gun'ko, I.F. Mironyuk, V.I. Zarko, E.F. Voronin, V.V. Turov, E.M. Pakhlov, E.V. Goncharuk, Y.M. Nychiporuk, N.N. Vlasova, P.P. Gorbik, O.A. Mishchuk, A.A. Chuiko, T.V. Kulik, B.B. Palyanytsya, S.V. Pakhovchishin, J. Skubiszewska-Zieba, W. Janusz, A.V. Turov, R. Leboda, J. Colloid Interface Sci. 289 (2005) 427–445.
[45] J.D. Allison, D.S. Brown, K.J. Novo-Gradac, MINTEQA2/PRODEFA2, A Geochemical Assessment Model for Environmental Systems, Version 3.0 User's Manual, vol. 106, 1991.
[46] A.E. Martell, R.M. Smith, R.J. Motekaitis, NIST Critically Selected Stability Constants of Metal Complexes, Database Software Version 3.0, Texas A & M University, College Station, TX, 1997.
[47] M. Dittrich, S. Sibler, Geol. Soc. London, Spec. Publ. 336 (2010) 51–63.
[48] P.F.G. Herben, N. Mozes, P.G. Rouxhet, Biochim. Biophys. Acta 1033 (1990) 184–188.
[49] J.R. Sloyer, M.E. Bayer, J. Virol. Methods 28 (1990) 207–216.
[50] F.A. Smith, N.A. Walker, New Phitolodist 86 (1980) 245–259.
[51] E.I. Kompantseva, I.A. Bryantseva, A.V. Komova, B.B. Namsaraev, Microbiology 76 (2007) 211–219.
[52] R.E. Blankenship, S. Sadekar, J. Raymond, G.F. Paul, H.K. Andrew, Evolution of Primary Producers in the Sea, Academic Press, Burlingto, 2007, pp. 21–35.
[53] M. Obst, B. Wehrli, M. Dittrich, Geobiology 7 (2009) 324–347.
[54] I.A. Bundeleva, L.S. Shirokova, P. Bénézeth, O.S. Pokrovsky, E.I. Kompantseva, Geophys. Res. Abstr., EGU Gen. Assembly 13 (2011) EGU2011–2636.
[55] I.A. Bundeleva, L.S. Shirokova, P. Bénézeth, O.S. Pokrovsky, E.I. Kompantseva, Geophys. Res. Abstr., EGU Gen. Assembly 12 (2010) EGU2010–9521.
[56] I.A. Bundeleva, L.S. Shirokova, P. Bénézeth, O.S. Pokrovsky, E.I. Kompantseva, in: Proceedings of 19th Annual V.M. Goldschmidt Conference, Davos, Switzerland, Geochim. Cosmochim. Acta, vol. 73, 2009 (21–26 June 2009).
[57] L.S. Shirokova, O.S. Pokrovsky, J. Schott, E.H. Oelkers, R. Martinez, E.I. Kompantseva, Geophys. Res. Abstr., EGU Gen. Assembly 10 (2008) EGU2008-A-04921.
[58] O.N. Lunina, I.A. Bryantseva, V.N. Akimov, I.I. Rusanov, E.S. Barinova, A.M. Lysenko, D.Y. Rogozin, N.V. Pimenov, Microbiology 76 (2007) 469–479.
[59] B. Michen, T. Graule, Appl. Microbiol. 109 (2010) 388–397.



Please cite this article in press as: I.A. Bundeleva et al., J. Colloid Interface Sci. (2011), doi:10.1016/j.jcis.2011.04.033

# Chapter IV

# Calcium carbonate precipitation by anoxygenic phototrophic bacteria

# Résumé en français

La biominéralisation des carbonates est considérée comme l'un des principaux processus contrôlant les niveaux de $CO_2$ dans l'atmosphère, aujourd'hui comme dans les temps passés. Contrairement aux nombreux travaux axés sur la calcification par les cyanobactéries, la biominéralisation par les bactéries anoxygéniques phototrophiques (APB) est restée longtemps sous-estimée, malgré leur rôle potentiel important dans la précipitation de $CaCO_3$ dans les biofilms. Ce chapitre rapporte les résultats obtenus lors de l'étude des vitesses de précipitation de $CaCO_3$ induite par deux types de bactéries anoxygéniques phototrophiques : *Rhodovulum steppens* A-20s haloalcaliphilique et *Rhodovulum* sp. S-17-65 neutrophilique halophilique, cultivées sur substrats organiques.

Afin de caractériser le lien entre le taux de croissance bactérienne (production de biomasse) et la vitesse apparente de précipitation de $CaCO_3$, des expériences cinétiques en présence de bactéries vivantes, mortes et inactivées ont été menées dans des solutions nutritives d'une part et dans une solution d'électrolyte inerte (NaCl) d'autre part. Les précipités obtenus ont ensuite été examinés par Microscopie Electronique à Balayage (MEB) et en Transmission (MET), ainsi que par spectroscopie de rayon X (XRD). Les résultats obtenus montrent une corrélation positive entre la vitesse de précipitation des carbonates et l'indice de saturation initial de la calcite ($\Omega_{calcite}$) pour les deux types de bactéries ($r^2$=0.80 et 0.75 pour A-20s et S-17-65, respectivement). Cependant, des analyses détaillées de la dépendance de l'indice de saturation sur la vitesse de précipitation apparente de la calcite, à $\Omega_{calcite}$ constant, montrent que [DIC] et [Ca] seuls ne peuvent contrôler les vitesses de précipitation de la calcite par les bactéries anoxygéniques phototrophiques. *Rhodovulum steppens* halophilique A-20s vivante précipite de la calcite à partir d'une solution initialement sursaturée ($\Omega_{calcite}$ =40 à 100), ce qui induit parfois une augmentation de $\Omega_{calcite}$ jusqu'à 100-120 juste avant la précipitation. En revanche, S-17-65 halophilique neutrophilique augmente toujours la sursaturation de 10-60 au début de la réaction à 100-140 après 5 à 7 jours de réaction, permettant ainsi la précipitation massive de $CaCO_3$. La quantité de précipité (en mole) est directement liée à la biomasse ($g_{wet}$) avec une pente allant de 0.1 à 0.8 et 0.1 à 0.5 pour A-20s et S-17-65, respectivement, en fonction de la composition initiale de la solution. Pour les deux souches, seules les bactéries vivantes et menant activement la photosynthèse sont capables de diminuer de manière effective la concentration de Ca et former $CaCO_3$ avec des vitesses apparentes de précipitation allant de 0.001 à 0.0150 mM/hr. Ces valeurs sont

similaires à celles des cyanobactéries et des bactéries hétérotrophiques et deux ordres de grandeur plus grandes que les taux de calcification typiques des algues corallines. Les analyses au MEB et par XRD des précipités révèlent que la phase calcite domine, accompagnée d'une certaine quantité de vatérite et de mono-hydro-calcite, formant des sphères de diamètre ≤100µm. Par contre, les analyses au MET des suspensions bactériennes prélevées à la fin des expériences de précipitation ne démontrent pas la présence de $CaCO_3$ à la surface ou à l'intérieur des cellules vivantes. Ceci suggère l'existence d'un processus cellulaire de protection contre la précipitation de carbonates. Etant donné l'efficacité des bactéries anoxygéniques phototrophiques à précipiter $CaCO_3$, leur rôle dans la calcification des biofilms pourrait être au moins aussi important que celui des cyanobactéries.

Les résultats obtenus, en particulier le rôle important de l'activité métabolique microbienne (photosynthèse) dans la précipitation de $CaCO_3$, sont décrits dans la section suivante sous la forme d'un manuscrit soumis à *Chemical Geology*.

# Calcium carbonate precipitation by anoxygenic phototrophic bacteria

Irina A. Bundeleva[1], Liudmila S. Shirokova[1,2], Pascale Bénézeth[1],

Oleg S. Pokrovsky[1]*, Elena I. Kompantseva[3], Stéphanie Balor[4]

[1]*Laboratoire Géosciences Environnement Toulouse (GET), Université de Toulouse, CNRS-IRD-OMP, 14 Avenue Edouard Belin, 31400 Toulouse, France*

[2] *Institute of Ecological Problems of the Northern Regions, Russian Academy of Science, 29 Naberezhnaja Sev. Dviny, Arkhangelsk , Russia*

[3] *Winogradsky Institute of Microbiology, Russian Academy of Science, Moscow, Russia*

[4] *Plateau de Microscopie électronique, FRBT CNRS FR3451, Bat. IBCG, 118 route de Narbonne, F-31062 Toulouse, France*

*corresponding author

e-mail: oleg@get.obs-mip.fr

**Key words:** Anoxygenic phototrophic bacteria, *Rhodovulum* sp., calcium carbonate, precipitation, kinetics, calcium, bicarbonate, calcite.

*Submitted to Chemical Geology, April 2011*

# Abstract

Carbonate biomineralization is considered as one of the main natural processes controlling $CO_2$ levels in the atmosphere both in the past and at present time. In contrast to extensive studies of cyanobacterial calcification, biomineralization of anoxygenic phototrophic bacteria (APB) remained largely underestimated, despite their potentially important role on $CaCO_3$ precipitation in the biomats. Haloalcaliphilic *Rhodovulum steppens* A-20s and halophilic neutrophilic *Rhodovulum* sp. S-17-65 were examined with respect to their ability to precipitate $CaCO_3$ under controlled laboratory conditions.

To characterise the link between the rate of bacterial growth (biomass production) and the rate of $CaCO_3$ precipitation, batch kinetic experiments with live, dead and inactivated bacteria both in nutrient solution and in inert electrolyte were performed and produced precipitates were examined by SEM, TEM and XRD. The results obtained show that there is a positive correlation between carbonate precipitation rate and the initial calcite saturation index ($\Omega_{calcite}$) for both bacterial species ($r^2$ = 0.80 and 0.75 for A-20s and S-17-65 respectively). Active haloalcaliphilic *Rhodovulum steppens* A-20s precipitated calcite from initially supersaturated solutions ($\Omega_{calcite}$ = 40 to 100) sometimes increasing $\Omega_{calcite}$ to 100-120 before the precipitation. In contrast, halophilic neutrophilic S-17-65 always increased supersaturation value from 10-60 at the beginning of reaction to 100-140 after 5-7 days of reaction thus promoting massive $CaCO_3$ precipitation. The amount of precipitated $CaCO_3$ (mole) was directly linked to bacterial biomass ($g_{wet}$) produced with a slope of dependence ranging from 0.1 to 0.8 and 0.1 to 0.5 for A-20s and S-17-65, respectively, depending on the initial solution composition. For both bacterial strains, only live actively photosynthetizing bacteria were capable of effectively decreasing Ca concentration and form $CaCO_3$ with apparent bulk precipitation rates ranging from 0.001 to 0.0150 mmol/hr, similar to rates reported for other bacteria. SEM and XRD analyses of precipitates reveal the dominance of calcite with some amount of vaterite and monohydrocalcite forming spheres up to 100 µm diameter. In contrast, TEM analysis of bacterial suspension at the end of precipitation experiments did not demonstrate the presence of $CaCO_3$ at the surface or in the vicinity of live cells. This suggests the existence of certain cell protection mechanism agains carbonate precipitation. Given the efficiency of APB to precipitate $CaCO_3$, their role in biomats calcification may be as much important as that of cyanobacteria.

# 1. Introduction

Microbial carbonate formation occurring for most of Earth's history was largely controlled by mineral nucleation processes driven by microbial metabolism (Bosak and Newman, 2003). Numerous works have addressed calcium carbonate formation via cyanobacterial activity (Thompson and Ferris, 1990; Hartley et al., 1995; Douglas and Beveridge, 1998; Obst and Dittrich, 2006; Dittrich and Sibler, 2010; Kranz et al., 2010; Martinez et al., 2010;), algal and coral (Ries, 2010) with a number of studies devoted to mineral precipitation via sulphate-reducing (Vasconselos et al., 1995; Warthmann et al., 2000; Van Lith et al., 2003; Bontognali et al., 2008), methanogenic archae (Kenward et al., 2009) and heterotrophic ureolitic (Ferris et al., 2004; Mitchell and Ferris, 2005, Dupraz et al., 2009) and aerobic halophilic (Sánchez-Román et al., 2011) bacteria. Whereas these studies are certainly helpful for understanding contemporary settings of microbial calcification, the deciphering of past biocalcification processes is still at the very beginning. Indeed, modern stromatolites are limited to a few tropical marine and quasi-marine sites, and to extreme environments, such as alkaline and hypersaline lakes or thermal springs (Riding et al., 1991; Lopez-Garcia et al., 2005; Papineau et al., 2005; Kazmierczak and Kempe, 2006). Precambrian stromatolites were formed by iterative accretive growth of microbial communities that precipitated and/or entrapped inorganic materials (Dupraz et al., 2006).

Although anoxygenic photosynthesis does not dominate primary production in the modern stromatolites, this metabolism may have been crucial for the growth of Archean and some Palaeoproterozoic stromatolites (Bosak et al., 2007). It has been suggested that anoxygenic photosynthesis could determine primary productivity in shallow marine environments before the rise of oxygenic photosynthesis and the widespread atmospheric oxygenation (Olson and Blankenship, 2004). Thus, biofilms formed by anoxygenic photosynthetic microorganisms would have helped building stromatolites even before cyanobacteria became the dominant primary producers in Precambrian reefs (Bosak et al., 2007). Even at present, α-proteobacteria anoxygenic phototrophs significantly contribute to genetic diversity, gross primary productivity and the biomass of the photosynthetic community, as it was demonstrated in Hamelin Pool stromatolithes (Papineau et al., 2005). Purple nonsulfur bacteria may play a previously underappreciated role in $CaCO_3$ formation

within some microbialites, particularly the microbial community associated with modern hypersaline stromatolites in Shark Bay (Bosak et al., 2007).

There is little doubt that present-day calcareous microbialites are formed via action of photosynthetic aerobic cyanobacteria that rise pH and increase $CaCO_3$ supersaturation. However, there is a certain paradox concerning the main processes responsible for massive calcium carbonate formation within a microbial mat. Previous field and recent laboratory observations demonstrated that the mineral formation occurs preferentially on dead than on live cyanobacteria (Krumbein et al., 1977; Chafetz and Buczynski, 1992; Martinez et al., 2010), after the decomposition of exopolymeric matrix by the heterotrophic bacteria (e.g., Arp et al., 1999a, b). In fact, live cyanobacterial cells are capable of protecting themselves to $CaCO_3$ incrustation via shed off of mineralized S-layer (Thompson et al., 1997; Douglas and Beveridge, 1998) and/or metabolically maintaining positive surface potential to avoid Ca adsorption (Martinez et al., 2008, 2010). Moreover, natural observations indicate that most of biocalcification in the biomats occur in the beginning of aphotic layer where dead cyanobacteria, heterotrophic bacteria and anoxygenic phototrophic bacteria (hereafter APB) dominate. However, in contrast to numerous laboratory and field studies of $CaCO_3$ precipitation by cyanobacteria (e.g., Altermann et al., 2006; Riding, 2006; Obst et al., 2009a, b; Kranz et al., 2010), quantification of reaction rates and characterization of mechanism of biocalcification by APB are very limited. To our knowledge, only one study investigated calcite precipitation by APB liquid cultures and biofilms (Bosak et al., 2007).

In order to better understand the processes and mechanisms of calcium carbonate precipitation by anoxygenic phototrophic bacteria, we selected two purple nonsulfur bacteria extracted from soda lakes: *Rhodovulum steppense* A-20s and *Rhodovulum sp.* S-17-65 extracted from soda lake and hypersaline water body, respectively (Kompantseva et al., 2007, 2009, 2010). Using laboratory modeling, we aimed at establishing the relationship between the growth rate of APB, environmental solution parameters and associated calcium carbonate precipitation.

# 2. Materials and Methods

## 2.1. Anoxygenic phototrophic bacteria (APB) cultures

Two distinct anoxygenic phototrophic bacteria (APB) were used in this study: Rhodovulum steppense A-20s (hereafter referred to as A-20s) and strain Rhodovulum sp. S-17-65 (hereafter referred to as S-17-65), which according to genotypic and phenotypic characteristics of the genus Rhodovulum (Kompantseva, 1985). Haloalcaliphilic A-20s with optimal growth conditions as a salinity of 10-50 g/L was isolated from steppe soda lake in southern Siberia (Kompantseva et al., 2010). The halophilic neutrophilic S-17-65 growing in 5-25% NaCl with optimum at 12 % was extracted from hypersaline water body in the Crimea steppe (Gorlenko et al., 1984). Natural aquatic environment of these APB is as follow: pH = 9.5, Dissolved Inorganic Carbon (DIC) = 0.1 mol/L, salinity = 40 g/L, T = 23-30°C for A-20s (Kompantseva et al., 2009) and pH = 7-8, DIC = 0.01 mol/L, salinity = 20 g/L and T = 25-35°C for S-17-65 (Gorlenko et al., 1984). Therefore, alkaliphilic Rhodovulum steppense A-20s grow in more alkaline, carbonate-bearing solutions but at much lower salinity compared to the neutrophilic halophilic Rhodovulum sp. S-17-65. By selecting these two contrasting species, it was possible to encompass a large variety of environmental conditions pertinent to modern and past biocalcification settings.

## 2.2. Growth and preparation of bacteria

Both APB were cultured in Pfenning growth medium of the following composition (Pfenning and Lippert, 1966; Kompantseva et al., 2010): $KH_2PO_4$ (330 mg/L), $MgCl_2*6H_2O$ (330 mg/L), $NH_4Cl$ (330 mg/L), KCl (330 mg/L), $Na_2SO_4$ (330 mg/L), $CaCl_2$ (50 mg/L), $NaHCO_3$ (5 g/L for A-20s, 0.5 g/L for S-17-65), NaCl (25 g/L for A-20s , 120 g/L for S-17-65), sodium acetate (1 g/L), casamino acids (0.1 g/L), yeast extract (0.1 g/L), $B_{12}$ (20 µg/L), and trace elements solution (1 ml/L (Fe, Zn, Cu, Co, Mn, Mo)). For S-17-65, $Na_2S$ (0.1 g/L) and cysteine (0.3 g/L) were added as a source of sulfur.

Unlike cyanobacteria, studied APB do not use dissolved $CO_2$ and $HCO_3^-$ during photosynthesis in the presence of organic substrate. This was proven by measuring DIC during bacterial growth without $CaCO_3$ precipitation: no significant variations of DIC (±10%, or 1-3 mM/L) were observed in experiments producing 1-1.5 $g_{dry}$/L biomass. Photolithoautotrophic growth of both strains is possible with reduced sulfur compounds as electron donors on mineral medium in the absence of organic matter (Kompantseva et al, 2010) but was not tested at experimental conditions of this study. Stock cultures of bacteria were kept in sealed glass bottles in oxygen-free conditions at 23-30°C, under constant 2000 lx white fluorescent light, and placed on a rotator shaker at 10 rpm to grow for 1 week till the stationary stage was reached. Note that the conversion factors of wet to freeze-dried weight applied for studied microorganisms were equal to 11.7 and 16.1 for A-20s and S-17-65, respectively. Cell suspensions of metabolically active A-20s or S-17-65 were used for kinetic experiments. The cells were rinsed in 0.1 mol/L NaCl and centrifuged twice at 10,000 rpm for 10 minutes at 20°C. Dead cells were preparated by autoclaving fresh bacterial suspension during 20 min at 120°C. Although the heat-killing procedure can significantly modify the cell surface structure, it still remains a widely used method for producing control alive material (e.g. Ngwenya, 2007; Pokrovsky et al., 2008; Kenward et al., 2009; Martinez et al., 2008, 2010). Scanning electron microscopic examination showed that heat-killed cells maintained their integrity and shape after heat treatment. Inactivated cells were prepared by rinsing part of the fresh (live) biomass in 0.01 mol/L $NaN_3$ during 1-2 hrs. Sodium azide inhibits bacterial growth by preventing cytochrome oxidase and is widely used for inactivating cells while keeping the surfaces physically and chemically intact (Urrutia Mera et al., 1992; Johnson et al., 2007; Hunter et al., 2010). Cell growth of both cultures in the presence of 0.01 M $NaN_3$ in nutrient solution was completely suppressed as proven in separate series of experiments.

The nutrient growth solution used for $CaCO_3$ precipitation experiments was slightly modified Pfenning media. Preliminary experiments on normal Pfenning media with addition of $CaCl_2$ and $NaHCO_3$ yielded Ca phosphate as the main precipitate. As such, phosphate-free growth solution was used in kinetic experiments. All manipulations were carried out in a laminar hood box class A100.

### 2.3. Experimental procedure and analyses.

All studied experimental conditions are listed in Table 1. Kinetic experiments were carried out with initial concentration of calcium chloride and sodium bicarbonate ranging from 1 to 10 and 5 to 20 mM, respectively. All biotic experiments were performed with initial biomass concentration between 1.6 and 3.5 $g_{wet}$/L. Precipitation experiments were carried out over a range of initial saturation index ($\Omega_{CaCO3}$) with respect to calcite varying between 8 and 230 for A-20s, and between 2 and 60 for S-17-65. The variation of all experimental parameters (pH, $[Ca^{2+}]$, [Alk] and biomass) as a function of time in each individual experiment is presented in the Appendix 3.

Kinetic experiments were performed at 25 ± 1°C in nutrient, $CaCl_2$, $NaHCO_3$-bearing solution and in nutrient-free inert electrolyte (0.1 M NaCl) with live, dead and $NaN_3$-inactivated cells. Experiments were conducted using discontinuous batch mode in two to three replicates. Mother suspension of cells in nutrient or inert electrolyte solution was mixed homogeneously and separated into 5-10 sealed 25-mL sterile glass bottles without headspace. The bottles were placed in a rotator mixer at 24 rpm and under continuous light 2000 lx. Periodically, one whole bottle was sampled to monitor the chemical and microbiological evolution of the system. The concentration of bacterial cells was estimated by measuring optical density at a 650 nm wavelength. Values of pH were measured using a Mettler Toledo® combined electrode, with an accuracy of ±0.02 units. Remaining solution was filtered through a 0.22 µm acetate cellulose membrane to measure [Ca], [Alk] and Dissolved Organic Carbon (DOC). DOC was analyzed with Shimadzu SCN Analyzer implying total combustion at 800°C after acidification, and, finally, infrared detection with an uncertainty of 3% and detection limit of $8\times10^{-3}$ mM/L. Calcium concentration was determined using flame atomic absorption spectroscopy via a Perkin Elmer AAnalyst 400 Spectrophotometer with an uncertainty of ±2% and a detection limit of 0.5 µmol/L. In organic-free solutions, alkalinity was determined following a standard HCl titration procedure using automatic titration cell TitroLine alpha TA10 plus (Schott Instruments®) with an uncertainty of ±2% and a detection limit of $5\times10^{-5}$ M. In organic-rich nutrient solutions, total dissolved inorganic carbon (DIC) was measured using Shimadzu SCN Analyzer after calibration of the instrument in a series of standard solutions prepared by addition of precise amount of $NaHCO_3$ into A-20s and S-17-65 carbonate-free organic-rich nutrient solution at pH = 8.

**Table IV. 1. Initial experimental conditions of kinetic experiments. APB strain A-20s.**

| № | Initial concentrations, mM | | Solution | Bacterial state | Experiment number Appendix 3 |
|---|---|---|---|---|---|
| | [$CaCl_2$] | [$NaHCO_3$] | | | |
| 1 | 1 | 5 | nutrient | live | 1 |
| 2 | 1 | 5 | nutrient | $NaN_3$-inactivated | 31 |
| 3 | 5 | 5 | nutrient | live | 2 |
| 4 | 5 | 5 | nutrient | $NaN_3$-inactivated | 32 |
| 5 | 10 | 5 | nutrient | live | 3, 4 |
| 6 | 10 | 5 | nutrient | $NaN_3$-inactivated | 33, 34 |
| 7 | 10 | 5 | nutrient | bacteria-free | 59 |
| 8 | 10 | 5 | nutrient | Absent+$NaN_3$ | 60 |
| 9 | 10 | 5 | nutrient | Dead (heat killed) | 61 |
| 10* | 10 | 5 | nutrient | live | 62 |
| 11 | 1 | 10 | nutrient | live | 5, 6 |
| 12 | 1 | 10 | nutrient | $NaN_3$-inactivated | 35, 36 |
| 13 | 1 | 19 | nutrient | bacteria-free | 63 |
| 14 | 5 | 10 | nutrient | live | 7, 8, 9 |
| 15 | 5 | 10 | nutrient | $NaN_3$-inactivated | 37, 38 |
| 16 | 5 | 10 | nutrient | bacteria-free | 64, 65, 66 |
| 17 | 10 | 10 | nutrient | live | 10, 11 |
| 18 | 10 | 10 | nutrient | $NaN_3$-inactivated | 39, 40 |
| 19 | 10 | 10 | nutrient | bacteria-free | 67 |
| 20 | 1 | 20 | nutrient | live | 12, 13 |
| 21 | 1 | 20 | nutrient | $NaN_3$-inactivated | 41, 42 |
| 22 | 5 | 20 | nutrient | live | 14 |
| 23 | 5 | 20 | nutrient | $NaN_3$-inactivated | 43 |
| 24 | 5 | 20 | nutrient | bacteria-free | 68 |
| 25 | 10 | 20 | nutrient | live | 15 |
| 26 | 10 | 20 | nutrient | $NaN_3$-inactivated | 44 |
| 27 | 0.3 | 40 | nutrient | live | 16 |
| 28 | 0.3 | 40 | nutrient | $NaN_3$-inactivated | 45 |
| 29 | 1.5 | 5 | inert electrolyte | live | 73 |
| 30 | 3 | 5 | inert electrolyte | live | 74 |
| 31 | 7 | 5 | inert electrolyte | live | 75 |
| 32 | 10 | 5 | inert electrolyte | live | 76 |
| 33 | 15 | 5 | inert electrolyte | live | 77 |
| 34 | 20 | 5 | inert electrolyte | live | 78 |
| 35 | 3 | 5 | inert electrolyte | Dead (heat killed) | 79 |
| 36 | 10 | 5 | inert electrolyte | Dead (heat killed) | 80 |
| 37 | 20 | 5 | inert electrolyte | Dead (heat killed) | 81 |
| 38 | 3 | 5 | inert electrolyte | bacteria-free | 82 |
| 39 | 10 | 5 | inert electrolyte | bacteria-free | 83 |
| 40 | 20 | 5 | inert electrolyte | bacteria-free | 84 |
| 41 | 5 | 10 | inert electrolyte | bacteria-free | 85 |

**Table IV. 1., continued. Initial experimental conditions of kinetic experiments. APB strain S-17-65**

| № | Initial concentrations, mM | | Solution | Bacterial state | Experiment number in Appendix 3 |
|---|---|---|---|---|---|
| | [$CaCl_2$] | [$NaHCO_3$] | | | |
| 42 | 1 | 5 | nutrient | live | 17, 18, 30 |
| 43 | 1 | 5 | nutrient | $NaN_3$-inactivated | 46, 47, 58 |
| 44 | 5 | 5 | nutrient | live | 19 |
| 45 | 5 | 5 | nutrient | $NaN_3$-inactivated | 48 |
| 46 | 10 | 5 | nutrient | live | 20, 21 |
| 47 | 10 | 5 | nutrient | $NaN_3$-inactivated | 49, 50 |
| 48 | 10 | 5 | nutrient | live | 69 |
| 49 | 1 | 10 | nutrient | Live | 22 |
| 50 | 1 | 10 | nutrient | $NaN_3$-inactivated | 51 |
| 51 | 5 | 10 | nutrient | Live | 23, 24, 25 |
| 52 | 5 | 10 | nutrient | $NaN_3$-inactivated | 52, 53 |
| 53 | 5 | 10 | nutrient | bacteria-free | 70, 72 |
| 54 | 10 | 10 | nutrient | Live | 26 |
| 55 | 10 | 10 | nutrient | $NaN_3$-inactivated | 54 |
| 56 | 10 | 10 | nutrient | Absent | 71 |
| 57 | 1 | 20 | nutrient | Live | 27 |
| 58 | 1 | 20 | nutrient | $NaN_3$-inactivated | 55 |
| 59 | 5 | 20 | nutrient | Live | 28 |
| 60 | 5 | 20 | nutrient | $NaN_3$-inactivated | 56 |
| 61 | 10 | 20 | nutrient | Live | 29 |
| 62 | 10 | 20 | nutrient | $NaN_3$-inactivated | 57 |
| 63 | 3 | 5 | inert electrolyte | Live | 89 |
| 64 | 7 | 5 | inert electrolyte | Live | 90 |
| 65 | 15 | 5 | inert electrolyte | Live | 91 |
| 66 | 5 | 10 | inert electrolyte | Live | 86, 87 |
| 67 | 5 | 10 | inert electrolyte | $NaN_3$-inactivated | 88 |

*****Experiment conducted in the darkness

For this, an inorganic (DIC) detection mode was used implying acidification, Ar flushing and infrared detection without high-T combustion. This yielded an uncertainty of ±10% and a detection limit of $4\times10^{-2}$ mM/L.

Mixtures of APB cells and precipitated mineral phase were subjected to digestion for removing organic matter using 2-3 days treatment in 10% $H_2O_2$ at the same solution pH as in experimental samples. Resulted solid phases were rinsed in MilliQ water, frozen at -80°C and freeze-dried. Selected samples were studied by X-ray diffraction (INEL CPS 120, $Co_{K\alpha}$, scan speed $0.02^{o}s^{-1}$) and microscopic examination was performed using a Jeol JSM840a Scanning

Electron Microscope (SEM) after carbon film coating deposition on the sample surface. Mineral-free bacterial cells and cell biomass with precipitated $CaCO_3$ were also observed using Transmission Electron Microscopy (TEM) with a JEOL JEM 12000 EX and JEOL JEM 2100F (equipped with a field emission gum (FEG) and PGT EDX detector) at 80 kV. Cell suspension was first rinsed using sterile nutrient solution and MilliQ water then centrifuged for about 2 min at 10 000 rpm. TEM samples for analyses were taken by immersing grids coated with a carbon film for 10 s in prepared bacterial suspension. Dried grids were used for TEM imaging.

### 2.4. Rate calculation

Anoxygenic phototrophic bacteria uptake organic ligands such as acetate or lactate (A-20s) and also cysteine, sulfide and hydrosulfide (S-17-65) at pH > 7.5, releasing $OH^-$ for charge compensation therefore rising the pH and increasing supersaturation degree. As a result, calcium carbonate precipitation by APB occurs, similar to other bacteria (Thompson and Ferris, 1990; Dittrich and Obst, 2004; Dittrich and Sibler, 2005; Mitchel and Ferris, 2006; Martinez et al., 2008) and according to the reaction:

$$Ca^{2+} + 2HCO_3^- \rightarrow CaCO_3 + CO_2 + H_2O \qquad (1)$$

The rates of calcium carbonate formation ($R_{CaCO3}$) were determined by fitting numerically the calcium concentration evolution with time using the integrated form of carbonate precipitation rate equation given by Morse (1983):

$$R_{CaCO_3} = \frac{d[Ca^{2+}]}{dt} = k_{CaCO_3} \times (\Omega_{CaCO_3} - 1)^n \qquad (2)$$

where $k_{CaCO3}$ stands for the rate constant and $[Ca^{2+}]$ refers to the aqueous calcium concentration, $t$ designates time, $n$ denotes the reaction order, $\Omega_{CaCO3}$ corresponds to the solution saturation state defined by:

$$\Omega_{CaCO_3} = \frac{a_{Ca^{2+}} \times a_{CO_3^{2-}}}{K^\circ_{CaCO_3}} \qquad (3)$$

where $a_{Ca}^{2+}$ and $a_{CO3}^{2-}$ represent the activity of the subscripted species, and $K°_{CaCO3}$ refers to the equilibrium constant taken as $10^{-8.48}$ for calcite at 25°C (Plummer and Busenberg,

1982). In order to verify the correctness of our calculation of $\Omega_{CaCO_3}$ using PHREEQC (Parkhurst et al., 1999) in highly saline, organic-rich nutrient media, calcite solubility experiments were performed in bacteria-free, sterile growth media. Results are presented in the Electronic Supporting Information (ESM Table 1). For most solutions, satisfactory agreement between calculated and measured calcite solubility was found thus allowing us using the modified PHREEQC database (Bénézeth et al., in preparation) for assessing the $\Omega_{CaCO_3}$ in experimental solutions.

The limited number of data points (typically 5-7) in each individual experiment did not allow rigorous quantification of *k* and *n* parameters (Eqn. 2). However, apparent precipitation rates ($R_i$) were calculated from the first derivative of the fluid phase Ca concentration with respect to time, using:

$$R_i = \frac{d[Ca]}{dt}. \qquad (4)$$

Resulting precipitation rates are presented in Table 2.

**Table IV. 2. Rate of calcium carbonate precipitation by APB.**

| Bacteria A-20s | | | Bacteria S-17-65 | | |
|---|---|---|---|---|---|
| Number in the Table ESP 2 | R mM/hrs | $\Omega_{calcite}$ | Number in the Table ESP 2 | R mM/hrs | $\Omega_{calcite}$ |
| 1 | 0.0010 | 7.76 | 17 | 0.00005 | 44.7 |
| 2 | 0.0038 | 100 | 18 | 0.00000 | 70.8 |
| 3 | 0.0099 | 77.6 | 19 | 0.0120 | 123 |
| 4 | 0.0130 | 36.3 | 20 | 0.0110 | 132 |
| 5 | 0.00009 | 30.9 | 21 | 0.0120 | 91.2 |
| 6 | 0.0005 | 7.94 | 22 | 0.00000 | 61.7 |
| 7 | 0.0019 | 72.4 | 23 | 0.0020 | 30.9 |
| 8 | 0.0038 | 33.9 | 24 | 0.0030 | 33.1 |
| 9 | 0.0025 | 39.8 | 25 | 0.0060 | 104 |
| 10 | 0.0037 | 77.6 | 26 | 0.0080 | 155 |
| 11 | 0.0044 | 123 | 27 | 0.00000 | 53.7 |
| 12 | 0.0004 | 38.0 | 28 | 0.0260 | 25.7 |
| 13 | 0.0020 | 66.1 | 29 | 0.0130 | 151 |
| 14 | 0.0020 | 83.2 | | | |
| 15 | 0.0088 | 239 | | | |
| 76 | 0.0010 | 97.7 | | | |
| 77 | 0.0010 | 102 | | | |
| 78 | 0.0010 | 112 | | | |

# 3. Results and discussion

91 precipitation experiments were performed to investigate the influence of physical, chemical and biological conditions on the nucleation and precipitation of $CaCO_3$ by both APB species (Table 1). These included 30 biotic experiments in growth medium, 28 experiments with $NaN_3$-inactivated bacteria and 14 abiotic experiments in growth media (with heat-killed bacteria, with live bacteria in the darkness, and without bacteria). Another 19 experiments were conducted in the inert electrolyte (organic-free electrolyte) with live and dead bacteria. About 30% of experiments were performed in duplicates and triplicates; typical experimental reproducibility in terms of Ca and DIC concentration was 10-20%. The list of conducted experiments and the range of investigated conditions are given in Table 1.

## 3.1. Bacterial biomass development

Bacterial growth in the nutrient medium included four consecutive phases: i) the latent phase when the bacteria adapt themselves to growth conditions, ii) exponential phase corresponding to active cell division, iii) stationary phase when the growth rate slows down as a result of nutrient depletion and accumulation of toxic products and the biomass remains constant, and iv) final death phase, marked by a decrease of cell concentration. The growth curves of APB A-20s and S-17-65 cultures in 10 mM $NaHCO_3$ and different $CaCl_2$ concentrations and in 5 mM $CaCl_2$ and different $NaHCO_3$ concentration are presented in Fig. 1. It can be seen from these figures that the growth curves are quite similar for different $CaCl_2$ and $NaHCO_3$ concentrations suggesting neither inhibition nor promotion of the cell growth by components of carbonate systems within the studied range of solution parameters. Note that the growth of both cultures in 2 and 10 times diluted nutrient solution was not achieved; as such, all kinetic experiments were conducted in normal growth media but depleted in phosphate to avoid Ca phosphate precipitation.

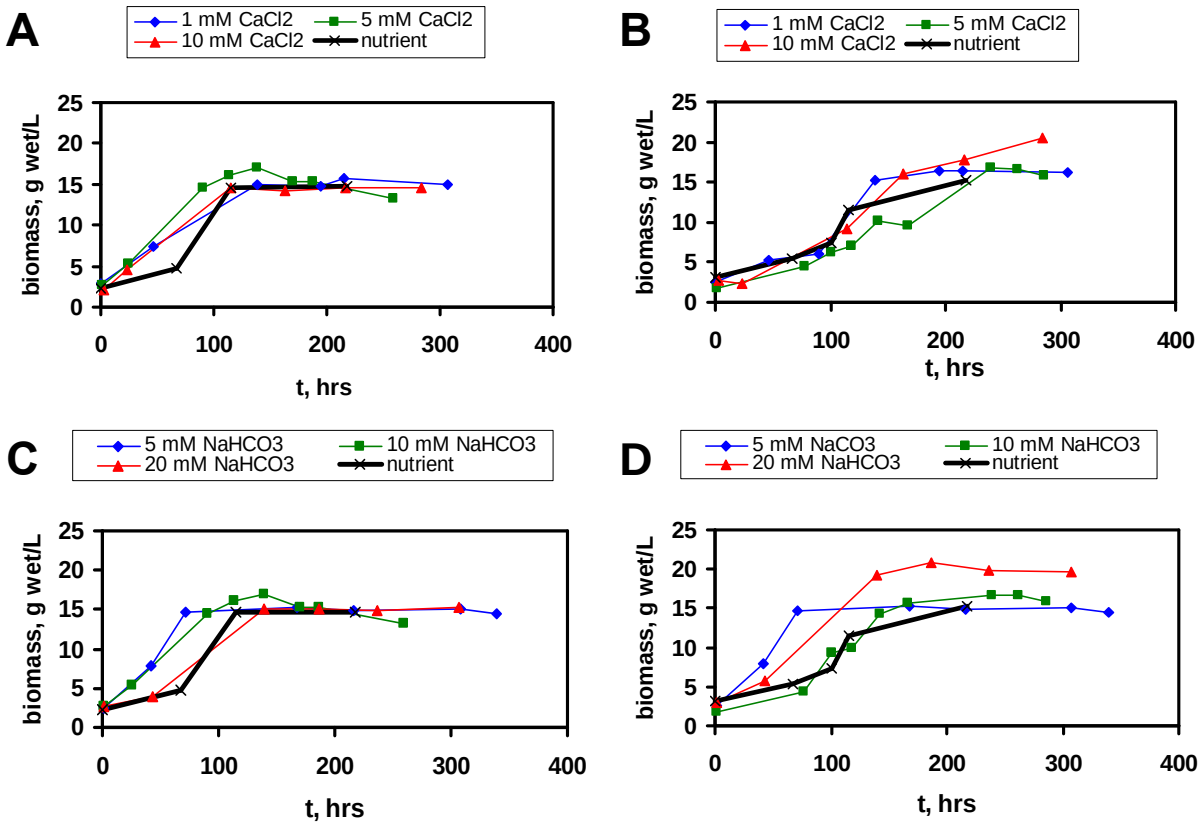


**Fig. IV. 1. Kinetic of APB A-20s (A, C) and S-17-65 (B, D) growth in the nutrient medium and in the kinetic experiments. Conditions of kinetic experiments: (A, B) 10 mM $NaHCO_3$, pH = 7.7 to 9.1; (C, D) 5 mM $CaCl_2$, pH = 7.7 to 9.4.**

### 3.2. Ca incorporation by APB cells

There exist 3 possible sinks of Ca in bacteria – solution system: (1) metabolic intracellular incorporation during growth, (2) reversible adsorption at the cell surface, and (3) calcium precipitation in the form of $CaCO_3$. To characterize the Ca metabolic uptake by both APB strains, Ca concentration evolution was followed in the experiments with nutrient solution, containing 0.3 and 1.0 mM Ca, for A-20s and S-17-65, respectively, where $CaCO_3$ precipitation did not occur. The results of these experiments are presented in Appendix 3 (Experiments 16, 17 and 30, hereinafter all experiments numbers from Table in Appendix 3). It can be seen from Table in Appendix 3 that there is an increase of the biomass (up to 18 $g_{we}t$/L) and pH (up to 9.1) during growth of both bacteria. At the same time, only small

decrease of calcium concentration (< 0.1-0.2 mM) is observed whereas the DIC concentration remains constant or slightly increases, indicating the absence of carbonate mineral precipitation. We believe that observed Ca concentration decrease is due to Ca adsorption plus intracellular incorporation; note that in $NaN_3$-inactivated suspension, no [Ca] decrease was observed (Experiments 45, 58). The maximal amount of calcium that active bacteria are capable of uptake during their growth can be calculated from the difference between the initial and final Ca concentration normalized to final cell biomass:

$$[Ca]_{uptake} = ([Ca]_{initial} - [Ca]_{final}) / biomass_{final} \quad (5)$$

For A-20s and S-17-65 cultures, maximal incorporation of calcium in the cells at our experimental conditions is equal to 12.7 ± 0.3 and 7.37 ± 0.34 µmol Ca /$g_{wet}$, respectively.

### 3.3. Mineral precipitation in biotic and abiotic experiments

Calcium carbonate precipitation in nutrient medium was evidenced by [Ca] decrease and also supported by microscopic examination of mineral phases. A typical plot of Ca concentration as a function of time in biotic and abiotic experiments is presented in Fig. 2. It can be seen from this figure that decrease of the aqueous calcium concentration is observed only in biotic experiment. No precipitation occurred in abiotic experiments, including those with heat-killed and $NaN_3$-inactivated bacteria, without bacteria, with live bacteria in the darkness, and with live bacteria in the inert electrolyte. Three experiments with live culture A-20s in the inert electrolyte (Experiments 76-78) also produced Ca carbonate as follows from Ca concentration evolution. This likely stem from the presence of intracellular nutrient resources that allowed bacteria to effectively metabolize and raise $\Omega_{CaCO_3}$ even in nutrient-free solutions.

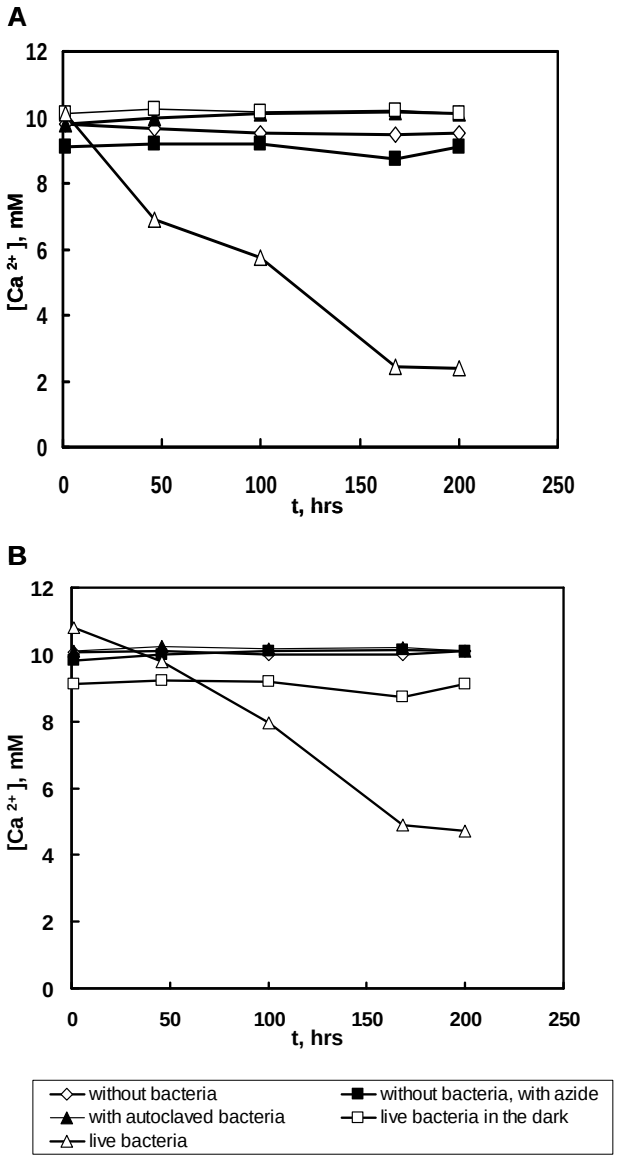


**Fig. IV. 2. Temporal evolution of the aqueous calcium concentration during biotic and abiotic experiments with *Rhodovulum* steppense A-20s (A) and *Rhodovulum* sp. S-17-65 (B) in nutrient medium. Initial experimental conditions: 10 mM $CaCl_2$ and 5 mM $NaHCO_3$.**

### 3.4. Characterization of solid phases

In the course of experiments, visual precipitates were formed on the glass walls of reactors after 5-7 and 7-9 days for A-20s and S-17-65, respectively. The XRD analysis of

biotic precipitates formed in nutrient-free inert electrolyte yielded calcite and vaterite as the main mineral phases of both APB species. The SEM images of the crystals are illustrated in Fig. 3A-D. Note that the mineral formation in the inert electrolyte was observed only in experiments with high initial biomass concentration (16 - 18 $g_{wet}$/L) with A-20s strain (Experiments 73-78). Calcite supersaturation degree in these experiments decreases from 53-135 at the beginning to 13-52 at the end of experiments. During these experiments, no change of the biomass concentration occurred indicating the lack of bacterial development in the absence of nutrients. Note that solution parameters ([Ca], alkalinity) in nutrient-free experiments with low initial biomass (2 - 3 $g_{biomass\ wet}$/L, Experiments 79-85, 86-87) remained constant and no calcium carbonate precipitation occurred. Significant pH and $\Omega_{CaCO_3}$ decrease (from 8.6-8.9 to 8.7-7.7 and 130-30 to 115-3, respectively) were measured for these nutrient-free experiments with both APB cultures.

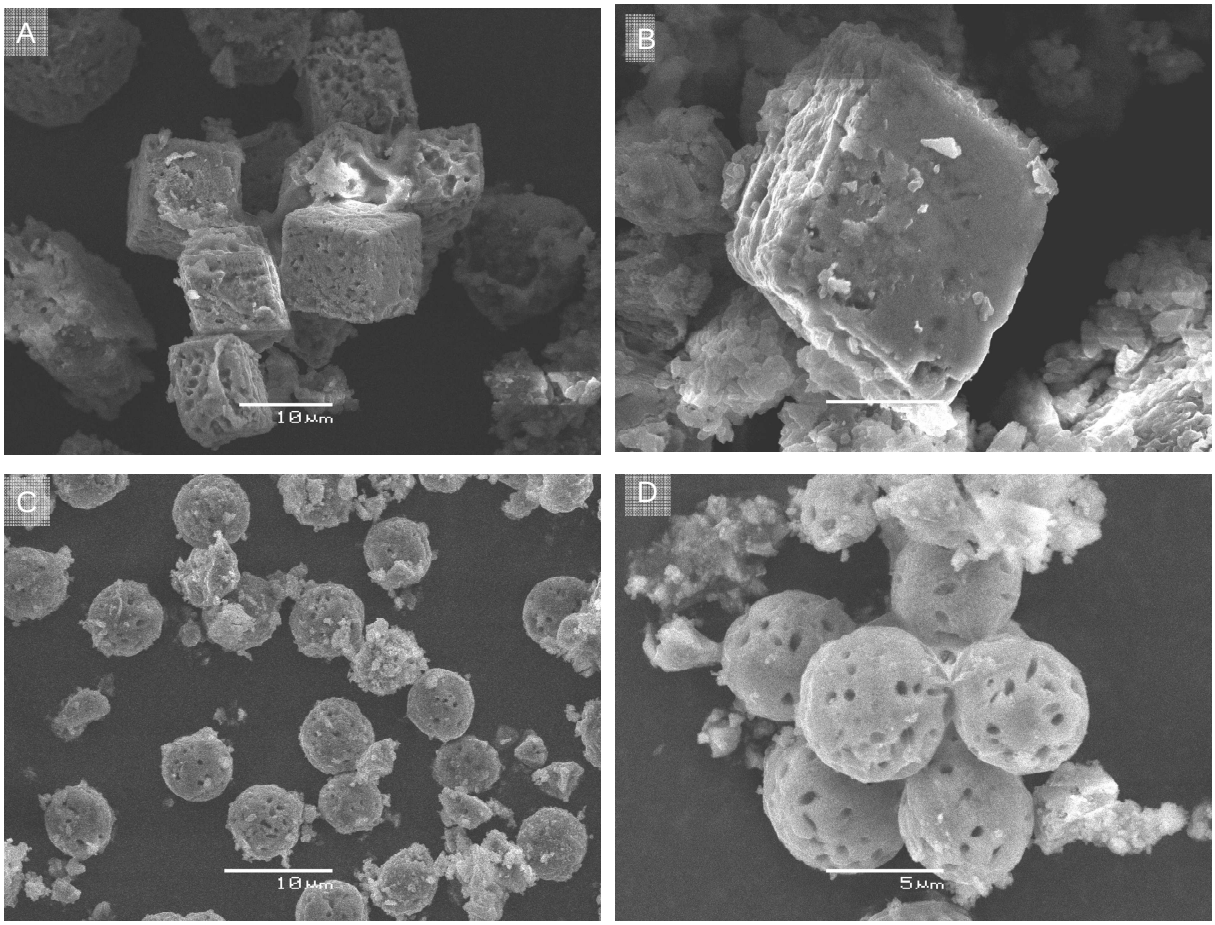


**Fig. IV. 3. SEM image of a precipitate collected from experiments performed in inert electrolyte (0.1 M NaCl) with APB A-20s in the presence of 5 mM $NaHCO_3$ and 10 mM $CaCl_2$ (A, B) or 20 mM $CaCl_2$ (C, D). A and B: calcite (Experiment 76, Table 1), C and D: vaterite (Experiment 78, Table 1).**

Significant increase of the biomass linked to an increase of pH and a decrease of calcium and DIC concentrations was observed in nutrient-rich biotic experiments with both APB cultures (Experiments 1-30, Table 1). The SEM images of precipitates from experiments 7-11 and 23-26 are shown in Fig. 4 (A-E).

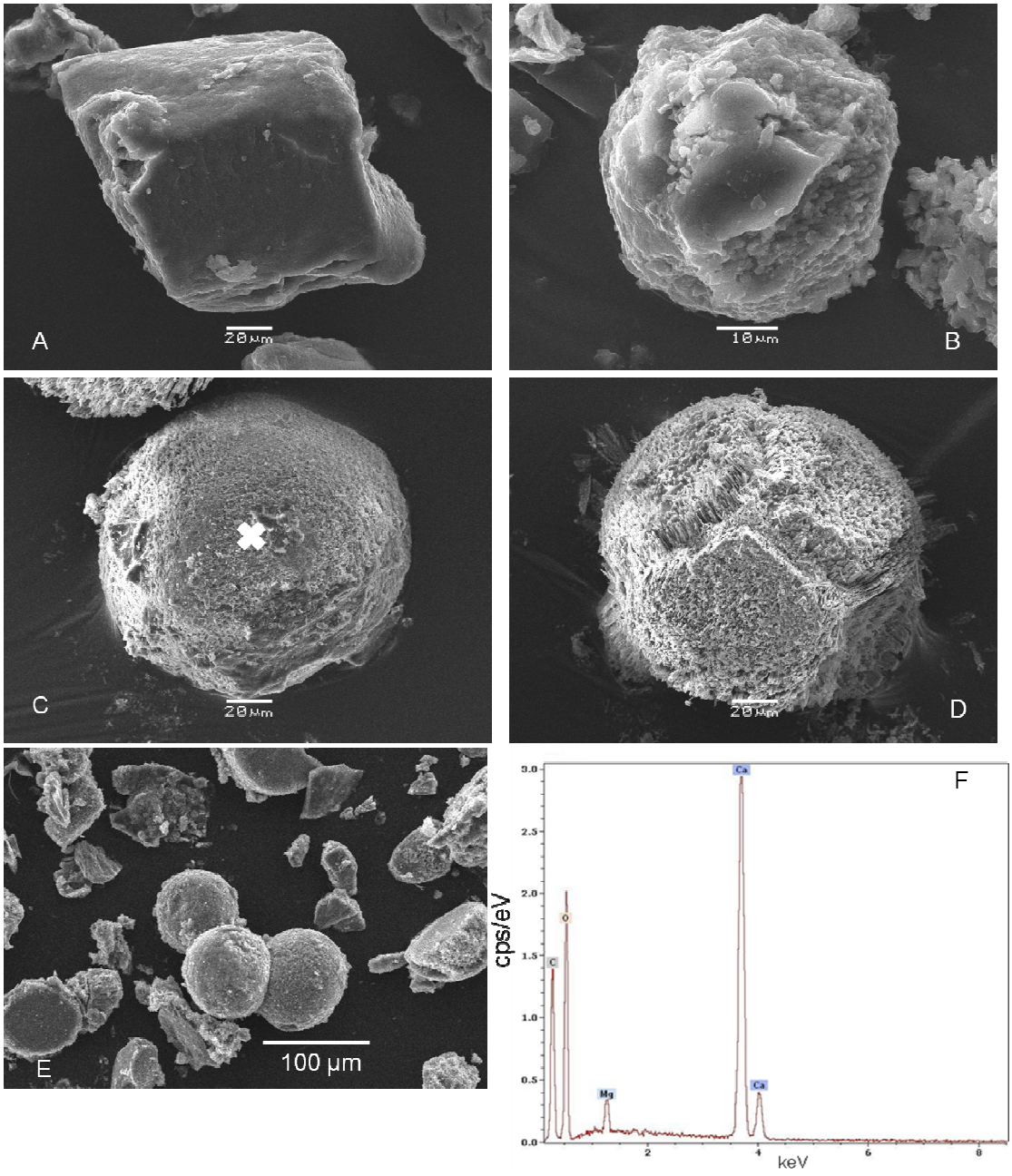


**Fig. IV. 4. SEM images of calcite formed in nutrient solution in the experiment with bacteria A-20s (A, B, E) and S-17-65 (C, D,). Initial experimental conditions: 5 mM $CaCl_2$ and 10 mM $NaHCO_3$ (A, C, E; Experiments 7-9 and 24-25 respectively, Table 1); 10 mM $CaCl_2$ and 10 mM $NaHCO_3$ (B, D, Experiments 10-11 and 26 respectively, Table 1). (F): Typical EDX spectrum of precipitate formed in nutrient solution in the experiment with bacteria A-20s (5 mM $CaCl_2$ + 10 mM $NaHCO_3$). The white cross in (C) indicates the position and approximate extent of the EDX analyses shown in (F).**

The elements detected by EDX (Fig. 4 F) on these crystals are mainly Ca, O and C with insignificant amount of Mg, P, N and S. The latter elements are likely to stem from contamination by the nutrient solution of the cell biomass. The XRD analysis of all precipitates showed only the presence of calcite for both APB species. The size and form of the crystals differ between experiments and during the course of the same experiment. There is no clear relationship between the experimental conditions and the shape and mineralogy (calcite vs. vaterite) of the crystals which is most likely linked to different rates of nucleation and crystal growth, accompanied by different transformation rate vaterite → calcite. Most precipitates range in size between 50 and 150 µm, having globular or rhombohedra shape with round edges and often associate in clusters (Fig. 4E).

Several experiments conducted at lowest calcium concentration (1 mM) with A-20s (Experiments 1, 5, 12, with $\Omega_{CaCO_3}$ (initial) ~ 25) yielded monohydrocalcite as evidenced by XRD analysis. The precipitates form spherical associates of 60-80 µm overall size (Fig. 5A).

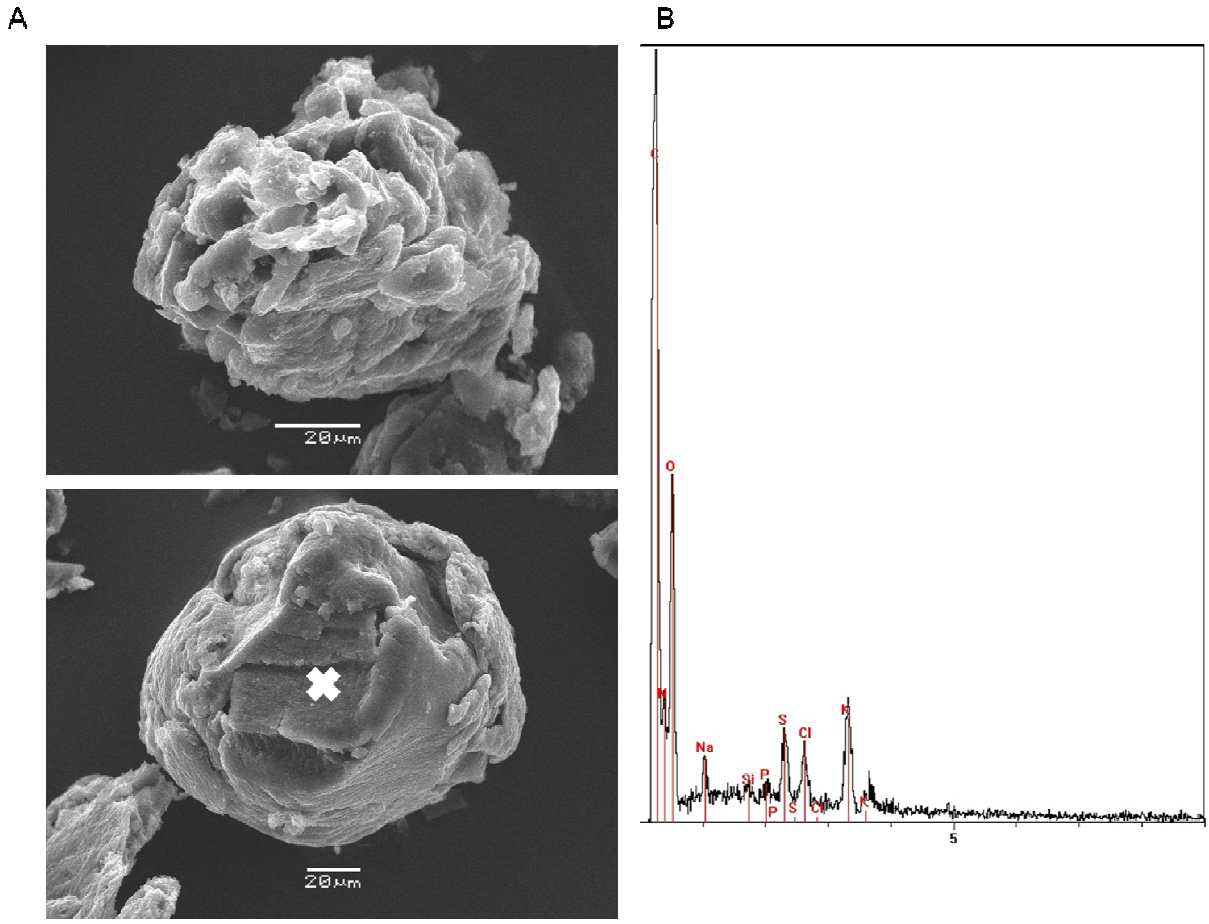


**Fig. IV. 5. (A) SEM images of monohydrocalcite formed in nutrient solution in the experiment with bacteria A-20s. Initial experimental condition: 1 mM $CaCl_2$ + 10 mM $NaHCO_3$ (Experiments 5, 6, Table 1). (B) EDX image. The white cross in (A) indicates the position and approximate extent of the EDX analyses shown in (B).**

However, the chemical analysis demonstrated the presence of mainly C, O, P and S without significant amount of Ca on the surface (Fig. 5B). This result suggests that the crystals of monohydrocalcite are covered by organic matter such as extracellular polymeric substances (EPS). This organic layer could preserve the metastable monohydrocalcite from recrystallization into more stable calcite. Indeed, the presence of organic polymers is known to extend the lifetime of metastable amorphous calcium carbonate (DiMasi et al., 2006). In bacterial experiments with extensive EPS production, the carbonate grains growing within the EPS matrix lacked cleavage and angular surfaces (Bontognali et al., 2008). In addition, viscous organic matrix and organic acids are known to influence calcium carbonate crystal morphology with a tendency to form round shapes (Braissant et al., 2003).

TEM imaging and chemical analysis were performed on A-20s and S-17-65 samples to further explore the cell arrangement and surface morphology linked to calcite precipitation. TEM imaging and EDX analysis of active cells following their growth during 10 days in the control (nutrient, mineral-free media) and calcite-supersaturated media are shown in Fig. 6 (A,B), 7(A,B) and Fig. 6 (C,D), 7(C,D). The elements detected on these cells and around with EDX are mainly C and O with some S, Si, P, Cl, and Na. No Ca was detected on these surfaces. It can be seen from these figures that the cell remains intact and perfectly preserve their shape and spatial organization. The surfaces remain clean, without traces of any mineral precipitate, except the presence of dark organic matter of extracellular origin or as cell debris. These observations suggest that calcium carbonate does not nucleate on live APB cell surfaces. The absence of Ca in the vicinity of live photosynthesizing cells was recently evidenced during calcium carbonate precipitation by cyanobacteria *Synechococcus* sp. and *Plantotrox* sp. (Martinez et al., 2010). This is also consistent with the result of Aloisi et al. (2006) who observed calcium carbonate precipitation on extracellular polymeric substances (EPS) released by heterotrophic sulfur reducing bacteria, rather than on the active cell surface itself.

### 3.5. Three stages of $CaCO_3$ precipitation by APB

In most experiments the precipitation process can be broken down into three stages: (1) initial pH-rise and Ca concentration decrease period, (2) significant biomass production

and massive precipitation reaction, and (3) a steady-state phase of culture development and solution equilibration with mineral. Examples of these stages are illustrated in Fig. 8.

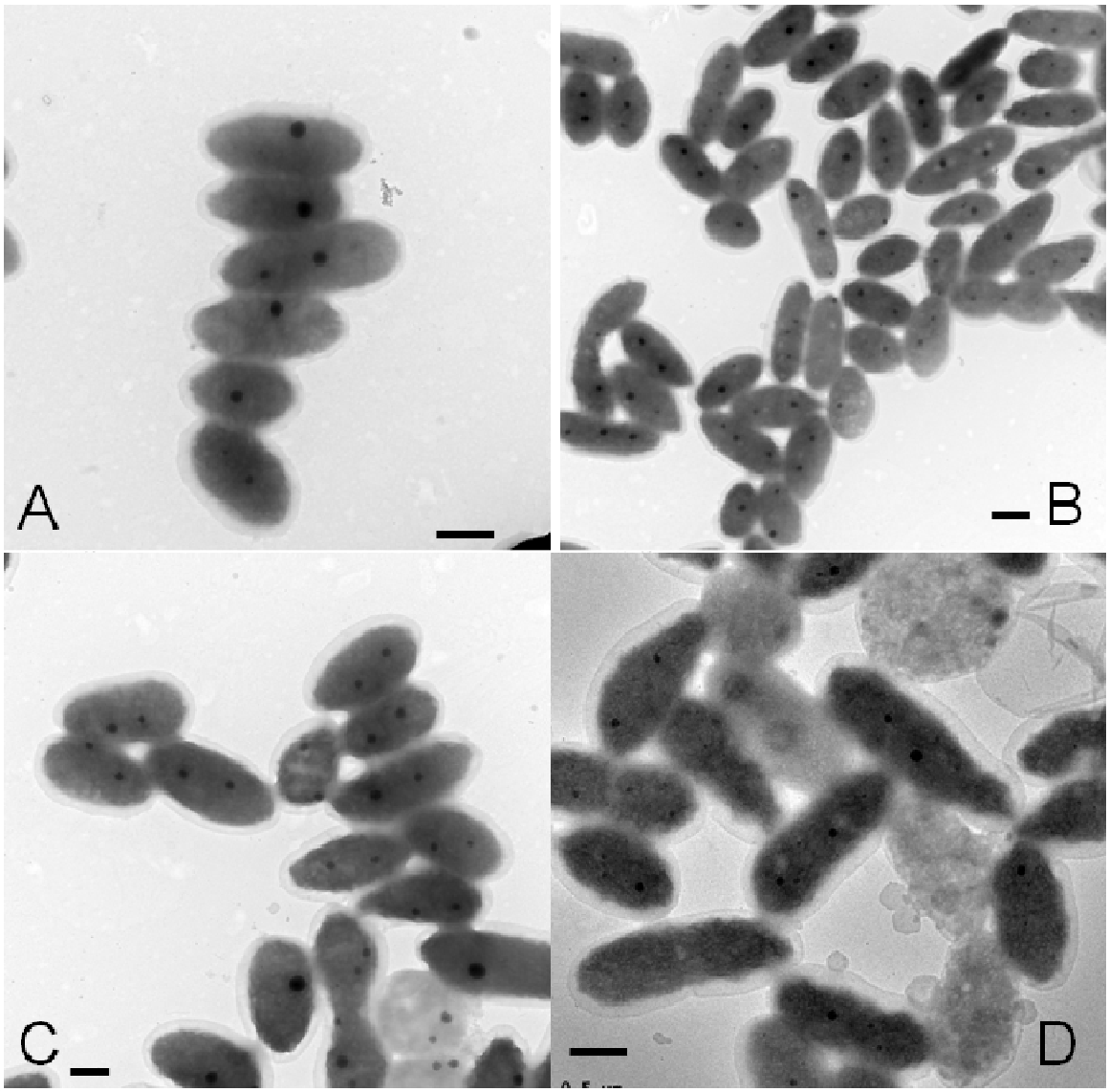


**Fig. IV. 6. TEM images of active A-20s in nutrient ($CaCO_3$-free) solution (A,B) and media supersaturated with respect to calcite (C,D) (Experiments 10, 11, 26). The black scale bars are 0.5 µm. No calcium carbonate is observed on the cell surfaces and around cells. Different cells color (C,D) indicate different stage of cells development.**

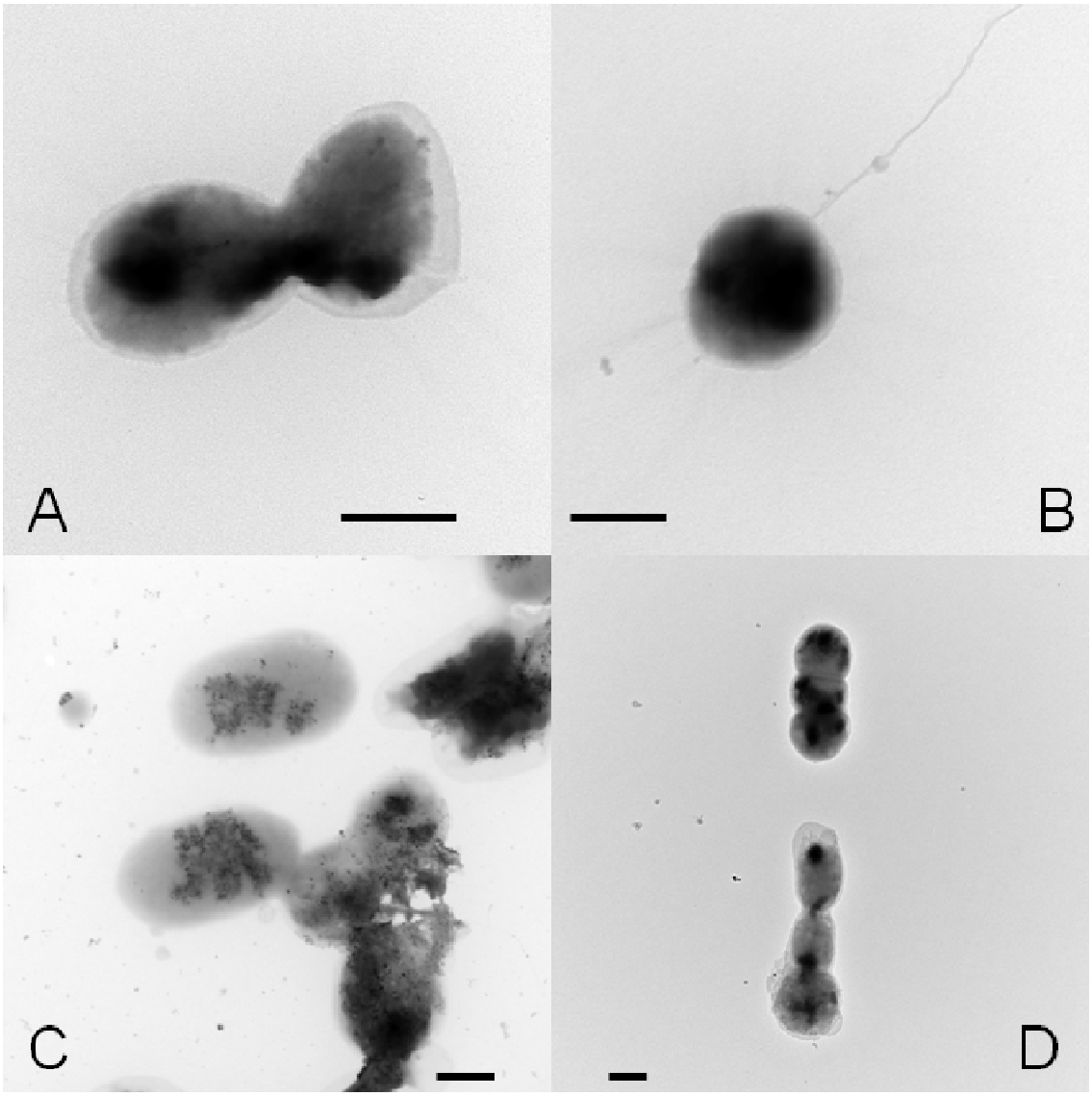


**Fig. IV. 7. TEM images of active S-17-65 in nutrient ($CaCO_3$-free) solution (A,B) and media supersaturated with respect to calcite (C,D) (Experiments 10, 11, 26). The black scale bars are 0.5 µm. No calcium carbonate is observed on the cell surfaces and around cells. The black substance in the vicinity of cells (C, D) is organic matter.**

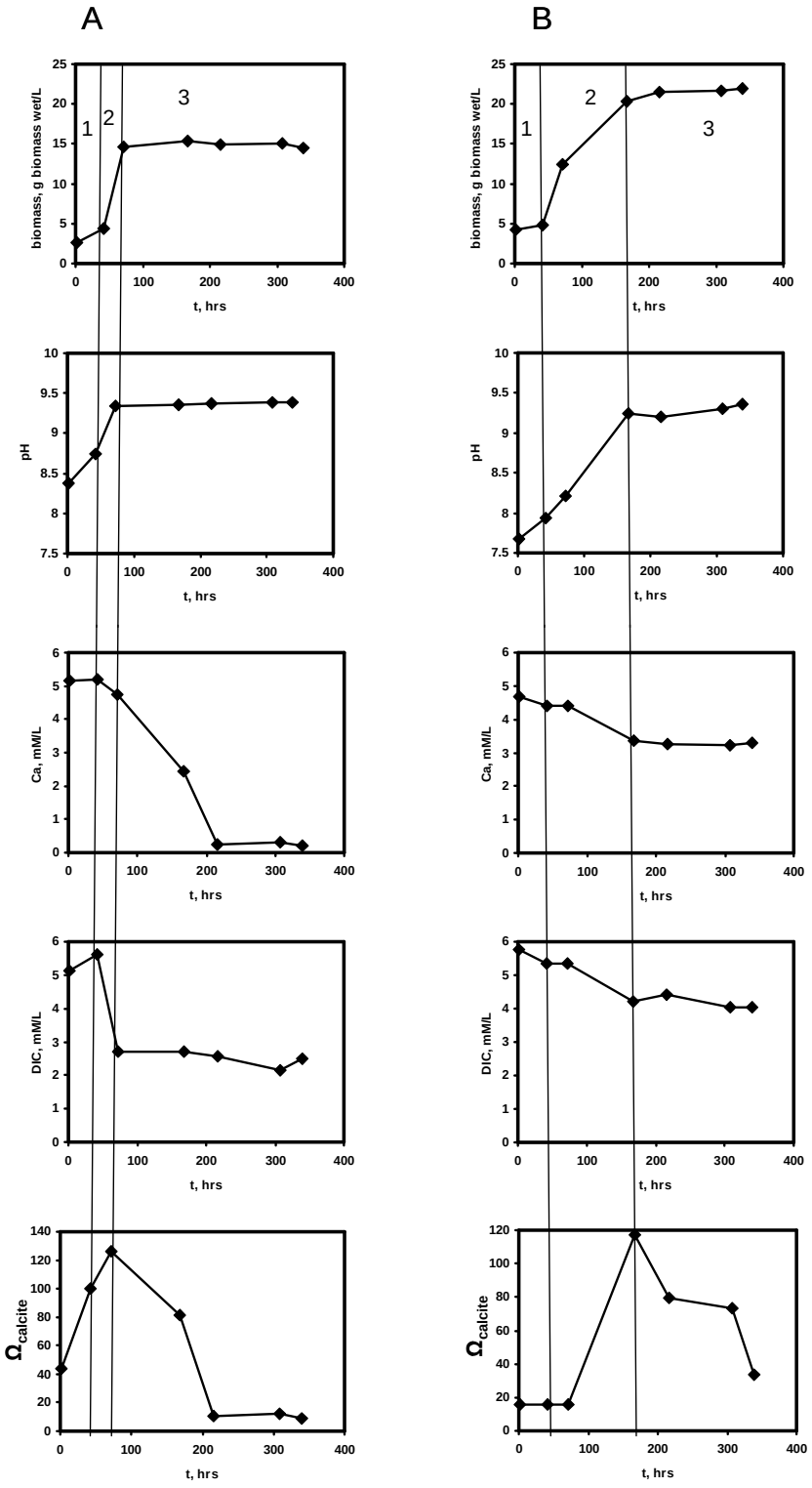


**Fig. IV. 8. Three phases of calcium carbonate precipitation by APB A-20s (A) and S-17-65 (B): (1) a pH-drift period, (2) the actual precipitation reaction, and (3) an equilibration phase.**

The first period lasts 40-100 hrs and is characterized by steady increase of bacterial biomass and pH increase from ~7.5 – 8 to some "critical value", between 8.5 and 9.2. During this period, Ca concentration slightly decreases whereas DIC concentration remains stable (e.g., experiments 1, 13, 15-18, 20, 21, 28, 30). It indicates that Ca removal from solution likely stem from Ca adsorption on the surface or intracellular uptake by live cells. The second period lasts 50-150 hrs and corresponds to exponential phase of culture growth; the pH increases to its maximal value (9.2-9.7 and 8.8-9.2 for A-20s and S-17-65, respectively), calcium and DIC concentrations abruptly decrease. There is much smaller relative [DIC] decrease compared to [Ca] decrease (a factor of 2 to 3) during experiments. The observed non-stoichiometry can be explained by $HCO_3^-/CO_3^{2-}$ production by APB during their metabolism or respiration. Overall, the evolution of solution composition strongly suggests that massive calcium carbonate precipitation occurs during the second period. Finally, after ~160 hrs of reaction, calcium and DIC concentration, pH and biomass achieve some steady-state values.

We observe dramatically different evolution of supersaturation degree with time between the two cultures (Fig. 9). In nutrient media with live A-20s cultures (Fig. 9A), values of $\Omega_{CaCO_3}$ decrease from 60-100 to 5-10. In the case of lower initial $\Omega_{CaCO_3}$ ($\leq$ 40), the bacteria increase the saturation index to 100-120 and then it decreases again to 20-40. In nutrient media with inactivated A-20s or in the inert electrolyte with live strain, there is a steady decrease of $\Omega_{CaCO_3}$ with time, mostly due to solution pH decrease. In contrast to alkaliphilic strain A-20s, the neutrophilic strain S-17-65 always increases $\Omega_{CaCO_3}$ from c.a. 10-30 to 100-120 whereas in the inert electrolyte and in the nutrient solution with $NaN_3$-inactivated cells, the supersaturation degree remains very high over full duration of the experiment, up to 80-120 (Fig. 9B).

Calcite supersaturation index is the result of combination of a number of solution characteristics (pH, [Ca], [DIC], salinity, presence of organic ligands). For the studied APB, the main governing factor of $\Omega_{CaCO_3}$ evolution during experiments is the initial pH ($pH_{initial}$). For bacteria A-20s and S-17-65 the $pH_{initial}$ is equal to 8.2±0.3 and 7.7±0.3, respectively. As a result, at the same initial [Ca] and [DIC], the $\Omega_{initial}$ for bacteria S-17-65 is significantly lower than that for A-20s. Consequently, in most experiments with A-20s calcium carbonate precipitation starts much earlier than that with S-17-65 strain. The latter have to increase $\Omega_{calcite}$ to some critical value (around 100-150) to initiate calcium carbonate precipitation.

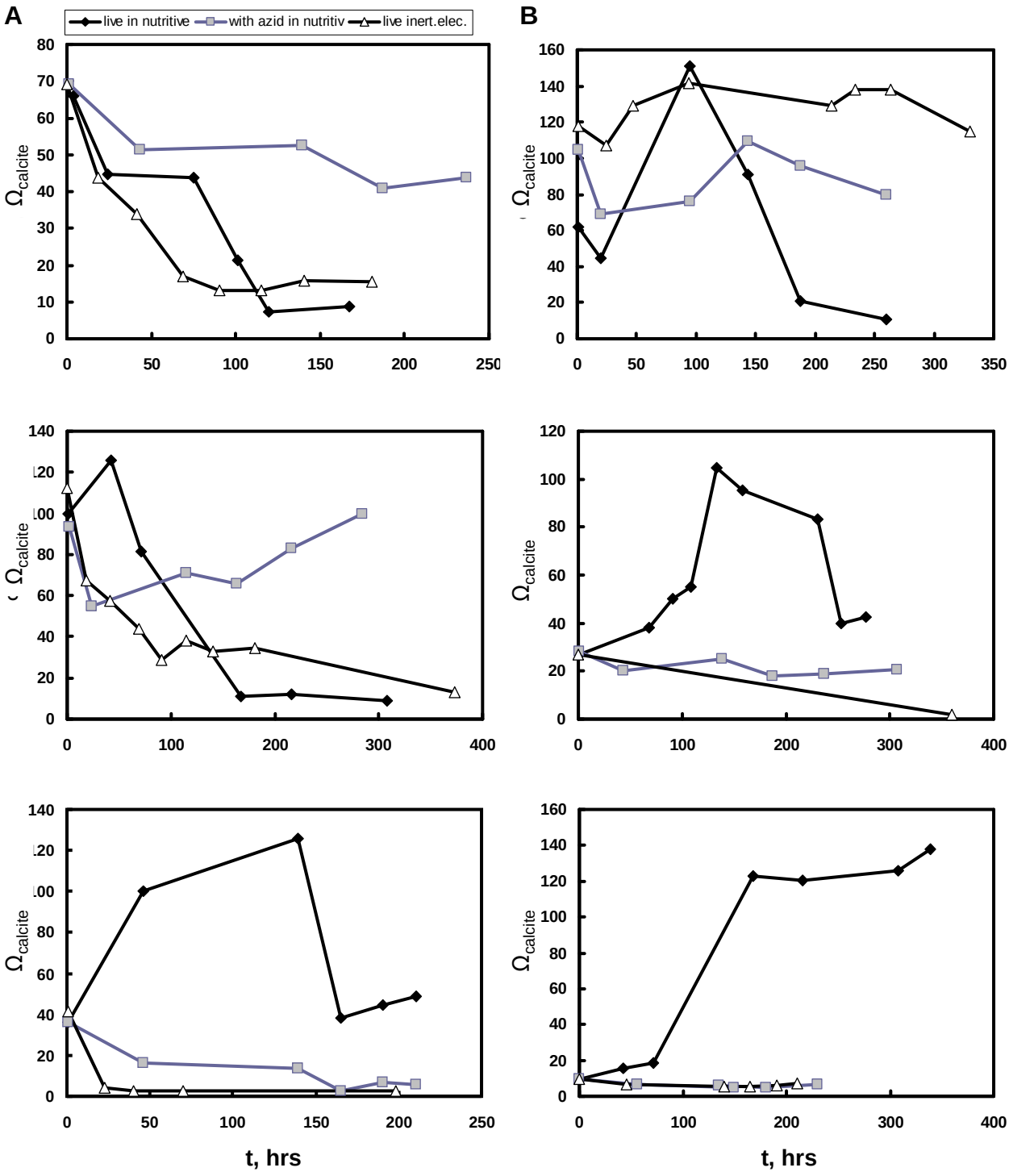


**Fig. IV. 9. $\Omega_{CaCO3}$ dependence on elapsed time during biotic and abiotic experiments. Column (A) A-20s; column (B) S-17-65.**

It can be seen from Fig. 8 that the maximal rate of calcium removal from solution corresponds to the sharp increase of the biomass during the first 100 hrs before the stationary

phase of culture development. This indicates that calcium carbonate formation is strongly controlled by the concentration and activity of bacterial cells. Note again that this [Ca] decrease is unlikely to be linked to Ca uptake by bacterial surface. Indeed, with an overall biomass increase of approximately 10 $g_{wet}$/L and typical Ca adsorption density of 20-30 µmol Ca/$g_{wet}$ (Bundeleva et al., 2011), this yields 0.2-0.3 mM Ca decrease, which is significantly smaller than the overall Ca decrease in experiments (typically from 1 to 10 mM). The amount of Ca incorporated in the cells is on the order of 10 µmol/$g_{wet}$ or maximum 0.1 mM at 10 $g_{wet}$/L of biomass (section 3.2).

Note that similar periods were observed in other experimental studies on calcium carbonate precipitation by green algae (Hartley et al., 1995), cyanobacteria (Dittrich and Obst, 2004), and heterotrophic bacteria (Ferris et al., 2004; Mitchell and Ferris, 2005). The rate of pH increase varied from one species to another depending on the relative growth rate of bacterial. As a general trend, there was a correlation between the degree of pH increase and the cell number in the suspension (Dittrich et al., 2004). For APB, we observe a clear correlation between the absolute increase of bacterial biomass ($g_{wet}$) and the amount of precipitated $CaCO_3$ (mM) for both bacterial species illustrated. The slope of dependence ranges from 0.1 to 0.8 and 0.1 to 0.5 for A-20s and S-17-65, respectively depending on the $CaCl_2$ and DIC concentrations. This dependence allows a first-order evolution of the quantity of $CaCO_3$ as a function of bacterial productivity rate at studied conditions.

### 3.6. Kinetics of calcium carbonate precipitation by APB.

We calculated apparent rates of $CaCO_3$ precipitation from the experimental slope of [Ca] vs. times at the second stage of reaction corresponding to massive $CaCO_3$ formation (zone 2 in Fig. 8). Apparent precipitation rates measured at 150±20 hrs after the beginning of experiment range between 0.001 and 0.010 mM/hr, and between 0.005 and 0.015 mM/hr for A-20s and S-17-65 APB cultures, respectively. For comparison, the rate of $CaCO_3$ precipitation during bacterial ureolysis by *Bacillus pasteurii* is 0.011 mM/hr (Mitchell and Ferris, 2005), and during photosynthesis of cyanobacteria *Synechococcus sp.* and *Planktothrix sp.* is 0.030 and 0.036 mM/hr, respectively (Martinez et al., 2010). Noteworthy that bacterial calcification rates are 2 to 3 orders of magnitude higher than those of microorganisms largely responsible for $CaCO_3$ formation on the Earth – calcareous algae such as *Halimeda,*

*Penicillus* and *Udotea*. For these algae, typical calcification rates range between 0.00005 and 0.0005 mM/hr (0.1 to 1.2 mg $CaCO_3$ $day^{-1}$) (Ries, 2010).

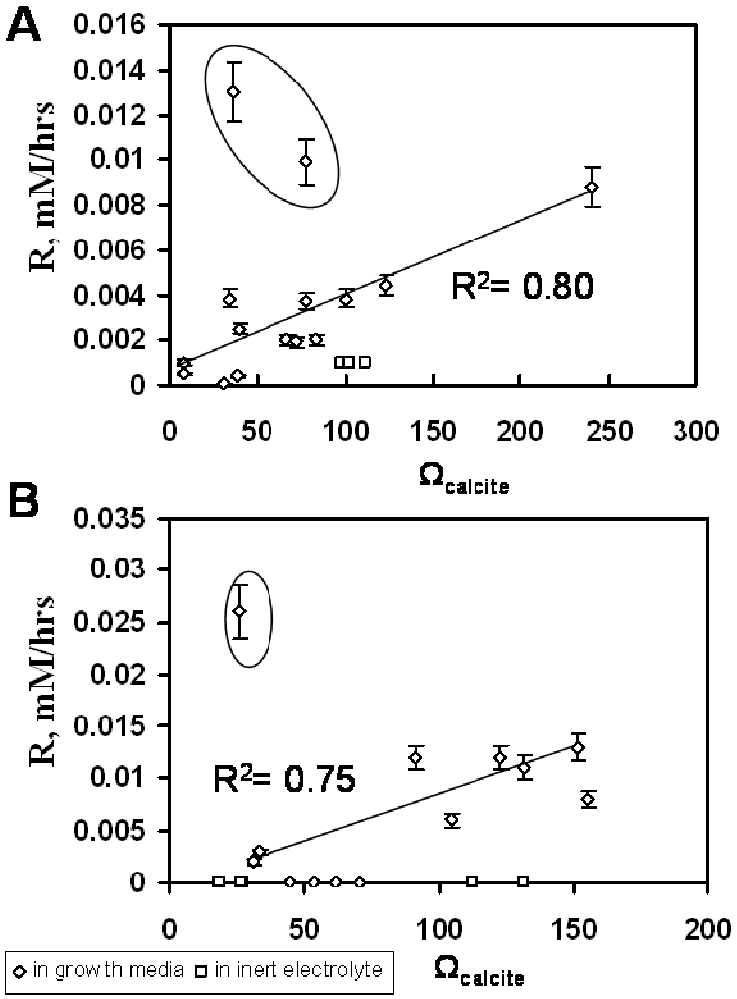


**Fig. IV. 10. Dependence between the apparent rate (calculated for period 2 in Fig. 6) of calcium carbonate precipitation by APB A-20s (A) and S-17-65 (B) and the saturation index of calcite.**

The dependence between calcium carbonate precipitation rate and calcite saturation state measured at the beginning of calcium concentration decrease after (40-100 hrs of reaction) is shown the Fig. 10. There is significant correlation between these parameters for both bacterial species ($r^2$ = 0.80 and 0.75 for A-20s and S-17-65, respectively). For A-20s culture, two experiments (Experiments 3 and 4) deviate significantly from the linear dependence (encircled in Fig. 10A). They show a factor of 3 to 5 higher precipitation rate at the same saturation degree ($\Omega_{CaCO_3}$ (1) = 40-45). These two experiments were conducted at the same initial conditions ([Ca]=10 mM, [DIC]=5 mM). For S-17-65 strain, one experiments (Experiment 19) performed at the same solution composition exhibit a factor of 10 higher

apparent rates compared to the general trend. Therefore, the saturation degree alone does not control the overall precipitation rate. Apparently, the minimal $NaHCO_3$ and maximal $CaCl_2$ concentrations are the optimal factors of both inorganic precipitation and biological activity (cell growth) creating sufficient number of nucleation sites. As an empirical rule, low [DIC] ($\leq$ 5 mM) is most favorable for significant pH and $\Omega_{CaCO_3}$ rise at the beginning of reaction promoting fast massive $CaCO_3$ formation. As such, $CaCO_3$ precipitation in studied bacterial systems is controlled by a complex interplay of physico-chemical and biological factors. In particularly, detailed analysis of $\Omega_{CaCO_3}$ - rate dependencies at constant $\Omega_{CaCO_3}$ and various Ca and DIC values demonstrate that [DIC] or [Ca] alone are not able to control overall precipitation rates by the APB. But there is a pH value around 8.5 above which the live cell precipitate $CaCO_3$ where as the dead and inactivated cells exhibit zero precipitation rate below pH 8.5. It follows that the elevated pH is important prerequisite for live APB to form $CaCO_3$ even at high supersaturation degrees.In fact, high DIC concentration precludes sufficient pH rise during photosynthesis and hampers massive $CaCO_3$ precipitation. This result corroborates the observations of the lack of carbonate precipitation in microbial mats in strongly alkaline environments (e.g., Arp et al., 1999a, b). The paucity of $CaCO_3$ precipitation in solutions having [DIC] $\geq$ 20-40 mM provides important constrains on the possibility of APB calcification under early soda ocean scenario (Kempe and Kazmierzhak, 1990; Kempe and Degens, 1985).

Overall, we can conclude that high rate of carbonate precipitation results from combination of favorable inorganic and biological conditions which are similar for both APB species. Curiously, these conditions (5 mM DIC, 10 mM Ca) are the closest to modern seawater composition (2.3 mM DIC, 10 mM Ca). Note that, similar to any other experimental work on biocalcification with bacteria that use the organic substrates, the final chemical composition of the media (pH and, therefore, supersaturation degree) depends on the nature of initial organic compound. The use of acetate by APB provokes significant alcalinization of the media and thus, massive $CaCO_3$ precipitation. We believe that these conditions, which are necessary to provide sufficient biomass growth and to quantify the rates, are nevertheless applicable to natural settings of essentially alkaline environments of studied bacteria. The similarity of apparent calcification rates between two contrasting species further confirms the validity of laboratory approach.

### 3.7. APB cell protection against $CaCO_3$ incrustation?

The first main result of the present study is that the actively growing APB's are capable of increasing pH and supersaturation of solution thus inducing calcium carbonate precipitation. Dead (heat-killed) and metabolically inactive bacteria are not capable of precipitating $CaCO_3$ in the full range of studied conditions (pH of 7.5 to 9.5; Ca of 0.3 to 10.7 mM, DIC of 4.5 to 45 mM) at comparable values of $\Omega_{CaCO_3}$ (40 to 100). Some earlier works (e.g., Braissant et al., 2003; Bosak and Newman, 2005, Gautret et al., 2006) suggested that actively growing bacteria consume various nutrients from solution, especially those capable of inhibiting mineral precipitation such as phosphate. As a result, precipitation in bacterial culture may simply happen due to removal of $CaCO_3$ inhibitor via cell metabolism. We do not expect this mechanism to occur under the conditions of our experiments. Indeed, there was no measurable $CaCO_3$ precipitation in nutrient (inhibitor)-free solutions at $\Omega_{CaCO_3}$ values comparable to those of nutrient-rich solutions (40 to 120) as illustrated in Fig. 9. Moreover, results of this work unambiguously demonstrate the capacity of live APB to precipitate $CaCO_3$ during their growth, whereas inactivated and dead cells could not appreciably decrease Ca concentration at similar supersaturation degree but lower pH in the nutrient media.

Plotted in Fig. 11 are the apparent bulk precipitation rates as a function of solution pH at the end of 2$^{nd}$ stage of $CaCO_3$ precipitation (zone 2 in Fig. 8). It can be seen that there is a "threshold" pH value around 8.5 above which the live cell precipitate $CaCO_3$ where as the dead and inactivated cells exhibit zero precipitation rate below pH 8.5. It follows that the elevated pH is important prerequisite for live APB to form $CaCO_3$ even at high supersaturation degrees.

The possible presence of the EPS in the vicinity of live cell surfaces (as it is visible on the TEM images of A-20s and S-17-65 strains, Fig. 6 and Fig.7, respectively) does not seem to be an inhibiting factor of $CaCO_3$ precipitation by both studied *Rhodovulum* species, in accord with recent results on other APB species, *Rhodopseudomonas palustris* (Bosak et al., 2007).

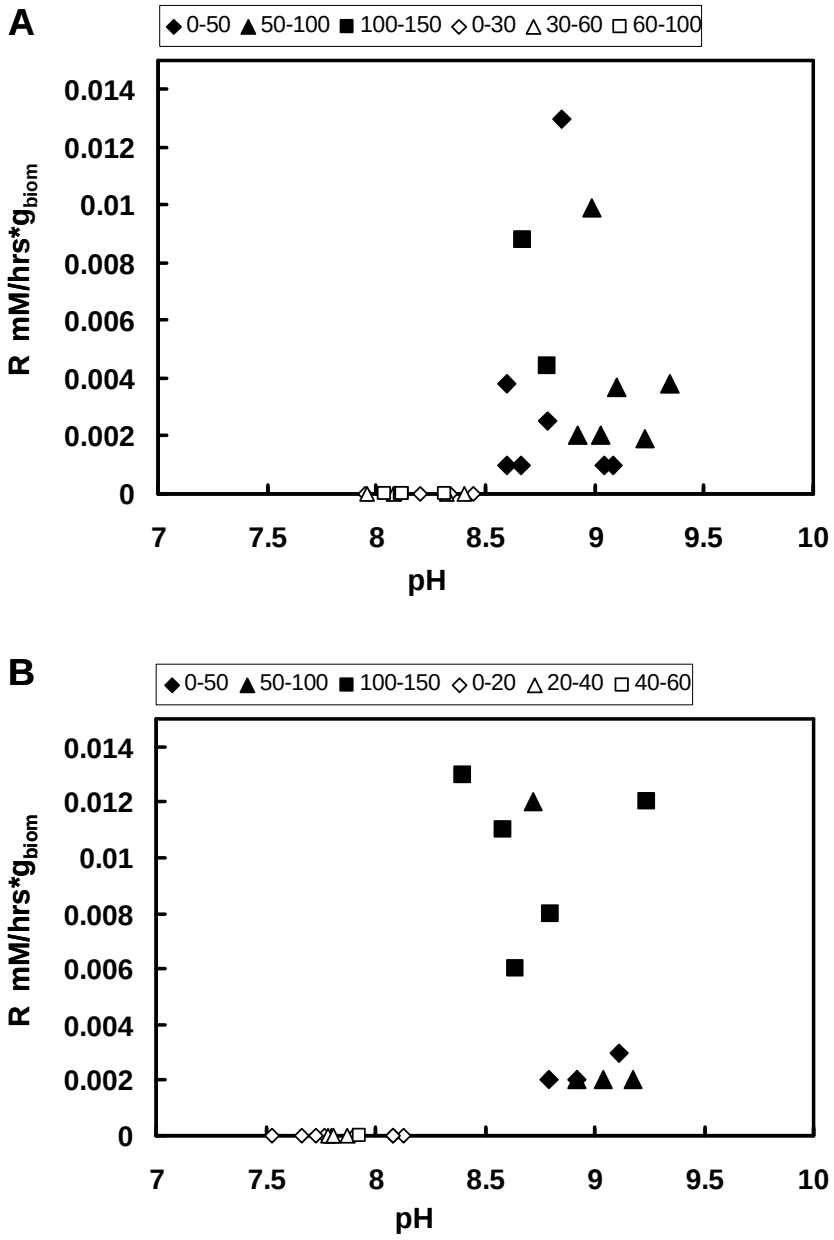


**Fig. IV. 11. Apparent bulk precipitation rates as a function of solution pH at the end of 2$^{nd}$ stage of $CaCO_3$ precipitation (zone 2 in Fig. 8). All experiments are performed in nutrient solution with A-20s (A) and S-17-65 (B) strains. Different symbols correspond to different ranges of $\Omega_{CaCO_3}$ with closed and open symbols representing live and $NaN_3$-inactivated cultures, respectively.**

Interestingly the results shown in Fig. 10 do not demonstrate existence of a plateau of rate - $\Omega_{CaCO_3}$ dependence. What should be expected here is a decrease of cell growth at highest supersaturation due to progressive cell incrustation and decrease of nucleation center concentration. This strongly suggest that whether there is a cell protection mechanisms of live

calcifying APB, established recently for cyanobacteria (Martinez et al., 2010) and some heterotrophic sulfate reducing bacteria (Aloisi et al., 2006; Bontognali et al., 2008) or the precipitation of $CaCO_3$ occurs at a certain distance from the cell surface and the cells remain intact as also supported by TEM images presented in section 3.4.

The possible presence of cell protection mechanism for APB consisting of non-precipitation of $CaCO_3$ in the vicinity of live cells but only in the bulk solution is in accordance with previous studies of *Synechococcus* sp. and *Planktothrix* sp. cyanobacteria demonstrating the metabolic maintenance of a positive surface charge at alkaline pH for protecting active cell against Ca adsorption and subsequent calcite embedding (Martinez et al., 2010). Similarly, spectroscopic and microscopic observations suggested that precipitation of an amorphous $CaCO_3$ layer within the external EPS sheaths of cyanobacteria at a certain distance from the cell wall could serve as a protection mechanism against uncontrolled precipitation of a thermodynamically stable phase calcite on their surface (Obst et al., 2009a). Another well-documented mechanism allowing cyanobacteria to calcify in continuous regime is shed off of mineralized S-layers (Thompson et al., 1997; Douglas and Beveridge, 1998). Heterotrophic sulfate-reducing bacteria (SRB) *D. desulfuricans* were also demonstrated to avoid calcium carbonate encrustation with dead cells being more active promoters of heterogeneous nucleation from strongly supersaturated solutions compared to live cells (Bosak and Newman, 2003). Another SRB, *Desulfovibrio brasiliensis*, exhibited a self-preservation behavior against dolomite formation via secreting extracellular polymeric substances that were responsible for mineral nucleation and growth at microscopic distances from the cells (Bontognali et al., 2008). Similarly, calcium carbonate formation initiated on 60-200 nm-size EPS globules formed near the cells of *Desulfonatrum lacustre* SRB, but calcify significantly only when released to the culture medium (Aloisi et al., 2006).

Most previous works documented a cell-protection mechanism were conducted at initially strongly saturated solutions when both live and dead cells could serve as carbonate nucleation centers. A straightforward application of such experiments to natural environments is not warranted. In contrast, results of the present study demonstrate an unequivocal role of live bacteria for raising the solution pH, creating the supersaturation ($\Omega_{CaCO_3}$) in the course of bacterial growth (from 10-40 to 60-100) and thus fostering massive $CaCO_3$ nucleation. Note that the metabolic regulation of APB cell surface less-negative charge occurs at pH above 9.5 because there is an increase of zeta potential with a maximum value of -10 to -20 mV at a pH of 9 to 10.5) (Bundeleva et al., 2011). These solution conditions correspond to the period of

massive mineral precipitation. Therefore, we can conclude, that active APB can apparently protect themselves from carbonate incrustation by creating a more positive charge on their surface at the pH of massive $CaCO_3$ nucleation. Note that in the microbial consortia such as biomats, where cyanobacterial photosynthesis essentially regulates the *in-situ* pH above 10 (Jørgensen and Revsbech, 1983; Visscher and van Gemerden, 1991; Visscher and Stolz, 2005), the APB will certainly manifest their self-protection properties against mineral incrustation..

# Conclusions

This study reports the first results on $CaCO_3$ precipitation rates induced by two contrasting strain anoxygenic phototrophic bacteria, haloalcaliphilic *Rhodovulum steppens* A-20s and neutrophilic halophilic *Rhodovulum* sp. S-17-65 growing on organic substrates. The optimal initial precipitation conditions for both strains were as following: Ca = 10 mM; DIC = 5 mM , pH = 8.1±0.1 and $\Omega_{CaCO_3}$ = 70-100. At the main stage of massive $CaCO_3$ precipitation, the bulk rates range between 0.001 and 0.010 mM/hr, and between 0.005 and 0.015 mM/hr for A-20s and S-17-65 APB cultures, respectively, similar to cyanobacteria and heterotrophic bacteria and being 2 orders of magnitude higher than typical calcification rates of coralline algae. Measured bulk precipitation rates are unaffected, within the experimental uncertainty of 10-20%, by Ca adsorption at the cell surface and by intracellular Ca uptake during cell growth. The rates are positively correlated with $\Omega_{CaCO_3}$ , but detailed analysis of $\Omega_{CaCO_3}$ - rate dependencies at constant $\Omega_{CaCO_3}$ and various Ca and DIC values demonstrate that the [DIC] and [Ca] alone are not able to control overall precipitation rates by APB. There is a pH value around 8.5 above which the live cell precipitate $CaCO_3$ where as the dead and inactivated cells exhibit zero precipitation rate below pH 8.5. It follows that the elevated pH is important prerequisite for live APB to form $CaCO_3$ even at high supersaturation degrees.In case of dead and inactivated cells in nutrient media and for live cultures in nutrient-free electrolyte solution, precipitation of $CaCO_3$ did not occur despite significant supersaturation degree of solution. The most plausible scenario of massive $CaCO_3$ precipitation in the presence of growing APB is bulk solution pH raise due to bacterial metabolism followed by heterogeneous nucleation on cell debris and EPS of the live cells which serve as nucleation

centers, once the required pH and $\Omega_{CaCO_3}$ are attained. TEM analyses of reaction products does not demonstrate the presence of $CaCO_3$ crystals in the vicinity of live cells, yet calcite and monohydrocalcite were identified as main precipitates of the bulk solution. The results presented in this study suggest the existence of a mechanism preventing carbonate biomineral formation by active APB, which can protect them from carbonate incrustation by creating a more positive charge on their surface at the pH of massive $CaCO_3$ nucleation.

**Acknowledgments**

The authors thank Michel Thibaut and Thierry Aigouy for XRD and SEM analyses, respectively; Carole Causseran for help in Mg, DIC and DOC analyses; and Lucien Datas of the TEMSCAN unit at the University of Toulouse for his help with TEM/EDX methods.

# ESM 1. Solubility of calcite in nutrient media of APB.

Experiments on calcite solubility in nutrient solutions were aimed at verifying the correctness of ion activity product calculation (and, correspondently, $\Omega_{calcite}$) using conventional equilibrium speciation code in experimental solution containing high amount of organic ligands (up to 1 g/L acetate for A-20s strain), and high ionic strength (up to 2 M NaCl for S-17-65 strain).

Calcite ($CaCO_3$) dissolution experiments were carried out in the closed batch reactors. Altogether, three experiments (in duplicates) were performed: two experiments in nutrient solution of A-20s strain, with and without organic ligands addition (Exp. 1, and 2, respectively of the ESM Table 1) and experiment in nutrient solution of S-17-65 strain with organic ligands addition (Exp. 3 of ESM Table 1). Optical clear Iceland spar from Siberian traps almost free of impurities (see Pokrovsky et al., 2005) for analysis was used in concentration of 50 g/L. Experiments were performed in polypropylene flasks under continuous shaking at 25±0.5°C.

Reactive solutions of all experiments were regularly sampled, pH was measured and solution was filtered (0.45 µm) for analyses of pH, calcium, alkalinity and DIC concentrations as described in section 2.3. These measured solution parameters together with all other components of the system were used for calculation of calcite saturation degree using Phreeqc code with implemented Phreeqc Interactive 2.15.0 (llnl.dat) database (Bénézeth et al., 2011, in preparation).

The evolution of calcite saturation index with reaction time is demonstrated in Fig. ESM-1 and measured experimental parameters are listed in Table ESM-1. It can be seen from this figure that after 15-20 days the $\Omega_{calcite}$ value is stable and equal to 1±0.5 for all experiments. This result indicates that available solution speciation code is suitable for calcite saturation degree calculation without additional adjustment of the existing database with respect to activity coefficient calculation or the $Ca^{2+}$ complexation with dissolved organic ligands.

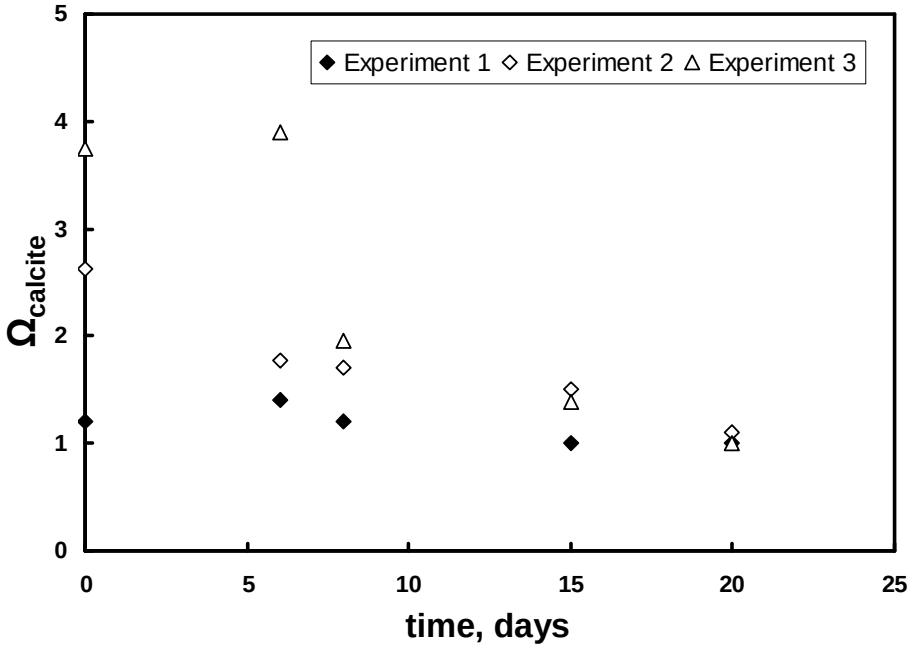


**ESM Fig. 1. The evolution of calcite supersaturation degree with time during representative experiments.**

**ESM Table 1. Results of experiment on calcite solubility measurements in nutrient media at 25±0.5°C.**

| № | t, days | pH | pH* | [Ca], mM | [Ca], mM* | Alk /DIC, mM | Alk/DIC, mM* | $\Omega_{calcite}$ | $\Omega^*_{calcite}$ |
|---|---|---|---|---|---|---|---|---|---|
| 1 | 0 | 8.23 | 8.24 | 0.090 | 0.083 | 45.67 | 45.13 | 1.2 | 1.0 |
| | 6 | 8.37 | 8.35 | 0.080 | 0.053 | 45.13 | 44.04 | 1.4 | 1.0 |
| | 8 | 8.34 | 8.38 | 0.075 | 0.047 | 44.81 | 43.28 | 1.2 | 1.0 |
| | 15 | 8.69 | 8.53 | 0.032 | 0.042 | 45.13 | 45.67 | 1.0 | 1.0 |
| | 20 | 8.62 | 8.48 | 0.034 | 0.037 | 44.81 | 43.28 | 1.0 | 1.0 |
| 2** | 0 | 8.20 | 8.18 | 0.084 | 0.073 | 45.13 | 45.13 | 2.6 | 2.2 |
| | 6 | 7.78 | 7.75 | 0.128 | 0.143 | 44.81 | 44.81 | 1.8 | 1.9 |
| | 8 | 7.63 | 7.57 | 0.166 | 0.190 | 45.13 | 43.28 | 1.7 | 1.7 |
| | 15 | 7.75 | 7.60 | 0.177 | 0.259 | 44.04 | 45.67 | 1.5 | 1.5 |
| | 20 | 7.84 | 7.82 | 0.136 | 0.196 | 45.67 | 43.28 | 1.1 | 1.2 |
| 3** | 0 | 8.22 | 8.23 | 0.387 | 0.449 | 4.34 | 4.45 | 3.8 | 3.6 |
| | 6 | 8.24 | 8.29 | 0.476 | 0.432 | 4.92 | 4.34 | 3.9 | 3.6 |
| | 8 | 7.14 | 7.72 | 0.765 | 0.559 | 4.75 | 4.45 | 2.0 | 1.4 |
| | 15 | 7.41 | 7.34 | 1.146 | 1.115 | 4.70 | 4.34 | 1.4 | 1.1 |
| | 20 | 7.26 | 7.81 | 1.158 | 1.161 | 4.81 | 4.70 | 1.0 | 1.0 |

*Replicate

**DIC measurements.

# Chapter V

# Experimental modeling of calcium carbonate precipitation by cyanobacteria *Gloeocapsa* sp.

# Résumé en français

Des expériences cinétiques en réacteurs fermés couplées à des analyses microscopiques au MEB, MET et aux rayons-X ainsi que des mesures d'adsorption de Ca à la surface des cyanobactéries ont été menées afin de mettre en évidence et de caractériser les processus métaboliques qui protégent les cyanobactéries *Gloeocapsa* sp. contre la précipitation de minéraux carbonatés à leur surface. Ces expériences cinétiques ont été réalisées dans des solutions initialement sursaturées (15.1-147.9) par rapport à la calcite à pH 9.0±0.4 et 25°C, en présence de cyanobactéries *Gloeocapsa* sp. actives.

Les résultats suggèrent que *Gloeocapsa* sp. prend part à la précipitation de $CaCO_3$. Les observations au MEB démontrent la présence de différents types de cristaux. Ceci indique que la précipitation se produit selon des processus différents: inorganiques (cristaux rhomboédriques), typiques des processus abiotiques, et biologiques de par la présence de cavités correspondantes à *Gloeocapsa* sp. à la surface des cristaux et de nano-globules couverts de matière organique. Les analyses MET/EDX montrent la présence de $Ca^{2+}$ à la surface de *Gloeocapsa* sp. active et de précipités de $CaCO_3$ à leur proximité. Les mesures par électrophorèse réalisées sur ces bactéries confirment qu'il n'y a aucun potentiel de surface positif à pH 8-10 (Pokrovsky et al., 2008), ce qui correspond temporellement à la phase de nucléation de $CaCO_3$. Ces observations mettent en évidence l'absence d'un mécanisme métabolique de maintenance d'une charge de surface positive à pH alcalin protégeant les bactéries actives contre l'adsorption et la précipitation ultérieure de carbonates à leur surface.

Cette étude apporte de nouveaux résultats aux travaux existants de Pokrovsky et al. (2008). De plus, le couplage de notre étude à leurs principaux résultats permet de proposer un modèle de mécanisme de précipitation de $CaCO_3$ en présence de *Gloeocapsa* sp. active. En particulier nous supposons que les macromolécules chargées négativement à la surface de *Gloeocapsa* sp. et agissant comme site de nucléation, sont capables de lier et d'accumuler des ions métalliques comme $Ca^{2+}$. Dans le microenvironnement proche de la membrane cellulaire de la bactérie, le pH pourrait être plus élevé que dans la solution environnante à cause de la libération d'ions $OH^-$ par certaines cellules, consécutivement à la consommation de $HCO_3^-$ durant la photosynthèse (Dittrich et al., 2004). Ainsi, la sursaturation de la couche de surface autour de la cellule aurait tendance à surpasser celle de la phase aqueuse principale et la précipitation de carbonate de calcium deviendrait possible, préférentiellement à cet endroit.

Cette étude ainsi que les résultats obtenus, sont décrits dans la section suivante sous la forme d'un manuscrit qui sera soumis dans le journal *Geobiology*.

# Experimental modeling of calcium carbonate precipitation by cyanobacteria *Gloeocapsa* sp.

Irina A. Bundeleva[1], Liudmila S. Shirokova[1,2],Oleg S. Pokrovsky[1]*,

Pascale Bénézeth[1], Stéphanie Balor[3]

[1]*Laboratoire Géosciences Environnement Toulouse (GET), Université de Toulouse, CNRS-IRD-OMP, 14 Avenue Edouard Belin, 31400 Toulouse, France*

[2] *Institute of Ecological Problems of the Northern Regions, Russian Academy of Science, 29 Naberezhnaja Sev. Dviny, Arkhangelsk , Russia*

[3] *Plateau de Microscopie électronique, FRBT CNRS FR3451, Bat. IBCG, 118 route de Narbonne, F-31062 Toulouse, France*

*corresponding author

e-mail: oleg@get.obs-mip.fr

**Key words:** Cyanobacteria, *Gloeocapsa* sp., calcium carbonate, precipitation, kinetics, calcium, bicarbonate, calcite.

*Prepared for Geobiology, May 2011*

# Abstract

Batch reactor kinetic experiments, SEM and TEM imaging, EDX and XRD analyses, and measurements of calcium adsorption onto bacterial surface and Ca intracellular assimilation were used to assess the existence of metabolic process responsible for calcium carbonate mineralization on *Gloeocapsa sp.* cyanobacteria surfaces. Carbonate precipitation experiments were performed at initial pH of 9.0±0.4 and 25 C in supersaturated solutions ($\Omega_{calcite}$ = 15 to 150) in the presence of active cyanobacteria cells. During cyanobacterial photosynthesis, solution pH increased up to 10.5-10.8 after the first 10-20 days of growth, Ca concentration decreased and the supersaturation index attained a maximum followed by gradual decrease due to progressive $CaCO_3$ precipitation. Ca adsorption at the surface of live and inactivated *Gloeocapsa* sp. cell and Ca intracellular assimilation during cell growth were measured as a function of pH and Ca concentration in solution. Experiments under light and in the darkness resulted in very similar adsorption edge and surface site densities in the wide range of solution pH and Ca concentration. The TEM imaging and EDX analysis indicated the presence of $Ca^{2+}$ on active *Gloeocapsa* sp. surfaces and $CaCO_3$ precipitation in the vicinity of bacterial cell surfaces. Scanning Electron Microscope analyses demonstrated cyanobacterial cell encrusting by $CaCO_3$ precipitated in the form of nano-spheres adjacent to the cell surface. In contrast to previously investigated calcifying bacteria, no cell protection mechanism against $Ca^{2+}$ adsorption and subsequent carbonate precipitation has been demonstrated for studied cyanobacteria. As such, *Gloeocapsa sp.* cyanobacteria exhibit significant calcifying potential, both in the biofilm and in planktonic culture.

# 1. Introduction

Geochemical modeling and laboratory experiments demonstrated the importance of physico-chemical mineral nucleation/precipitation processes rather than specific metabolic reactions, in overall microbially-induced $CaCO_3$ biomineralization processes occurring for most of Earth's history (Bosak and Newman, 2003). From the early Proterozoic and certainly since Precambrian-Cambrian boundary until the end of the Cretaceous, calcifying cyanobacteria frequently occur in normal marine environments (Ries, 2010). After the end of the Cretaceous, however, they seem to be restricted to non-marine settings. At the present time, calcification by cyanobacteria occurs almost exclusively in freshwater, alkaline and hypersaline or brackish water (Merz, 1992).

Various carbonate biomineralization mechanisms based on cyanobacteria cellular metabolism and surface composition have been proposed (Merz et al., 1993; McConnaughey and Whelan, 1997; Dittrich and Obst, 2004; Martinez et al., 2008; Obst et al., 2009 a,b). Cyanobacteria are undoubtedly associated with freshwater calcium carbonate biomineralization; some attribute this link to $Ca^{2+}$ binding to cyanobacteria surfaces (Thompson and Ferris, 1990; Castanier et al., 1999; Dittrich and Sibler, 2005, 2006). It has also been postulated that cyanobacterial calcification results from cell surface acidification stemming from proton discharge and/or bicarbonate/nutrient assimilation (Merz et al., 1993; McConnaughey and Whelan, 1997). Yet other studies concluded that calcium carbonate nucleation is initiated on inert bacteriogenic organic nano-globules and exopolymeric substances (Aloisi et al., 2006) and precipitation of amorphous $CaCO_3$ within the extracellular polymers of cyanobacteria could serve as a protection mechanism against uncontrolled precipitation of calcite at their surface (Obst et al., 2009a). Indeed, microbial cell surface and excreted extracellular polymeric substances (EPS), which carry a net negative electric charge and have the capacity to bind $Ca^{2+}$ ions, are frequently considered as sites of carbonate nucleation (Dupraz et al., 2004). The role of photosynthetic cyanobacteria on carbonate mineralization is, however, paradoxical, which was noted only recently (Martinez et al., 2010). To successfully photosynthesize, these bacteria must acquire aqueous bicarbonate ions. Bicarbonate ion consumption generates hydroxide ions, increasing pH and thus inducing calcite supersaturation and precipitation (e.g., Thompson and Ferris, 1990; Merz, 1992; Verrecchia et al., 1995). Different cyanobacteria (Martinez et al., 2010) as well as heterotrophic aerobic and anaerobic bacteria (Aloisi et al., 2006; Bontognali et al., 2008)

possess a self-protection mechanism against uncontrolled $CaCO_3$ coating and live cell embedding. For *Synechococcus* and *Plankothrix* and anoxygenic phototrophic bacteria (APB), this protection mechanism consists of maintaining a positive surface potential in alkaline solutions avoiding Ca adsorption at the cell surface (Martinez et al., 2008; Bundeleva et al., 2011). The surface potential regulation occurs via multiple and still poorly identified molecular and physiological mechanisms occurring in the vicinity of cell membrane such as conformational changes in the S-layer protein arrangement (Rachel et al., 1997), lysine-rich protein production within the cytoplasmic membrane (Zinovieva et al., 1998), proton secretion by the APB cell wall via proton-pumping (McConnaughey and Whelan, 1997) and enhanced respiration under alkaline conditions required to keep the proton gradient stable (Bazant et al., 2009) .

A typical freshwater cyanobacterium, *Gloeocapsa* sp., is dramatically different from other unicellular microorganisms studied so far in the sense that it possesses a thick polysaccharidic capsule surrounding several cells attached together. The presence of this capsule increases the distance between the cell surface membrane and the external environment. As a result, the electrostatic individual cell protection mechanisms may not be recognized at the macroscopic scale of cell aggregates. In this case, live *Gloeocapsa* cells may turn out to be extremely efficient calcifiers capable of extensive $CaCO_3$ precipitation in the vicinity of the cells directly during their life cycle, without necessary participation of dead cells or heterotrophic bacteria as it is known for other calcifying cultures.

The present work is aimed at verifying this hypothesis and assessing the rates and mineralogical nature of $CaCO_3$ precipitation during *Gloeocapsa* photosynthesis. Towards this goal, carbonate precipitation experiments have been conducted in closed-system reactors in the presence of active *Gloeocapsa* sp. under the light and in the dark. Complementary observations were made using scanning and transmission electron microscopy, coupled to energy-dispersive X-ray spectroscopy for cell surface analysis (SEM and TEM/EDX), and measurements of Ca adsorption and assimilation by live bacteria.

# 2. Materials and Methods

## 2.1. Gloeocapsa sp. cultures

Cyanobacterium *Gloeocapsa* sp. f-6gl (from the culture collection of the Institute of Microbiology RAS in Moscow, isolated from a warm spring (30–40°C) in Kamchatka) used in this study is represented by small number of cells grouped within concentric mucilage envelopes. The individual colonies are spherical, microscopic, and enclosed within larger masses of mucilage.

The concentration of the bacterial cell suspensions was quantified by (1) measurement of the optical density (O.D.) of suspensions using a spectrophotometer at a wavelength of 750 nm; the calibration curve O.D. – humid weight was linear up to 0.9 a.u.; (2) weighing the wet centrifuged pellets (20 min at 5000 *g*); and, (3) freeze-drying the centrifuged pellets. The conversion factor humid/dry (lyophilized) weight for *Gloeocapsa* sp. was $8.2 \pm 0.4$ (Pokrovsky et al., 2008). The biomass quantification via light absorbance measurement could be biased due to the presence of mineral precipitates. This wavelength (750 nm) was selected after full spectra recording in the region 300-800 nm of both mineral-free live cells of *Gloeocapsa* sp. cyanobacteria and cell-free calcite suspensions. The mineral suspension exhibits no adsorption in the region 650-800 nm whereas the cyanobacterial cells exhibit a distinct peak at 700-750 nm. The overall light absorbance of mineral suspension is lower by a factor of 10 than that of live biomass, when expressed per dry and wet weight. As a result, the maximum uncertainty in optical biomass measurements induced by the presence of minerals via absorbance at 750 nm is no more than 10%, which is within the experimental reproducibility. The O.D. calibration curve – humid weight was linear up to 1.3 absorbance units and the ratio between humid and freeze-dried weight of *Gloeocapsa* sp. was $10.0 \pm 2.0$.

## 2.2. Growth and preparation of Gloeocapsa sp.

*Gloeocapsa* sp. were cultured until stationary growth phase in Cyanobacteria BG-11 Fresh-water Solution Medium (Sigma-Aldrich C3061) of the following composition: $NaNO_3$

(150 g/L), $K_2HPO_4*3H_2O$ or $K_2HPO_4$ (40 g/L or 30 g/L), $MgSO_4*7H_2O$ (75 g/L), $CaCl_2*2H_2O$ (36 g/L), Citric Acid (6 g/L, Ammonium Citrate (6 g/L), $Na_2CO_3$ (20 g/L), Trace metal solution (1 ml/L) (composition of trace metal solution: $H_3BO_3$ (2.86 g/L), $MnCl_2*4H_2O$ (1.81 g/L), $ZnSO_4*7H_2O$ (0.222 g/L), $NaMoO_4*5H_2O$ (0.39 g/L), $CuSO_4*5H_2O$ (0.079 g/L), $Co(NO_3)_2*6H_2O$ (0.0494 g/L). Stock culture of *Gloeocapsa* sp. were kept at 25 ± 1°C under constant cool white fluorescent light (2000 lx) on a Ping-Pong Fisher shaker.

The cultures for experiments were harvested at the late exponential – stationary growth stage by centrifugation at 10,000 rpm (7000 g) for 10 min at 20°C. The cells were rinsed in 0.1 mol/L NaCl corresponding to optimal physiological conditions and centrifuged twice at 10,000 rpm for 10 minutes. Finally, bacterial suspension was washed in appropriate electrolyte solution and centrifuged.

Inactivated cells were prepared by rinsing part of the fresh (live) biomass in 0.01 mol/L sodium azide ($NaN_3$) during 1-2 hrs. Sodium azide suppresses bacterial activity by inhibiting cytochrome oxidase and is widely used for inactivating cells while keeping the surfaces physically and chemically intact (Hunter, 2010). Cell growth of *Gloeocapsa sp.* culture in the presence of 0.01 M $NaN_3$ in nutrient solution was completely suppressed as proven in a separate series of experiments.

## 2.3. Experimental procedure and analyses

### 2.3.1. Ca adsorption on cell surfaces

In this study, two aspects of $Ca^{2+}$ adsorption process were characterized: *i*) adsorption at constant initial calcium concentration in solution as a function of pH (pH-dependent adsorption edge) and *ii*) adsorption at constant pH as a function of calcium concentration in solution (adsorption isotherm). All experiments were performed in undersaturated solutions with respect to any calcium carbonate phase as verified by speciation calculations with the MINTEQA2 computer code and corresponding database (Alisson et al., 1991).

In experiments with *Gloeocapsa* sp. initial calcium concentration at variable pH ranged between 2.3 and 17 µmol/L, whereas Ca concentration at constant pH was between 4.2 and 25 µM/L (Table 1). The pH was adjusted by adding aliquots of NaOH (0.1 and 0.01

mol/L) or HCl (1.0, 0.1 and 0.01 mol/L), whereas, the constant pH of 7.6, 9.0 and 11.8 was maintained by adding 5 mM HEPES (4-(2-hydroxyethyl)-1-piperazineethanesulfonic acid), 5 mM $NaHCO_3$+$Na_2CO_3$ and 5 mM $Na_2CO_3$ buffers, respectively.

The effect of light on $Ca^{2+}$ adsorption onto surface of *Gloeocapsa* sp. was also investigated. For this, adsorption experiments were run under light (2000 lx light) or in the darkness, by wrapping the vials with aluminum foil. Adsorption experiments were conducted in 8 mL sterile polypropylene vials during 2.5, 19 and 24±1 hrs at 25 ± 0.2°C, in continuously agitated bacteria suspension with an ionic strength of 0.1 mol/L NaCl. The biomass concentration was kept constant at 10 $g_{wet}$/L. Live, freshly harvested (stationary stage) cells, sodium azide-inactivated and heat-killed (autoclaved 20 min at 120°C) bacteria were used in the adsorption experiments. The cells were rinsed in 0.1 mol/L NaCl and 0.01 mol/L EDTA solutions for 12 minutes and again in 0.1 mol/L NaCl solution prior the experiments. This procedure allowed desorption of all possible $Mg^{2+}$, $Ca^{2+}$ ions from the cell's surfaces that might occurred during the cyanobacteria culture.

The adsorption of calcium on cell surfaces was quantified by subtracting, at each solution pH, the concentration of calcium remaining in bacterial suspension from the concentration of calcium added in the supernatant. The adsorption of calcium on reactor walls and cellular Ca release from the biomass in the full range of studied pH was negligible (<10%) compared to the initial amount of Ca added. This was routinely verified by Ca analyses in the supernatant and in the zero-added-Ca cell suspension experiments. Nonetheless, the measured Ca concentrations in these blank experiments (to the limit of detection) were explicitly taken into account to calculate the adsorption isotherm.

All filtered (0.22 µm) solutions were analyzed for aqueous Ca concentration using flame atomic absorption spectroscopy (Perkin Elmer AAnalyst 400) with an uncertainty of ±2% and a detection limit of 0.5 µmol/L. Dissolved organic carbon (DOC) was analyzed using a Carbon Total Analyzer (Shimadzu SCN) with an uncertainty of 3% and a detection limit of 0.1 mg/L. The DOC concentration during adsorption measurements remained quite low, between 5 and 10 mg/L and did not vary with pH and ionic strength in any systematic manner, suggesting negligible cell lysis and degradation in the full range of studied solution conditions.

### 2.3.2. Ca and DIC uptake during cell growth

There are 3 possible sinks for Ca in bacterial suspension: (1) metabolic intracellular incorporation during growth, (2) reversible adsorption at the cell surface, and (3) calcium precipitation in the form of $CaCO_3$. To characterize the Ca metabolic uptake by live cyanobacteria, Ca concentration evolution was followed in the experiments with nutrient solution, containing 0.5 and 5 mM Ca where $CaCO_3$ precipitation did not occur. Experiments were performed in ventilated glass bottles shaken under light at 25 ± 1°C. Periodically, aliquots of homogeneous suspension were sampled and used for measurements of biomass, pH, and, in <0.45 µm filtered samples, of Ca and alkalinity. Regular optical examination of cyanobacterial cells demonstrated that they remained intact, preserving their envelopes and structural organization in 2-4 cell associates within a single capsule.

### 2.3.3. Mineral precipitation experiments

Kinetic experiments were performed in nutrient phosphate-free solution and in inert electrolyte (0.1 M NaCl) at 25 ± 1 °C in closed Schott® 1L glass bottle reactors containing 800 mL of the initial solution. Preliminary experiments in BG-11 containing normal phosphate concentration enriched in Ca and bicarbonate yielded Ca phosphate as mineral precipitates induced during cell photosynthesis. To avoid phosphate mineral precipitation and phosphate effect on $CaCO_3$ precipitation rates, all nutrient solution used for kinetic experiments were exempt of orthophosphate.

Kinetic experiments were carried out with initial concentration of calcium chloride and sodium bicarbonate ranging from 1 to 50 and 5 to 10 mM, respectively. All biotic experiments were performed with initial biomass concentration between 0.04-0.66 (in nutrient solution) and 1.5-1.7 $g_{wet}$/L (in inert electrolyte). Precipitation experiments were carried out over a range of initial saturation index ($\Omega_{calcite}$) varying between 15 and 150 in the nutrient solution and between 66 and 83 in the inert electrolyte. Approximately 20 % of experiments were conducted in duplicates. Experimental conditions investigated in this study are listed in Table 2. Several experiments have been performed with atmospheric air bubbling but most experiments were run in glass vessels with sterile ventilated caps Biosilico® allowing efficient gas exchange with the atmosphere.

Temporal variation of all experimental parameters in each individual experiment is presented in the Appendix 4. Numbers of experiments in Table 2 correspond to the ones in the Appendix 4.

Regularly, an aliquot of ~7 mL was removed from the closed-system reactor, using a sterile syringe or pipette, to monitor the chemical and microbiological evolution of the system Approximately 2 mL of this aliquot were used to estimate the concentration of bacterial cells in the reactor by measuring pH and optical density at a 650 nm wavelength. The remaining 5 mL were filtered through a 0.22 μm filter to remove biomass from the suspension. The filtrate was analyzed for alkalinity and calcium concentration.

The pH in each unfiltered sample was measured using a Fisher® pH combined electrode, with an uncertainty of 0.01 units, previously calibrated using pH 4.01, 6.86, 9.18, and 10.01 buffer solutions at 25°C. Alkalinity was determined through potentiometric analysis, using a Schott autotitrator system (Titroline alpha plus, TA10plus). Ca concentration was determined using flame atomic absorption spectroscopy via a Perkin Elmer 5100 PC Spectrophotometer with an uncertainty of ±2% and a detection limit of 0.05 mg/L.

### 2.3.4. Solid phase's analysis

Mixtures of *Gloeocapsa* sp. cells and precipitated mineral phase were subjected to digestion for removing organic matter using 2-3 days treatment in 10% $H_2O_2$ at the same solution pH as in experimental samples. Resulted solid phases were rinsed in MilliQ water, frozen at -80°C and freeze-dried. Selected samples were studied by X-ray diffraction (INEL CPS 120, $Co_{K\alpha}$, scan speed $0.02^{o}s^{-1}$) and microscopic examination was performed using a Jeol JSM840a Scanning Electron Microscope (SEM) after carbon film coating deposition on the sample surface.

Aliquots of suspensions containing live bacterial cultures and precipitated mineral were also examined using Transmission Electron Microscopy (TEM) with a JEOL JEM 12000 EX and JEOL JEM 2100F (equipped with a field emission gum and PGT EDX detector) at 80 kV. Cell suspension was rinsed using sterile nutrient solution (without sodium chloride addition) or MilliQ water, centrifuged 2 min at 10 000 rpm. TEM samples for analyses were taken by immersing grids coated with a carbon film for 10 s in prepared bacterial suspension. Dried grids were used for TEM analyses

# 3. Results and discussion

## 3.1. Calcium adsorption

The pH-dependent adsorption edge for *Gloeocapsa sp.* performed in 0.1 mol/L NaCl and with a biomass of 10 $g_{wet}$/L exposed for 3 hrs in the dark is illustrated in Fig. 1.

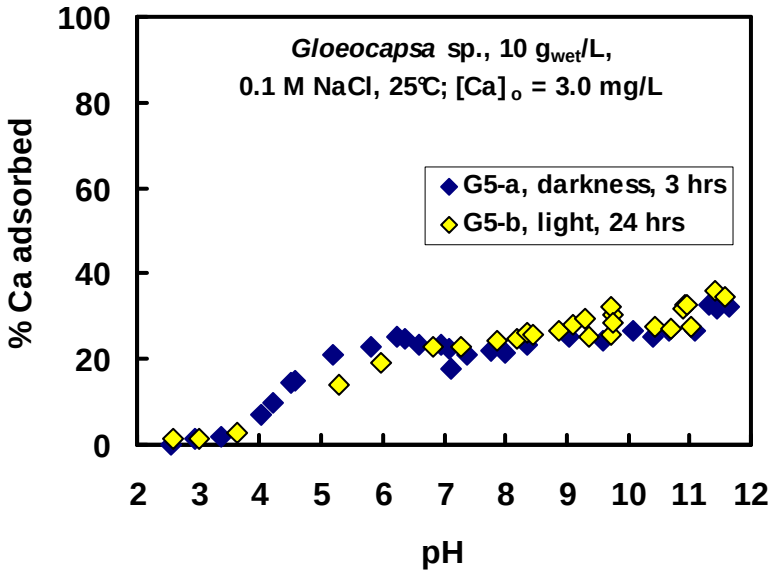


**Fig. 1. Percentage of adsorbed calcium as a function of pH for live *Gloeocapsa* sp. culture in the darkness (blue diamonds) and under light (yellow diamonds). Experimental conditions: 25°C, $[Ca]_o$ = 75 µmol/L, 10 $g_{wet}$ biomass/L in 0.1 M NaCl and 3 to 24 hours of exposure time. The error bars are within the symbol size.**

It can be seen from this figure that the adsorption is very low at pH < 3, it increases to 25-30% at pH = 5-6 and gradually increase to 30-35% with further pH increase, up to 11.5. There is no significant difference in the adsorption yield for cells kept in the darkness during 3 hrs and those exposed to light during 24 hrs. The maximal concentration of adsorbed Ca is 2 to 3 µmol/$g_{wet}$.

Calcium adsorption isotherms recorded for live *Gloeocapsa* sp. at three constant pHs (5.5, 5.9 and 6.7) and Ca concentrations from 10 to 100 µmol/L are illustrated in Fig. 2**.** The adsorption is rather similar at all three studied pH values and the measured maximal adsorption density is close to 2 µmol/$g_{wet}$, in accord with results of pH-dependent adsorption edge.

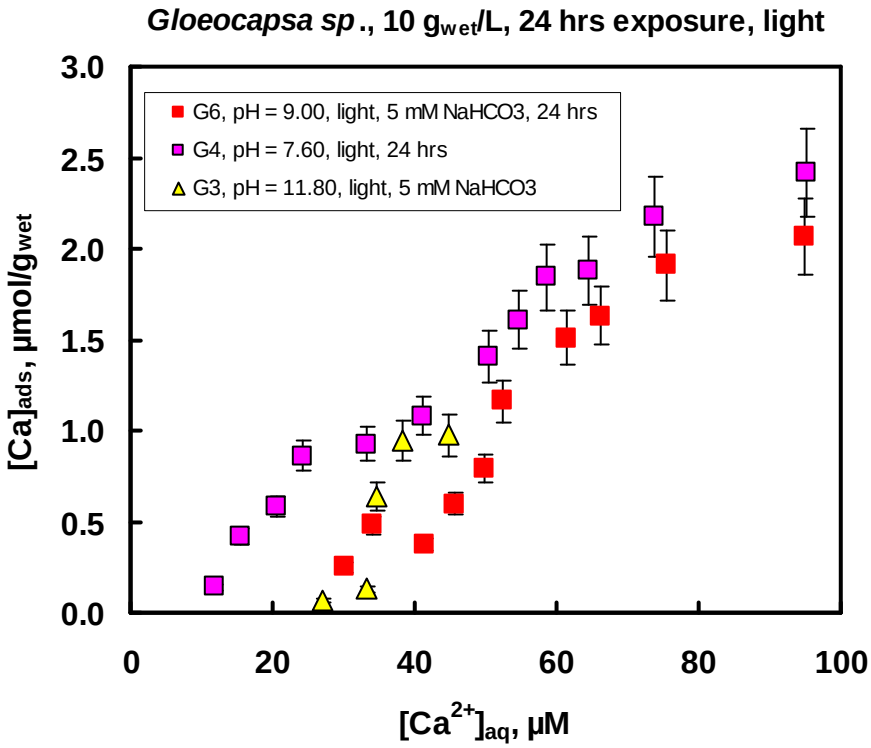


**Fig. 2. Concentration of adsorbed calcium as a function of calcium concentration in solution (constant-pH adsorption isotherm) for live *Gloeocapsa* sp.. Experimental conditions: 25°C, pH 7.6, 9.0 and 11.8, 10 $g_{wet}$ biomass/L in 0.1 M NaCl and 24 hour of exposure time under light.**

Experimental condition and range of all parameters in adsorption experiments are shown in Table 1.

**Table 1. Summary of Ca adsorption with *Gloeocapsa* sp.**

| № | durations, hrs | biomass, mg wet/L | Conditions | [Ca] range, µM/L | pH range |
|---|---|---|---|---|---|
| pH adge adsorption | | | | | |
| 1 | 2.5 | 10 | 0.1 M $NaNO_3$ | 2.28-19.1 | 2.981-11.429 |
| 2 | 2.5 | 10 | 0.1 M NaCl | 3.30-70.1 | 2.537-8.011 |
| 3 | 24 | 10 | 0.1 M NaCl | 12.6-81.2 | 2.564-11.206 |
| 4 | 24 | 10 | 0.1 M NaCl | 17.0-65.4 | 2.578-11.588 |
| Langmurian adsorption | | | | | |
| 5 | 24 | 20 | 0.1 NaCl | 24.5-50.0 | 7.74-7.89 |
| 6 | 19 | 10 | 6 ml 0.1 M NaCl+0.3 ml 0.1 M $NaHCO_3$ | 13.6-69.1 | 11.80-11.82 |
| 7 | 24 | 10 | 6 ml 0.1 M NaCl + 0.3 ml 0.1 M HEPES | 13.7-93.6 | 7.60-7.62 |
| 8 | 24 | 10 | 6 ml 0.1 M NaCl + 0.3 ml 0.1 M HEPES | 4.20-75.7 | 8.99-9.10 |
| 9 | 24 | 10 | 6 ml 0.1 M NaCl + 0.3 ml 0.1 M HEPES | 5.25-718 | 7.51-7.48 |
| 10 | 23 | 10 | 6 ml 0.1 M NaCl + 0.3 ml 0.1 M HEPES | 6.80-727 | 6.95-7.56 |

### 3.2. Ca and DIC uptake during bacterial growth

The results of Ca uptake during cyanobacterial growth are presented in Appendix 4 (Exp. 29-34) and illustrated in Fig. 3. Plotted in this figure are the biomass, pH, and Ca concentration evolution in experiments that lasted 65 days. It can be seen that there is an increase of the biomass (up to 1.15 $g_{we}t/L$) and pH (up to 11.4) during growth in the presence of various Ca concentration. At the same time, only small decrease of calcium concentration (< 0.11-0.46 mM) is observed whereas the DIC concentration remains constant or slightly increased, indicating the absence of carbonate mineral precipitation. We believe that observed Ca concentration decrease is due to Ca adsorption plus intracellular incorporation. The maximal amount of calcium that active bacteria are capable of uptake during their growth can be calculated from the difference between the initial and final Ca concentration normalized to final cell biomass:

$$[Ca]_{uptake} = ([Ca]_{initial} - [Ca]_{final}) / biomass_{final} \quad (1)$$

For *Gloeocapsa* sp., the maximal incorporation of calcium in the cells at our experimental conditions ranged from 86 to 430 µmol Ca $g_{wet}$ $L^{-1}$, being significantly higher than the experimental adsorption site density (~ 2 µmol/$g_{wet}$, see section 3.1). At the same time, Ca incorporation in live *Gloeocapsa* cells is much higher than that in anoxygenic phototrophic bacteria (13 to 8 µmol Ca /$g_{wet}$ $L^{-1}$ see **Chapter 4**; Bundeleva et al., submitted). Taken together, the maximal metabolic and passive adsorptive Ca uptake by live *Gloeocaopsa* sp. not linked to carbonate mineral precipitation is 430 µmol/$g_{wet}$. $L^{-1}$.

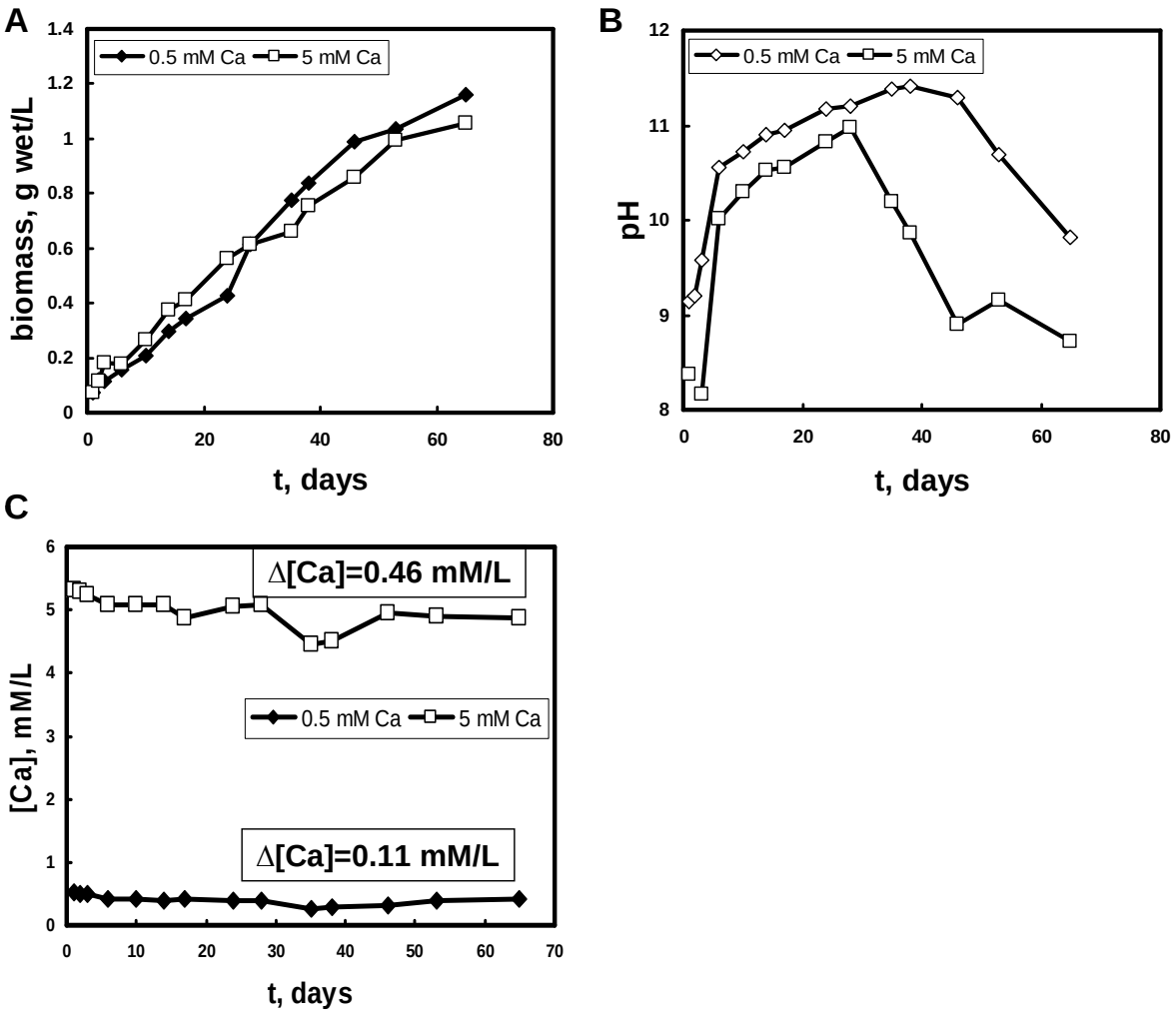


**Fig. 3. Evolution of biomass (A), pH (B) and calcium concentration (C) in experiments with live *Gloeocapsa sp.* without mineral precipitation at different initial Ca concentration (Exp. 31-34). The error bars are within the symbol size and represent the average of two duplicates.**

### 3.3. Kinetic of $CaCO_3$ precipitation in the presents of *Gloeocapsa* sp.

Three types of biotic kinetic experiments were conducted (Table 2): with live culture in inert electrolyte (0.1 M NaCl) and with live culture with and without light in nutrient phosphate-free solution.

In most experiments conducted in this work, the precipitation process can be broken down into three stages: (1) initial pH-rise period, (2) the actual massive precipitation reaction,

and (3) an equilibration phase (Fig. 4). Calcium carbonate precipitation was evidenced by Ca concentration decrease and also supported by microscopic examination of produced mineral phases. Typical plots of bacterial biomass, pH, [Ca], [Alkalinity] and Ω as a function of elapsed time in biotic experiments in nutrient solution with and without light are presented Fig. 4. It can be seen from this figure that significant decrease of calcium concentration is observed in both types of biotic experiment. The precipitation under light in biotic experiment started earlier than that in the darkness although the initial calcite saturation index was similar in both experiments ($\Omega_{calcite}$ = 23). Moreover, light experiments demonstrated significant increase of bacterial biomass which was accompanied by a dramatic increase in solution pH, and, as a result, $\Omega_{calcite}$ increase to 62, which coincided with the beginning of massive calcium carbonate precipitation. In the absence of light, there were no increase of the biomass and pH, Ω values remained stable or increased insignificantly. These results suggest that the presence of active *Gloeocapsa* sp. crucially affect calcite precipitation rates compared to biotic controls without light. This result corroborates that of Obst et al. (2009b) who reported little difference in calcite nucleation rates measured in the presence of active and inactive cyanobacteria *Synechococcus leopoliensis* and that of Martinez et al. (2010), who observed enhancement of $CaCO_3$ precipitation rate in biotic experiments with two strain of cyanobacteria *Synechococcus* sp. and *Planktotrix* sp. compared to bacteria-free experiments.

Table 2. Kinetic experiments with *Gloeocapsa* sp.: conditions, rates and mineralogy of precipitates.

| № | duration, hrs | biomass range, g wet/L | pH range | [Alkalinity] range mM/L | [Ca] range mM/L | precipitation rate, μM/hrs | Ω range | [DOC], mM/L | mineralogy |
|---|---|---|---|---|---|---|---|---|---|
| Experiments in nutrient solution | | | | | | | | | |
| 1 | 624 | 0.62-1.46 | 9.56-9.01 | 2.84-3.36 | 2.77-2.74 | 3.06 | 89.1-54.9 | | |
| 2 | 624 | 0.68-1.22 | 9.10-8.71 | 2.44-2.98 | 5.80-7.73 | 0.00 | 70.8-58.9 | | |
| 3 | 408 | 0.18-1.92 | 9.00-9.07 | 4.56-2.66 | 2.75-1.47 | 6.48 | 69.2-30.9 | | |
| 4 | 408 | 0.14-2.62 | 8.83-9.46 | 4.53-1.49 | 4.83-3.47 | 9.12 | 79.4-50.1 | | |
| 5 | 408 | 0.14-2.7 | 8.69-9.10 | 1.43-1.89 | 9.19-7.46 | 19.2 | 30.9-61.6 | | |
| 6 | 408 | 0.12-2.92 | 8.58-9.82 | 0.70-1.47 | 13.11-10.75 | 15.8 | 15.1-79.4 | | |
| 7 | 408 | 0.12-2.76 | 8.44-9.45 | 3.75-1.03 | 20.60-18.82 | 25.0 | 74.9-54.9 | | |
| 8 | 408 | 0.12-1.98 | 8.27-9.56 | 2.61-0.94 | 45.00-38.20 | 54.2 | 57.7-53.7 | | |
| 9 | 356 | 0.15-1.22 | 9.37-9.49 | 10.00-7.95 | 1.00-0.09 | 2.57 | 75.8-6.70 | | |
| 10 | 356 | 0.15-1.74 | 8.79-9.19 | 10.00-2.53 | 5.00-0.24 | 22.1 | 147-9.80 | | |
| 11 | 168 | 0.15-0.9 | 8.17-9.51 | 10.00-0.5 | 10.00-2.13 | 65.6 | 81.3-13.8 | | calcite |
| 12 | 356 | 0.10-1.52 | 7.71-8.54 | 10.00-0.31 | 20.00-9.26 | 53.5 | 50.1-8.10 | | calcite |
| 13 | 356 | bacteria free | 7.42-7.89 | 10.00-0.81 | 20.00-9.04 | 30.8 | 26.9-4.70 | | |
| 14# | 264 | 0.15-1.88 | 9.37-9.73 | 10.00-4.40 | 1.00-0.87 | 7.64 | 75.9-8.90 | | |
| 15# | 264 | 0.15-3.16 | 8.51-9.10 | 10.00-4.85 | 5.00-0.46 | 21.2 | 93.3-18.2 | | |
| 16# | 120 | 0.15-1.48 | 7.75-8.58 | 10.00-0.97 | 10.00-1.80 | 68.3 | 34.7-43.7 | | calcite |
| 17# | 120 | 0.15-0.84 | 7.46-8.34 | 10.00-0.59 | 20.00-10.86 | 76.1 | 29.5-7.80 | | calcite+aragonite |
| 18# | 120 | bacteria free | 7.40-8.01 | 10.00-0.83 | 20.00-7.96 | 100 | 25.7-4.70 | | calcite |
| 19# | 284 | 0.04-1.98 | 8.86-9.14 | 4.27-2.80 | 1.80-0.13 | 14.2 | 38.1-6.30 | | |
| 20# | 284 | 0.04-1.20 | 8.82-8.75 | 4.30-0.88 | 4.50-0.57 | 56.2 | 70.8-6.30 | | |
| 21# | 284 | 0.04-2.28 | 8.73-8.62 | 4.96-0.77 | 9.00-2.69 | 135 | 107-12.3 | | calcite |
| 22# | 284 | bacteria free | 8.60-7.89 | 4.47-0.80 | 9.00-5.45 | 12.5 | 79.4-2.70 | | |

Table 2. (Continued) Kinetic experiments with *Gloeocapsa* sp.: conditions, rates and mineralogy of precipitates.

| № | duration, hrs | biomass range, g wet/L | pH range | [Alkalinity] range mM/L | [Ca] range mM/L | precipitation rate, μM/hrs | Ω range | [DOC], mM/L | mineralogy |
|---|---|---|---|---|---|---|---|---|---|
| 23 | 3275 | 0.17-1.08 | 8.64-9.76 | 4.43-2.32 | 1.52-0.09 | 2.92 | 23.1-6.64 | 0.81-2.96 | calcite |
| 24* | 3275 | 0.08-0.17 | 8.37-9.17 | 4.91-2.68 | 1.52-0.12 | 2.44 | 23.4-3.90 | 0.17-0.44 | |
| 25# | 552 | 0.19-0.45 | 8.62-9.02 | 4.36-3.12 | 1.48-0.31 | 2.12 | 42.6-5.30 | | |
| 26 | 3275 | 0.17-1.02 | 8.66-9.75 | 17.53-6.63 | 0.77-0.07 | 6.48 | 24.5-8.30 | 0.66 | calcite |
| 27* | 3275 | 0.08-0.18 | 8.66-9.69 | 6.99-13.34 | 0.77-0.08 | 0.05 | 24.5-6.80 | 0.21 | |
| 28# | 548 | 0.21-0.46 | 9.07-9.35 | 10.90-9.59 | 0.74-0.13 | 2.32 | 54.9-11.7 | | |
| Experiments of Ca uptake during cyanobacterial growth in nutrient solution | | | | | | | | | |
| 29 | 1518 | 0.08-1.308 | 9.32-10.15 | | 0.008-0.000 | | | | |
| 30 | 1518 | 0.097-1.324 | 9.30-9.96 | | 0.011-0.000 | | | | |
| 31 | 1518 | 0.074-1.159 | 9.15-9.82 | | 0.53-0.42 | | | | |
| 32 | 1518 | 0.074-1.189 | 9.18-9.68 | | 0.55-0.39 | | | | |
| 33 | 1518 | 0.074-1.055 | 8.37-8.72 | | 5.33-4.87 | | | | |
| 34 | 1518 | 0;069-1.019 | 8.13-8.80 | | 5.23-4.83 | | | | |
| Experiments in inert electrolyte | | | | | | | | | |
| 35" | 96 | 1.64-1.96 | 9.07-10.80 | 4.42-3.98 | 3.40-3.05 | 1.82 | 83.2-186 | | |
| 36" | 96 | 1.66-2.00 | 8.96-10.92 | 4.95-2.93 | 3.45-2.59 | 9.68 | 66.1-117 | | |
| 37" | 96 | 1.60-1.74 | 8.90-10.64 | 4.18-2.40 | 5.11-3.94 | 40.5 | 93.3-107 | | |
| 38" | 96 | 1.50-1.80 | 8.84-10.73 | 4.62-2.08 | 6.52-5.49 | 12.0 | 85.1-114 | | |

* experiments in the dark

\# experiments with bubbling

" experiments with stirring

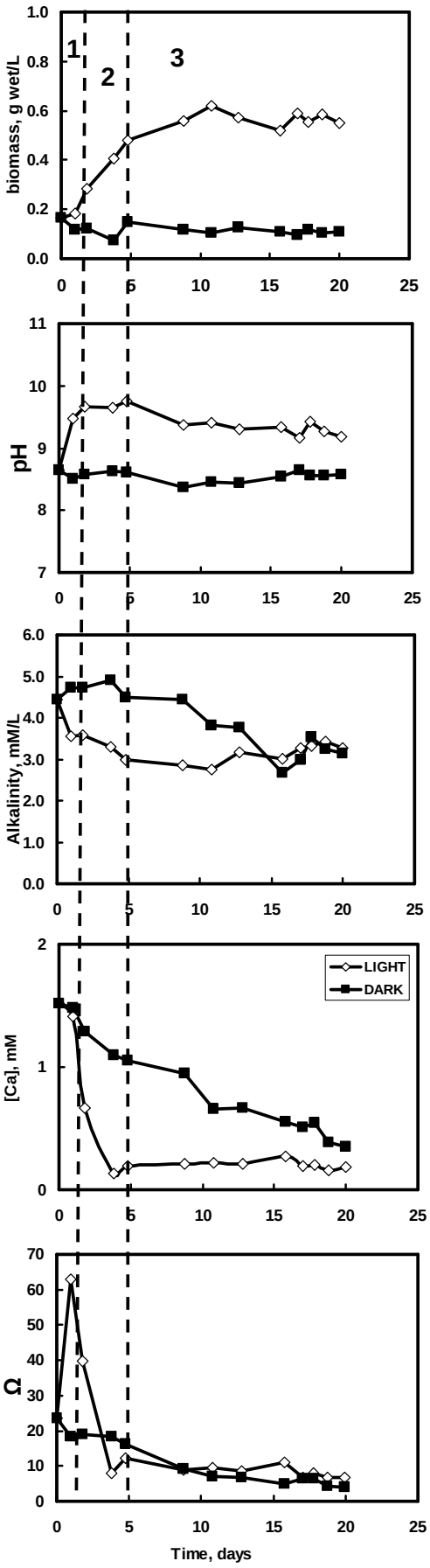


**Fig. 4. Three phases of calcium carbonate precipitation in nutrient solution under light (open symbols) and in the darkness (solid symbols) by *Gloeocapsa sp.* (Exp. 23 and 24 respectively): (1) a pH-drift period, (2) massive precipitation reaction, and (3) an equilibration phase.**

Biotic precipitation experiments were conducted at different initial $\Omega_{calcite}$ (from 15 to 150). The $\Omega_{calcite}$ evolution with time exhibited similar pattern among different experiments. At the beginning of experiments we observed an increase of $\Omega_{calcite}$ until a maximal value is attained (70-150) which induced massive $CaCO_3$ precipitation and subsequent $\Omega_{calcite}$ decrease. The duration of this increase and the maximal value of $\Omega_{calcite}$ varied from one experiment to the other depending on the initial experimental conditions (Fig. 5).

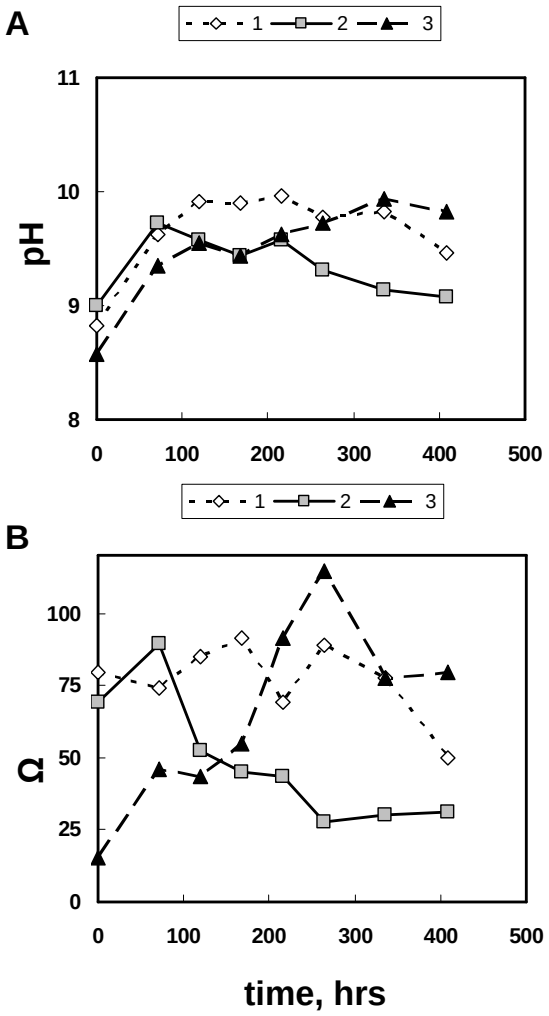


**Fig. 5. Evolution of pH (A) and $\Omega_{calcite}$ (B) in biotic experiments in nutrient solution. The numbers in the legend correspond to the following initial experimental conditions: (1) 3 mM $CaCl_2$, 5 mM $NaHCO_3$, biomass 0.14 g $_{wet}$/L (Exp.4 ); (2) 3 mM $CaCl_2$, 5 mM $NaHCO_3$, biomass 0.18 g $_{wet}$/L (Exp.3); (3) 13 mM $CaCl_2$, 9 mM $NaHCO_3$, biomass 0.12 g $_{wet}$/L (Exp.6).**

In contrast to biotic nutrient-rich experiments, in biotic experiments performed in the inert electrolyte, Ca concentration decrease was much less pronounced (Fig. 6). During these experiments, only insignificant increase of the biomass (between 0.3 and 0.08 g $_{wet}$/L) occurred indicating the lack of bacterial development in the absence of nutrients (Fig. 6A).

Despite the lack of bacterial growth, there is a significant pH increase in all biotic experiments performed in the inert electrolyte (from 8.9 at the beginning to 10.7 at the end of experiment, Fig. 6B).

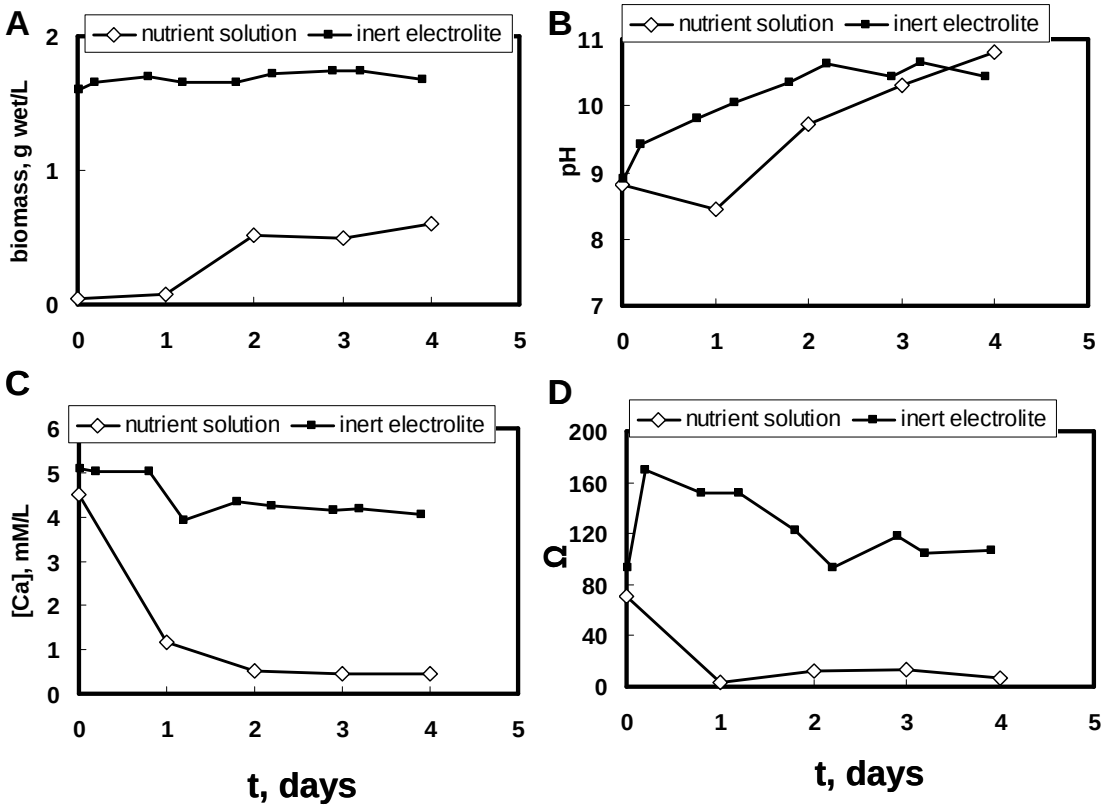


**Fig. 6. Evolution of aqueous solution parameters during biotic experiments in nutrient solution and inert electrolyte (Exp. 20 and 37 respectively). Initial conditions: 5 mM $CaCl_2$ and 5 mM $NaHCO_3$. (1) biomass development; (B) pH; (C) calcium concentration; (D) $\Omega_{calcite}$.**

The increase of pH without active development of bacterial biomass in the experiment in inert electrolyte may stem from on-going photosynthetic bacterial activity due to sufficient intracellular nutrient resources. As a result, calcite supersaturation degree increased from 66-90 at the beginning to 110-120 at the end of experiments with a maximum of ~190 attained in the first day of reaction.

Apparent precipitation rates ($r_i$) were calculated from the first derivative of the fluid phase Ca concentration with respect to time, using

$$r_i = \frac{d[Ca]}{dt} \qquad (2)$$

This equation has been applied to each experimental data series, typically at the stage 2 (Fig. 4) when the largest change in Ca concentration occurred. Resulting precipitation rates are listed in Table 2. Due to paucity of experimental data points and low temporal resolution

of long-term experiments, it was not possible to provide the uncertainties attached to these rate values but they are estimated to be 20-30%.

### 3.4. Solid phase characterization

In the course of experiments, visual white precipitates were formed on the glass walls of reactors and in the bacterial suspension after 5-7 days of culture growth. Although calcium carbonate precipitation was observed in biotic and abiotic experiments, the shape and size of precipitates was different. The SEM images of calcite formed in abiotic nutrient-free, biotic nutrient-free and biotic nutrient-rich solutions are shown in Fig. 7, 8 and 9, respectively. The XRD analysis identified calcite formations in all experiments except the experiment 17 (Table 2) in nutrient media with initial biomass 0.15 g $_{wet}$/L at $\Omega_{initial}$ 30 that produced aragonite.

Abiotic nutrient-free experiments produced typical rhomobohedral calcite crystals 5 to 10 µm in size, often associate in clusters (Fig. 7).

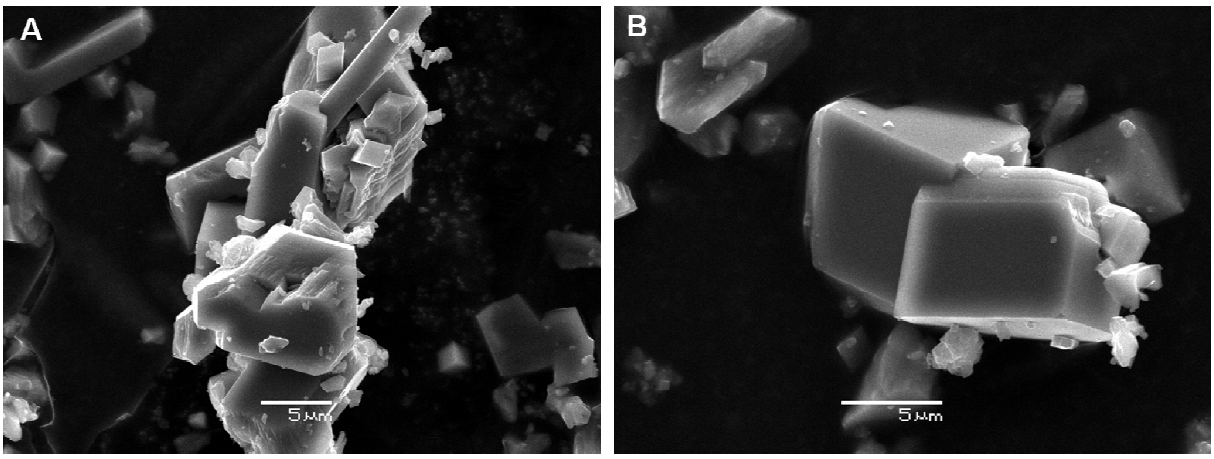


**Fig. 7. Calcite precipitated in abiotic (cell-free BG 11) experiment (initial conditions: 20 mM $CaCl_2$, 10 mM $NaHCO_3$) (Exp. 18).**

The size and shape of the crystals formed in biotic precipitation in the inert electrolyte and in nutrient solution are dramatically different and vary both in the course of the same experiment and among different initial solution conditions. First, there are large, 50 to 100 µm crystal associates without clear geometric form (Fig. 8A) or having spherical, rounded shape of 5 to 15 µm diameter (Fig. 8 B). In both associated crystals, rounded and elliptical holes 2 to 4 µm in diameter most likely representing the imprints of *Gloeocapsa* sp. Bacteria, are visible at the surface (Fig. 8 C, D). The same imprints are also visible at the surface of crystals formed in nutrient-rich media (see below). Similar "porous" crystals have also been found in experiments with $CaCO_3$ precipitation by algae (Stabel, 1986), cyanobacteria *Synechococcus*,

eukaryotic picoplankton *Mychonastes* sp. and *Chlorella* sp. (Dittrich et al., 2004). The second possible type of precipitate is represented by rhomboid crystals with the longest facet of 10-15 µm (Fig. 8 E), similar to those formed in abiotic experiments. The rhombohedral crystals and "porous" associates are often linked together, both in nutrient-free and nutrient-rich solutions (Fig. 8 D and 9 A, B). In addition, the rhombohedral and spherical associates of 10-15 µm in diameter are often formed in experiment with live cells in the inert electrolyte (Fig. 8F)

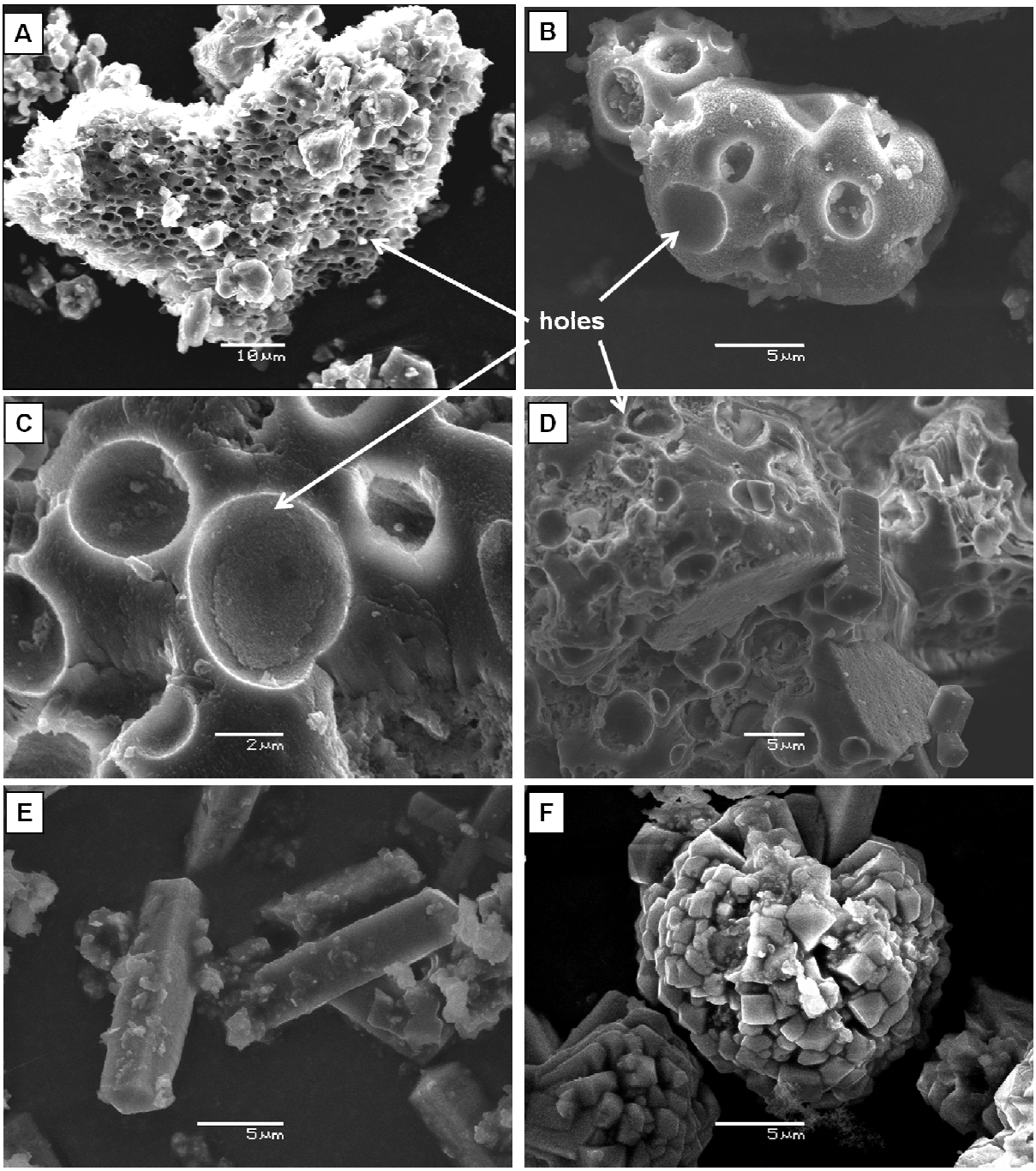


**Fig. 8. Calcite precipitated in biotic experiments with *Gloeocapsa* sp. in inert electrolyte. (A,B) Exp. 36; (C,D) Exp. 37; (E,F) Exp. 38.**

The third type of formed crystals is nano-globular associates. They are often found in biotic experiments in nutrient solution and represented by small individual crystals associated in large aggregates (Fig. 9 C), typically covered by organic matter, probably in the form of EPS (Fig. 9 D). The presence of organic matter is confirmed by the EDX analysis which demonstrated very high C content at the surface of these crystals.

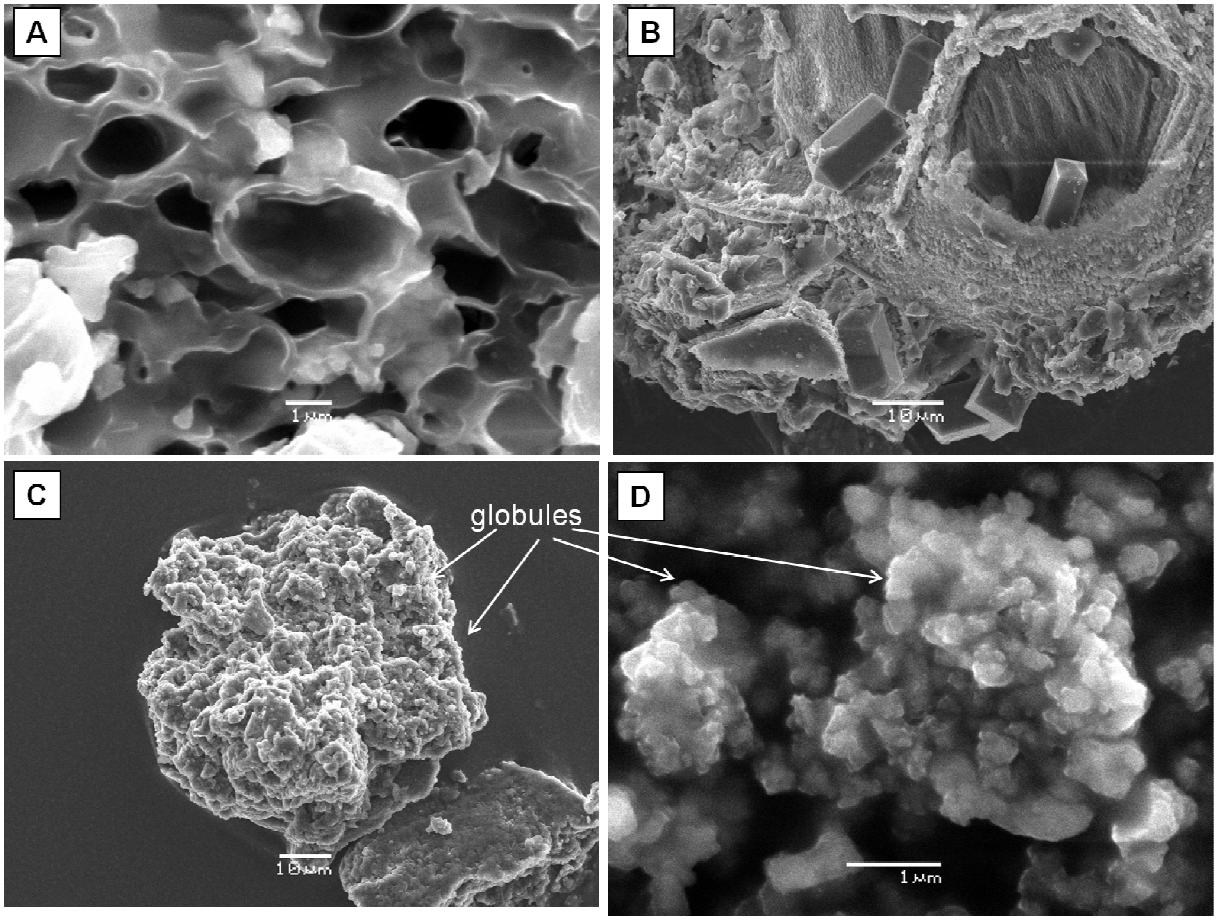


**Fig. 9. Calcite precipitated in biotic experiment with *Gloeocapsa* sp. in nutrient solution.(A) Exp. 15; (B, D) Exp. 26; (C) Exp. 23.**

Overall, the obtained results imply strong participation of cyanobacteria *Gloeocapsa* sp. in $CaCO_3$ precipitation. The existence of different types of crystals in biotic experiments suggests that $CaCO_3$ precipitation is driven by different pathways: inorganic precipitation as evidenced by the presence of rhombohedral crystals, typical for abiotic experiments and biologically-affected precipitation evidenced by the presence the *Gloeocapsa*-size pores on the surfaces of crystals and the nano-globules covered by the organic matter.

Further insights on mechanisms of $CaCO_3$ precipitation were acquired using TEM technique. Results of Transmission Electron Microscopy analysis of active cells following their presence in the control (nutrient, mineral-free media) and calcite-supersaturated

solutions are shown in Fig. 10. The cells in nutrient media appear intact without traces of precipitation within the surface (Fig. 10 A). The elements detected on and around live cells in nutrient medium are mainly C and O with some S, Si, P, Cl, and Na. No Ca was detected on these surfaces. In contrast, it can be seen from Fig. 10 B that significant $CaCO_3$ precipitation occurs in the vicinity of bacterial cell in calcite-supersaturated medium at $\Omega_{calcite}$ = 25. In these experiments, Ca was detected in precipitates formed at the surface and at some distances from *Gloeocapsa* sp. cells.

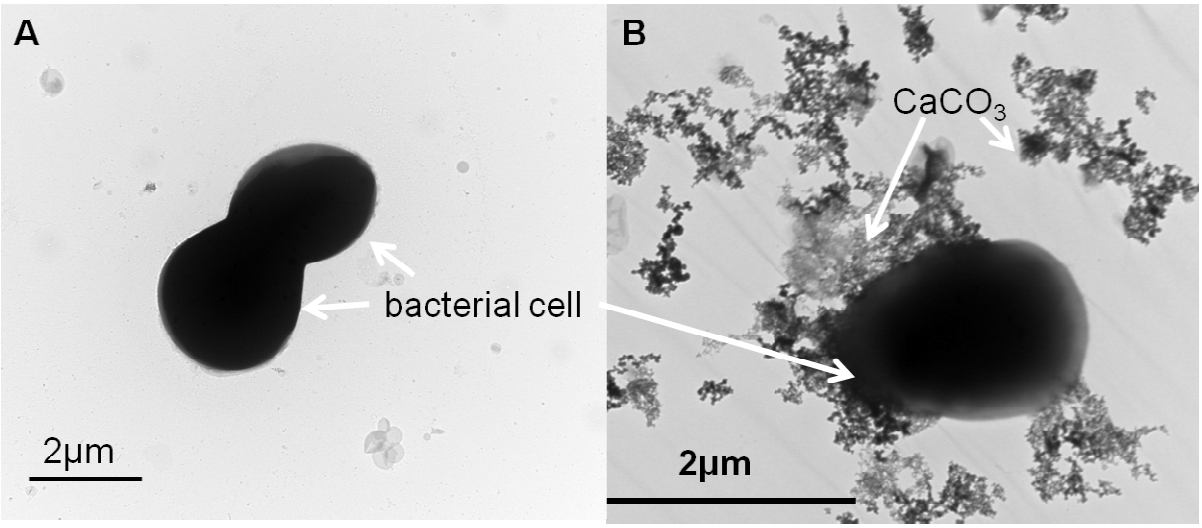


**Fig. 10. TEM images of cells of Gloeocapsa sp. (A) In nutrient solution; (B) in calcite-supersaturated media (1 mM $CaCl_2$, 10 mM $NaHCO_3$) (Exp. 26).**

The TEM images of cyanobacterial cells with mineral globules and agglomerates formed in precipitation experiment are further illustrated in Fig. 11. The size distribution of the globules is irregular; a large number of globules are in the 60-100 nm size range (small globules). These small globules are mostly attached to the surface of bacterial cells (Fig. 11 A). Some cells may be completely covered by the globules so that the surface is not visible (Fig. 11 B). There are also large globules (100-200 nm) that occur in the extracellular space, being separated from the *Gloeocapsa* sp. cells (Fig. 11 C, D).

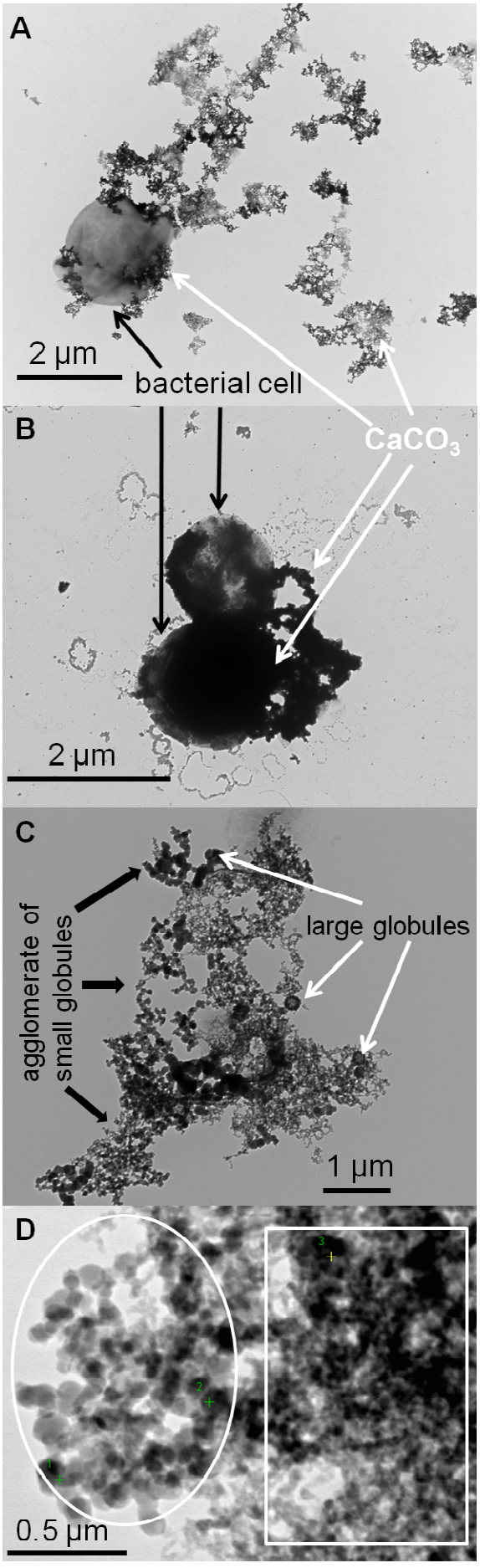


**Fig. 11. TEM image of *Gloeocapsa* sp. cells and globules of calcium carbonate formed in calcite-supersaturated media (1 mM $CaCl_2$, 10 mM $NaHCO_3$). (A) General view of the bacterial cells and $CaCO_3$ precipitated in the vicinity of the cell surface and at some distance; (B) Cell aggregate completely covered by small $CaCO_3$ globules; (C) Extracellular globular associates; (D) Detail of globular associats with aggregates of small globules (white rectangle) and large globules (white oval). Aggregate of small globules attached to the cell (not shown in this picture) (Exp. 26).**

# 4. Discussion: rates and mechanisms of calcium carbonate formation by *Gloeocapsa* sp.

The typical decrease of Ca concentration at the stage of massive $CaCO_3$ precipitation is 1 to 4 mmol/L over the first 2-7 days, accompanied by the biomass increase of 0.2 to 0.5 $g_{wet}$/L (Fig. 4, 6). This decrease, linked mainly to $CaCO_3$ precipitation (5 to 8 mmol/$g_{wet}$) is at least an order of magnitude higher than that induced by Ca adsorption at the cell surface and intracellular assimilation during cyanobacterial growth (sections 3.1 and 3.2). As a result, the rate of Ca scavenging during cyanobacterial cells growth is largely due to extracellular $CaCO_3$ precipitation rather than intracellular and surface Ca uptake. Indeed, results of the present work allowed establishing a direct relationship between the amount of precipitated calcium and the amount of biomass produced during culture growth (Fig. 12).

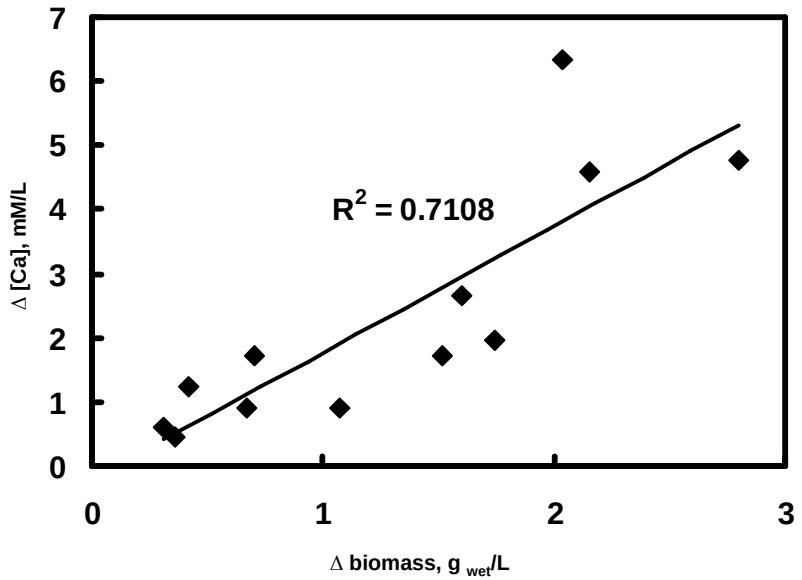


**Fig. 12. Relationship between the amount of precipitated Ca (mM/L) and increase of the biomass ($g_{wet}$/L) in biotic experiments with *Gloeocapsa sp.* in nutrient solution. Experimental conditions: $\Omega_{initial}$ = 15-150; pH = 8.6-9.6.**

Quantitative analysis of the amount of precipitated mineral (mole of Ca removed from solution) as a function of biomass production yielded a clear relationship with a slope of 2.0 following the relationship:

$$Ca_{precipitated}\ (moles) = (2.0) \times Biomass_{produced}\ (g_{wet}) \quad (3)$$

This finding corroborates reported linear relationship between the amount of hydromagnesite precipitated and the absolute biomass increase in experiments of hydrous Mg

carbonate precipitation due to photosynthetic activity of another cyanobacteria (*Synechoccocus sp.*) yielding the coefficient in Eqn. 3 of 1.45±0.23 (Appendix 1).

Despite this clear tendency of active cells to precipitate $CaCO_3$, there is no straightforward relationship between apparent calcite precipitation rates and solution supersaturation degree as shown in Fig. 13. This most likely stems from 1) microenvironment of solution pH and supersaturation degree adjacent to active photosynthesizing cells and 2) processes of Oswald ripening consisting of initial nucleation of amorphous $CaCO_3$ or monohydrocalcite at high supersaturation degree in the vicinity of cell surface, at $\Omega_{calcite}$ values significantly higher than that of the bulk solution, followed by rapid recrystallization of metastable phases to aragonite and, finally, calcite. The existence of aragonite as final precipitates in some experiments (Exp. 17 in Table 2) conducted at $\Omega_{initial} \sim 30$, indirectly witnesses the existence of such transformation reactions, also demonstrated in previous experiments with anoxygenic phototrophic bacteria (Bundeleva et al., 2011, Chapter 3 of this thesis).

$CaCO_3$ precipitation by cyanobacteria *Gloeocapsa* sp. includes several consecutive stages. In the first step, metal ions present in the aqueous surroundings of the cell interact electrostatically with negatively charged groups of cell surface and capsules (*i.e.*, Douglas & Beveridge, 1998) and cell exopolysaccharides which may act as nucleation sites capable to accumulate significant quantities of $Ca^{2+}$ (Dittrich et al., 2004, 2010). Once Ca is bound, it attracts the carbonate ion, given that cyanobacterial metabolism increases the microenvironmental pH facilitating transformation of DIC into $CO_3^{2-}$.

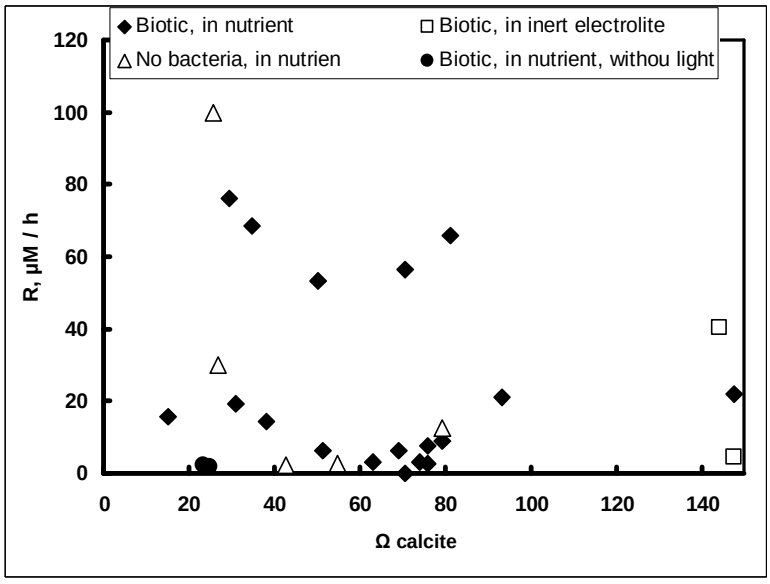


**Fig. 13. Plot of apparent Ca precipitation rates as a function of calcite supersaturation degree in the bulk solution.**

This mechanism is driven by $HCO_3^-$ uptake into the cell and its conversion by carbonic anhydrase to $CO_2$ and $OH^-$ (Miller and Colman, 1980). The $CO_2$ is incorporated into the cell biomass while $OH^-$ ions are released into the cell's microenvironment (Miller et al., 1990) and getting concentrated around the cell, and as a result around and within the capsules. Indeed, *Gloeocapsa* sp. grown under the light is capable of increasing solution pH from 8.5-8.6 to 9.5-9.6 within 48 h. This hypothesis is further confirmed by the TEM and SEM analyses: in calcite-supersaturated media, abundant $CaCO_3$ precipitation is observed around bacterial cells (Fig. 10B, 11A) with some cells and cell associates being completely encrusted by calcite (Fig. 8 A, B and C). Additional mechanism of cyanobacterial biomineralization, suggested first by Douglas and Beveridge (1998), is that cyanobacteria continuously shed off patches of mineralized S-layer which is rapidly replaced by new material. The quantitative contribution of this mechanism to biocalcification of *Gloeocapsa* sp. cannot be determined in this study; however, given that precipitated $CaCO_3$ is located not only adjacent to the cells but also at some micron-scale distance from the cells surface (Fig. 10B and 11 A, C and D), such an exopolysaccharidic shed-off pathway is certainly plausible.

Noteworthy is the typical spatial organization of cyanobacterial carbonate precipitates presented as honeycomb, highly porous calcite crystal associates, inheriting the capsules associates of bacteria (Fig. 8). The TEM images of cell – $CaCO_3$ precipitates demonstrated the tight link between the cell surface and the nano-globules of precipitated $CaCO_3$. Similar nano-spheres and globules were found during calcium carbonate precipitation by heterotrophic sulfate reducing bacteria (Aloisi et al., 2006). In their study, calcium carbonate precipitation was observed on extracellular polymeric substances (EPS) and near the microbial cell wall in the form of nano-globules. A number of recent studies with other types of anaerobic and aerobic heterotrophic bacteria (*e.g.*, Bontognali et al., 2008, Spadafora et al., 2010) also confirmed the governing role of mineral nano-globules in microbially-induced Ca and Mg carbonate formation.

The absence of self-protection mechanisms against $CaCO_3$ incrustation in *Gloeocapsa* sp. cyanobacteria sheds new light on mechanisms and capacities of photosynthetizing organisms to form carbonate mineral deposits. It has been earlier argued that the sole action of cyanobacteria, notably in the biomats is insufficient to provide massive calcium carbonate deposition. Numerous field observation and modeling experiments (Krumbein et al., 1977; Chafetz and Buczynski, 1992) demonstrated that precipitation of calcium carbonate occurs predominantly within the mats in the aphotic zone, in the deeper parts of the mats where the

degradation of organic compounds by heterotrophic bacteria occurs. In modern Ca-Mg carbonate stromatolites, formed in association with microbial mats in hypersaline coastal lagoons, degradation of organic matter of soft mats leads to the development of lithified Ca-Mg carbonate laminate via sub-micron polyhedral crystal formation of high-Mg calcite and/or Ca dolomite as a result of the coalescence of carbonate nano-globules around degraded organic matter nuclei (Spadafora et al., 2010). Furthermore, dead cyanobacteria were coated with calcium carbonate quicker and to a greater extent than live cyanobacteria (Chafetz and Buczynski, 1992) in agreement with the earlier observation that $CaCO_3$ precipitation within the mats is governed by the degradation of organic carbon compounds by bacteria (Krumbein et al., 1977). In addition to well-established S-layer shed off (Thompson et al., 1997), this observation may be linked to metabolic maintenance of positive surface potential and self-protection of live cyanobacterial cells from the incrustation (Martinez et al., 2008, 2010). Another mechanism of bacteria self-protection against uncontrolled encrustation is extracellular polymeric substances (EPS) secreted by the microbial community as it is the case for *Desulfovibrio brasiliensis*, whose cells are predominantly located outside of the EPS aggregates where mineral growth takes place. As a result, they remain mobile and are rarely entombed within the mineral (Bontognali et al., 2008). Similarly, another SRB bacterium, *Desulfonatronum lacustre*, produces individual globules 6-20 nm in diameter that originates from the cell surface but calcify significantly only when released to the culture medium (Aloisi et al., 2006). The idea that EPS of cyanobacteria serve as effective $Ca^{2+}$-buffers, thus preventing seed crystal nucleation even in a highly supersaturated macroenvironment has been also suggested from numerous field studies of biofilms in alkaline salt lakes (*e.g.*, Arp et al., 1999a, b).

In this regard, the ability of cyanobacteria *Gloeocapsa* sp. to efficiently calcify, even in life cell culture, is most likely linked to its unique cellular organization. Indeed, several *Gloeocapsa* sp. cells are usually grouped together in a single external capsule having essential polysaccharidic composition. In addition, the major surface functional groups of *Gloeocapsa* sp. cells are carboxylate, amine, phosphoryl/phosphodiester and hydroxyl stemmed from the presence of protein, lipid and carbohydrate components on the external envelopes of cells and cell associates such as capsules (Pokrovsky et al., 2008).

In contrast to other cyanobacteria such as *Synechococcus* sp. and *Planktothrix* sp. (Martinez et al., 2010) and anoxygenic phototrophic bacteria (Bundeleva et al., 2011), the *Gloeocapsa* sp. cells do not increase their zeta-potential at $9 \leq pH \leq 11$ (Pokrovsky et al., 2008). This result, together with massive cell incrustation by $CaCO_3$ and mineral formation in

the vicinity of the cell walls, microscopically confirmed in the present study, suggest the absence of specific "cell protection mechanism" against cells incrustation during active phase of $CaCO_3$ nucleation.

# 5. Conclusions

This study presents the first step towards the quantification of $CaCO_3$ precipitation by live photosynthetizing cyanobacteria, *Gloeocapsa* sp., having untypical cellular organization. Biotic experiments performed in strongly supersaturated solutions yielded different type of crystals reflecting that $CaCO_3$ precipitation in these experiments can be driven by different mechanisms: inorganic precipitation producing rhomboid calcite crystals, typical for abiotic experiments, and cell-induced precipitation producing the porous crystals with honeycomb – like structure bearing the imprints of *Gloeocapsa* sp. cell associates. Detailed TEM analyses revealed the presence of nano-globules covered by organic matter in the vicinity of cell surface but also at some micron-scale distance from the cells. Overall, microscopic examination of reaction products obtained in various environmental conditions does not suggest the existence of any self-protection mechanism against uncontrolled $CaCO_3$ encrustation of live *Gloeocapsa* sp. cells, in contrast to that established earlier for other cyanobacteria, anoxygenic phototrophic bacteria and heterotrophic anaerobic bacteria. The lack of this self-protection mechanism, also supported by electrostatic surface properties of *Gloeocapsa* sp. cell capsular associates, and high laboratory calcification rates measured at relatively low biomass produced during bacterial growth, place these bacteria among the most efficient bacterial calcifies on Earth. Indeed, apparent bulk rates of $CaCO_3$ precipitation due to *Gloeocapsa* sp. photosynthesis (0.01-0.100 mM/h) are similar or higher than those reported for capsule-free cyanobacteria *Synechococcus sp.* and *Planktothrix sp.* (0.03-0.04 mM/hr, Martinez et al., 2010), aerobic ureolithic bacteria (0.01 mM/hr, Micthel and Ferris, 2005) and anoxygenic phototrophic bacteria (0.001-0.0150 mM/hr, Bundeleva et al., 2011, Chapter 3). The absence of direct correlation between the apparent $CaCO_3$ precipitation rates and calcite supersaturation degree or other solution chemical composition parameters is most likely linked to specific microenvironments, non detectable in the bulk solution, adjacent to cyanobacterial cell due to intensive photosynthetic activity and $OH^-$ ions release.

# Conclusions and perspectives

# Résumé en français de la conclusion

La présente étude décrit une approche conjointe de plusieurs techniques destinée à caractériser la précipitation de carbonate de calcium induite par deux types de souches bactériennes anoxygéniques phototrophiques (APB), *Rhodovulum steppense* A-20s haloalcaliphilique et *Rhodovulum* sp. S-17-65 neutrophilique halophilique, se développant sur des substrats organiques; ainsi que par une souche de cyanobactéries d'eau douce *Gloeocapsa* sp..

Dans le premier article publié nous avons décrits les mesures de mobilité électrophorétique et d'adsorption de Ca à la surface des APB A-20s et S-17-65 vivantes, inactive et mortes qui ont été effectuées afin de déterminer le degré pour lequel ces bactéries contrôlent métaboliquement leur potentiel de surface. Nous avons montré en particulier que ces APB sont capable de réguler leur potentiel de surface en solution alcaline (pH~10-10.5). Cela entraîne un potentiel zeta inhabituellement moins négatif, alors jamais reporté pour la plupart des bactéries, à l'exception des cyanobactéries. Cet effet n'est pas observé pour les cellules mortes et celles inhibées par $NaN_3$, et il est significativement réduit après l'ajout de 1 à 10 mM d'ions bicarbonates.

Par analogie avec d'autres bactéries, deux mécanismes fonctionnant en parallèle peuvent être mis en avant pour expliquer ce nouveau phénomène d'augmentation du potentiel zeta en présence d'APB en solution alcaline : *i)* l'extension de la consommation de micronutriments sous forme d'anions et *ii)* la répulsion des ions $Ca^{2+}$ par la surface cellulaire, la protégeant ainsi de l'incrustation de $CaCO_3$. Ce dernier mécanisme est en accord avec les résultats d'adsorption de calcium à la surface cellulaire dans la gamme physiologique de composition de la solution. Une légère différence dans le degré d'augmentation du potentiel zeta et d'adsorption de Ca a été observée entre les deux souches APB étudiées ce qui est compatible avec leurs différences de surface cellulaire effective et leurs gammes de compositions optimales de la solution.

Dans le second article, soumis, nous présentons les premiers résultats de précipitation de $CaCO_3$ par des bactéries anoxygéniques phototrophiques. Les conditions optimales initiales de précipitation pour les deux souches sont les suivantes : [Ca]=10mM ; [DIC]=5mM, pH=8.1±0.1 et $\Omega_{CaCO_3}$ =70-100. Au stade de précipitation massive de $CaCO_3$, les vitesses apparentes varient entre 0.001 et 0.010 mM/heure, et entre 0.005 et 0.015 mM/heure pour les cultures A-20s et S-17-65, respectivement. Ces valeurs sont similaires à celles reportées auparavant pour les cyanobactéries et les bactéries hétérotrophes, étant déjà

deux ordres de grandeur plus importantes que les taux de calcification typiques des algues corallines. Les vitesses apparentes de précipitation mesurées ne sont pas affectées, à 10-20% près, par l'adsorption de Ca à la surface des cellules et par la consommation intracellulaire de Ca pendant la croissance de celle-ci. Les vitesses apparentes de précipitation sont positivement corrélées avec $\Omega_{CaCO_3}$, mais il existe un seuil de pH (~8.5) au dessus duquel les cellules vivantes précipitent $CaCO_3$ alors que les cellules mortes et inactives ne montrent aucune précipitation. Il apparaît ainsi qu'un pH élevé est un prérequis important pour la précipitation de $CaCO_3$ par des APB vivantes, même pour des taux de sursaturation élevés.

Des analyses par microscopie électronique en transmission (MET) ne montrent aucune présence de $CaCO_3$ à l'intérieur des cellules vivantes. Cependant, la calcite et le monohydro-calcite ont été identifiés par microscopie électronique à balayage (MEB) et par diffraction de rayons X (XRD) comme étant les principales phases de carbonate de calcium ayant précipitées dans la solution. Ces résultats suggèrent fortement l'existence d'un mécanisme prévenant la biominéralisation de carbonates au sein des cellules vivantes des APB, qui peuvent ainsi se protéger d'incrustations incontrôlées. Ce mécanisme consisterait principalement en la création de charges plus positives à leur surface, pour des pH correspondant à la nucléation massive de $CaCO_3$.

La troisième partie de l'étude, également sous forme d'article, visait à analyser le rôle des cyanobactéries *Gloeocapsa* sp. dans la précipitation de $CaCO_3$ par des modèles expérimentaux en laboratoire. Afin de définir le lien entre la croissance bactérienne (production de biomasse) et les vitesses de précipitation de $CaCO_3$, des expériences cinétiques de précipitation avec les deux souches de APB et les cyanobactéries *Gloeocapsa* sp. en solution nutritive et d'électrolyte inerte ont été menées. Les phases solides précipitées ont été examinées par MEB, MET et XRD. Ces observations microscopiques ont permis de mettre en évidence différents mécanismes de précipitation de $CaCO_3$ en présence de *Gloeocapsa* sp.: inorganique, produisant de la calcite rhomboédrique typique d'expériences abiotiques, et biologiques. Ce dernier processus est mis en évidence par l'apparition de cristaux poreux et par des empreintes sur les cristaux rhomboédriques et sur les nano-globules de calcite précipitée recouverts de matière organique. Les analyses microscopiques montrent la présence de carbonate de calcium directement sur la membrane cellulaire et au sein des cellules vivantes des bactéries. Les expériences menées sur *Gloeocapsa* sp. ne montrent aucun lien entre la vitesse de précipitation apparente et le degré de sursaturation par rapport à $CaCO_3$. Ceci est plutôt lié à l'existence de microenvironnements (pH, [DIC], $\Omega_{CaCO3}$) autour des

cellules réalisant la photosynthèse, qui ne sont pas directement liés et/ou identiques à la composition globale de la solution.

L'ensemble des résultats de précipitation de $CaCO_3$ nous permet ainsi d'identifier deux types différents de biominéralisation en lien avec la photosynthèse bactérienne. ***Le premier est qualifié de nucléation suivie de précipitation passive en dehors de la membrane cellulaire pour les APB***, et ***le second de nucléation directe liée à la surface des cellules pour Gloeocapsa sp.***. Dans le premier cas, le scénario le plus plausible de précipitation de $CaCO_3$ consiste en l'augmentation du pH et du degré de saturation environnant par les APB au cours de leur métabolisme, entraînant un changement de la chimie de la solution. Il est peu probable que les cellules vivantes des APB puissent servir de sites de nucléation pour les carbonates, car selon nos observations, elles se protègent de l'incrustation par les précipités en créant un potentiel de surface positif à un pH typique de la photosynthèse et durant la phase de nucléation massive de carbonates. En revanche, l'absence d'un mécanisme de protection semblable pour les cyanobactéries *Gloeocapsa* sp., due à une organisation spatiale différente de leurs cellules, entraine une calcification efficace des dites cellules. Elles peuvent dans ce cas servir de site de nucléation de part la charge négative présente à la surface des capsules de *Gloeocapsa* sp., qui peuvent alors lier et accumuler les ions métalliques comme $Ca^{2+}$. De plus, au sein du microenvironnement proche des parois cellulaires bactériennes, le pH peut être plus élevé que celui de la solution à cause de l'intense photosynthèse qui s'y déroule. Cette composition très variable de la solution à la surface des bactéries ne permet pas l'observation d'une relation directe entre le degré de sursaturation de la solution et la vitesse apparente de précipitation de $CaCO_3$ en présence de *Gloeocapsa* sp. réalisant la photosynthèse.

Enfin, les deux derniers articles consignés dans cette thèse (Annexes 1 et 2) présentent l'étude de la formation de carbonates magnésiens hydratés et leurs fractionnements isotopiques associés en présence de bactéries vivantes réalisant la photosynthèse (*Gloeocapsa* sp. et *Synechoccocus* sp.). Nous avons ainsi montré, lors d'une série d'expériences et d'observations en milieu naturel, que les Mg-carbonates hydratés peuvent apparaître à la suite de photosynthèse cyanobactérienne dans les eaux de lacs, et que le fractionnement isotopique du magnésium entre le solide et la solution ($\Delta^{26}Mg_{solid\text{-}solution}$) associé à ce processus se situe entre -0.8 et -1.5‰. Il n'y a pas de différence significative entre les facteurs de fractionnement biotiques et abiotiques. La formation de Mg-carbonates hydratés se produit via un processus en cascade de cristallisation/recristallisation : nesquehonite $\rightarrow$ dypingite $\rightarrow$

hydromagnésite initié par la nucléation de nano globules au sein et à la surface de cellules vivantes.

Ce travail représente les premiers pas vers une évaluation quantitative du phénomène de biominéralisation bactérienne en cultures individuelles en solutions aqueuses. L'émergence de nouvelles techniques de mesures : chimiques in-situ de haute résolution, spectroscopiques et d'observations à l'échelle microscopique et macroscopique, actuellement employées par différents groupes de recherche dans le monde, pourraient conduire à une nouvelle compréhension, sur le plan qualitatif, des réactions et associations d'interactions minéral-cellule bactérienne, et de l'appliquer non seulement aux cultures individuelles mais aussi aux consortia de cellules, à la fois en conditions de laboratoire et en environnement naturel.

# Conclusions and perspectives

This study describes a concerted multi-technical approach to characterize calcium carbonate precipitation induced by two contrasting strains of anoxygenic phototrophic bacteria (APB), haloalcaliphilic *Rhodovulum steppens* A-20s and neutrophilic halophilic *Rhodovulum* sp. S-17-65 growing on organic substrates as well as typical freshwater cyanobacteria *Gloeocapsa* sp.

In the **first** paper of this work, electrophoretic mobility measurements and surface adsorption of Ca on living, inactivated, and heat-killed A-20s and S-17-65 APB cell surfaces were performed to determine the degree to which these bacteria metabolically control their surface potential equilibria. We demonstrate, in a suite of electrophoretic and macroscopic batch adsorption experiments, that these APB are capable of regulating their electric surface potential in alkaline solutions (pH ~ 10-10.5). This produces an unusual, less negative zeta potential at these conditions, previously non-reported for most bacteria except cyanobacteria. This effect is absent for heat-killed and $NaN_3$-inactivated cells and it is significantly suppressed in the presence of 1-10 mM added bicarbonate ions.

Based on analogy with other bacteria, two parallel mechanisms can be suggested to explain this novel feature of zeta potential increase of APB in alkaline solutions linked to the appearance of less-negative zeta-potential: *i*) enhancement of uptake of the micronutrients in the form of anions and *ii*) $Ca^{2+}$ ions repelling from the cell surface in order to protect the cells from $CaCO_3$ incrustation. The latter mechanism is consistent with the results of Ca adsorption on the cell surface in the physiological range of solution composition. A slight difference in the degree of zeta-potential increase and Ca adsorption was observed between the two studied APB strains, which is compatible with their differences in surface areas and optimal physiological range of solution parameters.

In the **second** paper of this work, we reported the first results on $CaCO_3$ precipitation by anoxygenic phototrophic bacteria. The optimal initial precipitation conditions for both strains were as following: Ca = 10 mM; DIC = 5 mM , pH = 8.1±0.1 and $\Omega_{CaCO_3}$ = 70-100. At the main stage of massive $CaCO_3$ precipitation, the bulk rates range between 0.001 and 0.010 mM/hr, and between 0.005 and 0.015 mM/hr for A-20s and S-17-65 APB cultures, respectively. These values are similar to those reported earlier for cyanobacteria and heterotrophic bacteria, being 2 orders of magnitude higher than typical calcification rates of coralline algae. Measured bulk precipitation rates are unaffected, within the experimental

uncertainty of 10-20%, by Ca adsorption at the cell surface and by intracellular Ca uptake during cell growth. The rates are positively correlated with $\Omega_{CaCO_3}$, but there is a threshold pH value around 8.5 above which the live cells precipitate $CaCO_3$ whereas the dead and inactivated cells exhibit zero precipitation rate below pH 8.5. It follows that the elevated pH is an important prerequisite for live APB to form $CaCO_3$ even at high supersaturation degrees.

TEM analyses of reaction products does not demonstrate the presence of $CaCO_3$ crystals in the vicinity of live cells, yet calcite and monohydrocalcite were identified using SEM and XRD techniques as main precipitates of the bulk solution. These results strongly suggest the existence of a mechanism preventing carbonate biomineral formation in the vicinity of live APB cells, which can protect them from uncontrolled carbonate incrustation. This mechanism most likely consists in creating a more positive charge on their surface at pH corresponding to massive $CaCO_3$ nucleation.

The **third** paper of this study analyzed the effect of cyanobacteria *Gloeocapsa sp.* on $CaCO_3$ precipitation via experimental laboratory modeling. To characterise the link between bacterial growth (biomass production) and the rate of $CaCO_3$ precipitation, and the precipitation process batch kinetic experiments with both strain of APB and with cyanobacteria *Gloeocapsa* sp. in nutrient solution and in inert electrolyte were performed and produced precipitates were examined by SEM, TEM and XRD techniques. The TEM and SEM analyses demonstrated the presence of different types of crystals formed in the biotic experiments. It follows that $CaCO_3$ precipitation in the presence of *Gloeocapsa sp.* can be driven by different mechanisms: inorganic precipitation (producing rhombohedral calcite, typical for abiotic experiments), and biological precipitation witnessed by appearance of porous crystals and imprints of cell associates in calcite rhombohedra as well as the nano-globules covered by organic matter. Microscopic analysis showed the presence of calcium carbonate directly on the cell membrane in the vicinity of live bacterial cells. Experiments on *Gloeocapsa* sp. demonstrated the absence of relationship between the apparent precipitation rates and the supersaturation degree with respect to $CaCO_3$. This is most likely linked to the existence of microenvironments (pH, DIC, $\Omega_{CaCO3}$) around the photosynthetizing cells, not directly related to the bulk solution composition.

Taken together, results of $CaCO_3$ precipitation allowed identification of two different types of biomineralization related to bacterial photosynthesis, namely ***unspecific passive nucleation and precipitation outside of the cell membrane for APB*** and ***direct, cell-surface related nucleation for Gloeocapsa sp***. For APB, the most plausible scenario of $CaCO_3$

precipitation consists in increasing the pH of the bulk solution during bacterial metabolism. The role of APB in precipitation is restricted to the change of bulk aqueous solution chemistry via increasing solution pH and saturation degree. It is unlikely that live APB cells may serve as nucleation sites for carbonate precipitation, because they apparently protect themselves from carbonate incrustation by creating a positive surface potential at the pH of photosynthesis and during the phase of massive $CaCO_3$ nucleation. In contrast, the absence of cell protection mechanism for cyanobacteria *Gloeocapsa* sp. due to different spatial organization of their cells allow them to efficiently calcify via direct embedding of cells by calcite. The cells in this case may serve as nucleation centers due to negative charge present on the surface of *Gloeocapsa* sp. capsules which can therefore bind and accumulate the metal ions such as $Ca^{2+}$. In addition, in the microenvironment close to the bacterial cell wall the pH might be higher than that in the bulk solution due to intense photosynthesis. This extremely variable solution composition in the vicinity of cell surface does not allow observing a straightforward relationship between the bulk solution supersaturation degree and apparent $CaCO_3$ crystallization rates in the presence of photosynthetizing *Gloeocapsa sp.*

Finally, the last two papers of this thesis (Appendix 1 and 2) present a study of hydrous Mg carbonate formation in the presence of live photosynthetizing bacteria (*Gloeocapsa* sp. and *Synechoccocus* sp.). We have shown, in a suite of laboratory experiments and natural observations, that hydrous Mg carbonate precipitation may occur due to cyanobacterial photosynthesis in the lake water and that Mg isotope fractionation between solid and solution ($\Delta^{26}Mg_{solid\text{-}solution}$) linked to this process ranges from -0.8 to -1.5 ‰. There is no significant difference between biotic and abiotic fractionation factors. Formation of hydrous Mg carbonate occurs via stepwise crystallization/recrystallization process nesquehonite $\rightarrow$ dypingite $\rightarrow$ hydromagnesite initiated by the nucleation of nanoglobules in the vicinity and on the live cell surfaces.

This work opens a number of perspectives for further research on bacterial biomineralization.

- Towards a better understanding of initial crystallization phenomena, cyanobacterial cell surface and EPS interaction with Ca and Mg are considered as important governing factors of mineral nucleation kinetics and thus deserve a separate study. Towards this goal, a multidisciplinary macroscopic/microscopic and spectroscopic approach can be envisaged.

- The present study, performed in batch reactors, demonstrated the difficulties of quantifying the rates of mineral growth and nucleation in closed system with continuously increasing biomass. Therefore, for rigorous assessment of crystallization rates and identification of governing parameters, continuous-flow, open-system biological reactors similar to those elaborated for mineral dissolution (e.g., Shirokova et al., 2011, submitted) have to be used. Such reactors will allow maintaining constant bacterial biomass (at the exponential or stationary stage) and constant solution parameters (pH, [Ca], [Mg], [DIC], [DOC]) including supersaturation degree $\Omega_{CaCO3}$, while continuously evacuating growthing biomass and mineral precipitation products.
- The ultimate goal of multidisciplinary physico-chemical study of bacterial biomineralization phenomena should be a construction of quantitative (and predictive) model that link the primary productivity (PP, or biomass growth) and the amount and mineralogy of precipitated mineral. A straightforward relationship between the amount of produced biomass and the moles of precipitated hydrous Mg carbonate (established for Synechoccocus sp. cyanobacteria of the Salda Lake water) provides a solid empirical background for such a model. Ideally, this model should incorporate the differential equations linking the PP of a single APB or cyanobacterial cell and the spatial distribution of pH, DIC, Ca(Mg) and Ω in the diffuse layer adjacent to bacterial surface (see for example, Pokrovsky and Savenko 1995a,b). Based on available nucleation and crystal growth rate models (constructed from independent abiotic experiments), a kinetic equation for carbonate precursor nucleation and metastable phase crystal growth in the vicinity of cell surface should be constructed. These relationships will be used to assess the time necessary to form the first mineral precursor (nesquehonite, monohydrocalcite, amorphous $CaCO_3$) depending on the intensity of photosynthesis and initial chemical composition of the media. The next step in this model should be a prediction of mineral transformation reactions in the sequence of classical Oswald ripening:

$CaCO_3$(amorp) → monohydrocalcite → vaterite → aragonite → calcite, and Nesquehonite → dypingite → hydromagnesite,

which occur under continuous photosynthesis leading to the increase of pH and Ω and decrease of [DIC] and [Ca]([Mg]). Again, the transformation (recrystallization) reaction rate driven essentially by physico-chemical inorganic mineral dissolution/precipitation reactions should be based on results of independent abiotic experiments.

Finally, this model should incorporate, at all stages of mineral growth and dissolution, the effect of cellular exometabolites and various excudates both on Ca(Mg) speciation in solution and on the mineral(nucleus) surface. Again, these kinetic and thermodynamic coefficients can be evaluated only from independent physico-chemical experiments with bacterially-produced dissolved and colloidal organic matter. Overall, it is anticipated that such a model, applied for the first time to bacterial monoculture, will allow quantitative reconstruction of the amount and nature of carbonate minerals formed during autotrophic bacterial activity both in the past and present aquatic environments.

- Despite a highly sophisticated physico-chemical and microscopic approach used in the present study to characterize the processes of carbonate biomineralization induced by axenic bacterial cultures, the direct extrapolation of these results to natural environments is not possible because of the dominance of microbial consortia (autotrophic and heterotrophic aerobic and anaerobic bacteria). The main differences of these consortia experiments from monocultural approach are: *i*) chemical gradients linked to PP and respiration are different and exhibit clear diurnal and much more heterogeneous spatial pattern and *ii*) cellular exometabolites and dead cells are not freely available to participate in mineral carbonation process, being essentially consumed by heterotrophic activity. Towards approaching the natural environment, a coupled (double) culture in the liquid media of autotrophic and heterotrophic bacteria should be developed. In such a microbial reactor, simultaneous control of both heterotrophic bacteria and cyanobacterial concentration, primary productivity and respiration together with all usuall solution parameters should be provided and the mineral precipitation rates may be assessed following the conceptual scheme described above for the monoculture reactor.
- An efficient way to address both spatial heterogeneity and species-species relationship in a complex microbial consortia is to use gel-like cell growth and mineral crystallization media thus approaching the cyanobacterial biofilm conditions typical for microbial mats or stromatolites. Although numerous previous studies used agar media for $Ca(Mg)CO_3$ crystallization in the presence of heterotrophic bacteria, the main shortcoming of these works was the lack of rigorous characterization of the chemical composition of the media. To overcome this barrier, Raman or confocal-based techniques allowing high-resolution imaging of chemical profiles around growing cells and precipitating mineral aggregates are envisaged.

Additional powerful technique allowing efficient tracing of specific biological, metabolic and physico-chemical (abiotic) processes of carbonate mineral formation is the measurement of stable isotope fractionation. Although the last part of this study failed to prove the specific

biological Mg isotope fractionation mechanism (manuscripts presented in Appendix 1 and 2), linked to Mg hydrous carbonate precipitation by cyanobacteria, the potential of using C, Ca and Mg isotopes but also traces such as B, Fe, metals for each of the reaction sequence step of the general model described in the third perspectives (presented above) is just at the beginning of its exploration.

Overall, this work represents only the first step towards quantitative assessment of bacterial biomineralization phenomena in individual cultures in aqueous solutions. Appearance of novel, in-situ high resolution tracing chemical, spectroscopic, microscopic but also macroscopic techniques, being currently applied by different research groups in the world, will allow achieving new qualitative understanding of mineral – bacterial cell interaction reaction and associations applied to individual cultures but also to cell consortia, both in laboratory conditions and in natural environment.

# Bibliographic list

Alekseev, O.L., Boiko, Yu.P., Ovcharenko, F.D., Shilov, V.N., Chubirka, L.A., 1988. Electroosmosis and some properties of the boundary layers of bounded water. *Kolloid. Zh.* **50**, 211-216.

Allison, J.D., Brown, D.S., Novo-Gradac, K.J. MINTEQA2/PRODEFA2, A Geochemical Assessment Model for Environmental Systems. Version 3.0 User's Manual, U.S. EPA, Athens, GA (1991) 106 pp.

Aloisi, G., Gloter, A., Kruger, M., Wallmann, K., Guyot, F., Zuddas, P., 2006. Nucleation of calcium carbonate on bacterial nanoglobules. *Geology* **34**, 1017-1020.

Altermann, W., Kazmierczak, J., Oren, A., Wright, D.T., 2006. Cyanobacterial calcification and its rock-building potential during 3.5 billion years of Earth history. *Geobiology* **4**, 147-166.

Arp, G., Reimer, A., Reitner, J., 1999a. Calcification in cyanobacterial biofilms of alkaline salt lakes. *Eur. J. Phycol.* **34**, 393-403.

Arp, G., Thiel V., Reimer, A., Michaelis, W., Reitner, J., 1999b. Biofilm exopolymers control microbialite formation at thermal springs discharging into the alkaline Pyramid Lake, Nevada, USA. *Sedimentary Geology* **126**, 159–176.

Arp, G., Reimer, A., Reitner, J., 2003. Microbialite formation in seawater of increased alkalinity, Satonda Crater Lake, Indonesia. *Journal Sedimentary Research* **73**, 105-127.

Bayer, E.M., Sloyer, J.L., 1990. The electrophoretic mobility of Gram-negative and gram-positive bacteria: and electrokinetic analysis. *Journal of General Microbiology* **136**, 867-874.

Bazant, M.Z., Kilic, M.S., Storey, B.D., Ajdari, A., 2009. Towards an understanding of induced-charge electrokinetics at large applied voltages in concentrated solutions. *Advances in Colloid and Interface Science* **152**, 48-88.

Belton, G., 1976. Langmuir adsorption, the gibbs adsorption isotherm, and interracial kinetics in liquid metal systems. *Metallurgical and Materials Transactions* **7**, 35-42.

Beukes, N., 2004. Biogeochemistry: early options in photosynthesis. *Nature*, **431**, 522-523.

Beveridge, T. J., Graham, L.L., 1991.Surface layers of bacteria. *Microbiol. Rev.* **55**, 684-705.

Beveridge, T.J., 1988. Wall ultrastructure: how little we know. In: Actor, P., Daneo-Moore, L., Higgins, M.L., Salton, M.R.J., Shockman, G.D.,(Eds.), Antibiotic Inhibition of Bacterial Cell Surface Assembly and Function. *American Society for Microbiology*, Washington, DC, USA, pp. 3-20.

Beveridge, T.J., Pouwels, P.H., Sára, M., Kotiranta, A., Lounatmaa, K., Kari, K., Kerosuo, E., Haapasalo, M., Egelseer, E.M., Schocher, I., Sleytr, U.B., Morelli, L., Callegari, M.-L., Nomellini, J.F., Bingle, W.H., Smit, J., Leibovitz, E., Lemaire, M., Miras, I., Salamitou, S., Béguin, P., Ohayon, H., Gounon, P., Matuschek, M., Sahm, K., Bahl, H., Grogono-Thomas, R., Dworkin, J., Blaser, M.J., Woodland, R.M., Newell, D.G., Kessel, M., Koval, S.F., 1997).V. Functions of S-layers. *FEMS Microbiology Reviews* **20**, 99-149.

Blankenship, R., Madigan, M.T., 2004. Taxonomy and Physiology of Phototrophic Purple Bacteria and Green Sulfur Bacteria. Anoxygenic Photosynthetic Bacteria. *Springer Netherlands* **2**, 1-15.

Blankenship, R.E., 1992. Origin and early evolution of photosynthesis. *Photosynth Res* **33**, 91-111.

Blankenship, R.E., 1994. Protein structure, electron transfer and evolution of prokaryotic photosynthetic reaction centers. *Antonie van Leeuwenhoek* **65**, 311-329.

Blankenship, R.E., Madigan, M.T., Bauer, C., 1995. Anoxygenic Photosynthetic Bacteria. *Kluwer Academic*, Netherlands.

Blankenship, R.E., Sadekar, S., Raymond, J., Paul, G.F., Andrew, H.K., 2007. The Evolutionary Transition from Anoxygenic to Oxygenic Photosynthesis. In: Evolution of Primary Producers in the Sea. *Academic Press*, Burlington, pp. 21-35.

Bontognali, T.R.R., Vasconcelos, C., Warthmann, R.J., Dupraz, C., Bernasconi, S.M., McKenzie, J.A., 2008. Microbes produce nanobacteria-like structures, avoiding cell entombment. *Geology* **36**, 663-666.

Borrok, D, Fein, J.B., 2004. Distribution of protons and Cd between bacterial surfaces and dissolved humic substances determined through chemical equilibrium modeling. *Geochimica et Cosmochimica Acta*, **68**, 3043-3052.

Bosak, T., Greene, S.E., Newman, D.K., 2007. A likely role for anoxygenic photosynthetic microbes in the formation of ancient stromatolites. *Geobiol.* **5**, 119-126.

Bosak, T., Newman, D.K., 2003. Microbial nucleation of calcium carbonate in the Precambrian. *Geology* **31**, 577-580.

Bosak, T., Newman, D.K., 2005. Microbial kinetic control on calcite morphology in supersaturated solutions. *Journal of Sedimentary Petrology* **75**, 190-199.

Bozzola, J.J., Russell, L.D., 1999. Electron microscopy: principles and techniques for biologists, *Jones and Bartlett Publishers*.

Braissant, O., Cailleau, G., Dupraz, C., Verrecchia, E.P., 2003. Bacterially induced mineralization of calcium carbonate in terrestrial environments: The role of exopolysaccharides and amino acids. *Journal of Sea Research* **73**, 485-490.

Briggs, W., 1989. Photosynthesis. *Alan Liss*., New York.

Bundeleva, I.A., Shirokova, L.S., Bénézeth, P., Pokrovsky, O.S., Kompantseva, E.I., 2009. Calcium carbonate precipitation in the presence of phototrophic anaerobic bacteria *Rhodovulum* sp. Proceedings of 19th Annual V.M. Goldschmidt Conference, Davos, Switzerland, 21-26 juin 2009. *Geochim. Cosmochim. Acta,* **73,** No 13, Suppl. S, p. A174.

Bundeleva, I.A., Shirokova, L.S., Bénézeth, P., Pokrovsky, O.S., Kompantseva, E.I., 2010. Experimental modelling of calcium carbonate precipitation in the presence of phototrophic anaerobic bacteria *Rhodovulum* sp. Geophysical Research Abstracts, EGU General Assembly 2010, Vol. **12**, EGU2010-9521.

Bundeleva, I.A., Shirokova, L.S., Bénézeth, P., Pokrovsky, O.S., Kompantseva, E.I., 2011. Zeta-potential of anoxygenic phototrophic bacteria and Ca adsorption at the cell surface: possible implications for cell protection from $CaCO_3$ precipitation in alkaline solutions. *J Colloid Interface Science* **360**, 100-109.

Burns, B.P., Goh, F., Allen, M. Nallan, B.A., 2004. Microbial diversity of extant stromatolites in the hypersaline marine environment of Shark Bay, Australia. Enviromental *Microbiology* **6**, 1096-1101.

Castanier, S., Métayer-Levrel, G.L., Perthuisot, J.-P., 1999. Ca-carbonates precipitation and limestone genesis -- the microbiogeologist point of view. *Sedimentary Geology* **126**, 9-23.

Castenholz, R., Pierson, B., 2004. Ecology of thermophilic anoxygenic phototrophs. In Advances in Photosynthesis and Respiration, (Eds. Blankenship R., Madigan M. and Bauer C.) *Kluwer Academic Publishers New York* **2**, 87-103

Chafetz, H.S., Buczynski, C., 1992. Bacterially induced lithification of microbial mats. *Palaios* **7**, 277-293.

Chesworth, W., Zasoski, R.J., 2008. Zeta potential. Encyclopedia Soil Science, *Springer Netherlands*, pp 841-845.

Deinega, Yu.F., Polyakova, V.M., Alexandrove, L.N., 1982. Electrophoretic mobility of particles in concentrated electrolyte solutions. *Kolloid. Zh.* **48**, 546-548.

DiMasi, E., Kwak, S.-Y., Amos, F.F., Olszta, M.J., Lush, D., Gower, L.B., 2006. Complementary control by additives on the kinetics of amorphous $CaCO_3$ mineralization at an organic interface. *Physical Review Letters* **97,** 045503-045504.

Dittrich, M., Kurz, P., 2004. The role of autotrophic Picocyanobacteria in calcite precipitation in an oligotrophic lake. *Geomicrobiol. J* **21**, 45-53.

Dittrich, M., Kurz, P., Wehrli, B., 2004. The role of autotrophic picocyanobacteria in calcite precipitation in an oligotrophic lake. *Geomocrobiol. J.* **53**, 45-53.

Dittrich, M., Obst, M., 2004. Are picoplankton responsible for calcite precipitation in lakes? *Ambio* **33**, 559-564.

Dittrich, M., Sibler, S., 2005. Cell surface groups of two picocyanobacteria strains studied by zeta potential investigations, potentiometric titration, and infrared spectroscopy, *J. Coll. Interf. Sci.* **286**, 487–495.

Dittrich, M., Sibler, S., 2006. Influence of $H^+$ and calcium ions on surface functional groups of *Synechococcus* PCC 7942 cells, *Langmuir* **22**, 5435–5442.

Dittrich, M., Sibler, S., 2010. Calcium carbonate precipitation by cyanobacterial polysaccharides. *Geol. Soc. London*, Spec. Publ. **336**, 51-63.

Douglas, S., Beveridge, T.J., 1998. Mineral formation by bacteria in natural microbial communities. *FEMS Microbiol. Ecol.* **26**, 79-88.

Dupraz, C., Pattisina, R., Verrecchia, E. P., 2006. Translation of energy into morphology: Simulation of stromatolite morphospace using a stochastic model. *Sedim. Geol.* **185**, 185-203.

Dupraz, C., Reid, R.P., Braissant, O., Decho, A.W., Norman, R.S., Visscher, P.Y., 2009. Processes of carbonate precipitation in modern microbial mats. *Earth-Science Reviewes* **96**, 141-162.

Dupraz, C., Visscher, P.T., Baumgartner, L.K., Reid, R.P., 2004. Microbe-mineral interactions: early $CaCO_3$ precipitation in a Recent hypersaline lake (Eleuthera Islands, Bahamas). *Sedimentology* **51**, 745-765.

Dupraz, S., Menez, B., Gouze, Ph., Leprovost, R., Bénézeth, P., Pokrovsky, O.S., Guyot, F., 2009. New experimental design for studying interactions between microorganisms and $CO_2$ injected in the subsurface. *Chem. Geol.* **265**, 54-62.

Duval, J.F.L., Gaboriaud, F., 2010. Progress in electrohydrodynamics of soft microbial particle interphases. *Current Opinion in Colloid & Interface Science* **15**, 184-195.

Farmer, J.D., 2000. Hydrothermal systems: doorways to early biosphere evolution. *GSA Today* **10**, 1-10.

Fein, J. B., Daughney, C. J., Yee, N., Davis, T. A., 1997. A chemical equilibrium model for metal adsorption onto bacterial surfaces. *Geochimica et Cosmochimica Acta* **61**, 3319-3328.

Fein, J.B., Martin, A.M., Wightman, P.G., 2001. Metal adsorption onto bacterial surfaces: Development of a predictive approach. *Geochimica et Cosmochimica Acta* **65**, 4267-4273.

Ferris, F. G., Phoenix, V., Fujita, Y., Smith, R. W., 2004. Kinetics of calcite precipitation induced by ureolytic bacteria at 10 to 20°C in artificial groundwater. *Geochim. Cosmochim. Acta* **68**, 1701-1710.

Fouke, B.W., Farmer, J.D., Des Marias, D.J., Pratt, L., Strurchino, N.C., Burns, P.C., Discipulo, M.K., 2000. Depositional facies and aqueous-solid geochemistry of

travertine-depositing hot springs (Angel Terrace, Mammouth Hot Springs, Yellowstone National Park, USA). *Journal of Sedimentary Research* **70**, 565-585.

Freytet, P., Verrecchia, E.P., 1999. Calcite radial palisadic fabric in freshwater stromatolites: diagenetic and recrystallized feature or physicochemical sinter crust. *Sedimentary Geology* **126**, 97-102.

Frigaard, N.-U., Bryant, D.A., 2004. Seeing green bacteria in a new light: genomics-enabled studies of the photosynthetic apparatus in green sulfur bacteria and filamentous anoxygenic phototrophic bacteria. *Archives of Microbiology* **182**, 265-276.

Frigaard, N.U., Dahl, C., 2009. Sulfur metabolism in phototrophic sulfur bacteria. *Microb Physiol.* **54**, 103-200.

Gautret, P., Wit, D., Camoin, G., Golubic, S., 2006. Are environmental conditions recorded by the organic matrices associated with precipitated calcium carbonate in cyanobacterial microbialites? *Geobiology* **4**, 93-107.

Gélabert, A., Pokrovsky, O.S., Schott, J., Boudou, A., Feurtet-Mazel, A., Mielczarski, J., Mielczarski, E., Mesmer-Dudons, N., Spalla, O., 2004. Study of diatoms/aqueous solution interface. I. Acid-base equilibria and spectroscopic observation of freshwater and marine species. *Geochimica et Cosmochimica Acta* **68**, 4039-4058.

González, A.G., Shirokova, L.S., Pokrovsky, O.S., Emnova, E.E., Martínez, R.E., Santana-Casiano, J.M., González-Dávila, M., Pokrovski, G.S., 2010. Adsorption of copper on Pseudomonas aureofaciens: protective role of surface exopolysaccharides. *Journal of Colloid and Interface Science* **350**, 305-314.

Gorlenko, V. M., Kompantseva, E. I., Korotkov, S. A., Pouchkova, N. N., Savvichev, A. S., 1984. Development conditions and species of phototrophic bacteria, inhabiting salty shallow reservoirs in Crimea. *Microbiology* **3**, 327-328.

Graef, M.D., 2003. Introduction to conventional transmission electron microscopy, *Cambridg*.

Gun'ko, V.M., Mironyuk, I.F., Zarko, V.I., Voronin, E.F., Turov, V.V., Pakhlov, E.M., Goncharuk, E.V., Nychiporuk, Y.M., Vlasova, N.N., Gorbik, P.P., Mishchuk, O.A., Chuiko, A.A., Kulik, T.V., Palyanytsya, B.B., Pakhovchishin, S.V., Skubiszewska-

Zieba, J., Janusz, W., Turov, A.V., Leboda, R. 2005. Morphology and surface properties of fumed silicas. *Journal of Colloid and Interface Science* **289**, 427-445.

Harden, V.P., Hearris J.O., 1952. The isoelectric point of bacterial cells. *Biochimica et Biophysica Acta* **65**, 198-202.

Hartley, A.M., House, W.A., Callow, M.E., Leadbeate, B.S.C., 1995. The role of green algae in the precipitation of calcite and the coprecipitation of phosphate in freshwater. *Internationale Revue der gesamten Hydrobiologie und Hydrographie* **80**, 385-401.

Hayashi, H., Tsuneda, S., Hirata, A., Sasaki, H., 2001. Soft particle analysis of bacterial cells and its interpretation of cell adhesion behaviors in terms of DLVO theory. *Colloids and Surfaces* **22**, 149-157.

Hell, R., Dahl, C., 2008. Systematics of Anoxygenic Phototrophic Bacteria. Sulfur Metabolism in Phototrophic Organisms. *Springer Netherlands* **27**, 269-287.

Herben, P.F.G., Mozes, N., Rouxhet, P.G., 1990. Variation of the surface properties of Bacillus licheniformis according to age, temperature and aeration. *Biochimica et Biophysica Acta (BBA) - General Subjects* **1033**, 184-188.

Hett, E.C., Rubin, E.J., 2008**.** Bacterial Growth and Cell Division: a Mycobacterial Perspective. *Microbiology and Molecular Biology Reviews* **72**, 126-156.

Hunter, R.J., 1989. Foundation of colloid science. *Claredon Press, Oxford* **1**.

Hunter, R.C., Phoenix, V.R., Saxena, A., Beveridge, T.J., 2010. Impact of growth environment and physiological state on metal immobilization by *Pseudomonas aeruginosa* PAO1. *Can. J. Microbiol.* **56**, 527-538.

Hunter, R.J., 1981. Zeta potential in Colloid Science. *Academic Press*, NY.

Hunter, R.J., 1998. Review. Recent developments in the electroacoustic characterization of colloidal suspensions and emulsions. *Colloids and Surfaces* **141**, 37-65.

Huzisige, H., Ke, B., 1993. Dynamics of the history of photosynthesis. *Photosynth. Res.* **38**, 185-209.

Ishikawa, T., Zhu, B.L., Maeda, H., 2006. Effect of sodium azide on the metabolic activity of cultured fetal cells. *Toxicology and Industrial Health* **22**, 337-341.

Jagannathan, B., Golbeck, J.H., Moselio, S., 2009. Photosynthesis: Microbial. In: Encyclopedia of Microbiology. *Academic Press, Oxford*, 325-341.

Johnson, K.J., Ams, D.A., Wedel, A.N., Szymanowski, J.E.S., Weber, D.L., Schneegurt, M.A., Fein, J.B., 2007. The impact of metabolic state on Cd adsorption onto bacterial cells. *Geobiology* **5,** 211–218.

Jørgensen, B.B., Revsbech, N.P., 1983. Photosynthesis and structure of benthic microbial mats: Microelectrode and SEM studies of four cyanobacterial communities. *Limnol. Oceanogr*. **28**, 1075-1093.

Kazmierczak, J., Kempe, S., 2006. Genuine modern analogues of Precambrian stromatolites from caldera lakes of Niuafo‘ou, Tonga. *Naturwissenschaften* **93**, 119-126.

Kempe, S., Degens, E.T., 1985. An early soda ocean? *Chem. Geol.* **53**, 95-108.

Kempe, S., Kazmierczak, J., 1990. Chemistry and stromatolites of the sea-linked Satonda Crater Lake, Indonesia: A recent model for the Precambrian sea? *Chem. Geol.* **81**, 299-310.

Kenward, P.A., Goldstein, R.H., Gonzalez, L.A., Roberts, J.A., 2009. Precipitation of low-temperature dolomite from an anaerobic microbial consortium: the role of methanogenic Archaea. *Geobiol*. **7**, 556–565.

Kompantseva, E.I., Bryantseva, I.A., Komova, A.V., Namsaraev, B.B., 2007. The structure of Phototrophic communities of soda lakes of the Southeastern Transbaikal region. *Microbiol.* **76**, 211-219.

Kompantseva, E.I., Komova, A.V., Kostrikina, N.A., 2010. *Rhodovulum steppense* sp. nov., an obligately haloalkaliphilic purple nonsulfur bacterium widespread in saline soda lakes of Central Asia. *Int. J. Syst. Evol. Microbiol*. **60**, 1210 - 1214.

Kompantseva, E.I., Komova, A.V., Krauzova, V.I., Kolganova, T.V., Panteleeva, A.N., 2009. Purple nonsulfur bacteria in weakly and moderately mineralized soda lakes of the Southern Transbaikal region and Northeastern Mongolia. *Microbiol.* **78**, 246-253.

Kompantseva, E.I., News halophilic purple bacteria *Rhodobacter euryhalinus sp.* nov., 1985. Microboil. **54**, 974-982.

Kosami, I.B., Obst, M., 2009. The influence of picocyanobacterial photosynthesis on calcite precipitation, *Int. J. Environ. Sci. Technol.* **6**, 557–562.

Kosmulski, M., 2009. pH-dependent surface charging and points of zero charge. IV. Update and new approach. *Journal of Colloid and Interface Science* **337**, 439-448.

Kosmulski, M., Saneluta, C., 2004. Point of zero charge/isoelectric point of exotic oxides: $Tl_2O_3$. *Journal of Colloid and Interface Science* **280**, 544-545.

Kosmulsky, M., Maczka, E., Janusz, W., Rosenholm, J.B., 2002. Multiinstrumentel study of the electrophoretic mobility of quartz. *Journal of Colloid and Interface Science* **250**, 99-103.

Kranz, S.A., Wolf-Gladrow, D., Nehrke, G., Langer, G., Rost, B., 2010. Calcium carbonate precipitation induced by the growth of the marine cyanobacterium *Trichodesmium*. *Limnol. Oceanogr*. **55**, 2563-2569.

Krumbein, W.E., Cohen, Y., Shilo, M., 1977. Solar Lake (Sinai). 4. Stromatolitic cyanobacterial mats. *Limnol. Oceanogr.* **22**, 635- 656.

Lopez-Garcia, P., Kazmierczak, J., Benzerara, K., Kempe, S., Guyot, F., Moreire, D., 2005. Bacterial diversity and carbonate precipitation in the giant microbialites from the highly alkaline Lake Van, Turkey. *Extremophiles* **9**, 263-274.

Lowenstam, H.A., Weaner, S., 1989. On biomineralization. *Oxford University Press. New York. Oxford*. 309 pp.

Lunina, O.N., Bryantseva, I.A., Akimov, V.N., Rusanov, I.I., Barinova, E.S., Lysenko, A.M, Rogozin, D.Y., Pimenov, N.V., 2007. Anoxygenic phototrophic bacterial community of Lake Shira (Khakassia). *Microbiology* **76**, 469–479.

Lyklema, J., 1993. Fundamentals of Interface and Colloid Science. *Academic Press* **1**.

Madigan, M.T., Martinko, J.M., Parker, J., 2000. Brock Biology of Microorganisms 9$^{th}$ edition. *Prentice Hall. Upper Saddle River*, NJ. 991 pp.

Madigan, M.T., Ormerod, J.G., 1995. Anoxygenic Photosynthetic Bacteria. In Blankenship et al., Kluwer Academic Publishers New York, 17-30.

Martell, A.E., Smith, R.M., 1997. NIST Critically selected stability constants of metal complexes. Database software Version 3.0. Texas A & M University, *College Station*, TX.

Martinez, R.E., Gardés, E., Pokrovsky, O.S., Schott, J., Oelkers, E.H., 2010. Do photosynthetic bacteria have a protective mechanism against carbonate precipitation at their surfaces? *Geochimica et Cosmochimica Acta* **74,** 1329-1337.

Martinez, R.E., Pokrovsky, O.S., Schott, J., Oelkers, E.H., 2008. Surface charge and zeta potential of metabolically active and dead cyanobacteria, *J. Coll. Interf. Sci.* **323**, 317–325.

McConnaughey, T., Whelan, J.F., 1997. Calcification generates protons for nutrient and bicarbonate uptake, *Earth-Science Reviews* **42**, 95–117.

Merz, M.U.E., Schlue, W.R., Zankl, H., 1992. The biology of carbonate precipitation by cyanobacteria. *Facies* **26**, 81-102.

Merz, M.U.E., Schlue, W.R., Zankl, H., 1993. PH-measurement in the sheath of calcifying filamentous cyanobacteria, *Biomineralization, Programs and Abstracts* **45**, 48.

Michen, B., Graule, T., 2010. Isoelectric points of viruses. *Journal of Applied Microbiology* **109**, 388-397.

Miller, A.G., Colman, B., 1980. Evidence for $HCO_3$- transport by the blue-green alga (cyanobacterium) Coccochloris peniocystis. *Plant Physiol*. **65**, 397–402.

Miller, A.G., Espie, G.S., Canvin, D.T. ,1990. Physiological aspects of $CO_2$ and $HCO_3$- transport by cyanobacteria. *Can. J. Bot*. **68**, 1291–1302.

Mishra, Y., Bhargavam P., Chaursia, N. and Rai, C.L., 2009. Proteomic evaluation of the non-survival of *Anabaena doliolum* (Cyanophyta) elevated temperatures. *Eur. J.Phycol*. **44**, 551 - 565.

Mitchel, A.C., Ferris, F.G., 2006. The Influence of *Bacillus pasteurii* on the nucleation and growth of calcium carbonate. *Geomicrobiol. J.* **23**, 213-226.

Mitchell, A.C., Ferris, F.G., 2005. The coprecipitation of Sr into calcite precipitates induced by bacterial ureolysis in artificial groundwater: Temperature and kinetic dependence. *Geochim. Cosmochim. Acta* **69**, 4199-4210.

Morse, J.W., 1983. The kinetics of calcium carbonate dissolution and precipitation. *Rev. Min.* **11**, 227–264.

Mozes, N., Rouxhet, P.G., 1990. Microbial hydrophobicity and fermentation technology. In: Doyle, R.J., Rosenberg, M. (Eds.), Microbial Cell Surface Hydrophobicity. *American Society for Microbiology*, Washington, DC, USA, pp. 75-105.

Mullen, M.D., Wolf, D.C., Ferris, F.G., Beveridge, T.L., 1989. Bacterial sorption of heavy metals. *Appl. Environ. Microbiol.* **55**, 3143-3149.

Newbury, D. E., Joy, D.C., 1986. Advanced scanning electron microscopy and X-ray microanalysis. New York, Kluwer Academic Plenum Publishers.

Ngwenya, B.T., 2007. Enhanced adsorption of zinc is associated with aging and lysis of bacterial cells in batch incubations. *Chemosphere* **67**, 1982–1992.

Novick, A., 1955. Growth of Bacteria. *Annual Review of Microbiology* **9**, 97–110.

Obst, M., Wehrli, B., Dittrich, M., 2009b. $CaCO_3$ nucleation by cyanobacteria: laboratory evidence for a passive, surface-induced mechanism, *Geobiology* **7**, 324–347.

Obst, M., Dittrich, M., 2006. Calcium adsorption and changes of the surface microtopography of cyanobacteria studied by AFM, CFM, and TEM with respect to biogenic calcite nucleation. *Gechem. Geophys. Geosyst*. **7**, pp.15.

Obst, M., Dynes, J.J., Lawrence, J.R., Swerhone, G.D.W., Benzerara, K., Karundakaran, C., Kaznatcheev, K., Tyliszcak, T., Hitchcock, A.P., 2009a. Precipitation of amorphous $CaCO_3$ (aragonite-like) by cyanobacteria: a STXM study of the influence of EPS on the nucleation process, *Geochim. Cosmochim. Acta* **73**, 4180–4198.

Olson, J.M., Blankenship, R.E., 2004. Thinking about the evolution of photosynthesis. *Photosynthesis Research* **80**, 373-386.

Papineau, D., Walker, J.J., Mojzsis, S.J., Pace, N.R., 2005. Composition and structure of microbial communities from stromatolites of hamelin pool in Shark Bay, Western Austria. *Applied and Environmental Microbiology* **71**, 4822-4832.

Parkhurst, D.L., Appelo, C.A.J., 1999. User's guide to PHREEQC (version 2) - a computer program for speciation, reaction-path, 1D-transport, and inverse geochemical calculations. US Geol. Surv. *Water Resour*. Inv. Rep. 99-4259, 312p.

Pentecost, A., 1978. Blue-green algae and freshwater carbonate deposits. *Proc. R. Soc. London B.* **200**, 43-61.

Pfenning, N., Lippert, K.D., 1966. Uber des Vitamin B12 - bedurfnis phototrophen Schwefelbakterien. *Archives fur Mikrobiologie* **55**, 245-256.

Plummer, L.N., Busenberg, E., 1982. The solubilities of calcite, aragonite and vaterite in $CO_2$-$H_2O$ solutions between 0 and 90°C, and an evaluation of the aqueous model for the system $CaCO_3$-$CO_2$-$H_2O$. *Geochim. Cosmochim. Acta* **46**, 1011-1040.

Pokrovsky, O.S., Martinez, R.E. , Golubev, S.V., Kompantseva, E.I., Shirokova, L.S., 2008. Adsorption of metals and protons on Gloeocapsa sp. cyanobacteria: A surface speciation approach. *Applied Geochemistry* **23**, 2574-2588.

Pokrovsky, O.S., Golubev, S.V. and Schott, J., 2005. Dissolution kinetics of calcite, dolomite and magnesite at 25°C and 0 to 50 atm $pCO_2$. *Chem. Geol.* **217**, 239-255.

Pokrovsky, O.S., Pokrovsky, G.S., Gelabert, A., Schott, J., Boudou, A., 2005. Speciation of Zn associated with diatoms using X-ray absorption spectroscopy. *Environmetal Science & Technology* **39**, 4039-4058.

Pokrovsky, O.S., Savenko, V.S., 1995a. Experimental modeling of crystallization processes of carbonates near photosynthesizing organisms in seawater. *Experiment in Geosciences* **4**, 41-42.

Pokrovsky, O.S., Savenko, V.S., 1995b.Experimental modeling of $CaCO_3$ precipitation at the conditions of photosynthesis in seawater. *Oceanology* **35**, 805-810

Rachel, R, Pum, D, Marda, J, Majs, D, Komrska, J, Krzyzánek, V, Rieger, G, Stetter, K, 1997. II. Fine structure of S-layers. *FEMS Microbiology Reviews* **20**, 13-23.

Reed, S.J.B., 2005. Electron Microprobe Analysis and Scanning Electron Microscopy in Geology, *Cambridge*.

Reid, R.P., James, N.P., Macintyre, I.G., Dupraz, C.P., Burne, R.V., 2003. Shark Bay stromatolites : microfabrics and reinterpretation of origin. *Facies* **49**. 299-324.

Reynolds, E.C., Wong, A., 1983. Effect of adsorbed protein on hydroxyapatite zeta-potentual and Streptococcus mutans Adherence. *Infection and Immunity* **39,** 1285-1290.

Richmond, D.V., Fisher, D.J., Rose, A.H., Tempest, D.W., 1973. The Electrophoretic Mobility of Micro-Organisms. In: *Advances in Microbial Physiology*. Academic Press, pp. 1-29.

Riding, R., 2006. Cyanobacterial calcification, carbon dioxide concentrating mechanisms, and Proterozoic-Cambrian changes in atmospheric composition. *Geobiol.* **4**, 299-316.

Riding, R., Braga, J.C., Martin, J.M., 1991. Oolite stromatolites and thrombolites, Miocene, Spain: analogues of Recent giant Bahamian examples.*Sedimentary Geology* **71**, 121-127.

Ries, J.B., 2010. Review: geological and experimental evidence for secular variation in seawater Mg/Ca (calcite-aragonite seas) and its effects on marine biological calcification. *Biogeosciences* **7**, 2795-2849.

Rippka, R., Deruelles, J., Waterbury, J., Herdman, M., Stanier, R., 1979. Generic assignments, strain histories and properties of pure cultures of cyanobacteria. *J. Gen. Microbiol*. **111**, 1-61.

Saito, T., Takatsuka, T., Kato, T., Ishihara, K., Okuda, K., 1997. Adherence of oral streptococci to an immobilized antimicrobial agent. *Arch. Oral Biol.* **42**, 539-545.

Sánchez-Román, M., Romanek, C.S., Fernández-Remolar, D.C., Sánchez-Navas, A., McKenzie, J.A., Pibernat, R.A., Vasconcelos, C., 2011. Aerobic biomineralization of Mg-rich carbonates: Implications for natural environments. *Chem. Geol.* **281**, 143-150.

Scanlan, D.J., Nyree J.W., 2002. Molecular ecology of the marine cyanobacterial genera *Prochlorococcu*s and *Synechococcus*. *FEMS Microbiology Ecology* **40**, 1-12.

Schopf, J.W., 2006. Fossil evidence of Archean life. Philosophical transactions of the Royal Society, *B* **361**, 869-885.

Schultze-Lam, S., Harauz, G., Beveridge, T.J., 1992. Participation of a cyanobacterial S layer in fine-grain mineral formation, *J. Bacteriol.* **174**, 7971–7981.

Sheindorf, C., Rebhun, M., 1981. A Freundlich-type multicomponent isotherm. *Journal of Colloid and Interface Science* **79**, 136-142.

Shirokova, L.S., Pokrovsky, O.S., Schott, J., Oelkers, E.H., Kompantseva, E.I., Martinez, R., 2008. Experimental modeling of $CaCO_3$ precipitation in the presence of oxygenic and anoxygenic phototrophic bacteria. *Geophysical Research Abstracts*, **10**, EGU2008-A-04921, 2008. SRef-ID: 1607-7962/gra/EGU2008-A-04921.

Skarstad, K., Steen, H.B., Boye, E., 1983. Cell cycle parameters of slowly growing Escherichia coli B/r studied by flow cytometry. *J. Bacteriol.* **154**, 656–662.

Sleytr, U.B., Beveridge, T.J., 1999. Bacterial S-layers. *Trends in Microbiology* **7**, 253-260.

Sloyer, J.R., Bayer, M.E., 1990. Automated electrokinetic analysis; description and application in virology and cell biology. *Journal of Virological Methods* **28**, 207-216.

Smith, A.J., 1982. The Biology of Cyanobacteria. *University of California Press*, Berkeley, 47-85.

Smith, F.A., Walker, N.A., 1980. Photosyntethis of aquatic plants: Effects of unstirred layers in relation to assimilation of $CO_2$ and $HCO_3^-$ and to carbon isotop discrimination. *New Phitolodist* **86**, 245-259.

Spadafora, A., Perri, E., McKenzie, J.A., Vasconcelos, C., 2010. Microbial biomineralization processes forming modern Ca:Mg carbonate stromatolites. *Sedimentology* **57**, 27-40.

Stabel, H.H., 1986. Calcite precipitation in Lake Constance: chemical equilibrium, sedimentation, and nucleation by algae. *Limnol. Oceanogr.* **31**, 1081-1093.

Suryanarayana, C., Grant Norton, M., 1990. X-Ray diffraction: a practical approach, *Library of Congress Cataloging in Publication Data*.

Thompson, J.B., Ferris, F.G., 1990. Cyanobacterial precipitation of gypsum, calcite, and magnesite from natural alkaline lake water, *Geology* **18**, 995–998.

Thompson, J.B., Shultze-Lam, S., Beveridge, T.J., Des Marais, D.J., 1997. Whiting events: Biogenic origin due to the photosynthetic activity of cyanobacterial picoplankton. *Limnol. Oceanogr.* **42**, 133-141.

Tice, M.M., Lowe, D.R., 2006. Hydrogen-based carbon fixation in the earliest known photosynthetic organisms. *Geology* **34**, 37-40.

Tourney, J., Ngwenya, B.T., 2010. The effect of ionic strength on the electrophoretic mobility and protonation constants of an EPS-producing bacterial strain. *Journal of Colloid and Interface Science* **348,** 348-354.

Urrutia Mera, M., Kemper, M., Doyle, R., Beveridge, T.J., 1992. The membrane-induced proton motive force influences the metal binding ability of Bacillus subtilis cell walls. *Appl. Environ. Microbiol*. **58**, 3837–3844.

Valleau, J.P., 1982. Electrical double layers. 4. Limitations of the Gouy-Chapman theory. *J. Phys. Chem.* **86**, 3251–3257.

Van Der Wal, A., Norde, W., Zehnder, A.J.B., Lyklema, J., 1997. Determination of the total charge in the cell walls of Gram-positive bacteria. *Colloids and Surfaces B: Biointerfaces* **9**, 81-100.

Van Lith, Y., Vasconcelos, C., Warthmann, R., McKenzie, J.A., 2003. Microbial fossilization in carbonate sediments; a result of the bacterial surface involvement in carbonate precipitation. *Sedimentology* **50**, 237–245.

Vasconcelos, C., Warthmann, R., McKenzie, J., Visscher, P.T., Bittermann, A.G., van Lith, Y., 2006. Lithifyling microbial mats in Lagoa Vermelha, Brazil: Modern Precambrian relics? *Sedimentary Geology* **185**, 175-183.

Vasconcelos, V.M., Sivonen, K., Evans, W.L.R., Carmichael, W.W. and Namikoshi, M., 1995. Isolation and characterization of microcystins (heptapeptide hepatotoxins) from Portuguese strains of *Microcystis aeruginosa* Kutz. Emend Elekin. Arch. *Hydrobiol.* **134**, pp. 295–305

Verrecchia, E.P., Freytet, P., Verrecchia, K.E., Dumont, J.-L., 1995. Spherulites in calcrete laminar crusts: Biogenic $CaCO_3$ precipitation as a major contributor to crust formation, *J. Sed. Res.* **65**, 690–700.

Visscher, P.T., Stolz, J.F., 2005. Microbial mats as bioreactors: populations, processes and products. *Palaeogeography, Palaeoclimatology, Palaeoecology* **219**. 87-100.

Visscher, P.T., Stolz, J.F., 2005. Microbial mats as bioreactors: populations, processes, and products. *PALAEO* **219**, 87-100.

Visscher, P.T., van Gemerden, H., 1991. Production and consumption of dimethylsulfoniopropionate in marine microbial mats. *Appl. Environ. Microbiol.* **57**, 3237-3242.

Warthmann, R., Van Lith, Y., Vasconcelos, C., McKenzie, J.A., Karpoff, A.M., 2000. Bacterially induced dolomite precipitation in anoxic culture experiments. *Geology* **28**, 1091-1094.

Williams, D. B., Carter, C.B., 2009. Transmission electron microscopy: a textbook for materials science, *Springer*.

Wilson, W.W., Wade, M.M., Holman, S.C., Champlin, F.R., 2001. Status of methods for assessing bacterial cell surface charge properties based on zeta potential measurements. *Journal of Microbiological Methods* **43**, 153-164.

Xiong, J., Bauer, C.E., 2002. A cytochrome *b* origin of photosynthetic reaction centers. *J. Mol. Biol.* **322**, 1025-1037.

Yurkov, V.V., Beatty, J.T., 1998. Aerobic Anoxygenic Phototrophic Bacteria. *Microbiology and Molecular Biology Reviews* **62**, 695-724.

Zembala, M., 2004. Electrokinetics of heterogeneous interfaces. *Advances in Colloid and Interface Science* **112**, 59-92.

Zinovieva, M., Fresneau, C., Arrio, B., 1998. Electrophoretic mobility variations of Synechococcus PCC 7942 plasmalemma vesicles with nitrogen source. *Bioelectrochemistry and Bioenergetics* **46**, 55-58.

Zwietering, M. H., Jongenburger, I., Rombouts, F.M., van T Riet, K., 1990. Modeling of the Bacterial Growth Curve. *Applied and Environmental Microbiology* **56**, 1875–1881.

# Appendix 1

# Mg isotope tracing of hydrous magnesium carbonate precipitation in alkaline lake with cyanobacterial stromatolites

# Mg isotope tracing of hydrous magnesium carbonate precipitation in alkaline lake with cyanobacterial stromatolites

L.S. Shirokova[1*], V. Mavromatis [1], I.A. Bundeleva[1], O.S. Pokrovsky[1], P. Benezeth[1], C. Pearce[3], E. Gérard[2], S. Balor[4], E.H. Oelkers[1]

[1] *Geoscience and Environment Toulouse (GET), CNRS, UMR 5563, Observatoire Midi-Pyrénées, 14 Avenue Edouard Belin, 31400 Toulouse, France*

[2]*Institut de Physique du Globe de Paris, 1 rue Jussieu, 75238 Paris, France*

[3] *Department of Earth and Environmental Sciences, The Open University, Walton Hall, Milton Keynes, MK7 6AA, UK.*

[4] *Plateau de Microscopie électronique, FRBT CNRS FR3451, Bat.IBCG,118 route de Narbonne, F-31062 Toulouse, France*

* On leave from the *Institute of Ecological Problems of the North, 23 Nab. Sev. Dviny, Russian Academy of Science, Arkhangelsk, Russia*

*Prepared for* ***Biogeosciences***

**Abstract**

Lake Salda (SE Turkey) is one of the few modern environments in Earth's surface where hydrous Mg-carbonates are the dominant precipitating minerals. Stromatolites consisting mainly of hydromagnesite formed by cyanobacterial activity are abundant in this aquatic ecosystem. Mg isotope analyses were performed on samples of incoming streams and groundwaters, lake waters and stromatolites/sediments composed of hydromagnesite. Laboratory modeling experiments of Mg hydrous carbonate precipitation were conducted on purified Salda lake cyanobacteria of *Chroococales* family (close to *Synechococcus* sp.) isolated from the lake water. The hydrous magnesium carbonates, nesquehonite ($MgCO_3 \cdot 3H_2O$) and dypingite ($Mg_5(CO_3)_4(OH)_2 \bullet 5(H_2O)$), were precipitated in batch reactors from aqueous solutions containing 0.05 M $NaHCO_3$ and 0.025 M $MgCl_2$ and natural Salda Lake water in the presence and absence of live photosynthesizing *Synechococcus* sp. Bulk precipitation rates are not affected by the presence of bacteria in case of air bubbling through solution. However, bacterial photosynthesis allowed nesquehonite precipitation in stirred non bubbled reactors, under conditions more similar to natural settings. In bacteria-free systems without air bubbling mineral precipitation did not occur despite similar or higher solution supersaturation degree. Mg isotope fractionation ($\Delta^{26}Mg_{solid\text{-}solution}$) between mineral and solution in the abiotic experiments is identical, within uncertainty, to that measured in cyanobacteria-bearing experiments and range from -1.4 to -0.7‰. The isotopic shift between the inflowing streams (and the groundwaters) feeding the lake ($\delta^{26}Mg \approx$ -1.1 to -1.4 ‰ DSM-3) and the lake water samples ($\delta^{26}Mg \approx$ 0.0 to 0.1 ‰ DSM-3) might be explained by the formation of hydromagnesite in the lake water with $\delta^{26}Mg \approx$ -0.8 to -1.1 ‰. This is consistent with results of laboratory experiments in this study and previous works on *Gloeocapsa* sp. cyanobacteria.

## 1. INTRODUCTION

In contrast to significant research efforts aimed at elucidating biogeochemical processes in lakes using traditional isotopic techniques (eg. C, O, N, S, B; Peterson and Fry, 1987; Pentecost and Spiro, 1990) new less-common stable isotopes of metals such as Ca, Cu, Fe, Li, Mg, Zn are just at the beginning of their utilization by limnologists. Among new isotopic couples, Mg provides a very promising proxy because 1) it is a major ionic

component of the lake water; 2) it is directly involved in chlorophyll*a* of aquatic microorganisms (Black et al., 2006, 2007); 3) it is capable forming individual minerals in the lake sediments (Castanier et al., 1993; Power et al., 2009) and 4) its stable isotopes are proven to fractionate more significantly compared to other alkaline earth metal such Ca and Sr (Galy et al., 2002; Tipper et al., 2006; Higgins and Schrag, 2010; Li et al., 2011; Schauble, 2011).

One of the most important processes controlling biogeochemical cycle of calcium and magnesium in continental waters is carbonate biomineralization (Lowenstum and Weiner, 1989; Dove, 2010). Cyanobacteria-induced mineralization occurred in both ancient and modern environments since the Precambrian (Kempe and Kazmierczak, 1990; Knoll et al., 1993; Brady et al., 2009; Planavsky et al, 2009; Raven and Giordano, 2009; Riding, 2000; Ries, 2010). The majority of modern freshwater cyanobacteria-dominated carbonate formations are observed in alkaline aquatic environments with high calcium to magnesium ratios (Scholl and Taft, 1964; Müller et al., 1972; Otsuki and Wetzel, 1974; Kelts and Hsü, 1978; Pentecost, 1978; Stabel, 1986; Thompson and Ferris, 1990; Pedone and Folk, 1996; Ferris et al., 1997; Thompson et al., 1997; Kazmierczak and Kempe, 2006; Dupraz et al., 2009; Power et al., 2011) producing various forms of calcium carbonate minerals. In contrast, the formation of Mg-rich carbonate minerals by cyanobacteria occurs only in specific Earth surface environments, such as Lake Salda in Turkey, which is fed by ultramafic rock weathering products (e.g. Braithwaite and Zedef, 1994), alkaline lakes such as those in British Columbia (Renaut, 1990; Power et al., 2007, 2009) and some saline lake sediments (Renaut and Long, 1989; Renaut and Douglas, 1990; Queralt et al., 1997). The interest to these $Mg(HCO_3)_2$ -dominated lakes has been recently stimulated by discovery of Mg carbonates on the surface of the Mars which may witness the existence of some Mg-rich waters precipitated hydrous Mg carbonates (Calvin et al., 1994; Russell et al., 1999; Edwards et al., 2005; Palomba et al., 2009).

Compared to relatively good knowledge of reaction rates and mechanisms of calcium carbonate precipitation associated with cyanobacterial activity, both in liquid suspension (Hartley et al., 1995, Obst and Dittrich, 2006; Obst et al., 2009; Dittrich and Sibler, 2010; Kranz et al., 2010) and in biofilms (Jorgensen et al., 1983; Cox et al., 1989; Hartley et al., 1996), the understanding of main biological and physico-chemical factors controlling hydrous Mg carbonate precipitation and Mg isotope fractionation in natural waters is still at the very beginning.

In this regard, alkaline Lake Salda (SW Turkey) represents an excellent natural laboratory where contemporary Mg carbonate precipitation occurs. Previous studies allowed

comprehensive understanding of its geology, lithology, biology and processes of mineral precipitation occurring in the lake basin (Braithwaite and Zedef, 1994, 1996). It is believed that hydromagnesite ($Mg_4(OH)_2(CO_3)_3 \cdot 3H_2O$) microbialites (stromatolites) developed along the lake coast are formed via cyanobacterial and algal activity (Braithwaite and Zedef, 1994). In this work, we sampled lake waters, sediments and stromatolites and we performed laboratory modeling experiments in order to assess the range and characterize the mechanisms of Mg isotope fractionation in lacustrine environment. This allowed us providing first quantitative experimental and field calibration of Mg isotope fractionation between aqueous solution and biotically and abiotically formed hydrous magnesium carbonates under conditions similar to the lake water. It is anticipated that obtained results should provide a firm basis for quantitative use of magnesium isotopes as proxies for tracing biomineralization processes in past and contemporary continental aquatic environments.

## 2. MATERIALS AND METHODS

### 2.1. Site description

Salda Gölü (lake in turkish), located in SW Turkey, has an area close to 45 $km^2$ and an average depth of 80 m with a maximal reported depth of 200 m (Fig. 1A). This lake was earlier extensively studied from limnological, geological and geochemical point of view (Schmid, 1987; Braithwaite and Zedef, 1994, 1996; Russell et al., 1999; Zedef et al., 2000; Kazanchi et al., 2004). It represents an ideal natural case of $CO_2$ sequestration because meteoric waters feeding the lake dissolve adjacent ultramafic rocks and precipitate hydromagnesite in shallow littoral zones, similar to what is recently described in British Columbia playas (Power et al., 2009). The lake has no outlet and the water level is varying from one year to another, being largely controlled by precipitation/evaporation regime.

Contemporary hydromagnesite stromatolites are developed in the littoral of SW part of the lake (Kocaadalar Burnu) where they form three large, 20 to 30 m islands about 50 m offshore rising ~10 m from the lake bottom and reaching within 3-4 m of the surface. Similar to Braithwaite and Zedef (1994, 1996), we define hereafter the modern, actively grown microbialite structures as stromatolites. Underwater diving examination of the deepest part of these islands at the end of the littoral did not evidenced any stromatolite presence at depth more than 6-10 m. Smaller, up to 1.5-3 m stromatolites are also found in other parts of the

lake within 10-20 m from the shoreline (Fig. 1B). Finally, at the littoral of the N side of the lake, most submerged stones are covered by actively forming, non-solidified stromatolites (Fig. 1C) having the same texture as that constituting the large islands (Fig. 1B)

Detailed underwater examination of the surface of stromatolites demonstrated that they are alive and actively growing. The mineral surface is covered by a layer of green algae, diatoms and cyanobacteria with oxygen bubbles adjacent to the surface of the microbial mats (Fig. 1D).

### 2.2. Sampling of lake water and minerals

We sampled all inflowing streams and the lake littoral zone for dissolved load in February 2008 and 2010 and in September 2010. Massive stromatolite islands of Kocaadalar Burnu and lake water column up to 70 m depth in the middle of the lake were sampled in September 2010 from a PVC boat.

Various pieces of air-exposed stromatolite islands as well as parts of stromatolites collected from 4-5 m depth were also investigated. Both mold, external surface and internal parts of stromatolites have been sampled (Fig. 1B to 1C). We also sampled hydromagnesite sand from the beach and carbonate mineral coating on submerged branches and grasses.

For bacterial culture in laboratory, large volumes of surface water filtered on-site using sterile Nalgene disposable filter unit (polycarbonate 0.22 µm) and sterile polypropylene flacons and stored at 5°C during transport to the laboratory.

For the water column sampling, horizontal polycarbonate water sampler (Aquatic Research Co) was used, applying ultraclean sampling procedures throughout all manipulations in the field (Shirokova et al., 2010). The water samples were immediately filtered through sterile, single-use Minisart® filter units (Sartorius, acetate cellulose filter) with pore sizes of 0.45 µm. The first 100ml of the filtrate was systematically discarded. Dissolved oxygen, pH and temperature were measured on-site with an uncertainty of 5%, 0.02 units, and 0.5°C, respectively. Concentrations of dissolved organic carbon (DOC), Cl, $SO_4$, alkalinity (Alk), cations and trace element (TE) were measured in our laboratory using methods routinely applied for analysis of lake and river water samples (Pokrovsky et al., 2010, 2011; Shirokova et al., 2010; Vasyukova et al., 2010).

### 2.3. Culture and characterization of cyanobacteria

A culture of family *Chroococales*. cyanobacteria was isolated from the surface of coastal stromatolites sampled in February 2008 from the depth of 1 m at 50 m from the shoreline of the Salda Lake, SW Turkey. Similar strains (*Chroococcus turgidus*, *Plankothrix, Anabaena* and *Microcystis*) were reported to occur in adjacent $Mg(HCO_3)_2$-rich alkaline lake Burdur, SW Turkey (Girgin et al., 2004). The culture was purified on the agar BG-11 or Pratt media and individual colonies were grown in synthetic, cyanobacteria BG-11 Freshwater Solution for 3 weeks until the stationary growth phase was reached. Continuous illumination at 2000 lx was provided from fluorescent lamps. Cyanobacterium *Synechoccocus* typically consists of isolated elongated cells, without significant amount of mucilage.

Their phylogenetic affiliation was performed by DNA extracting (UltraClean® Microbial DNA Isolation Kit MO BIO) and 16S RNA gene amplifying (bacterial-specific primers 27F (5'-AGAGTTTGATCCTGGCTCAG) and prokaryote-specific reverse primers 1492R (5'-GGTTACCTTGTTACGACTT), see Gerard et al. 2009 for the condition of PCR amplification) and sequencing (Cogenics, Beckman Coulter Genomics). The sequence was then identified by BLAST against the NCBI non-redundant nucleotides database. We found that purified culture and *Synechoccocus PCC XX*, already reported to occur in alkaline lakes and notably lake Salda (Girgin et al., 2004), share 75% identity at the level of their 16S RNA genes. The concentration of the bacterial cell suspensions was quantified via optical density (O.D.) using a spectrophotometer at a wavelength of 750 nm (Hu et al., 2000; Sarcina and Mullineaux, 2000). The O.D. calibration curve - wet weight was linear up to 1.3 absorbance units and the ratio between wet and freeze-dried weight of *Synechoccocus* sp. was 8.0±2.0.

Very similar cyanobacteria culture was also isolated from the interior part of the examined stromatolite and from the algal coating on the submerged branches in inflowing stream. Therefore, it can be considered as the most common and easily culturable cyanobacteria representative for Salda lake peryphyton. Note that other cyanobacterial species like *Gloeocapsa* sp. were also reported to occur in the Salda lake stromatolites and water column. As such, several experiments were performed with model *Gloeocapsa* sp. culture described previously (Pokrovsky et al., 2008; Mavromatis et al., 2011)

### 2.4. Laboratory Precipitation Experiments

Precipitation experiments were aimed at reproducing Mg hydrous carbonate formation in the presence of cyanobacterial cultures extracted from the Salda lake stromatolites under

controlled laboratory conditions. Experiments were performed in 1000 ml sterile borosilicate glass reactors containing either the low-phosphate (10% of normal content, 50 μM) BG-11 growth medium, or the cell supernatant (sterile filtered BG-11 media after 14-30 days of culture growth on the stationary phase), into which 0.025-0.03 M $MgCl_2$ and ~0.05 M $NaHCO_3$ were added. In addition, sterile Salda lake water (0.014 M Mg, 0.03 M DIC) amended with low-phosphate BG-11 nutrient components, was used for bacterial growth experiments. Details of all experiments performed in this study are given in Table 1.

Several distinct types of biotic experiments were performed at 25 ± 2°C. Experiments S-Bio-2, S-Bio-5 and S-Bio-7 were performed in reactors that were continuously stirred with a magnet stir bar and bubbled with sterile humid air with an average flow rate of 1.5 ± 0.3 L/min. Experiments S-Bio-1, S-Bio-3, S-Bio-4 and S-Bio-6 were performed in reactors that were stirred but without air bubbling. Salda lake water amended with components of BG-11 (S-Bio-3, 4) or without addition of BG-11 (S-Bio-6) as well as artificial solutions of different composition (0.025 M $MgCl_2$ + 0.05 M $NaHCO_3$, S-Bio-1, S-Bio-2, S-Bio-5) and 0.05 M $MgCl_2$ + 0.005 M $NaHCO_3$ (S-Bio-7) were used as growth media. Experiments S-Bio-8, 9 and 10 (0.025 M $MgCl_2$ + 0.05 M $NaHCO_3$ amended with BG-11) were run without shaking and bubbling. Each of these experiments was performed under continuous fluorescent light of 30 μmol photon $m^{-2}$ $s^{-1}$.

Abiotic cell-free control experiments were also performed at a variety of conditions. S-Abio-1 experiment was performed with stirring and air bubbling in the presence of a sterile supernatant of the *Synechoccocus* sp. cyanobacteria containing 50 ± 10 mg/L of dissolved organic carbon (DOC) in the form of cell exometabolites in which $MgCl_2$ and $NaHCO_3$ were added in concentrations similar to those of the biotic experiments. The supernatant solution used in these abiotic experiments was generated after centrifugation and filtration through a 0.22 μm sterile filter of the *Synechoccocus* sp. culture collected ~20 days after attainment of the stationary phase. Abiotic control experiments S-Abio-2, 5 and 6 were performed without air bubbling in sterile Salda lake water amended with low-phosphate BG-11 culture media. Experiment S-Abio-4 was performed also without air bubbling in solution having elevated concentrations of Mg and DIC (0.05 M $MgCl_2$ + 0.1 M $NaHCO_3$). All abiotic experiments were performed in the presence of 0.01 M $NaN_3$ to prevent possible microbial growth.

One additional experiment, S-f, was run to assess Mg consumption and isotopic fractionation by *Synechoccocus* sp. without carbonate precipitation. This experiment performed in the absence of dissolved $MgCl_2$ and $NaHCO_3$ and *Synechoccocus* sp. was grown

in BG-11 medium. The fluid phase and biomass in this experiment was sampled after 5 days and 3 months of growth.

### 2.5. Sampling and Analyses

30-50 ml aliquots of homogeneous suspension (containing the solution, precipitated mineral phase, and cells if present) were sampled periodically from the reactors in a sterile laminar hood box during each experiment. Optical density and pH were measured in liquid sub-samples, whilst the solution supernatants were initially filtered (< 0.22 µm) and later processed for alkalinity, DOC, and Mg concentration measurements. Trace elements were measured without preconcentration by the ICP-MS following procedure routinely used in our laboratory for lake and river water analyses (e.g., Pokrovsky et al., 2010, 2011). Alkalinity was determined following a standard HCl titration procedure using an automatic Schott TitroLine alpha $TA10^{plus}$ titrator with an uncertainty of ±2% and a detection limit of $5\times10^{-5}$ M. Dissolved Organic Carbon (DOC) was analyzed using a Shimadzu TOC-6000 SCN Carbon Total Analyzer with an uncertainty of 3% and a detection limit of 40 µM. Magnesium concentrations were measured by flame atomic absorption spectroscopy using a Perkin Elmer AAnalyst 400 with an uncertainty of ±2% and a detection limit of 0.2 µM. pH was measured using a Mettler Toledo combined electrode, with a precision of ±0.01. The uncertainty of biomass concentration determination via optical density is estimated at ±10%.

Prior to sample characterization by scanning electron microscopy (SEM), organic matter was removed by treating sampled solid phases with 10% $H_2O_2$ for 2-3 days at the same pH as the experimental fluids. The residual solid phases were then thoroughly rinsed with de-ionized water and freeze dried at -55°C. The mineral phases were characterized by SEM using a Jeol JSM840a, and by X-ray diffraction using an INEL CPS 120 $Co_{K\alpha}$, with a scan speed of $0.02^{o}\,s^{-1}$. Untreated solids were kept for chemical analysis as described below.

Transmission Electron Microscopy (TEM) analysis was performed using TEMSCAN facilities of the University of Toulouse, with a JEOL JEM 2100F unit equipped with a field emission gun (FEG) source and a PGT EDX detector. TEM samples for analyses were prepared by immersing 200 mesh copper grids coated with a carbon film for 10 seconds in solutions containing live bacteria taken from the experiments that either produced or not mineral precipitates. To minimize the potential effect of crystallization from salts present in reactor solution on TEM/EDX measurements, aliquots of 20 mL were centrifuged at 4000

rpm for 10 minutes and washed twice with sterile MilliQ water. Grids were dried and covered with a 20 nm carbon layer prior to TEM analysis.

### 2.6. Magnesium Isotope Analyses

Mg isotope compositions of liquid and solid samples collected in the field and produced during the experimental part of the present study, were analyzed following the procedure given in Mavromatis et al. (2011). Magnesium isotopic ratios were measured using a Thermo-Finnigan 'Neptune' Multi Collector Inductively Coupled Plasma Mass Spectrometer (MC-ICP-MS) at GET (Toulouse, France). Instrumental mass fractionation effects were corrected via sample-standard bracketing, and all results are presented in delta notation with respect to the DSM-3 international reference material (Galy et al., 2001):

$$\delta^{x}\mathrm{Mg} = \left( \frac{\left( \frac{^{x}\mathrm{Mg}}{^{24}\mathrm{Mg}} \right)_{sample}}{\left( \frac{^{x}\mathrm{Mg}}{^{24}\mathrm{Mg}} \right)_{DSM\,3}} - 1 \right) \cdot 1000 \qquad (1)$$

where *x* refers to the Mg mass of interest. Compatibility of results between the Neptune and Nu Instrument MC-ICP-MS used in this study was confirmed by replicate analyses of three international Mg reference standards (DSM, CAM-1 and OUMg), and by duplicate analyses of the carbonate standard J-Do 1. The $\delta^{26}$Mg reproducibility of these standards was typically <0.08 ‰.

The isotopic offset between the Mg in the fluid and that incorporated into the solid phase is defined as:

$$\Delta^{26}\mathrm{Mg}_{\text{solid-liquid}} \equiv \delta^{26}\mathrm{Mg}_{\text{solid}} - \delta^{26}\mathrm{Mg}_{\text{liquid}} \qquad (2)$$

This value was determined for all samples where both the fluid and solid phases were collected in the present study.

# 3. RESULTS

## 3.1. Chemical and Mg isotopic composition of Salda lake water and minerals

### 3.1.1. Hydrochemistry

Concentrations of Mg, Alk and pH values measured in Salda lake waters and inflowing streams are in general in agreement with values reported by Braithwaite and Zedef (1994, 1996) and Kazanci et al. (2004) over the past two decades. The chemical composition of major and trace elements in collected samples is listed in the electronic supporting information (ESM-1). In February 2008 and 2010, surface water temperature was around 8-10°C whereas in September 2010, it varied from 27.5°C at the surface to 13°C at 70 m depth. The summer period corresponds to the most significant growth of stromatolites (e.g. Braithwaite and Zedef, 1996) and as such, detailed chemical and isotopic analysis of the lake water composition was performed in water samples collected during September 2010. During this period, pH decreased from 9.20±0.05 at the surface to 9.03±0.03 at the bottom layer; [DOC] ranged from 4.1-4.5 to 3.5 mg/L, and Alk, Mg, Ca and Cl concentrations remained constant in the water column and were equal to 0.032±0.001 M, 390±5 mg/L, 4.0±0.1 mg/L and 195±5 mg/L, respectively. Solution saturation degree (Ω) with respect to nesquehonite, the first precipitating mineral (e.g., Mavromatis et al., 2011 and this study) ranged from 1.6-1.85 at the surface to 0.76 at the bottom layer. Therefore, precipitation of hydrous magnesium carbonates in the Salda lake water during summer is limited to the upper 20 meters. The Mg concentration of incoming streams and groundwaters was about 3 times lower compared to the lake water (e.g., 72 – 120 mg/L, see also Braithwaite and Zedef, 1996) and they were strongly undersaturated with respect to nesquehonite ($\Omega_{nesquehonite}$ = 0.03-0.12).

### 3.1.2. Mineralogy of stromatolites

Collected stromatolites are dominated by hydromagnesite as shown by XRD analysis of multiple spots of a 20 cm-thick representative stromatolite sample and littoral sediments. The carbonate sand on the littoral zone of the lake (white coastal deposits Fig. 1A) is also composed of hydromagnesite as it essentially originates from the wave abrasion of growing stromatolites (Braithwaite and Zedef, 1996). The external stromatolite surface has a typical honeycomb-like structure (Fig. 2A, B) probably formed due to heterotrophic degradation of cyanobacteria cell which are mineralized within their EPS layers (e.g., Dupraz et al., 2004). In

the deeper (interior) part of stromatolites, platelets of hydromagnesite are clearly seen (Fig. 2D) and similar needle-like habits occur on hydromagnesite covering the submerged solid support as tree branches (Fig. 2C). These three types of crystal forms were found to be highly reproducible and frequently found in all investigated hydromagnesite samples. The imprints of *Pyrogira* green algae are often seen by the SEM on the surface of stromatolites (not shown) as this algae efficiency to colonize active stromatolite surfaces forming visible air bubbles (Fig. 1D).

3.1.3. Mg isotopes

In September 2010, magnesium isotopic composition ($\delta^{26}Mg$) of the lake water was very homogeneous and did not vary among different sites on the littoral zone, with and without stromatolite presence, and along the water column down to the bottom (70 m), being equal in average to 0.118±0.043 ‰ (Table 2). The coastal lake water in February 2008 and 2010 had $\delta^{26}Mg$ of -0.005 and -0.02 ‰. The incoming spring and ground water are much lighter in Mg having $\delta^{26}Mg$ between -1.4 and -0.8‰. The internal and external parts of stromatolites and the littoral sand exhibit similar $^{26}Mg$ isotope signature of -0.99 ± 0.07 ‰.

### 3.2. Experimental modeling of hydrous Mg carbonate precipitation in laboratory

The measured chemical composition of the reactive fluids and the mineralogy of precipitated solid phases are listed in the Electronic Supplementary Material (Table ESM-2 (*as file ESM.pdf made of "Total compilation Salda cyanobacteria-March-2011.xls" file*) and are described in detail below.

3.2.1. Solid phases

X-ray diffraction results demonstrate the precipitation of nesquehonite ($MgCO_3 \cdot 3H_2O$) and dypingite ($Mg_5(CO_3)_4(OH)_2 \cdot 5H_2O$) at distinct times during the experiments. Nesquehonite precipitation is limited to the first 12-23 days of experiments S-Bio-2 and S-Bio-5, but it is present after 48 days in experiment S-Abio-4 performed in solutions two times more enriched in Mg and DIC (Fig. 2I). Two biotic runs (S-Bio-1 and S-Bio-2) yielded brucite at the end of experiment (Fig. 2G) with nesquehonite followed by dypingite at the

beginning. For the majority of abiotic (S-Abio-1, S-Abio-3) and some biotic experiments (S-Bio-2, 3 and 5), dypingite or mixtures of dypingite and hydromagnesite were the main mineral phases at the end of experiment. Experiments performed on Salda lake water without air bubbling often yielded the presence of hydromagnesite. Scanning electron microscopy images, such as shown in Fig. 2, reveal that nesquehonite exhibits a needle-like habit, whilst the dypingite is present as rosette-like aggregates of 2 to 10 µm diameter. The hydromagnesite was characterized by rounded elongated crystals of 0.5 - 1 µm size forming large associates (Fig. 2K). Overall, the sequence of precipitation and recrystallization events seems as: nesquehonite (needles 20-120 µm long, 10±5 µm large) → dypingite (rosettes 5-15 µm) → hydromagnesite (aggregates 20-40 µm).

It is important noting that the hydromagnesite crystal associates formed in solutions with *Gloeocapsa* sp. cyanobacteria (Fig. 2F, Exp H2) are surprisingly similar to the external surface of Salda lake stromatolites (Fig. 2A) whereas the rosette-like dypingite and hydromagnesite aggregates obtained in experiments with *Synechoccocus* sp. cyanobacteria (Fig. 2E, Exp S-Bio-10; Fig. 2J, K, Exp S-Bio-3) are also similar to natural hydromagnesite coatings of submerged surfaces in the Salda lake (Fig. 2C). Finally, the "platellets" of hydromagnesite precipitated in biotic experiment S-Bio-3 (Fig. 2K, L) resemble the interior part of natural stromatolite (Fig. 2D). Note the shape of hydromagnesite crystals formed in this experiment is similar to that of coccoid *Synechoccocus* sp. cyanobacteria (Fig. 3A) suggesting some embedding of the cells. Such an embedding of cells and cell associates is clearly seen in experiment with *Gloeocapsa* sp. cyanobacteria cultured during 100 days in Mg, $HCO_3$-enriched BG-11 media (Exp No H-5'', S-Bio-11) and it is likely to be responsible for typical honeycomb structure of Mg hydrous carbonates formed in the presence of cyanobacteria (Fig. 2E) as well as in natural stromatolites (Fig. 2A, B)

The TEM examination of bacteria grown during 2 weeks in hydromagnesite-supersaturation low-phosphate BG-11 nutrient media containing initially 0.025 M $MgCl_2$ + 0.05 M $NaHCO_3$ demonstrated the presence of nanometer-size spherulite crystals assembled in network-like associates of 1-2 µm size, usually adjacent to the very surface of live cells (Fig. 3A, D, E). In addition, mineral coating of the whole cell surfaces (Fig. 3C) or cell sheaths (Fig. 3B) was frequently observed. Cells grown in Mg, $HCO_3^-$ low nutrient media remained clean, without any mineral precipitation on the surface (Fig. 3F).

3.2.2. Chemical Composition of the Fluid Phase

The temporal evolution of Mg concentration and pH in all experiments and the temporal evolution of alkalinity and biomass concentration during representative experiments are illustrated in Fig. 4. The Mg concentration and alkalinity of the reactive fluids tend to decrease and the pH tends to increase with time during all biotic experiments, notably those with air bubbling (Fig. 4A, C, E). In the biotic and abiotic experiments, the reactive fluid Mg concentration and alkalinity decreased during the first 10±5 days, becoming almost constant thereafter, suggesting the attainment of near-equilibrium conditions with most insoluble Mg carbonate phase, hydromagnesite or dypingite. Abiotic stirred experiments without air bubbling did not produce measurable [Mg] and [Alk] decrease although slight pH increase was observed (Fig. 4B, D, F). Biotic stirred experiments with and without air bubbling demonstrated very similar pattern of pH, [Mg] and [Alk] dependence on time (Fig. 4), although the biomass production was a factor of two higher in experiments with air bubbling (Fig. 5). The amendment of Salda lake water with nutrient BG-11 components exhibit significant effect on biomass production and Mg hydrous carbonate precipitation as follows from Mg concentration decrease (Fig. 6).

Quantitative analysis of the amount of precipitated mineral (mole of Mg removed from solution) as a function of biomass production yielded a clear relationship with a slope of 7.1 ± 0.9 following the relationship

$$Mg_{precipitated}\,(moles) = (7.1\pm0.9) \times Biomass_{produced}\,(g_{wet}) \quad (3)$$

or, converting mole of Mg into mole of precipitated mineral (Fig. 7):

$$Hydromagnesite\ (mol) = (1.45\pm0.23) \times Biomass_{produced}\,(g_{wet}) \quad (4)$$

Given the large variety of investigated conditions (BG-11 media, Salda lake water, air bubbling and no-bubbling regime), we consider this dependence as universal suitable for quantitative prediction (±25%) of the amount of precipitated Mg hydrous carbonate in the presence of photosynthesizing cyanobacteria. Another important conclusion that may be drawn from this dependence is that the mineral yield due to microbial photosynthesis and, thus, mineral precipitation rates, are very similar among experiments with different solution conditions (Mg, DIC concentration and pH), duration and biomass concentration, and air bubbling or no-bubbling regime.

The speciation and saturation state of the reactive fluids with respect to potentially precipitating mineral phases for all experiments was calculated using PHREEQC together

with its MINTEQA2 database (Parkhurst and Appelo, 1999) after adding to it thermodynamic properties for nesquehonite and hydromagnesite reported by Cheng and Li (2010a,b). The calculated aqueous speciation of Mg is reported in Table ESM-3 (file Total compilation 2011 Avril.exl). The speciation of aqueous Mg during the experiments was dominated by aqueous $Mg^{2+}$, but also contained 30-50% $MgCO_3^{-}{}_{(aq)}$ and $MgHCO_3°$. Reactive fluids were undersaturated ($\Omega$ = 0.2-0.4) with respect to, first precipitating phase, nesquehonite, found to be near to equilibrium with respect to nesquehonite after 5-10 days of reaction, during the beginning of massive precipitation, and undersaturated with respect to nesquehonite and hydromagnesite at the end of each experiment. The saturation state of these fluids with respect to dypingite was not calculated owing to lack of relevant thermodynamic data. The evolution of the saturation state of the fluids of biotic and abiotic experiments with and without air bubbling is illustrated in Fig. 8A and B, respectively. The initial supersaturation degree with respect to nesquehonite, the first precipitating phase, ranged from 0.2 to 0.6, at the beginning of the experiments, to 0.8 - 1.6 in the middle of reaction, before massive mineral precipitation and finally decreased to 0.1 - 0.3. Experiments with lower concentrations of $HCO_3^-$ and thus lower supersaturation degree ($\leq$ 0.3) failed to produce sufficient mineral precipitation.

Note that the abiotic experiments yielded mineral precipitation only at the conditions of air bubbling, where as stirred unbubbled experiments failed to precipitate any detectable quantity of hydrous Mg carbonate, despite the fact that $\Omega_{nesquehonite}$ was similar or even higher than that in biotic experiments (Fig. 8B). Similarly, experiments with Salda lake water amended (S-Bio-4) and not amended (S-Bio-6) with BG-11 yielded similar precipitation indices after 5 and 20 days of experiment (Fig. 8C); however, no mineral precipitation was observed in nutrient-free Salda lake water.

Apparent precipitation rates ($r_i$) were calculated from the first derivative of the fluid phase Mg concentration with respect to time, from the onset of precipitation to the attainment of constant fluid Mg concentrations using

$$r_i = \frac{dc_{Mg}}{dt} . \qquad (4)$$

where $c_{Mg}$ stands for the concentration of Mg in the reactive fluid and $t$ designates time. All experiments performed in the presence of sterile humid air bubbling attained steady-state Mg concentrations over shorter time periods (12±3 days) and exhibit approximately twice higher apparent precipitation rates compared to bubbling-free experiments. Under similar environmental conditions (Mg, DIC, bubbling regime), the precipitation rate measured

in biotic (S-Bio-2) experiment is significantly higher than that measured in abiotic experiment (S-Abio-1): -1.22 and -0.50 mmol Mg $day^{-1}$, respectively.

### 3.2.3 Magnesium Isotopic Composition

Mg-isotope analyses were performed on selected samples of experiments S-Bio-1, S-Bio-2, S-Abio-1, 4 and 5 where nesquehonite and dypingite were the main precipitated mineral phases except the last sample of S-Bio-2 which yielded brucite as the main phase. The Mg isotope compositions of all analyzed samples are given in Table 2 and the temporal evolution of $\Delta^{26}Mg_{solid\text{-}solution}$ (Eqn. 2) during experiments is plotted in Fig. 10. All experiments exhibited mass-dependent fractionation between the fluid and the solid phase. The precipitated hydrous Mg carbonates have $\delta^{26}Mg$ compositions that are 0.5-1.4 ‰ lighter than their liquid counterparts. Precipitated brucite is only 0.1-0.2 ‰ lighter than the aqueous solution. Isotopic composition of *Synechoccocus* sp. cells from the mineral-free experiment was 0.15 ‰ enriched in heavier Mg isotopic composition compared to the growth medium.

There is no statistically significant correlation between the extent of Mg fractionation and the reactive fluid pH, $IAP_{hydromagnesite}$, Mg, alkalinity and biomass concentrations (not shown) as also follows from data on other cyanobacteria of the family *Chroococcales*, *Gloeocapsa* sp. (Mavromatis et al., 2011). Generally, within the course of experiments with a single mineral hydrous Mg carbonate phase present (eg. S-Bio-5, S-Abio-1), the $\Delta^{26}Mg_{solid\text{-}liquid}$ values are almost constant as a function of elapsed time (Fig. 10A) or the fraction of Mg remaining in solution (Fig. 10B) and consistent with closed system equilibrium exchange between the fluid and solid phase.

## 4. DISCUSSION

### 4.1. Mineralogy of Salda lake sediments and laboratory precipitates.

Although the stromatolites of the Salda lake were extensively studied in the past, the present study confirms the dominance of hydromagnesite ($Mg_5(CO_3)_4(OH)_2 \cdot 4H_2O$) as the main mineral of these microbialites. The external surface of stromatolite is extremely porous, void-like, honeycomb-like structure bearing the presence of bacterial associates or cyanobacterial colonies. The persistence of hydromagnesite both in the lake littoral sediments and in live microbialites confirms its ultimate long-term stability at the conditions of lake

water temperature and pH. This is also in accord with reports on hydromagnesite dominance in alkaline playas of British Columbia (Power et al., 2009) and the hydromagnesite persistence in other alkaline lake sediments (Renaut and Long, 1989; Queralt et al., 1997).

The bottom waters of the lake and incoming streams are undersaturated with respect to hydromagnesite and nesquehonite which suggest the importance of both *i*) microbial photosynthetic activity and *ii*) surface temperature in creating sufficient supersaturation degree favorable for *in-situ* mineral formation.

In contrast to natural samples, experimental precipitation both in biotic and abiotic systems yielded mainly nesquehonite and dypingite. Although the transformation of nesquehonite into hydromagnesite is relatively fast, on the order of weeks, it has only been studied at elevated temperatures (Davies and Bubela, 1973; Hopkinson et al., 2008). The same authors also suggested that dypingite ($Mg_5(CO_3)_4(OH)_2 \bullet 5(H_2O)$ may represent an intermediate metastable phase during the transition of nesquehonite to hydromagnesite. This observation, together with the results of our long term experiments (100 days; S-Bio-8, 9 and 10) were hydromagnesite was formed, may explain the presence of less stable intermediate phases (nesquehonite and dypingite) in experiments run at room temperature for relatively short period of time (2 to 6 weeks). Similar to our results, Power et al. (2007), working with microbial consortia isolated from Atlin Playas, British Columbia, Canada, reported dypingite formation in biotic mesocosm experiments, and nesquehonite formation in abiotic control experiments at a pH of ~9.5

A striking similarity is observed between Mg hydrous carbonate forming at the surface of live stromatolites in the Salda lake (Fig. 2B) and those precipitating in long-term laboratory experiments with *Gloeocapsa* sp. (Fig. 2F) as well as in numerous field observations (see Fig. 9c and Fig. 11 in Dupraz et al., 2004). Dupraz et al. (2009) observed that discontinuous EPS calcification generates a micropeloidal structure resulting from the presence of clusters of coccoid or remnants of filamentous bacteria. Furthermore the same authors report that no precipitation is observed in or on the sheaths of cyanobacteria, and only a negligible amount of precipitation is directly associated with the well-organized and active filamentous cyanobacteria (in deeper layers of the mat). Instead, the precipitation occurs at the uppermost layer of the mat, which is composed of EPS, empty filamentous bacteria and coccoids (*Gloeocapsa* spp.). Results of the present study corroborates the mechanism of honeycomb -

like structures formation for hydrous Mg carbonates due to the presence of EPS and cell capsules evidenced earlier only for biocalcification phenomena.

### 4.2. Physico-chemical mechanisms of Mg carbonate precipitation in the presence of cyanobacteria

Carbonate mineral formation in the presence of photosynthetic bacteria may be attributed to the alkaline environment produced due to release of hydroxyl ions as a result of photosynthesis (Thompson and Ferris, 1990; Douglas and Beveridge, 1998). pH was observed to increase in all experiments although this increase was much smaller in abiotic experiments without air bubbling. In abiotic experiments, this increase originates from the degassing of the initial reactive fluid which contained $3\text{-}5\times10^{-2}$ mol/kg $NaHCO_3$ at pH ~ 8.2-9.2. Owing to this high aqueous bicarbonate content, these initial fluids have a $pCO_2$ of $\sim(0.3\text{-}10)\times10^{-2.0}$ atm, supersaturated with respect to the atmosphere. The bubbling of sterile humid air liberates $CO_2$ from the reactive fluid leading to both an increase in pH and degree of supersaturation with respect to Mg carbonate minerals. In biotic experiments, this $pCO_2$ decrease was accompanied by additional pH increase due to photosynthetic uptake of $HCO_3^-$ ions and $OH^-$ release.

In contrast, the lack of precipitation in abiotic, non-bubbling experiments may stem from insufficient local supersaturation occurring in the vicinity of cells during photosynthesis (Pokrovsky and Savenko, 1994). This micro-environment supersaturation well known for microbial mats and stemmed from local pH rise (Jorgensen and Revsbech, 1983) are necessary to initiate nesquehonite precipitation. However, it may not be detectable in the plot of bulk solution Ω versus time (Fig. 8). Therefore, at the experimental conditions investigated in this work, the live photosynthesizing cells act as nucleation centers due to high local supersaturation, not occurring in abiotic, no-bubbling experiments. The contrast between bubbling and non-bubbling regime should be more significant in non-stirred experiments; however, given the low pertinence of such an experimental setup to highly agitated coastal zones of the Salda Lake subjected to wave abrasion, these experiments were not conducted.

Results of the experiments in axenic culture performed in the present study suggest that the role of studied cyanobacteria is both in increasing pH of the bulk solution capable directly controlling crystallization process and in providing specific organic template and EPS for nucleation. Given the presence of microcrystalline mineral precipitates at the vicinity of the cell walls and directly at the cell surface (Fig. 3) we suggest that the role of cyanobacterial polysaccharides in Mg hydrous carbonate precipitation is significant as also established for

calcium carbonate (e.g., Braissant et al., 2003, 2007; Dittrich and Sibler, 2010). This is further confirmed by the similarity of Mg hydrous carbonate crystals observed in natural microbialites and that in laboratory cultures (Fig. 2B and 2F). The demonstrated capacity of one single culture to precipitate carbonate crystals very similar in shape to those of microbial consortia of Salda lake stromatolites may have important consequences on the mechanisms of Mg-rich carbonates formation in the past, before the appearance of massive $CaCO_3$ formation in the ocean. If the presence of live cyanobacteria is capable of inducing hydromagnesite precipitation simply by increasing pH and supersaturation and without specific action of other bacteria, then the formation of Mg-rich stromatolites in Precambrian period could occur via the simplest life form. This may question the necessity of important control by postmortem decomposition of cyanobacterial sheaths by precipitation-inducing heterotrophic bacteria as suggested for ancient dendritic reef structures (Laval et al., 2000).

At the present time, it is widely accepted that actively metabolizing microbial cells are capable of avoiding calcium carbonate mineral encrustation and cell entombment (Thompson et al., 1997; Aloisi et al., 2006; Bontognali et al., 2008; Martinez et al., 2010) via various mechanisms of cell electric potential regulation, S-layer formation and extracellular EPS generation as evidenced from numerous laboratory experiments and field observations (e.g., Krumbein et al., 1977; Chafetz and Buczynski, 1992; Arp et al., 1999a, b). Unlike in experiments and observations on biocalcification (Dupraz et al., 2009; Martinez et al., 2010), hydrous Mg carbonate formation does not trigger a cell protection mechanism. The presence of nanoclusters of hydrous Mg carbonates at the very surface of live cells detectable in the TEM images (Fig. 3A, D, E) and complete cell encrustation by precipitated mineral seen by the SEM (Fig. 2F, N, O) unequivocally supports the major role of cell surface in governing Mg mineral formation in the presence of cyanobacterial cells.

In addition to different but still unknown requirements (pH, $pCO_2$, EPS concentration) of calcite and hydrous Mg carbonate nucleation at the vicinity of photosynthesizing cells, another reason for this difference may be the different size of forming crystals. Unlike calcite or dolomite submicron nano-globulles (e.g. Aloisi et al., 2006; BontognalI et al., 2008; Spadafora et al., 2010), the first precipitated hydrous Mg carbonate, nesquehonite, is represented by crystals of 50 to 200 µm length (Fig. 2I) and as such it can not embed the small *Synechoccocus* sp. cells. Similarly, rosette-like dypingite crystal aggregates (Fig. 2E, J and M) formed at the second stage of experiment are also too large to cover completely the cyanobacterial cells at the beginning of incrustation. Only at the stage of hydromagnesite

formation at the end of experiment (Fig. 2K, 2L) at the end of experiments, massive embedding and encrusting becomes possible due to *i*) small size of hydromagnesite platelets, and *ii*) the presence of dead cells which are easier to mineralize (e.g., Chafetz and Buczynski, 1992; Martinez et al., 2010)

### 4.3. Fractionation of Mg isotopes

Mg isotope fractionation between cells and aqueous solutions ($\Delta^{26}Mg_{solid\text{-}solution}$) linked to adsorption by cyanobacterial cell surface and intracellular uptake during *Synechoccocus* sp. growth, assessed in mineral-free bacterial growth experiments (S-f), is equal to 0.152 ‰. This is in agreement with previous results on *Gloeocapsa* sp. cyanobacteria (0.05-0.2 ‰, Mavromatis et al., 2011). At the same time, Black et al. (2006) reported that chlorophyll*a* isolated from cyanobacterium *S. elongatus* preferentially incorporates light Mg isotopes with a fractionation factor of -0.71 to -0.53 ‰ depending on the growth stage. The chlorophyll represents small fraction of total cell Mg pool, compared to the cytoplasm. As such, there may be significant variation of Mg isotopic ratio in different cell pools, with cytoplasm being much "heavier" than the chlorophyll. Note that, unlike other essential metals, $Mg^{2+}$ is not exchanged during a cell division cycle, but once taken by the cells, remains inside them (Silver and Walderhaug, 1992). This explains the persistence of light Mg isotope composition in mineral-free biomass, collected after 5 days and 3 months (-0.82 and -1.18 ‰, respectively).

During the abiotic experiment S-Abio-1 in the presence of air bubbling, the precipitated dypingite exhibits a $\Delta^{26}Mg_{solid\text{-}solution}$ value between -1.4‰ and -1. 25‰, whereas abiotic experiment S-Abio-4 without bubbling produced only nesquehonite with $\Delta^{26}Mg_{solid\text{-}solution}$ = -0.47‰. In contrast, the biotic experiment with bubbling (S-Bio-5) yielded nesquehonite slightly lighter than the abiotic counterpart and depleted in $^{26}Mg$ compared to fluid with $\Delta^{26}Mg_{solid\text{-}solution}$ equal to -0.7‰ to -1.0 ‰. Finally, biotic experiments with brucite precipitation had $\Delta^{26}Mg_{solid\text{-}solution}$ = -0.2‰ to -0.1‰. Therefore, we observe a systematic enrichment of mineral solid phase by light isotope in the order brucite < nesquehonite < dypingite with maximal fractionation factors of -0.7 to -1.4 ‰ similar to that reported for hydrous Mg carbonates formation in the presence *Gloeocapsa* sp. cyanobacteria (Mavromatis et al., 2011). Overall, the depletion of heavy isotopes in our samples is also coherent with the results of previous studies on Mg isotope fractionation between aqueous fluids and biogenic skeletal carbonates (Chang et al., 2004; Buhl et al., 2007; Hippler et al., 2009), abiotically

precipitated low Mg-calcite (Galy et al., 2002; Immenhauser et al., 2010), dolomite (Higgins and Schrag, 2010), and magnesite (Pearce et al., 2009).

The nearly constant $\Delta^{26}Mg_{solid\text{-}liquid}$ values for a given dominant mineral phase are consistent with a closed-system fractionation equilibrium model suggesting a continuous isotopic exchange/equilibration between the precipitated hydrous Mg-carbonates and the reactive fluid (Criss, 1999). Taking into account earlier results for dypingite (Mavromatis et al., 2011) and for other hydrous Mg carbonates (this work), it can be assumed that hydrous Mg-carbonate minerals are in a continuous isotopic equilibrium when present in aquatic environments. The exchange does not seem to appreciably affected by physicochemical factors such as pH, bubbling, Mg and DIC concentration or the biological activity.

The isotopic shift between solid and solution observed in the laboratory is in reasonable agreement with that found in the Salda lake ecosystem. In the latter, an offset of 1.0-1.4 ‰ between the incoming streams and groundwaters from the one hand and the lake water from the other hand is consistent with formation of 1.0-1.4 ‰ isotopically lighter hydromagnesite via cyanobacterial activity in the stromatolites. It is important to note that the presence of biofilms and other, heterotrophic bacteria in the microbial community of stromatolites apparently, have no significant effect on overall isotopic fractionation factor compared to laboratory monocultures of cyanobacteria. Given that abiotic precipitation experiments yielded similar fractionation factor, the use of Mg isotopes for tracing the role of microbial activity in Mg hydrous carbonate formation is unwarranted.

## 5. CONCLUSIONS

The hydrochemistry of the Salda lake system and field observations suggest strong microbial control on hydrous Mg carbonates formation in the upper layers of the lake surface. Laboratory experiments with cyanobacteria culture *Chroococcales* sp. isolated from live stromatolite yielded the precipitation of hydrous magnesium carbonates, nesquehonite and dypingite under varying laboratory conditions. We discovered a universal dependence between the amount of precipitated Mg carbonate and bacterial biomass production which can be used for reconstructing paleoproductivity based on the amount of accumulated Mg carbonates. All experiments yielded similar bulk precipitation rates, although the pH of reactive fluid was 0.5-1.0 units higher in biotic compared to abiotic experiments. Taken together these observations suggest that the presence of cyanobacteria is necessary to increase solution pH and therefore, supersaturation degree and to provide the sites for nucleation at the microenvironments of the cell surface. No cell protection mechanisms known for

biocalcification phenomena have been evidenced in case of hydrous Mg carbonate precipitation. The difference between mineral (nesquehonite and dypingite) and solution $^{26}Mg$ isotope ratio ($\Delta^{26}Mg_{solid\text{-}liquid}$) obtained from abiotic experiments are similar within the uncertainty of those obtained in the presence of *Synechoccocus* sp. and earlier *Gloeocapsa* sp. cyanobacteria.

## ACKNOWLEDGMENTS

Jerome Chmeleff and Carole Casseraund are acknowledged for their assistance with the MC-ICP-MS and atomic absorption analyses in Toulouse. This work was supported by ANR CO2-FIX, MC ITN DELTA-MIN (ITN-2008-215360), MC RTN GRASP-$CO_2$ (MRTN-CT-2006-035868) and MC MIN-GRO (MRTN-CT-2006-035488) and the programs: INTERVIE (INSU), and the Associated European Laboratory LEAGE.

## REFERENCES

Aloisi, G., Gloter, A., Kruger, M., Wallmann, K., Guyot, F. and Zuddas, P.: Nucleation of calcium carbonate on bacterial nanoglobules, Geology 34, 1017-1020, 2006.

Arp, G., Reimer, A. and Reitner, J.: Calcification in cyanobacterial biofilms of alkaline salt lakes, Eur. J. Phycol. 34, 393-403, 1999a.

Arp, G., Thiel, V., Reimer, A., Michaelis, W. and Reitner, J.: Biofilm exopolymers control microbialite formation at thermal springs discharging into the alkaline Pyramid Lake, Nevada, USA, Sedimentary Geology 126, 159–176, 1999b.

Black, J. R., Yin, Q. Z. and Casey, W. H.: An experimental study of magnesium-isotope fractionation in chlorophyll-a photosynthesis, Geochim. Cosmochim. Acta 70, 4072-4079, 2006.

Black, J. R., Yin, Q.-Z., Rustad, J. R. and Casey, W. H.: Magnesium-isotope equilibrium in chlorophylls, J. Am. Chem. Soc. 129, 8690-8691, 2007.

Bontognali, T. R. R., Vasconcelos, C., Warthmann, R. J., Dupraz, C., Bernasconi, S. M. and McKenzie, J. T.: Microbes produce nanobacteria-like structures, avoiding cell entombment, Geology 36; 663-666; doi: 10.1130/G24755A.1, 2008.

Brady, A. L., Slater, G., Laval, B., and Lim, D. S.: Constraining carbon sources and growth rates of freshwater stromatolites in Pavilion Lake using $^{14}C$ analysis, Geobiology 7**,** 544-555, 2009.

Braissant, O., Cailleau, G., Dupraz, C. and Verrecchia, A. P.: Bacterially induced mineralization of calcium carbonate in terrestrial environments: The role of exopolysaccharides and amino acids, J. Sediment. Res. 73, 485-490, 2003.

Braissant, O., Decho, A. W., Dupraz, C., Glunk, C., Przekop, K. M. and Visscher, P. T.: Exopolymeric substances of sulfate-reducing bacteria: Interactions with calcium at alkaline pH and implication for formation of carbonate minerals, Geobiology 5, 401-411, 2007.

Braithwaite, C .J. R. and Zedef, V.: Hydromagnesite stromatolites and sediments in an alkaline lake, Salda Gölü, Turkey, J. Sed. Res. 66**,** 991-1002, 1996.

Braithwaite, C. J. R. and Zedef, V.: Living hydromagnesite stromatolites from Turkey, Sediment. Geol. 92, 1-5, 1994.

Buhl, D., Immenhauser, A., Smeulders, G., Kabiri, L., and Richter, D. K.: Time series $\delta^{26}$Mg analysis in speleothem calcite: Kinetic versus equilibrium fractionation, comparison with other proxies and implications for palaeoclimate research, Chem. Geol. 244, 715-729, 2007.

Calvin, W. M., King, T. V. V. and Clark, R. N.: Hydrous carbonates on Mars? evidence from Mariner 6/7 infrared spectrometer and ground-based telescopic spectra, J. Geophys. Res. 99, 14659-14675, 1994.

Castanier, S., Bernet-Rollande, M.-C., Maurin, A. and Perthuisot, J.-P.: Effects of microbial activity on the hydrochemistry and sedimentaology of Lake Logipi, Kenya, Hydrobiologia 267**,** 99-112, 1993.

Chafetz, H. S. and Buczynski, C.: Bacterially induced lithification of microbial mats, Palaios, 7**,** 277-293, 1992.

Chang, V. T. C., Williams, R. J. P., Makishima, A., Belshawl, N. S., and O'Nions, R. K.: Mg and Ca isotope fractionation during $CaCO_3$ biomineralisation, Biochem. Biophys. Res. Commun. 323, 79-85, 2004.

Cheng, W. T. and Li, Z. B.: Controlled Supersaturation Precipitation of Hydromagnesite for the $MgCl_2$-$Na_2CO_3$ System at Elevated Temperatures: Chemical Modeling and Experiment, Ind. Eng. Chem. Res. 49, 1964-1974, 2010a.

Cheng, W. T. and Li, Z. B.: Nucleation kinetics of nesquehonite ($MgCO_3 \cdot 3H_2O$) in the $MgCl_2$-$Na_2CO_3$ system, J. Cryst. Growth 312, 1563-1571, 2010b.

Cox, G., James, J. M., Leggett, K. E. A., Armstrong, R. and Osborne, L.: Cyanobacterially deposited speleothems: Subaerial stromatolites, Geomicrobiol. J. 7, 245-252, 1989.

Criss, R. E.: Principles of Stable Isotope Distribution, Oxford University Press, Oxford, 254, 1999.

Davies, P. J. and Bubela, B.: The transformation of nesquehonite into hydromagnesite, Chem. Geol. 12, 289-300, 1973.

Dittrich, M. and Sibler, S.: Calcium carbonate precipitation by cyanobacterial polysaccharides. In Pedley, H.M. and Rogerson, M. (eds.) Tufas and Speleotherms: Unravelling the microbial and physical controls, Geol. Soc. London Spec. Publ. 336, 51-63, doi: 10.1144/SP336.4, 2010.

Douglas, S. and Beveridge, T. J.: Mineral formation by bacteria in natural microbial communities, FEMS Microbiol. Ecol. 26, 79-88, 1998.

Dove, P. M.: The Rise of Skeletal Biominerals, Elements 6, 37-42, 2010.

Dupraz, C., Reid, R. P., Braissant, O., Decho, A. W., Norman, R. S., and Visscher, P. T.: Processes of carbonate precipitation in modern microbial mats, Earth-Sci. Rev. 96, 141-162, 2009.

Dupraz, C., Visscher, P. T., Baumgartner, L. K. and Reid, R. P.: Microbe–mineral interactions: early carbonate precipitation in a hypersaline lake (Eleuthera Island, Bahamas), Sedimentology 51, 745–765 doi: 10.1111/j.1365-3091.2004.00649.x, 2004.

Edwards, H. G. M., Moody, C. D., Newton, E. M., Villar, S. E. J. and Russell, M. J.: Raman spectroscopic analysis of cyanobacterial colonization of hydromagnesite, a putative martian extremophile, Icarus, 175, 372-381, 2005.

Ferris, F. G., Thompson, J. B. and Beveridge, T. J.: Modern freshwater microbialites from Kelly Lake, british Columbia, Canada. Palaios, 12, 213-219, 1997.

Galy, A., Bar-Mattews, M., Halicz, L. and O'Nions, R. K.: Mg isotopic composition of carbonate: insight from speleotherm formation, Earth Plganet. Sci. Lett. 201, 105-115, 2002.

Galy, A., Belshaw, N. S., Halicz, L. and O'Nions, R. K.: High-precision measurement of magnesium isotopes by multiple-collector inductively coupled plasma mass spectrometry Internat, J. Mass Spec. 208, 89-98, 2001.

Girgin, S., Kazanci, N. and Dügel, M.: On the limnology of deep and saline lake Burdur in Turkey, Acta Hydrochim. Hydrobiol. 32, 189-200, 2004.

Hartley, A. M., House, W. A., Callow, M. E. and Leadbeater, B. S. C.: The role of a green alga in the precipitation of calcite and the coprecipitation of phosphate in freshwater, Internat. Rev. Hydrobiol. Hydrograpie, 80, 385-401, 1995.

Hartley, A. M., House, W. A., Leadbeater, B. S. C. and Callow, M. E.: The use of microelectrodes to study the precipitation of calcite upon algal biofilms, J. Colloid Interface Sci. 183, 498-505, 1996.

Higgins, J. A. and Schrag, D. P.: Constraining magnesium cycling in marine sediments using magnesium isotopes, Geochim. Cosmochim. Acta 74, 5039-5053, 2010.

Hippler, D., Buhl, D., Witbaard, R., Richter, D. K., and Immenhauser, A.: Towards a better understanding of magnesium-isotope ratios from marine skeletal carbonates, Geochim. Cosmochim. Acta 73, 6134-6146, 2009.

Hopkinson, L., Rutt, K. and Cressey, G.: The transformation of nesquehonite to hydromagnesite in the system CaO-MgO-$H_2O$-$CO_2$: An experimental spectroscopic study, J. Geol. 116, 387-400, 2008.

Immenhauser, A., Buhl, D., Richter, D., Niedermayr, A., Riechelmann, D., Dietzel, M. and Schulte, U.: Magnesium-isotope fractionation during low-Mg calcite precipitation in a limestone cave – Field study and experiments, Geochim. Cosmochim. Acta 74, 4346-4364, 2010.

Jørgensen, B. B. and Revsbech, N. P.: Photosynthesis and structure of benthic microbial mats: Microelectrode and SEM studies of four cyanobacterial communities, Limnol. Oceanogr. 28, 1075-1093, 1983.

Kazanci, N., Girgin, S. and Dügel, M.: On the limnology of Salda Lake, a large and deep soda lake in southwestern Turkey: future management proposals, Aquatic Conservation: Mar. Freshw. Ecosyst. 14: 151-162. DOI: 10.1002/aqc.609, 2004.

Kazmierczak, J. and Kempe, S.: Genuine modern analogues of Precambrian stromatolites from caldera lakes of Niuafo'ou Island, Tonga. Naturwissenschaften 93**,** 119-126, 2006.

Kelts, K., and Hsu, J.: Freshwater carbonate sedimentation, In A. Lerman [ed.], Lakes – chemistry, geology, physics. Springer, 295-323, 1978.

Kempe, S. and Kazmierczak, J.: Chemistry and stromatolites of the sea-linked Satonda Crater Lake, Indonesia: A recent model for the Precambrian sea? Chem. Geol. 81, 299-310, 1990.

Knoll, A. H., Fairchild, J. J. and Sweet, K.: Calcified microbes in Neoproterozoic carbonates: Implications for our understanding of the Proteroizic/Cambrian transition. Palaios, 8, 512-525, 1993.

Kranz, S. A., Wolf-Gladrow, D., Nehrke, G., Langer, G. and Rost, B.: Calcium carbonate precipitation induced by the growth of the marine cyanobacterium *Trichodesmium*. Limnol. Oceanogr. 55, 2563-2569, 2010.

Krumbein, W. E., Cohen, Y. and Shilo, M.: Solar Lake (Sinai). 4. Stromatolitic cyanobacterial mats, Limnol. Oceanogr. 22, 635- 656, 1977.

Laval, B., Cady, S. L., Pollack, J. C., McKay, C. P., Bird, J. S., Grotzinger, J. P., Ford, D. C. and Bohm, H. R.: Modern freshwater microbialite analogues for ancient dendritic reef structures, Nature, 407, 626-629, 2000.

Li, W., Beard, B. L. and Johnson, C. M.: Exchange and fractionation of Mg isotopes between epsomite and saturated $MgSO_4$ solution, Geochimica et Cosmochimica Acta, 75, 1814-1828, 2011.

Lopez-Garcia, P., Kazmierczak, J., Benzerara, K., Kempe, S., Guyot, F., and Moreire, D.: Bacterial diversity and carbonate precipitation un the gaint stromatolites from the highly alkaline Lake Van, Turkey. Extremophiles 9, 263-274, 2005.

Lowenstam, H. A. and Weiner, S.: On biomineralization, Oxford University Press, Oxford, New York, 1989.

Martinez, R. E., Gardes, E., Pokrovsky, O. S., Schott, J. and Oelkers, E. H.: Do photosynthetic bacteria have a protective mechanism against carbonate precipitation at their surfaces? Geochim. Cosmochim. Acta 74, 1329-1337, 2010.

Martinez, R., Pokrovsky, O. S., Schott, J. and Oelkers, E. H.: Surface charge and zeta-potential of metabolically active and dead cyanobacteria, J. Colloid Interface Sci. 323, 317-325, 2008.

Mavromatis, V. M., Pearce, C., Shirokova, L. S., Bundeleva, I. A., Pokrovsky, O. S., Benezeth, P. and Oelkers, E.H.: Magnesium isotope fractionation during inorganic and cyanobacteria-induced hydrous magnesium carbonate precipitation, Geochim. Cosmochim. Acta, submitted, 2011.

Müller, G., Irion, G. and Förstner, U.: Formation and diagenesis of inorganic Ca-Mf carbonates in the lacustrine environment, Naturwissenschaften 59, 158-164, 1972.

Obst, M, Wehrli, B. and Dittrich, M.: $CaCO_3$ nucleation by cyanobacteria: laboratory evidence for a passive, surface-induced mechanism, Geobiology, 7, 324-347, 2009.

Obst, M. and Dittrich, M.: Calcium adsorption and changes of the surface microtopography of cyanobacteria studied by AFM, CFM, and TEM with respect to biogenic calcite nucleation, Gechemistry Geophysics Geosystems, 7, 15, 2006.

Otsuki, A. and Wetzel, R. G.: Calcium and total alkalinity budgets and calcium carbonate precipitation in a small hard-water lake, Arch. Hydrobiol. 73, 14-30, 1974.

Palomba, E., Zinzi, A., Cloutis, E. A., D'Amore, M., Grassi, D. and Maturilli, A.: Evidence for Mg-rich carbonates on Mars from a 3.9 µm absorption feature. Icarus, 203, 58-65, 2009.

Parkhurst, D. L. and Appelo, C. A. J.: User's Guide to PHREEQC (Version 2) - A Computer Program for Speciation, Batch- Reaction, One-Dimensional Transport, and Inverse Geochemical Calculations, U.S. Geological Survey Water-Resources Investigations Report 99-4259, 310, 1999.

Pearce, C. R., Saldi, G. D., Schott, J., Burton, K.W. and Oelkers, E.H.: Experimental quantification of kinetic Mg-isotope fractionation during magnesite precipitation, Geochim. Cosmochim. Acta 73, 13, A1003, 2009.

Pedone, V. A. and Folk, R. L.: Formation of aragonite cement by nannobacteria in the Great Salt Lake, Utah. Geology, 24, 763-765, 1996.

Pentecost, A. and Spiro, B.: Stable Carbon and Oxygen Isotope Composition of Calcites Associated with Modern Fresh-Water Cyanobacteria and Algae, Geomicrobiol. J. 8, 17-26, 1990.

Pentecost, A.: Blue-green algae and freshwater carbonate deposits, Proc. R. Soc. London B. 200, 43-61, 1978.

Peterson, B. J. and Fry, B.: Stable isotopes in ecosystem studies, Annu. Rev. Ecol. Syst. 18, 293-320, 1987.

Planavsky, N., Reid, R. P., Lyons, T. W., Myshrall, K. L. and Visscher, P. T.: Formation and diagenesis of modern marine calcified cyanobacteria, Geobiology 7, 566-576, 2009.

Pokrovsky, O. S. and Savenko, V. S.: Experimental modeling of CaCO3 precipitation at the conditions of photosynthesis in seawater, Oceanology 35, N6, 805-810, 1995.

Pokrovsky, O. S., Shirokova, L. S., Kirpotin, S. N., Audry, S., Viers, J. and Dupré, B.: Effect of permafrost thawing on the organic carbon and metal speciation in thermokarst lakes of western Siberia, Biogeosciences, Special issue Siberian Arctic Land-Shelf-Atmosphere Interface, 8, 565-583, doi:10.5194/bg-8-565-2011, 2011.

Pokrovsky, O. S., Viers, J., Shirokova, L. S., Shevchenko, V. P., Filipov, A. S. and Dupré, B.: Dissolved, suspended, and colloidal fluxes of organic carbon, major and trace elements in Severnaya Dvina River and its tributary, Chem. Geol. 273, 136–149, 2010.

Power, I. M., Wilson, S. A., Dipple, G. M. and Southam, G.: Modern carbonate microbialites from an asbestos open pit pond, Yukon, Canada, Geobiology, 180-195, DOI: 10.1111/j.1472-4669.2010.00265.x, 2011.

Power, I. M., Wilson, S. A., Thom, J. M., Dipple, G. M. and Southam, G.: Biologically induced mineralization of dypingite by cyanobacteria from an alkaline wetland near Atlin, British Columbia, Canada, Geochem. Trans. 8: 13, doi: 10.1186/1467-4866-8-13, 2007.

Power, I. M., Wilson, S. A., Thom, J. M., Dipple, G. M., Gabites, J. E. and Southam, G.: The hydromagnesite playas of Atlin, British Columbia, Canada: A biogeochemical model for $CO_2$ sequestration, Chem. Geol. 260, 286-300, 2009.

Queralt, I., Julia, R., Plana, F. and Bischoff, J. L.: A hydrous Ca-bearing magnesium carbonate from playa lake sediments, Saline Lake, Spain, Amer. Mineral. 82**,** 812-819, 1997.

Raven, J. A. and Giordano, M.: Biomineralization by photosynthetic organisms: Evidence of co-evolution of the organisms and their environment? Geobiology 7, 140-154, 2009.

Renault, R.W.: Recent carbonate sedimentation and brine evolution in the saline lake basins of the Cariboo Plateau, British Columbia, Canada, Hydrobiologia, 197, 67-81, 1990.

Renaut R. W. and Long, P. R.: Sedimentaology of the saline lakes of the Cariboo Plateau, Interior British Columbia, Canada, Sed. Geol. 64, 239-264, 1989.

Renaut, R. W. and Stead, D.: Recent Magnesite-Hydromagnesite sedimentation in Playa Basins of the Caribou Plateau, British Columbia, Geological Fieldwork 1990, Paper 1991-1. British Columbia Geological Survey Branch, pp. 279-288. http://www.em.gov.bc.ca/DL/GSBPubs/GeoFldWk/1990/279-288-renaut.pdf, 1990.

Riding, R.: Microbial carbonates: the geological record of calcified bacterial-algal mats and biofilms, Sedimentology 47, 179-214, 2000.

Ries, J. B.: Review: geological and experimental evidence for secular variation in seawater Mg/Ca (calcite-aragonite seas) and its effects on marine biological calcification, Biogeosciences 7, 2795-2849, 2010.

Russell, M. J., Ingham, J. K., Zedef, V., Maktav, D., Sunar, F., Hall, A. J. and Fallick, A. E.: Search for signs of ancient life on mars: expectations from hydromagnesite microbialites, Salda Lake, Turkey, J. Geol. Soc. London, 156**,** 869-888, 1999.

Schauble, E. A.: First-principles estimates of equilibrium magnesium isotope fractionation in silicate, oxide, carbonate and hexaaquamagnesium(2+) crystals, Geochim. Cosmochim. Acta 75**,** 844-869, 2011.

Schmid, I. H.: Turkey's Salda Lake, a generic model of Australia's newly discovered magnesite deposits, Industrial Minerals 239, 19-31, 1987.

Scholl, D. W. and Taft, W. H.: Algae, contributors to the formation of calcareous tufa, Mono Lake, California, J. Sedimentary Research, 34, 309-319, 1964.

Shirokova, L. S., Pokrovsky, O. S., Viers, J., Klimov, S. I., Moreva, O. Yu., Zabelina, S. A., Vorobieva, T. Ya. and Dupré, B.: Diurnal variations of trace elements and heterotrophic bacterioplankton concentration in a small boreal lake of the White Sea basin, Ann. Limnol. - Int. J. Lim., 46, 67–75, DOI: 10.1051/limn/2010011, 2010.

Silver, S. and Walderhaug, M.: Gene regulation of plasmid- and chromosome-determined inorganic ion transport in bacteria, Microbiol. Rev. 56, 195-228, 1992.

Spadafora, A., Perri, E., McKenzie, J. A. and Vasconcelos, C.: Microbial biomineralization processes forming modern Ca:Mg carbonate stromatolites, Sedimentology, 57, 27-40, 2010.

Stabel, H.-H.: Calcite precipitation in Lake Constance: Chemical equilibrium, sedimentation, and nucleation by algae, Limnol. Oceanogr. 31, 1081-1093, 1986.

Thompson, J. B. and Ferris, F. G.: Cyanobacterial Precipitation of Gypsum, Calcite, and Magnesite from Natural Alkaline Lake Water, Geology 18, 995-998, 1990.

Thompson, J. B., Shultze-Lam, S., Beveridge, T. J. and Des Marais, D. J.: Whiting events: Biogenic origin due to the photosynthetic activity of cyanobacterial picoplankton, Limnol. Oceanogr. 42**,** 133-141, 1997.

Tipper, E. T., Galy, A., Gaillardet, J., Bickle, M. J., Elderfield, H. and Carder, E. H.: The magnesium isotope budget of the modern ocean: constraints from riverine magnesium isotope ratios, Earth Planet Sci. Lett. 250, 241-253, 2006.

Vasyukova, E. V., Pokrovsky, O. S., Viers, J., Oliva, P., Dupré, B., Martin, F. and Candaudaup, F.: Trace elements in organic- and iron-rich surficial fluids of the Boreal zone: Assessing colloidal forms via dialysis and ultrafiltration, Geochim. Cosmochim. Acta, 74, 449-468, 2010.

Zedef, V., Russell, M. J. and Fallick, A. E.: Genesis of vein stockwork and sedimentary magnesite and hydromagnesite deposits in the ultramafic terranes of Southwestern Turkey: A stable isotope study, Econ. Geol., 95, 429-445, DOI: 10.2113/gsecongeo.95.2.429, 2000.

**Table 1:** Experimental conditions during the experiments performed in this study. All abiotic experiments were conducted in the presence of 0.01 M $NaN_3$.

| Experiment | Medium | Duration (days) | conditions | Biomass range, $g_{wet}$/L | pH range | Mg range (mM) | DOC, mg/L | Rate (Mg slope) mmol $day^{-1}$ | Solid phase |
|---|---|---|---|---|---|---|---|---|---|
| S-BIO-1 H-10 | BG-11 | 43 | Stirring, no bubbling | 0.1-3.1 | 8.7-10.6 | 25.6-2.2 | 17-62 | -0.86 | Dypingite+brucite |
| S-BIO-2 H-16 | BG-11 | 30 | Stirring, bubbling | 0.2-3.7 | 8.2-10.5 | 30.8 - 4.1 | 60 | -1.22 | Nesquehonite, Dypingite, brucite |
| S-BIO-3 H-46 | BG-11 on Salda lake water | 34 | Stirring, no bubbling | 0.2-2.2 | 9.2 - 10.8 | 15-2.5 | 7-18 | -0.38** | Dypingite, hydromagnesite |
| S-BIO-4 H-50 | BG-11 on Salda lake water | 36 | Stirring, no bubbling | 0.1 - 3.0 | 9.3 - 10.8 | 14 - 3 | 9-17 | -0.435** | Dypingite, hydromagnesite |
| S-BIO-5 H-20 | BG-11 | 30 | Stirring, bubbling | 0.4 - 2.8 | 8.2 – 10.4 | 31 - 7 | 23 - 29 | -0.71 | Nesquehonite, dypingite |
| S-BIO-6 H-47 | Salda lake water w/o BG-11 | 34 | Stirring, no bubbling | 0.2-0.9 | 9.2 - 9.6 | 9.5-12 | | No precipitation | |
| S-BIO-7 H-29 | 0.05 M MgCl2+0.005 M NaHCO3 | 31 | Stirring, bubbling | 0.05 - 3.0 | 8.1 - 10.0 | 52-40 | | No precipitation | |
| S-BIO-8* H-2* | BG-11: 0.025 M $MgCl_2$ + 0.036 M $NaHCO_3$ | 100 | No stirring, no bubbling | 0.05 - 4.0 | 8.4 - 10.4 | 25-5 | 20-120 | N.D. | Hydromagnesite |
| S-BIO-9 H-3 | BG-11: 0.025 M $MgCl_2$ + 0.036 M $NaHCO_3$ | 100 | No stirring, bubbling | 0.05 - 3.5 | 8.4 - 10.7 | 25-5 | 10-65 | N.D. | Hydromagnesite |
| S-BIO-10 H-4 | BG-11: 0.025 M $MgCl_2$ + 0.036 M $NaHCO_3$ | 100 | No stirring, no bubbling | 0.05 -3.5 | 8.5 - 10.8 | 25-5 | 10-40 | N.D. | Hydromagnesite |
| S-BIO-11* H-5* | BG-11: 0.025 M $MgCl_2$ + 0.05 M $NaHCO_3$ | 40 | Stirring, no bubbling | 0.2-2.2 | 8.7-10.6 | 25-4 | 6.2-90 | N.D. | Dypingite, brucite |
| | | | | | | | | | |
| S-ABIO-1 H-18 | Supernatant | 25 | Stirring, bubbling | | 8.15-9.3 | 23-9 | 90-30 | **-0.50** | |
| S-ABIO-2 H-49 | BG-11 on Salda lake water | 35 | Stirring, no bubblinh | 0 | 9.2-9.39 | 13-12 | 7.4 | No precipitation | |
| S-ABIO-3 H-22 | Supernatant | 25 | Stirring, no bubbling | 0 | 8.1 - 9.25 | 37 - 13 | 30 | **-1.39** | Dypingite |
| S-ABIO-4 H-27 | 0.05 M MgCl2 + 0.1 M NaHCO3 | 48 | Stirring, no bubbling | 0 | 8.33 - 8.90 | 52-27 | | **-0.67** | Nesquehonite, dypingite |
| S-ABIO-5 H-48 | BG-11 on Salda lake water | 35 | Stirring, no bubblinh | 0 | 8.2-9.46 | 21-22 | | No precipitation | |
| S-ABIO-6 H-51 | BG-11 on Salda lake water | 40? | Stirring, no bubbling | 0 | 9.3 - 9.4 | 13.1 - 13.8 | | No precipitation | |

* Gloeocapsa sp. Culture; ** The rates are significantly lower due to lower initial Mg concentration

| Expt. | Sample No. | Time (Days) | LIQUIDS $\delta^{25}$Mg | 2 s.d. | $\delta^{26}$Mg | 2 s.d. | SOLIDS $\delta^{25}$Mg | 2 s.d. | $\delta^{26}$Mg | 2 s.d. | $\Delta^{26}$Mg solid-liquid | Mineralogy |
|---|---|---|---|---|---|---|---|---|---|---|---|---|
| **Laboratory samples** | | | | | | | | | | | | |
| | 1 | 0 | -0.2699 | 0.0343 | -0.5235 | 0.0504 | | | | | | |
| **S-Bio-1 (H-10)** | 8 | 13 | 0.0477 | 0.0599 | -0.0172 | 0.0561 | | | | | | |
| | 13 | 37 | -0.0905 | 0.0546 | -0.4620 | 0.0258 | -0.0501 | 0.0708 | -0.5666 | 0.0052 | **-0.105** | Brucite |
| **S-Bio-2 (H-16)** | 6 | 7 | -0.07978 | 0.0589 | -0.16762 | 0.1025 | -0.80708 | 0.0318 | -1.57317 | 0.0161 | **-1.406** | Nesquehonite |
| | 10 | 15 | -0.4093 | 0.0716 | -0.75737 | 0.1207 | -0.56523 | 0.0396 | -1.06708 | 0.0356 | **-0.310** | Dypingite |
| | 14 | 26 | -0.2328 | 0.0500 | -0.4472 | 0.0264 | -0.3658 | 0.0096 | -0.6992 | 0.0408 | **-0.252** | dypingite+brucite |
| **S-ABIO-1 (H-18)** | 4 | 6 | -0.074 | 0.041 | -0.103 | 0.033 | -0.738 | 0.016 | -1.428 | 0.005 | **-1.325** | Dypingite |
| | 8 | 13 | 0.1130 | 0.0356 | 0.2129 | 0.0114 | -0.5905 | 0.0321 | -1.1911 | 0.0197 | **-1.404** | Dypingite |
| | 13 | 25 | 0.0900 | 0.0277 | 0.1949 | 0.0314 | -0.5554 | 0.0226 | -1.0608 | 0.0295 | **-1.256** | Dypingite |
| | | | | | | | | | | | **-1.328** | |
| **S-BIO-5 (H20)** | 4 | 10 | -0.0677 | 0.0677 | -0.16521 | 0.1025 | -0.4668 | 0.0168 | -0.96494 | 0.0548 | **-0.800** | nesquehonite |
| | 9 | 20 | -0.02475 | 0.0300 | -0.10091 | 0.0505 | -0.3676 | 0.0021 | -0.76927 | 0.1294 | **-0.668** | nesquehonite |
| | 11 | 26 | 0.18442 | 0.0299 | 0.36078 | 0.0728 | -0.33207 | 0.0507 | -0.70502 | 0.0874 | **-1.066** | nesquehonite |
| | | | | | | | | | | | **-0.845** | |
| **S-ABIO-4 (H-27)** | 10 | 40 | -0.2059 | 0.0257 | -0.38161 | 0.0630 | -0.4176 | 0.0446 | -0.84917 | 0.0936 | **-0.468** | nesquehonite |
| | | | | | | | | | | | | |
| **S-f-5 culture** | 5 days | 5 | -0.47447 | 0.0462 | -0.97307 | 0.0525 | -0.38499 | 0.0525 | -0.82143 | 0.0667 | **0.152** | |
| | 3 months | | | | | | -0.582 | 0.0046 | -1.18436 | 0.0187 | **-0.211** | |
| **Natural samples** | | | | | | | | | | | | |
| **T3 Salda Lake coast and stromatholites** | | | 0.1337 | 0.0162 | 0.2569 | 0.0721 | -0.3648 | 0.0477 | -0.6955 | 0.0357 | **-0.952** | Hydromagnesite |
| **Salda coastal water & Sand on the beach** | | | -0.0637 | 0.0772 | -0.1360 | 0.1509 | -0.5040 | 0.0665 | -0.9933 | 0.1537 | **-0.857** | Hydromagnesite |
| **Stromatolite - Interior part** | | | | | | | -0.5324 | 0.0407 | -1.0384 | 0.0315 | **-1.118*** | Hydromagnesite |
| **Stromatolite - Exterior part** | | | | | | | -0.4794 | 0.0037 | -0.9378 | 0.0225 | **-1.018*** | Hydromagnesite |
| **Salda-Water February 2010** | | | -0.0053 | 0.0077 | -0.0208 | 0.0046 | | | | | | |
| **Live stromatolites + bacteria** | | | | | | | -0.3953 | 0.0260 | -0.7541 | 0.0178 | | |
| **Lake depth profile:** | | | | | | | | | | | | |
| **T07-0** | 0 | | 0.075 | 0.017 | 0.150 | 0.010 | | | | | | |
| **T07-20** | 20 | | 0.035 | 0.044 | 0.094 | 0.049 | | | | | | |
| **T07-40** | 40 | | 0.100 | 0.031 | 0.167 | 0.031 | | | | | | |
| **T07-60** | 60 | | 0.040 | 0.034 | 0.117 | 0.080 | | | | | | |
| **T07-70** | 70 | | 0.079 | 0.011 | 0.137 | 0.063 | | | | | | |
| **T08, Stromatolite islands** | | | 0.050 | 0.024 | 0.084 | 0.027 | | | | | | |
| **T11, 1.5 m depth, fragm. stromatolites** | | | 0.045 | 0.024 | 0.080 | 0.042 | | | | | | |
| | | | | | 0.118 | | | | | | | |
| **T09, Incoming spring** | | | -0.733 | 0.042 | -1.402 | 0.053 | | | | | | |
| **T10, Spring under mountain, Yuoruk MZL** | | | -0.535 | 0.101 | -1.010 | 0.107 | | | | | | |
| | | | | | | | | | | | | |
| **T1, Coastal lake water, Feb 2008** | | | -0.019 | 0.046 | -0.005 | 0.070 | | | | | | |
| **T2 Incoming spring, Feb 2008** | | | -0.384 | 0.049 | -0.759 | 0.028 | | | | | | |
| | | | | | | | | | | | | |
| **Epsomite deposits at the wood** | | | | | **0.1000** | | -0.1830 | 0.0226 | -0.3401 | 0.0466 | -0.4401 | Epsomite |

*** Assuming $\delta^{26}$Mg in Salda lake water of 0.08‰**

**Table 2. Mg isotopic composition in natural and laboratory samples**

**Figure 1. (A): View of the Salda lake coast. The white and light blue layers at the littoral zone represent the hydromagnesite sand formed due to modern and paleostromatolites wave abrasion. (B): Modern stromatolite formations in the littoral zone. (C): stromatolite coating of the peridote rock debris from 1-1.5 depth in the littoral zone. (D): surface of active stromatolite covered by Pyrogira algae and diatoms with oxygen bubbles illustrating active on-going photosynthesis.**

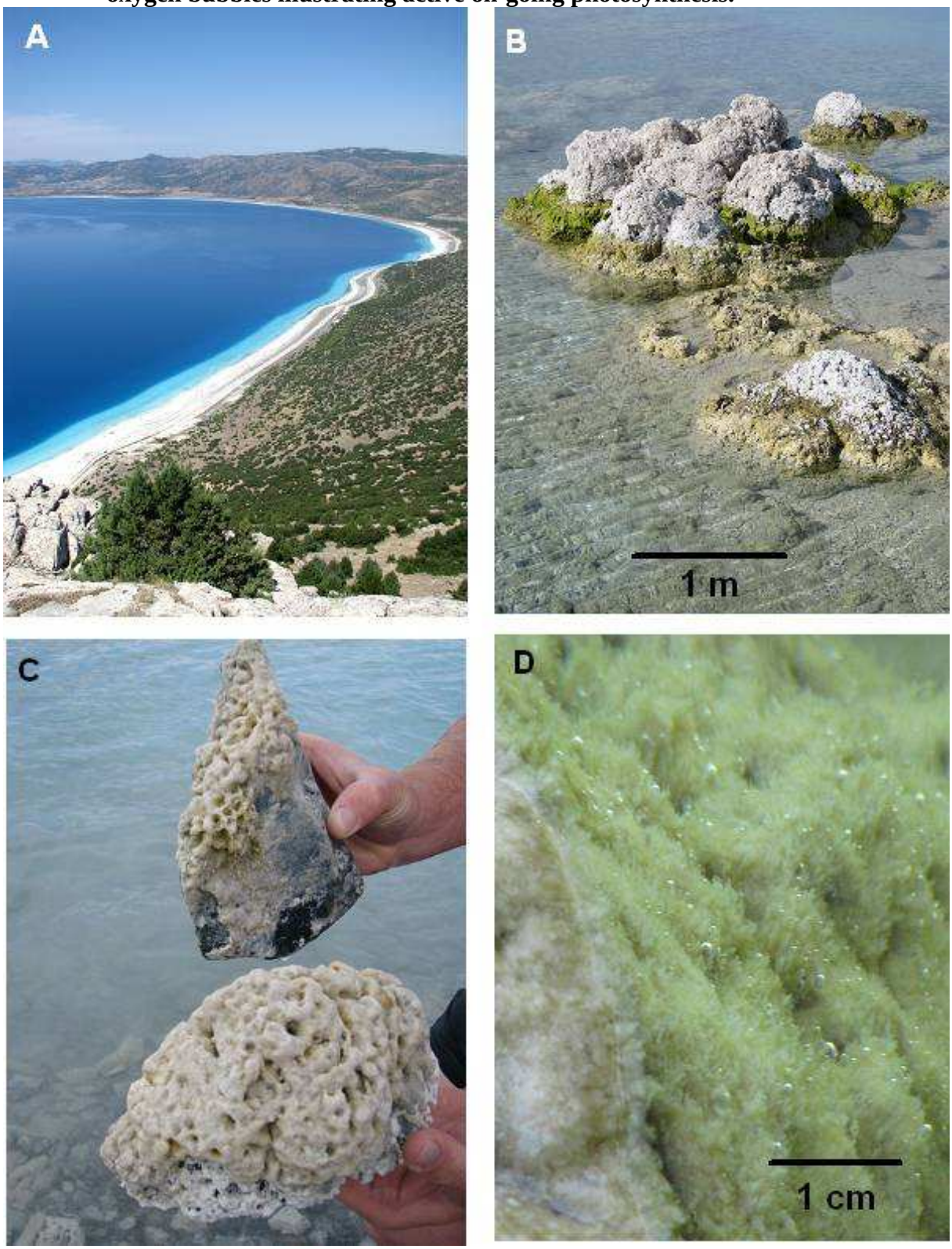

**Figure 2. SEM images of natural stromatolites and experimentally precipitated minerals**

**(A): sample T3-1 of the coastal zone, representing the external surface of stromatolite with a zoom (B). (C): Scratch of 2-10 mm thick mineral coating on grasses and tree branches in the littoral zone water. (D) : Deep interior part of the microbialite. EDS analyses demonstrated o the presence of only C, Mg, and O in all natural samples (A – D).**

**E-N: Laboratory precipitates of Experiment S-Bio-10 with dypingite (E), S-Bio-8 with hydromagnesite (F), S-Bio-2 with dypingite + brucite (G), S-Abio-4 with nesquhonite + dypingite (I), S-Bio-3 with dypingite (J), S-Bio-3 with hydromagnesite (K, L), S-Abio-1 with dypingite (M), and S-Bio-11 with dypingite and hydromagnesite (N, O).**

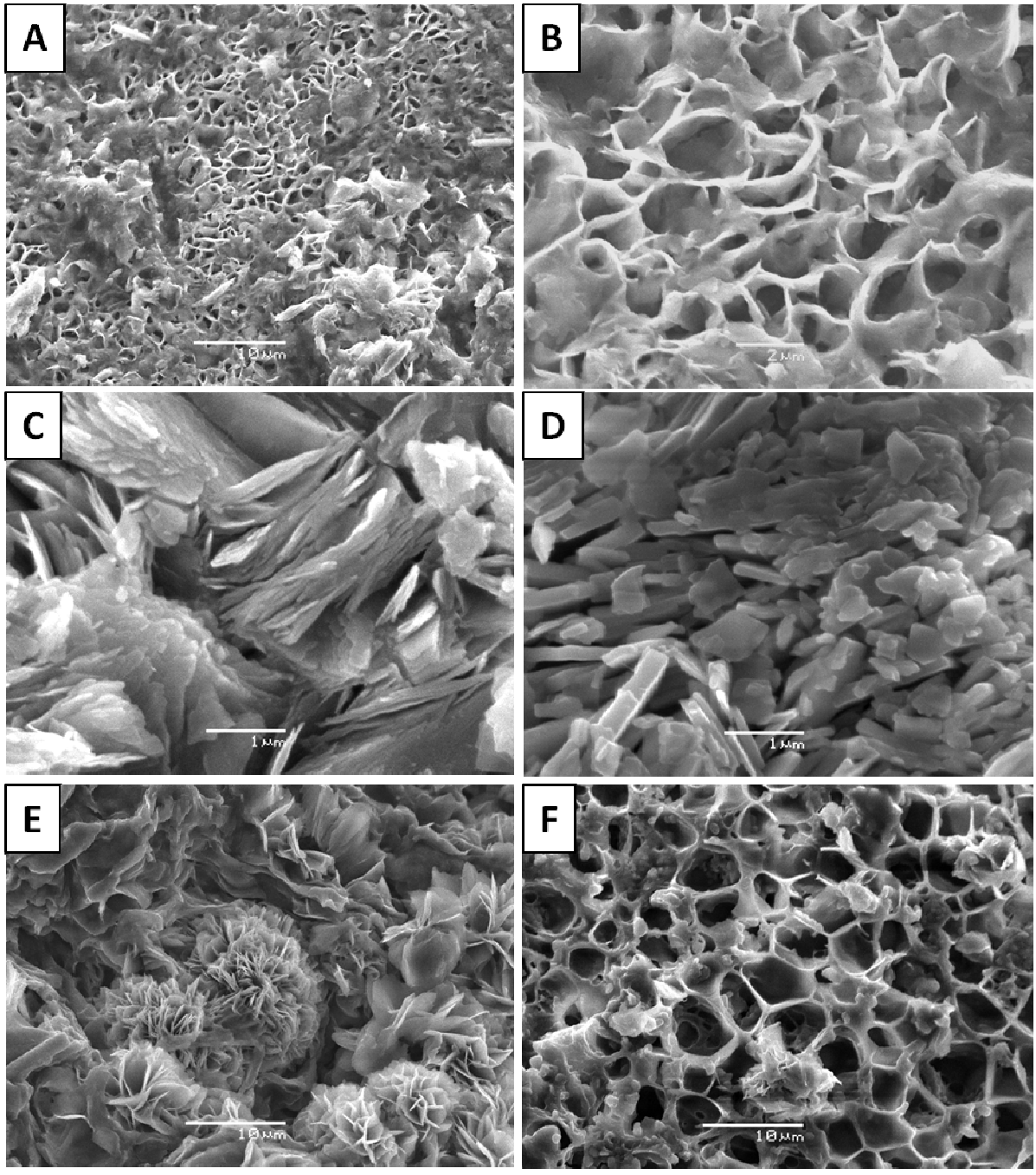

**Figure 3. TEM images of hydrous Mg carbonate precipitation after 14 days in 0.025 M $MgCl_2$ + 0.05 M $NaHCO_3$ (A-E) and *Synechococcus sp.* growth during 14 days in BG-11 media without mineral precipitation (F).**

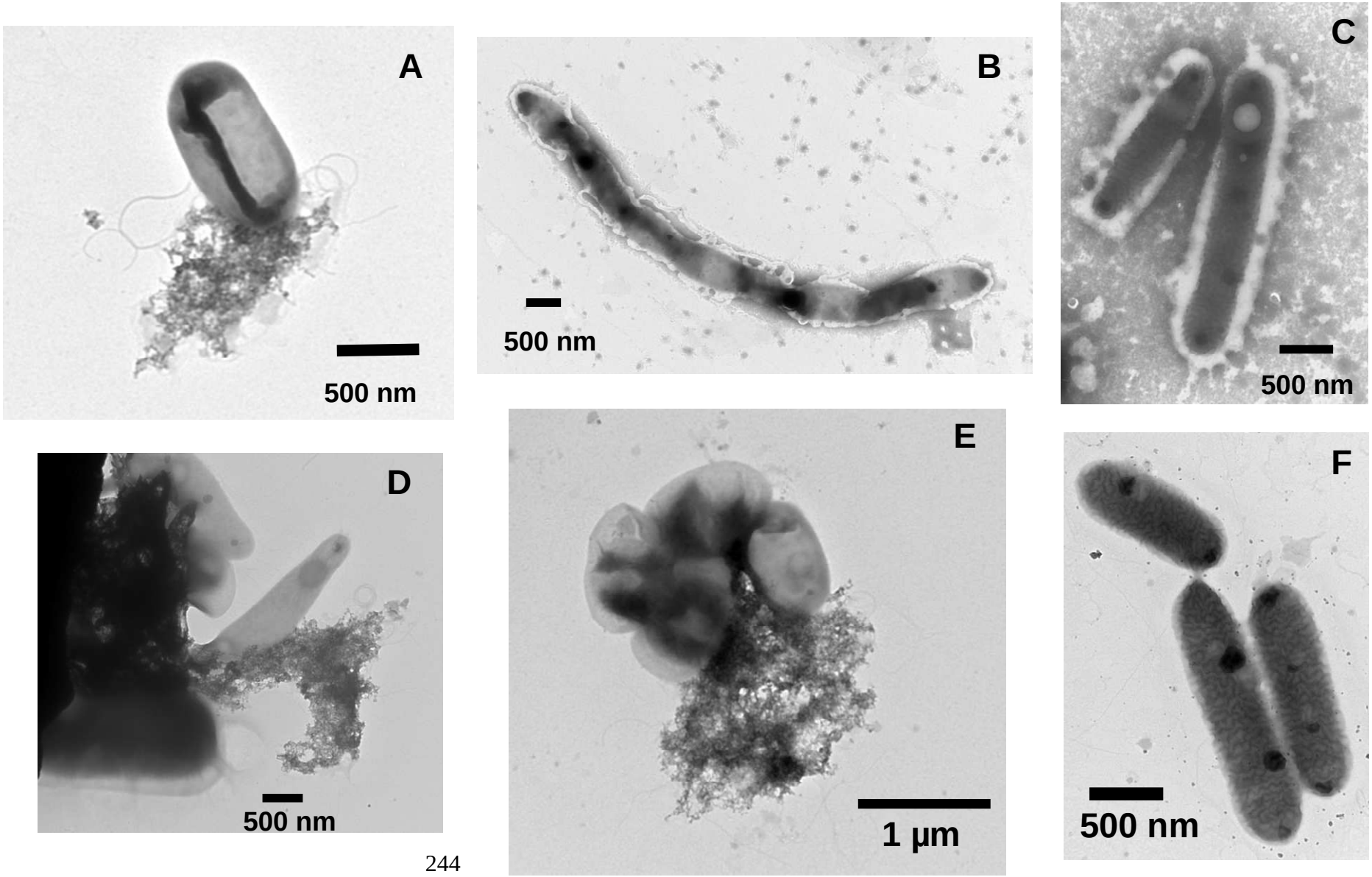

**Figure 4. Reactive fluid evolution during experiments performed in this study. Temporal evolution of pH (A, B), Mg concentration (C, D), and Alkalinity concentration (E, F) during experiments in continuously stirred reactors with air bubbling (left panel, A, C, E) and without air bubbling (right panel, B, D, F). The symbol size is within the uncertainty of the analyses.**

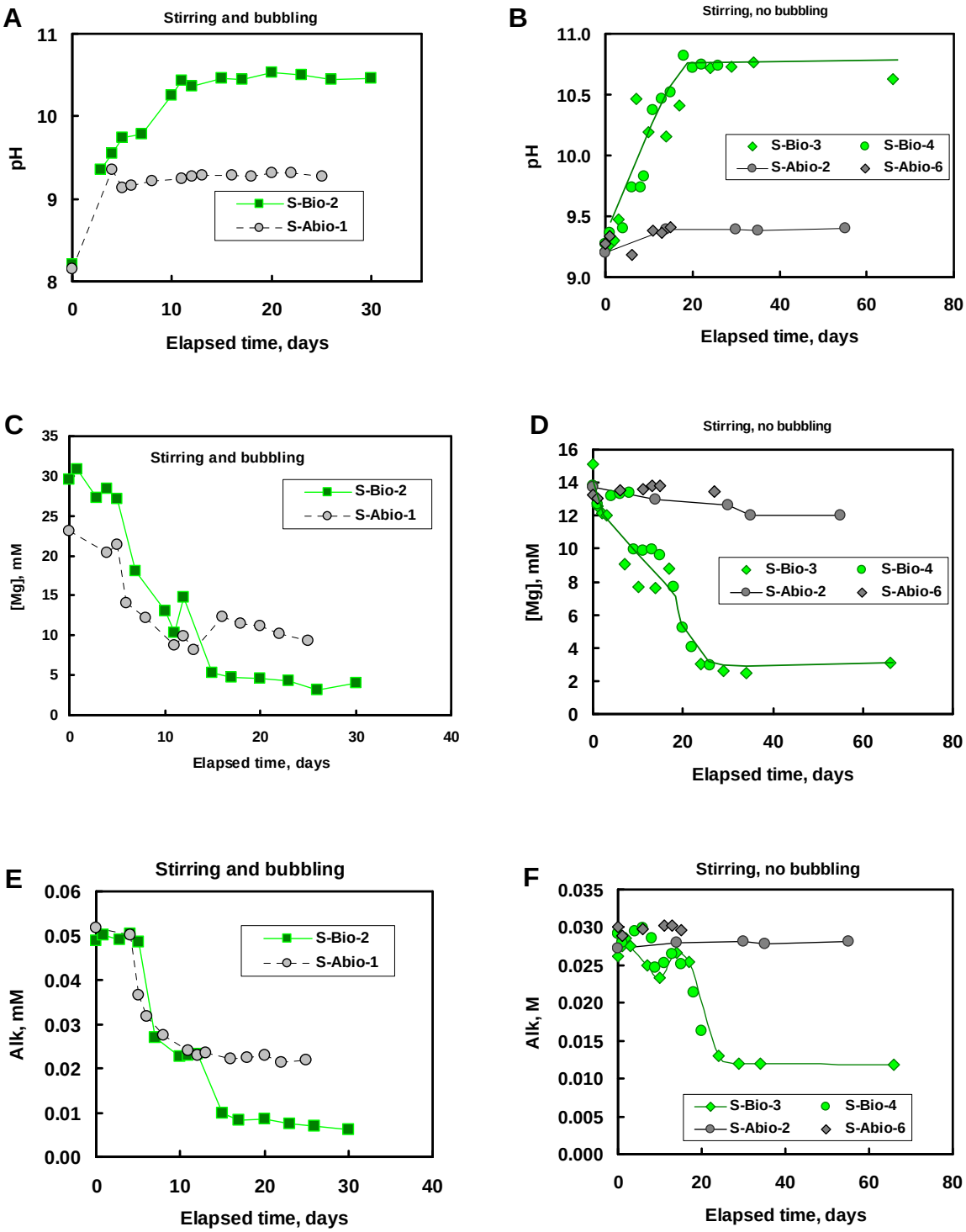

**Figure 5. The biomass evolution during experiments in stirred reactors with bubbling (S-Bio-2, circles) and without air bubbling (S-Bio-3, 4, diamonds and triangles)**

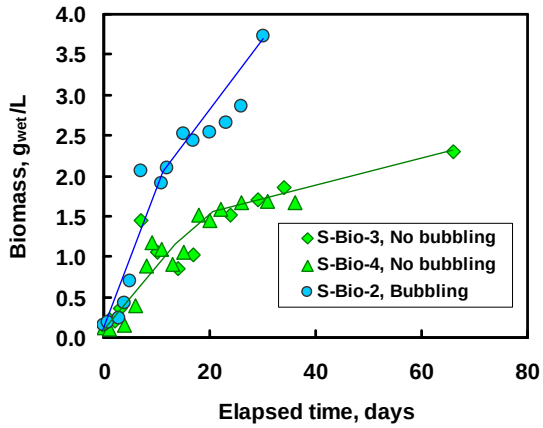

**Figure 6. Magnesium and biomass concentration evolution during experiments in stirred reactors with Salda lake water amended with BG-11 components (S-Bio-4, squares) and without BG-11 (S-Bio-6, squares)**

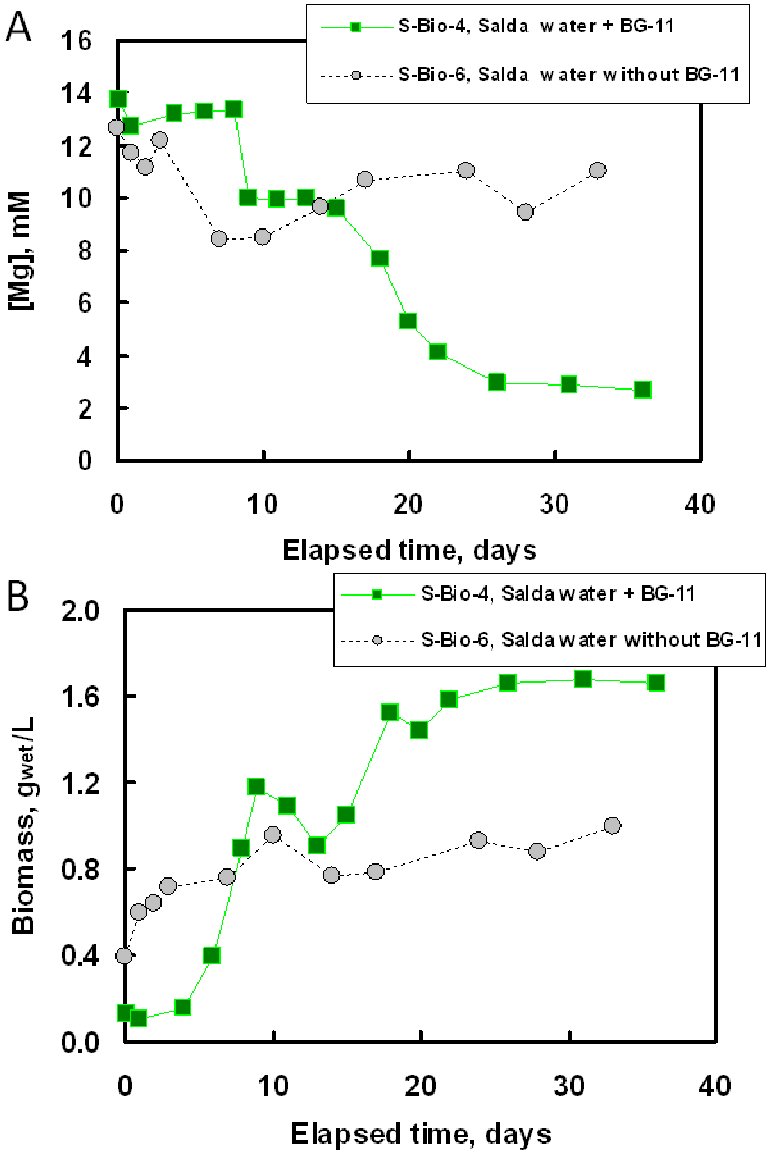

**Figure 7. Relationship between the amount of precipitated hydromagnesite (mmol) and the increase of the biomass ($g_{wet}$) in different biotic experiments.**

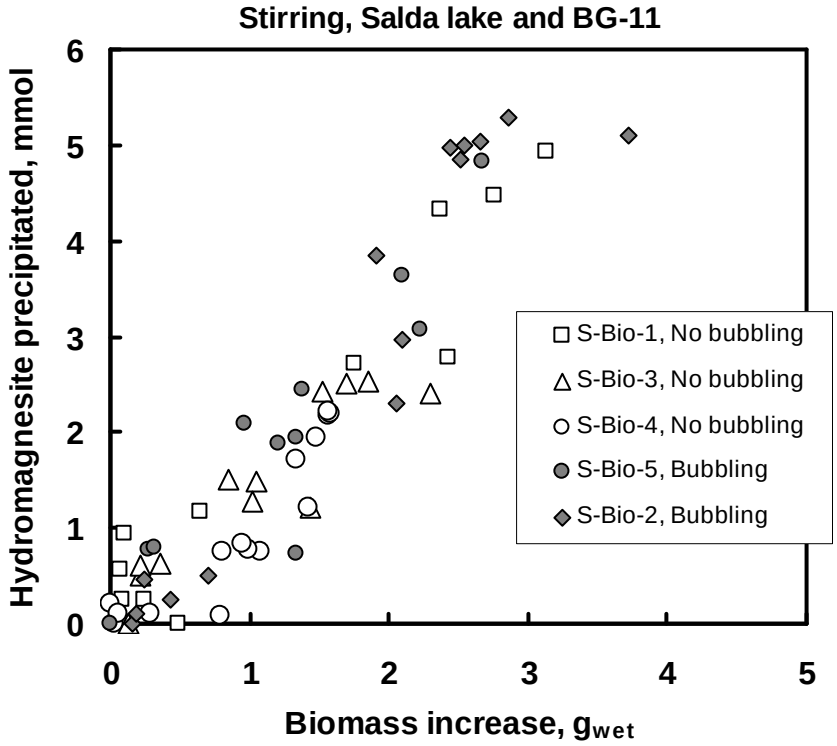

**Figure 8. Temporal evolution of degree of saturation of nesquehonite ($\Omega_{nesquehonite}$) of the reactive fluids in stirred experiments. A: During biotic (S-Bio-2) and abiotic (S-Abio-1) experiments with air bubbling; B: During biotic and abiotic experiments without air bubbling; C: During biotic experiments with Salda lake water amended with BG-11 components (S-Bio-4, squares) and without BG-11 (S-Bio-6, squares)**

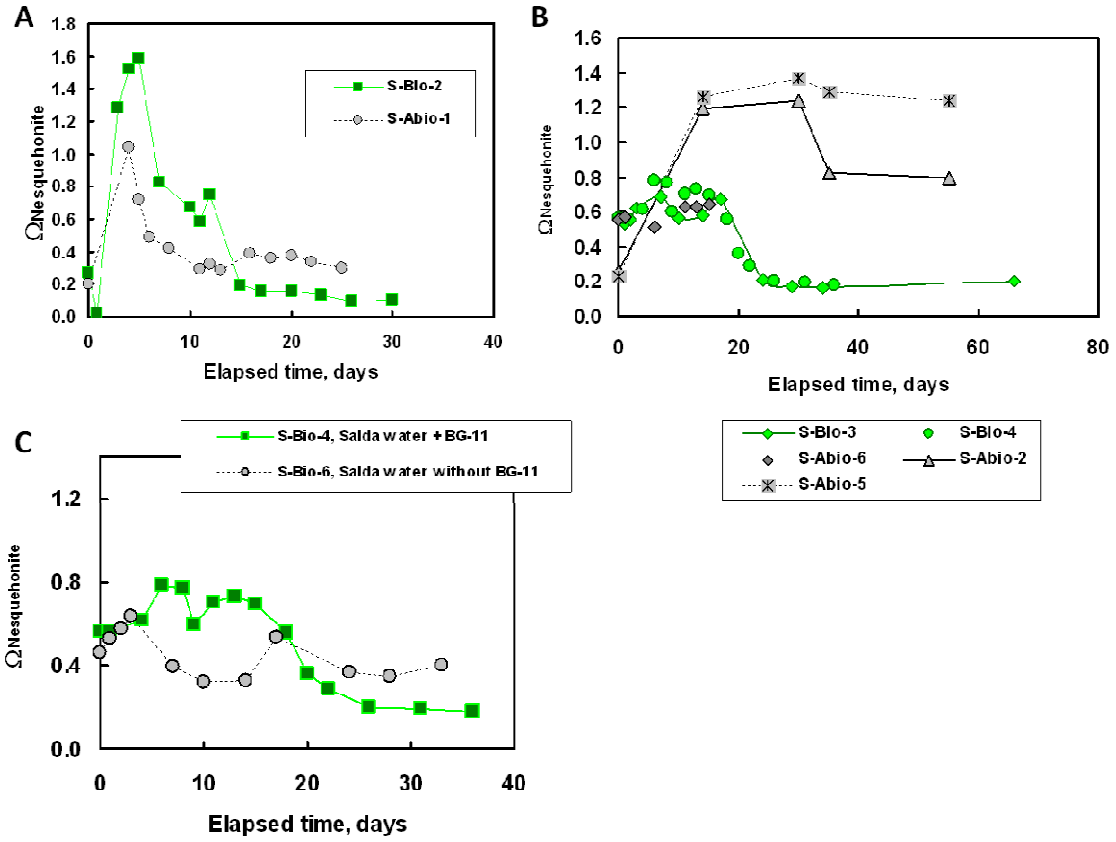

**Figure 9. Mg isotopic composition in Salda lake water (blue diamonds), inflowing springs (pink squares), stromatolites and sediments (yellow triangles).**

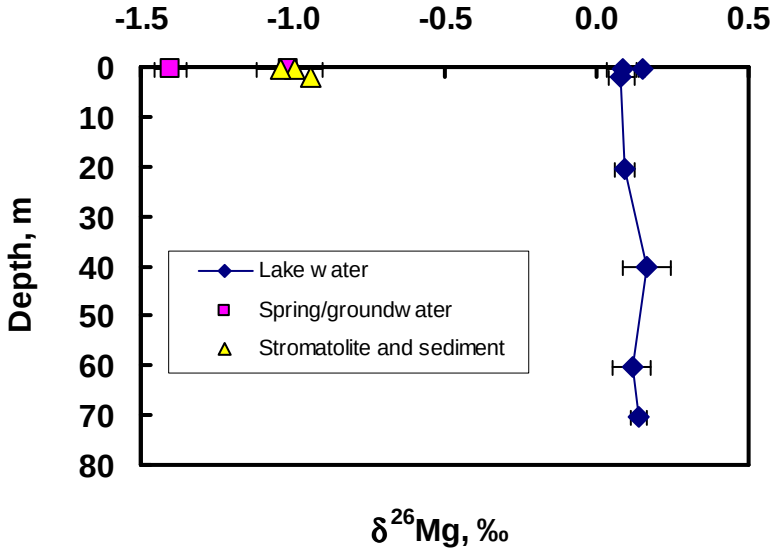

**Figure 10. Temporal evolution of $\delta^{26}Mg$ in the liquid and solid samples collected during experiments Bio-A and Abio-A plotted as a function of elapsed time (A) and fraction of Mg remaining in solution (B). The size of the symbols incorporates the uncertainty (2σ) on $\delta^{26}Mg$.**

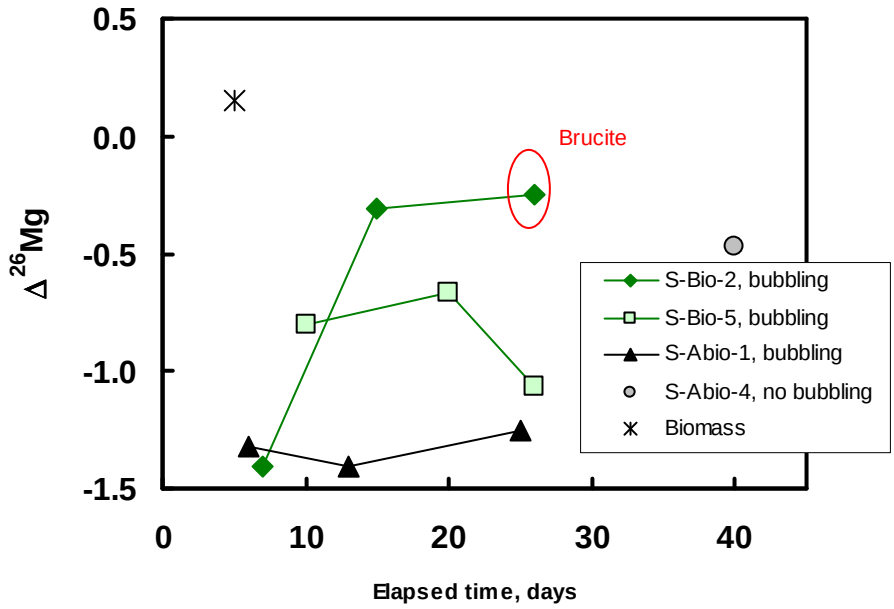


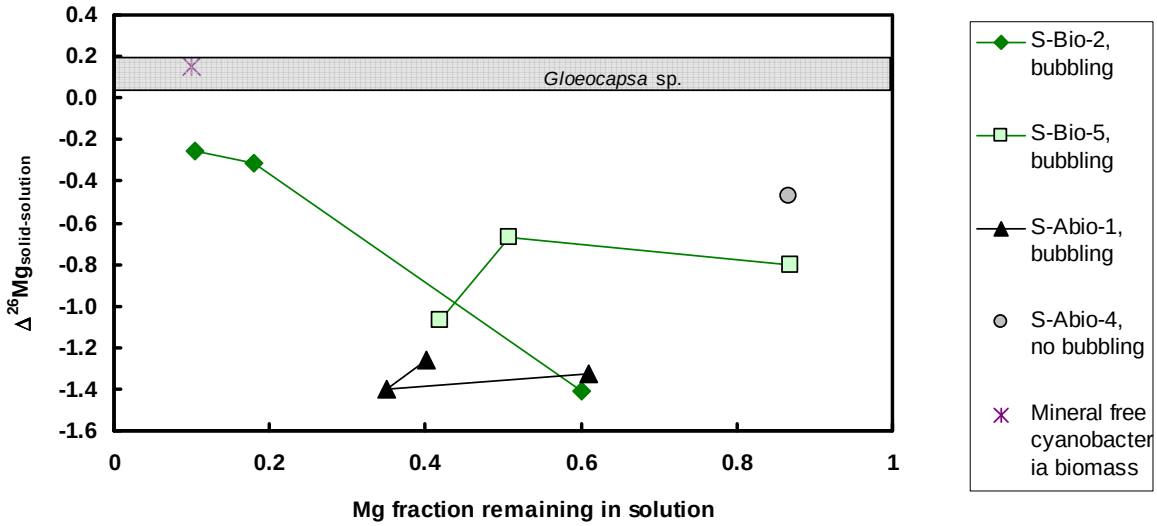

# Appendix 2

# Magnesium isotope fractionation during hydrous magnesium carbonate precipitation with and without cyanobacteria

# Magnesium isotope fractionation during hydrous magnesium carbonate precipitation with and without cyanobacteria

Vasileios Mavromatis[1], Christopher R. Pearce[1,2], Liudmila S. Shirokova[1,3], Irina A. Bundeleva[1], Oleg S. Pokrovsky[1], Pascale Benezeth[1], Eric H. Oelkers[1]

[1] *Geosciences Environment Toulouse (GET), CNRS, UMR 5563, Observatoire Midi-Pyrénées, 14 Avenue Edouard Belin, 31400 Toulouse, France*

[2] *Present address: Department of Earth and Environmental Sciences, The Open University, Walton Hall, Milton Keynes, MK7 6AA, UK.*

[3] *Institute of Ecological Problems of the North, 23 Nab. Sev. Dviny, Russian Academy of Science, Arkhangelsk, Russia*

*Submitted to Geochimica et Cosmochimica Acta, April 2011*

## Abstract

The hydrous magnesium carbonates, nesquehonite ($MgCO_3 \cdot 3H_2O$) and dypingite ($Mg_5(CO_3)_4(OH)_2 \cdot 5(H_2O)$), were precipitated in batch reactors from aqueous solutions containing 0.05 M $NaHCO_3$ and 0.025 M $MgCl_2$ and in the presence and absence of live photosynthesizing *Gloeocapsa* sp. cyanobacteria at various conditions (i.e. stirring and bubbling, continuous light, darkness, day/night cycle). Bulk precipitation rates are not affected by the presence of bacteria although the solution pH and the degree of fluid supersaturation with respect to magnesium carbonates increase due to photosynthesis.. Lighter Mg isotopes are preferentially incorporated into the precipitated solids in all experiments. Mg isotope fractionation between mineral and solution in the abiotic experiments is identical, within uncertainty, to that measured in cyanobacteria-bearing experiments; measured $\delta^{26}Mg$ ranges from -1.54 to -1.16 ‰ in all experiments. Mg isotope fractionation is also found to be independent of reactive solution pH and Mg, $CO_3^{2-}$ and biomass concentrations. Taken together, these observations suggest that *Gloeocapsa* sp. cyanobacterium does not appreciably affect the magnesium isotope fractionation between aqueous solution and hydrous magnesium carbonates both in laboratory and natural conditions. These results may have significant implications for past environmental reconstruction of hydrous magnesium carbonates precipitation in the cyanobacterial mats.

# 1. INTRODUCTION

Biomineralization is the most important carbonate mineral formation mechanism in the hydrosphere (Lowenstum and Weiner, 1989; Chafetz and Buczynski, 1992; Ferris et al., 1997; Douglas and Beveridge 1998; Dove, 2010). Cyanobacteria induced mineralization occurred in both ancient and modern environments (Brady et al., 2009; Planavsky et al, 2009; Raven and Giordano, 2009); cyanobacteria-dominated carbonate formation occurred in oceans, lakes, springs, and soils during the Precambrian (Riding, 2000), whilst modern cyanobacteria-dominated carbonate formation occurs in highly alkaline aquatic environments (Thompson and Ferris, 1990; Braithwaite and Zedef, 1994; Dupraz et al., 2009; Power et al., 2009). The formation of Mg-rich carbonates by cyanobacteria occurs only in specific Earth surface environments, such as Lake Salda in Turkey, which is fed by ultramafic rock weathering products (e.g. Braithwaite and Zedef, 1994), and alkaline lakes such as those in British Columbia (Power et al., 2007, 2009).

The chemical and isotopic composition of bio-precipitated minerals is routinely used to reconstruct past environmental conditions (Altermann et al., 2006), with particular emphasis on carbon and oxygen fractionation in carbonates (e.g. Pentecost and Spiro, 1990; Power et al., 2007). Until recently, little attention has been paid to the possibility of isotopic fractionation of the major divalent cations within carbonate minerals (i.e. Ca, Mg and Sr) owing to the more complex analytical procedures required to quantify these effects (Chang et al., 2003; Young and Galy, 2004). The importance of Mg in biogeochemical cycles, and the ~8% mass difference between $^{24}Mg$ and $^{26}Mg$ suggest that Mg isotopes are potentially useful for resolving mass fractionation mechanisms during carbonate precipitation. The potential for magnesium isotope fractionation in carbonate minerals has been recently documented for Mg-bearing carbonates (Chang et al., 2004; Buhl et al., 2007; Hippler et al., 2009) and may be significant in cyanobacterial induced mineralization (Black et al., 2006).

In this study the rates and magnitude of Mg isotope fractionation has been determined during the abiotic and *Gloeocapsa* sp. induced precipitation of hydrous Mg-carbonates. These results 1) enable the quantitative calibration of Mg isotope fractionation between aqueous solutions and biotically and abiotically formed magnesium carbonates at Earth surface

conditions, and 2) allow assessment of the possible role of cyanobacteria on Mg isotope fractionation during carbonate biomineralization.

## 2. MATERIALS AND METHODS

### 2.1. Culture and Characterization of Cyanobacteria

An axenic culture of mesophilic *Gloeocapsa* sp. f-6gl cyanobacteria was obtained from the Institute of Microbiology RAS (Moscow). This culture was originally isolated from a thermal spring having a temperature ranging from 30 to 40 $^{o}$C in Kamchatka (Russia). The bacterium was grown in synthetic, low-phosphate (10 % of normal content) cyanobacteria BG-11 Freshwater Solution for 3 weeks until the stationary growth phase was reached (Martinez et al., 2008). Cyanobacterium *Gloeocapsa* sp. typically consists of a small number of spherical individual colonies, containing 3 to 10 cells enclosed within larger masses of mucilage. The concentration of the bacterial cell suspensions was quantified via optical density (O.D.) using a spectrophotometer at a wavelength of 750 nm. This wavelength was selected after full spectra recording in the region 300-800 nm of both mineral-free live cells of *Gloeocapsa* sp. cyanobacteria and cell-free dypingite suspensions. The mineral suspension exhibits no adsorption in the region 650-800 nm whereas the cyanobacterial cells exhibit a distinct peak at 700-750 nm. The overall light absorbance of mineral suspension is lower by a factor of 10 than that of live biomass, when expressed per dry and wet weight. As a result, the maximum uncertainty in optical biomass measurements induced by the presence of minerals via absorbance at 750 nm is no more than 10%, which is within the experimental reproducibility. The O.D. calibration curve – humid weight was linear up to 1.3 absorbance units and the ratio between humid and freeze-dried weight of *Gloeocapsa* sp. was $10.0 \pm 2.0$.

Although the experiments were conducted under fully sterile conditions, possible reactor contamination by other cyanobacterial species was assessed by detailed optical microscopic examination of bacterial culture during growth, approximately once a week. The same periodicity was employed for monitoring contamination by culturable aerobic heterotrophic bacteria after inoculation on agar plates. In both cases, no detectable contamination was observed even during long-term experiments.

### 2.2. Precipitation Experiments

Precipitation experiments were performed in 1000 ml sterile borosilicate glass reactors containing either the low-phosphate BG-11 growth medium (10% of normal content, 50 µM), or the cell supernatant, into which 25-30 mM $MgCl_2$ and ~50 mM $NaHCO_3$ were added. These conditions were found to be the most suitable for Mg carbonate precipitation and correspond closely to conditions found in natural settings where hydromagnesite precipitation has been reported (Braithwaite and Zedef, 1994; Power et al., 2007). Experiments with lower concentrations of $Mg^{2+}$ and $HCO_3^-$ failed to produce sufficient precipitation for analysis, whereas higher concentrations led to rapid and uncontrolled hydrous Mg carbonate precipitation. The bacteria used in the experiments were pre-cultured in BG-11 media before being placed in the reactors. The bacteria continued to grow while mineral precipitation occurred; biomass typically increased by a factor of 10 during the first 2-4 weeks then increased less rapidly for the rest of the experiment. Details of all experiments performed in this study are given in Table 1.

Several distinct types of biotic experiments were performed at 25 ± 2°C. All biotic experiments were initiated by adding a known quantity of previously grown *Gloeocapsa* sp. cyanobacteria to the reactors. Experiments Bio-A and Bio-B were performed in reactors that were continuously stirred and bubbled with sterile humid air with an average flow rate of 1.5 ± 0.3 L/min. Experiments Bio-C and Bio-F were performed in reactors that were neither stirred nor bubbled with air. Experiment Bio-D was shaken continuous using a Fisher PingPong 400 shaker, whereas experiment Bio-E was continuous stirred but both were performed in the absence of bubbling. Each of these experiments was performed under continuous fluorescent light of 30 µmol photon $m^{-2}$ $s^{-1}$. In addition, experiment Bio-G was run under a normal day/night cycle without stirring and bubbling and experiment Bio-I was shaken and run in complete darkness without bubbling. Furthermore, experiments Bio-G and Bio-I run for 143 days to allow for i) achievement of end of stationary growth phase and beginning of the cell death phase and ii) to account for long-term mineral transformation reactions. This allowed for a better approximation of natural conditions and a more rigorous characterization of mineral transformation reactions.

All abiotic experiments performed at 25 ± 2$^o$C but at various conditions. Experiments Abio-A, Abio-B, Abio-C, and Abio-E were performed in the presence of a sterile supernatant of the *Gloeocapsa* sp. cyanobacteria to which were added $MgCl_2$ and $NaHCO_3$ in similar concentrations to those of the biotic experiments and 50 ± 10 mg/L of dissolved organic

carbon (DOC) in the form of cell exometabolites. Note that by cell exometabolites we mean dissolved (< 0.22 µm) organic substances of undefined structure and chemical composition, largely dominated by exopolysaccharides. Furthermore, phytoplankton-originated exopolymeric substances represent the major pool of autochtonous organic matter in natural waters, including the lakes where hydrous Mg carbonate precipitation occurs. The amount of Mg initially present in the supernatant was always less than 5% of that added in the form of $MgCl_2$ The concentration of DOC used in these experiments is similar to that measured in the experiments containing the live *Gloeocapsa* sp. The supernatant solution for these abiotic experiments was generated by centrifugation and filtration through a 0.22 µm sterile filter of *Gloeocapsa* sp. culture collected ~20 days after attainment of the stationary phase. Abiotic control Abio-D1 and Abio-D2 experiments were performed in sterile low-phosphate (10 % of normal content) and normal BG-11 culture media respectively. Experiments Abio-A, Abio-B, Abio-D1, Abio-D2 and Abio-E were bubbled with sterile humid air at similar flow rates as that of experiments Bio-A and Bio-B. All abiotic experiments were performed in the presence of 0.01 M $NaN_3$ to prevent possible microbial contamination.

One additional experiment, P-f, was run to assess Mg consumption and isotopic fractionation by *Gloeocapsa* sp. in the absence of carbonate precipitation. This experiment was performed in the absence of dissolved $MgCl_2$ and $NaHCO_3$ and *Gloeocapsa* sp. was grown in BG-11 medium. The fluid phase and biomass in this experiment were sampled after 11 and 44 days of growth.

### 2.3. Sampling and Analyses

30-50 ml aliquots of homogeneous suspension (containing the solution, precipitated mineral phase, and cells if present) were sampled periodically from the reactors in a sterile laminar hood box during each experiment (see Table ESM-1). Optical density and pH were measured in liquid sub-samples, whilst the solution supernatants were filtered using MilliPore 0.22 µm cellulose acetate filters, then used for alkalinity, DOC, and Mg concentration measurements. Alkalinity was determined following a standard HCl titration procedure using an automatic Schott TitroLine alpha $TA10^{plus}$ titrator with an uncertainty of ± 2% and a detection limit of $5\times10^{-5}$ M. Dissolved Organic Carbon (DOC) was analyzed using a Shimadzu TOC-6000 Carbon Total Analyzer with an uncertainty of 3% and a detection limit of 0.1 mg/L. Magnesium concentrations were measured by flame atomic absorption spectroscopy using a Perkin Elmer AAnalyst 400 with an uncertainty of ±2% and a detection

limit of 0.0002 mM. pH was measured using a Mettler Toledo combined electrode, with a precision of ±0.001. The uncertainty of biomass concentration determination via optical density is estimated at ±10%.

Organic matter was removed from the surfaces of a subset of the recovered minerals prior to their surface characterization by treating them with 10% $H_2O_2$ for 2-3 days at the same pH as the experimental fluids. The residual solid phases were then thoroughly rinsed in de-ionized water and freeze dried at -55°C. The resulting mineral phases were characterized by scanning electron microscopy (SEM) using a Jeol JSM840a, and by X-ray diffraction using an INEL CPS 120 $Co_{k\alpha}$, with a scan speed of $0.02^o\ s^{-1}$. Mineral-free bacterial cells and cell biomass with precipitated $MgCO_3$ were also observed using Transmission Electron Microscopy (TEM) with a JEOL JEM 12000 EX and JEOL JEM 2100F (equipped with a field emission gum (FEG) and PGT EDX detector) at 80 kV. TEM samples were prepared by first rinsing cell suspension with sterile nutrient solution and MilliQ water then centrifuging them for about 2 min at 10000 rpm. TEM analyses were then performed on grids coated with a carbon film that was submerged in the prepared bacterial suspension for 10 s then dried.

### 2.4. Magnesium Isotope Analyses

Mg isotope compositions of both filtered fluids and solid phases were measured. The Mg composition of the solids were made before any pre-treatment; as such resulting Mg compositions reflect contributions of the precipitated mineral and some organic material, including cells of cyanobacteria and chlorophyll*a*. Because precipitation was performed under controlled conditions, the potential for isobaric interferences from double charged ions (e.g. $^{48}Ca^{2+}$, $^{48}Ti^{2+}$, $^{50}Ti^{2+}$, $^{50}V^{2+}$, $^{50}Cr^{2+}$ and $^{52}Cr^{2+}$) was minimal. Galy et al. (2001), however, demonstrated that the presence of $Na^+$ and other species within the sample matrix could also result in mass bias effects. Consequently all samples were chemically purified prior to Mg isotopes analysis via cation exchange chromatography. Filtered acidified fluids were evaporated to dryness and re-diluted in 1 M $HNO_3$, while the freeze-dried solid samples and mineral-free organic samples obtained from P-f experiment were digested in 16 M $HNO_3$, before being evaporated and re-dissolved in 1 M $HNO_3$. Mg separation was achieved using the protocol of Teng et al. (2007), with the AG 50W-X12 exchange resin held in a 10 ml Bio-Rad poly-prep column. Complete recovery of Mg from the columns, which is essential to avoid isotopic fractionation (Chang et al., 2003; Teng et al., 2007) was confirmed by replicate passes of samples with different matrices through the purification procedure (Pearce et al.

2009). A single pass was generally sufficient to reduce the cation/Mg ratio in the sample to <0.05, thereby avoiding potential interferences during mass spectrometry analysis (Galy et al., 2001).

Magnesium isotopic ratios were measured using a Thermo-Finnigan 'Neptune' Multi Collector Inductively Coupled Plasma Mass Spectrometer (MC-ICP-MS) at both the LMTG (Toulouse, France) and at The Open University (Milton Keynes, UK). All solutions were prepared in 0.32 M $HNO_3$ and were introduced into the Ar plasma using a standard spray chamber. Instrumental mass fractionation effects were corrected via sample-standard bracketing, and all results are presented in delta notation with respect to the DSM3 international reference material (Galy et al., 2001):

$$\delta^{x}\mathrm{Mg} = \left( \frac{\left( \frac{^{x}\mathrm{Mg}}{^{24}\mathrm{Mg}} \right)_{sample}}{\left( \frac{^{x}\mathrm{Mg}}{^{24}\mathrm{Mg}} \right)_{DSM3}} - 1 \right) \cdot 1000 \quad (1)$$

where *x* refers to the Mg mass of interest. Compatibility of results between the two MC-ICP-MS used in this study was confirmed by replicate analyses of three international Mg reference standards (DSM, CAM-1 and OUMg), and by duplicate analyses of the carbonate standard J-Do 1. The $\delta^{26}$Mg reproducibility of these standards was typically <0.07 ‰.

The isotopic offset between the Mg in the fluid and that incorporated into the solid phase can be defined as:

$$\Delta^{26}\mathrm{Mg}_{\text{solid-liquid}} \equiv \delta^{26}\mathrm{Mg}_{\text{solid}} - \delta^{26}\mathrm{Mg}_{\text{liquid}} \quad (2)$$

This value was determined for all samples where both the fluid and solid phases were collected in the present study.

The evolution of the Mg isotopic composition of the solid phase ($\delta^{26}\mathrm{Mg}_{\text{solid}}$) precipitating at equilibrium in a closed system experiment can be calculated from mass balance constraints using (Criss, 1999):

$$\delta^{26}\mathrm{Mg}_{\text{solid}} = \delta^{26}\mathrm{Mg}_{\text{initial}} + A(\Delta^{26}\mathrm{Mg}_{\text{solid-liquid}} - 1)\cdot 10^{3} \quad (3)$$

where *A* stands for the percent of Mg precipitated from the liquid phase, and $\delta^{26}\mathrm{Mg}_{\text{initial}}$ refers to the isotopic composition of the initial fluid phase.

## 3. RESULTS

The measured chemical composition of the reactive fluids (e.g. the fluid phase in the reactor during the experiments) and the mineralogy of precipitated solid phases in all samples are listed in the Electronic Supplementary Information table ESM-1 (file ESM.pdf) and are described in detail below.

### 3.1. Mineralogy of the Precipitated Phases

Examples of X-ray diffraction patterns of the solid phases precipitated during the experiments are shown in Fig. 1. X-ray diffraction results demonstrate the precipitation of nesquehonite ($MgCO_3$ $3H_2O$) and dypingite ($Mg_5(CO_3)_4(OH)_2$ $5H_2O$) at distinct times during the experiments. Nesquehonite precipitation is limited to the first hours of experiments Bio-A and Abio-A. After ~100 hours of reaction time, dypingite was the only mineral phase present in these experiments. Experiments Bio-C, Bio-D and Abio-D2 exhibit dypingite formation whereas experiments Bio-F, Bio-G, Bio-I, Abio-B, Abio-C, Abio-D1 and Abio-E exhibit nesquehonite formation. Co-existence of both mineral phases was observed only in the final solid sample collected from experiment Bio-E. In general, all the collected nesquehonite XRD patters exhibited close agreement with corresponding reference patterns (see Fig. 1B), whilst the collected XRD patterns of collected dypingite exhibit some minor difference compared to their corresponding reference patterns (see Fig. 1A). No clear connection between the mineralogy of the precipitated phase and the experimental/ physical conditions of the experiment is evident. Scanning electron microscopy images, reveal that nesquehonite exhibits a needle-like habit with needles ranging from 5 to 15 μm in length (see Fig. 2A), whilst the dypingite is present as rosette-like aggregates of 2 to 8 μm diameter (see Fig. 2B and 2C). Transmission electron microscopy demonstrated the presence of nanometer size mineral precipitates in the vicinity of cell surfaces in solutions supersaturated with respect to hydrous Mg carbonates (see Fig. 3A) suggesting a direct link between the bacteria and some precipitates. Such precipitates around cells were absent in control media (see Fig. 3B).

### 3.2. Chemical Composition of the Fluid Phase

The temporal evolution of Mg concentration and pH in all experiments as well as alkalinity and biomass concentration during representative experiments are illustrated in Fig.

4. The Mg concentration and alkalinity of the reactive fluids tend to decrease and the pH tends to increase with time during all biotic experiments. Some significant differences, however, are evident among these biotic experiments. For example, an initial latent stage lasting ~4 days is observed in experiments Bio-A, Bio-B, Bio-E, Bio-F, where the reactive fluid exhibits a slight increase in Mg concentration and alkalinity. This latent stage is followed by a rapid decrease in reactive fluid Mg concentration and alkalinity during the next 10-15 days, before attainment of a quasi-stationary state. Experiments Bio-C, Bio-D, Bio-G, and Bio-I exhibit similar temporal Mg concentration and pH variations, although a pH drop accompanied by an increase in the Mg concentration and alkalinity are observed after 40-60 days. For all of these biotic experiments other than Bio-I, this final pH drop is concurrent with a decrease of fluid optical density suggesting that this observation stems from cyanobacterial death. A decrease in photosynthetic activity due to decreasing cyanobacterial activity can result in decreasing pH which favors Mg-carbonate dissolution.

In the abiotic experiments, the reactive fluid Mg concentration and alkalinity decreased during the first 10±5 days, becoming almost constant thereafter, suggesting the attainment of near-equilibrium conditions. During the same period, the reactive fluid pH increased to 9.2-9.3 and then remained approximately constant until the end of each experiment (see Fig. 4 and Table ESM-1).

The speciation and saturation state of the reactive fluids with respect to potentially precipitating mineral phases for all experiments was calculated using PHREEQC together with its MINTEQA2 database (Parkhurst and Appelo, 1999) after adding to it thermodynamic properties for nesquehonite and hydromagnesite reported by Cheng and Li (2010a,b). The saturation state of these fluids with respect to dypingite was not calculated owing to lack of relevant thermodynamic data. A summary of these saturation state calculations is provided in Table 2. The evolution of the saturation state of the fluids of experiments Bio-A and Abio-A are illustrated as a function of time in Fig. 5. The calculated aqueous speciation of Mg is reported in Table ESM-2 (file ESM.pdf). The aqueous speciation of Mg during the experiments was dominated by aqueous $Mg^{2+}$, but also contained 30-50% of $MgCO_3^-{}_{(aq)}$ and minor quantities of $MgHCO_3°$ and $MgOH^+$.

Apparent precipitation rates ($r_i$) were calculated from the first derivative of the fluid phase Mg concentration with respect to time, from the onset of precipitation to the attainment of constant fluid Mg concentrations using

$$r_i = \frac{1}{\nu_{\mathrm{Mg},i}} \frac{dc_{\mathrm{Mg}}}{dt}. \quad (4)$$

where $c_{\mathrm{Mg}}$ stands for the concentration of Mg in the reactive fluid, *t* designates time, and $\nu_{\mathrm{Mg},i}$ denotes the number of moles of Mg in one mole of the $i^{\mathrm{th}}$ mineral. Resulting precipitation rates are presented in Table 2. All experiments performed in the presence of sterile humid air bubbling attained steady-state Mg concentrations over shorter time periods (12±3 days) and exhibit higher apparent precipitation rates compared to bubbling-free experiments. Note that the Mg concentration in all the biotic experiments attained a lower stationary-state compared to those of the abiotic experiments. There is, however, no statistical difference in the precipitation rates obtained from the biotic (Bio-A and Bio-B) and abiotic (Abio-A, Abio-B, Abio-D1, Abio-D2, and Abio-E) experiments performed with either stirring or air bubbling during first 10-15 days with rates equal to $-143 \pm 33 \times 10^{-3}$ and $-118 \pm 16 \times 10^{-3}$ mol dypingite $L^{-1}$ $day^{-1}$, respectively as calculated using Eq. (4).

### 3.3. Magnesium Isotopic Composition

The Mg isotope compositions of all analyzed samples are given in Table 3. Mg isotope analyses were performed on selected samples of experiments Bio-A, Bio-B, Bio-C, Bio-D, and Abio-A where dypingite was the main precipitated mineral phase. Furthermore, the temporal evolution of $\delta^{26}$Mg during experiments Bio-A and Abio-A was studied in detail and is plotted in Fig. 6.

All experiments exhibited mass-dependent fractionation between fluid and solid phase. The precipitated solids have $\delta^{26}$Mg values that are 0.6-1.55 ‰ lighter than their liquid counterparts. The solid samples obtained from Bio-A do not exhibit a systematic temporal trend, whilst the solid phases from the Abio-A experiment show a slight isotopic enrichment with time, concurrent with a corresponding enrichment in the reactive fluid from the same experiment. Isotopic compositions from the mineral-free experiment (P-f) show that the *Gloeocapsa* sp. cells have slightly heavier Mg isotopic values compared to the growth medium. The observed shift of $\delta^{26}$Mg between the biomass and the nutrient media over the 44 days of growth during experiment P-f is ~0.2 ‰.

The fractionation factors, $\Delta^{25}Mg_{\text{solid-liquid}}$, and $\Delta^{26}Mg_{\text{solid-liquid}}$, calculated from corresponding solid and liquid samples are listed in Table 3. In the presence of *Gloeocapsa* sp., $\Delta^{26}Mg_{\text{solid-liquid}}$ calculated from the first collected sample (~ after 4 hours) of experiment

Bio-A is significantly lower than that of the latter samples; this is the only Mg isotope concentration measurement made on nesquehonite in this study. The samples collected between 8 and 25 days from the Abio-A control experiment exhibit $\Delta^{26}Mg_{solid\text{-}liquid}$ values similar to those measured in most of the biotic experiments. There is no statistically significant correlation between the extent of Mg fractionation and the reactive fluid pH, $IAP_{hydromagnesite}$, Mg, alkalinity and biomass concentrations as illustrated in Fig. ESM-1. In addition, no statistically significant correlation was found between the fractionation factor and the aqueous speciation of Mg as shown in Fig. ESM-2 for $MgCO_3°(aq)$.

The temporal $\delta^{26}Mg_{solid\text{-}liquid}$ evolution of experiments Bio-A and Abio-A are plotted against fraction of Mg remaining in solution in Fig. 7. Most data from these experiments fall on parallel linear trends corresponding to constant $\Delta^{26}Mg_{solid\text{-}solution}$ and consistent with closed system equilibrium exchange between the fluid and solid phase calculated with Eq. (4).

## 4. DISCUSSION

### 4.1. Chemical Composition of Solutions and Mineralogy of Precipitants

pH was observed to increase with time in all abiotic and biotic experiments. In the abiotic experiments, this increase originates from the degassing of the initial reactive fluid, which contained a $5x10^{-2}$ mol/kg $NaHCO_3$ at pH~8.5. Owing to this high aqueous bicarbonate content, these initial fluids have a $pCO_2$ of $10^{-2.0}$ atm, which is supersaturated with respect to the atmosphere. The bubbling of sterile humid air liberates $CO_2$ from the reactive fluid leading to both an increase in pH and degree of supersaturation of this fluid with respect to Mg carbonate minerals. Note that all experiments were oversaturated with respect to hydromagnesite, although this mineral phase was never observed in the precipitates. In biotic experiments, this $pCO_2$ decrease was accompanied by additional pH increase due to photosynthetic uptake of $HCO_3^-$ ions and $OH^-$ release. This enhanced pH increase is evident in our experiments; the pH in our biotic experiments increases by 0.8-2.2 units compared to a 0.7-1.4 units increase in our abiotic experiments. Similar pH increases due to biological activity were documented by Power et al. (2007) who performed field experiments using a consortium of cyanobacteria isolated from microbial mats of hydromagnesite playas in British Columbia, Canada. The evolution of fluid composition during our experiments, as illustrated in Fig. 4, shows that, in the presence of cyanobacteria, there is initial induction period lasting up to 5 days, during which little mineral precipitation occurs. At the end of this induction

period, hydroxyl ions produced by photosynthetic activity increase pH and the degree of fluid supersaturation with respect to hydrous magnesium carbonates leading to their precipitation (Thompson and Ferris, 1990). Indeed, the TEM images shown in Fig. 3, of active *Gloeocapsa* sp. cyanobacteria suspension in solutions oversaturated with respect to magnesium carbonates show formation of fine grained mineral phase in the near their surfaces, indicating a strong link between cyanobacterial cells and precipitating Mg hydrous carbonate.

The final mineral phase precipitated in our experiments was either dypingite, a rare hydrous magnesium carbonate mineral compositionally similar to hydromagnesite (Raade, 1970) or nesquehonite. Power et al. (2007) reported dypingite formation in biotic mesocosm experiments, and nesquehonite formation in abiotic control experiments at a pH of ~9.5. The transformation of nesquehonite to hydromagnesite is known to occur through intermediary hydrous magnesium carbonate phases such as dypingite (Davies and Bubela, 1973; Hopkinson et al., 2008). Although it has been argued that such mineralogical changes could be an artifact of the sample drying (Botha and Strydom, 2001), we did not observe any significant difference in the XRD patterns of samples prepared via freeze-drying and those oven-drying at 50°C, and thus conclude that mineralogical changes did not occur during sample preparation. All previous work reported on the transformation of nesquehonite to hydromagnesite was performed at temperatures above 45 $^{o}$C, suggesting that this is an optimum temperature for this reaction. Formation of hydromagnesite, however, in natural environments (e.g. Lake Salda, Turkey; British Columbia, Canada) likely ocurrs at significantly lower temperatures, similar to those considered in our experiments (Braithwaite and Zedef, 1994; Power et al., 2007, 2009). The results above suggest that at ambient temperatures the transformation from nesquehonite to hydromagnesite occurs via a dypingite intermediary both in the laboratory and in nature. However the physicochemical factors controlling these transformation reactions are currently unknown. Note that a slow transition from dypingite to hydromagnesite, might explain the differences reported above between our XRD spectra and the reference standard.

### 4.2. Role of cyanobacteria in Mg concentration and isotopic composition changes

Bacterial cell surfaces, chlorophyll-*a*, and cellular cytoplasm are strong adsorbers of aqueous ions; as such some Mg could have absorbed to cell walls in our experiments (Pokrovsky and Kompantseva, 2007; Pokrovsky et al., 2008). For example, Jasper and Silver (1977) reported that Mg can be incorporated into chlorophyll-*a* and cellular cytoplasm during

cyanobacterial growth. Black et al. (2006) reported that chlorophyll-*a* isolated from cyanobacterium *S. elongatus* preferentially incorporates light Mg isotopes. This process has also been observed to enrich cells in heavy Zn isotopes (Gélabert et al., 2006). The maximum surface site density of *Gloeocapsa* sp., as revealed by proton Ca-Mg exchange experiments, is ~$0.7x10^{-3}$ mol $g_{dry}^{-1}$ (Pokrovsky et al., 2008). This suggests that the maximum amount of Mg removed from solution during our experiments performed in the presence of cyanobacteria, which contained 2-3 $g_{dry}$ biomass $L^{-1}$ is no more than $1.4\text{-}2.1x10^{-3}$ mol $L^{-1}$. This is significantly smaller than the 15-25 $10^{-3}$ mol/L of Mg removed from solution by mineral precipitation in our experiments. The small role of bacterial adsorption in this study is confirmed by the results of experiment P-f. This experiment, performed to quantify Mg uptake and fractionation by *Gloeocapsa* sp. shows that only $1.5x10^{-5}$ to $2.5x10^{-5}$ mol/L of the aqueous Mg concentration in the reactive fluid was taken up by the biomass. Therefore, unless the isotopic fractionation linked to Mg adsorption at cyanobacteria surface is orders of magnitude larger than suggested by previous studies, Mg adsorption on the cell surface should be negligible compared to the effects of mineral precipitation.

Note that the magnesium isotope compositions of the solid samples retrieved after 1 hr and 4 days of Bio-A experiment deviate from closed system fractionation trend shown in Fig. 7a. The observed differences between solid and fluid phases may reflect the change in the mineralogy from the initially precipitated nesquehonite to the more stable dypingite, if each mineral has a distinct fractionation factor. Another possibility is that precipitation rates are fast at the onset of the experiment, so this deviation may stem from kinetic isotopic fraction effects.

### 4.3. Magnesium Isotope Fractionation between Mineral and Reactive Fluid

The reactive fluids of Bio-A, Bio-B, Bio-C, Bio-D, and Abio-A experiments exhibit an increase in $\delta^{26}$Mg values of 0.5-1.5 ‰ (see Table 3 and Fig. 6). This demonstrates that lighter Mg isotopes are preferentially incorporated into the solid phase. This observation is coherent with the results of previous studies on Mg isotope fractionation between aqueous fluids and biogenic skeletal carbonates (Chang et al., 2004; Buhl et al., 2007; Hippler et al., 2009), abiotically precipitated low Mg-calcite (Galy et al., 2002; Immenhauser et al., 2010), dolomite (Higgins and Schrag, 2010), and magnesite (Pearce et al., 2009). The origin of the Mg isotope fractionation likely stems from the change in Mg coordination, symmetry, and bond distances in the reaction forming the mineral from the aqueous fluid. One of the main changes during

this reaction is the loss of the strongly attached hydration shell surrounding Mg, which has 6 water molecules located at a distance of 2.08 Å (Di Tommaso and de Leeuw, 2010). In contrast, Mg in hydrous Mg carbonate minerals is contained in a three-dimensional framework of $MgO_6$ octahedra and triangular carbonate ions. For example, the average Mg-O distances in hydromagnesite are 2.10 and 2.04 Å where the Mg(1) atom is surrounded by 4 oxygen atoms from carbonate ions, 1 hydroxyl group and 1 water molecule, while the Mg(2) atom is surrounded by 4 oxygen atoms from carbonate groups and 2 hydroxyl groups (Akao et al., 1974). As such, the Mg-O octahedral in hydromagnesite is more distorted than that in the aqueous solution. Quantum mechanic theory suggests that heavier isotopes will concentrate in the species in which they are most strongly bounded (i.e. the aqueous solution), meaning the lighter, less stable isotopes will be favored in the solid phase (Criss, 1999).

The $\Delta^{26}Mg_{solid\text{-}liquid}$ values of abiotic experiments range from -1.43 to -1.17 ‰. These factors are similar to those found in the experiments performed in the presence of *Gloeocapsa* sp., which range from -1.55 to -1.19 ‰. Measured $\Delta^{26}Mg_{solid\text{-}liquid}$ values are consistent with a closed system equilibrium model (Fig. 7) suggesting a continuous isotopic exchange/equilibration between the precipitated hydrous Mg-carbonates and the reactive fluid, probably via a stepwise dissolution/re-precipitation process, which itself is consistent with the equilibrium fraction model (Criss, 1999). Such a process can also explain the small temporal variations in $\Delta^{26}Mg_{solid\text{-}liquid}$ values observed during the experiments. The small deviations in $\Delta^{26}Mg_{solid\text{-}liquid}$ equilibrium values observed at the end of experiments may arise from small changes in the chemical composition of aqueous fluid. The final $\Delta^{26}Mg_{solid\text{-}liquid}$ values can be affected by: 1) the low amount of remaining suspension as well as modification of stirring and bubbling regime at these conditions; and 2) cell lysis and intracellular "organic" Mg release at the end of long-term experiment.

The observation that $\Delta^{26}Mg_{solid\text{-}liquid}$ values are identical, within uncertainty (defined as the standard deviation of all samples where solid and liquid phase were measured and is equal to ± 0.14 ‰), in the presence and the absence of *Gloeocapsa* sp. suggests that, Mg carbonate sediments formed via abiotic processes, or provoked by cyanobacterial photosynthesis will exhibit similar Mg isotopic signatures. Moreover no affect of reactor stirring or air bubbling was found on Mg isotope fractionation. This suggests that the experimental fractionation factors determined in this study may be applicable to natural processes. The only exception to this might be Mg-carbonate formation in biofilms that exhibit a high cell:mineral ratio, as cyanobacteria can store $Ca^{2+}$ and $Mg^{2+}$ ions in organic envelopes (Braissant et al., 2003, 2007). In such systems, "organic" Mg originated from cell decay and lysis would be

isotopically lighter than the bulk fluid phase. Given that the $\Delta^{26}Mg_{solid\text{-}liquid}$ value for cell biomass is significantly less negative than that for inorganic carbonates, the release of Mg from cyanobacterial sheaths and cell envelopes, and subsequent precipitation of Mg carbonates in the vicinity of the cyanobacterial cyanobacterial mats, might be expected to produce minerals that are isotopically heavier than those precipitated directly from supersaturated aqueous fluids at having a high fluid to cell biomass ratio.

## 5. CONCLUSIONS

The hydrous magnesium carbonates, nesquehonite and dypingite, were precipitated in the presence and absence of cyanobacteria *Gloeocapsa* sp. under varying laboratory conditions (i.e. stirring and bubbling, continuous light, darkness, day/night cycle). All experiments yielded similar bulk precipitation rates, although the pH of the reactive fluids were 0.5-1.0 units higher in biotic experiments compared to abiotic experiments. Similarly, retrieved $\Delta^{26}Mg_{solid\text{-}liquid}$ values obtained from abiotic experiments are identical within uncertainty of those obtained in the presence of *Gloeocapsa* sp. Taken together these observations suggest that the presence of cyanobacteria affects neither the rates nor the Mg isotopic fractionation of the precipitated hydrous magnesium carbonates in natural systems.

## ACKNOWLEDGMENTS

The authors thank E.I. Kompantseva for providing the *Gloeocapsa* sp. culture. Remi Meyer and Jerome Chmeleff are acknowledged for their assistance with the MC-ICP-MS analyses in Toulouse and Manuela Fehr is acknowledged for her assistance with MC-ICP-MS analyses at the Open University. This work was supported by MC ITN DELTA-MIN (ITN-2008-215360), MC RTN GRASP-$CO_2$ (MRTN-CT-2006-035868) and MC MIN-GRO (MRTN-CT-2006-035488) and the programs: INTERVIE (INSU), EPOV (CNRS), and the Associated European Laboratory LEAGE.

## REFERENCES

Akao M., Marumo F. and Iwai S. (1974) The Crystal Structure of Hydromagnesite. *Acta Cryst*. **B30**, 2670.

Altermann W., Kazmierczak J., Oren A., and Wright D.T. (2006) Cyanobacterial calcification and its rock-building potential during 3.5 billion years of Earth history. *Geobiology* **4**, 147-166.

Black J. R., Yin Q. Z. and Casey W. H. (2006) An experimental study of magnesium-isotope fractionation in chlorophyll-a photosynthesis. *Geochim. Cosmochim. Acta* **70**, 4072-4079.

Botha A. and Strydom C. A. (2001) Preparation of a magnesium hydroxy carbonate from magnesium hydroxide. *Hydrometallurgy* **62**, 175-183.

Brady A. L., Slater G., Laval B., and Lim D. S. (2009) Constraining carbon sources and growth rates of freshwater microbialites in Pavilion Lake using $^{14}C$ analysis. *Geobiology* **7,** 544-555.

Braissant O., Cailleau G., Dupraz C. and Verrecchia A. P. (2003) Bacterially induced mineralization of calcium carbonate in terrestrial environments: The role of exopolysaccharides and amino acids. *J. Sediment. Res.* **73**, 485-490.

Braissant O., Decho A. W., Dupraz C., Glunk C., Przekop K. M. and Visscher P. T. (2007) Exopolymeric substances of sulfate-reducing bacteria: Interactions with calcium at alkaline pH and implication for formation of carbonate minerals. *Geobiology* **5**, 401-411.

Braithwaite C. J. R. and Zedef V. (1994) Living Hydromagnesite Stromatolites from Turkey. *Sediment. Geol*. **92**, 1-5.

Buhl D., Immenhauser A., Smeulders G., Kabiri L., and Richter D. K. (2007) Time series $\delta^{26}Mg$ analysis in speleothem calcite: Kinetic versus equilibrium fractionation, comparison with other proxies and implications for palaeoclimate research. *Chem. Geol*. **244**, 715-729.

Chafetz, H.S. and Buczynski C. (1992) Bacterially induced lithification of microbial mats. Palaios 7, 277-293.

Chang V. T. C., Makishima A., Belshaw N. S. and O'Nions R. K. (2003) Purification of Mg from low-Mg biogenic carbonates for isotope ratio determination using multiple collector ICP-MS. *J. Anal. At. Spectrom.* **18**, 296-301.

Chang V. T. C., Williams R. J. P., Makishima A., Belshawl N. S., and O'Nions R. K. (2004) Mg and Ca isotope fractionation during $CaCO_3$ biomineralisation. *Biochem. Biophys. Res. Commun.* **323**, 79-85.

Cheng W. T. and Li, Z. B. (2010a) Controlled Supersaturation Precipitation of Hydromagnesite for the $MgCl_2$-$Na_2CO_3$ System at Elevated Temperatures: Chemical Modeling and *Experiment. Ind. Eng. Chem. Res*. **49**, 1964-1974.

Cheng W. T. and Li Z. B. (2010b) Nucleation kinetics of nesquehonite ($MgCO_3 \cdot 3H_2O$) in the $MgCl_2$-$Na_2CO_3$ system. *J. Cryst. Growth* **312**, 1563-1571.

Criss R.E. (1999) *Principles of Stable Isotope Distribution*. Oxford University Press, Oxford.

Davies P. J. and Bubela B. (1973). Transformation of Nesquehonite into Hydromagnesite. *Chem. Geol*. **12**, 289-300.

Di Tommaso D. and de Leeuw N. H. (2010) Structure and dynamics of the hydrated magnesium ion and of the solvated magnesium carbonates: insights from first principles simulations. *Phys. Chem. Chem. Phys*. **12**, 894-901.

Douglas S. and Beveridge T.J. (1998) Mineral formation by bacteria in natural microbial communities. *FEMS Microbiol. Ecol.* **26**, 79-88.

Dove P.M. (2010). The Rise of Skeletal Biominerals. *Elements* **6**, 37-42.

Dupraz C., Reid R. P., Braissant O., Decho A. W., Norman R. S., and Visscher P. T. (2009) Processes of carbonate precipitation in modern microbial mats. *Earth-Sci. Rev.* **96**, 141-162.

Ferris F.G., Thompson J.B., Beveridge T.J. (1997) Modern freshwater microbialites from Kelly Lake, British Columbia, Canada. Palaios, 12, 213-219.

Galy A., Belshaw N. S., Halicz L. and O'Nions R. K. (2001) High-precision measurement of magnesium isotopes by multiple-collector inductively coupled plasma mass spectrometry. Internat. *J. Mass Spec.* **208**, 89-98.

Galy A., Bar-Mattews M., Halicz L., O'Nions R.K. (2002) Mg isotopic composition of carbonate: insight from speleotherm formation. *Earth Planet. Sci. Lett.* **201**, 105-115.

Gélabert A., Pokrovsky O. S., Viers J., Schott J., Boudou A., and Feurtet-Mazel A. (2006) Interaction between zinc and freshwater and marine diatom species: Surface complexation and Zn isotope fractionation. *Geochim. Cosmochim. Acta* **70**, 839-857.

Higgins J.A. and Schrag, D.P. (2010) Constraining magnesium cycling in marine sediments using magnesium isotopes. *Geochim. Cosmochim. Acta* **74**, 5039-5053.

Hippler D., Buhl D., Witbaard R., Richter D. K., and Immenhauser A. (2009) Towards a better understanding of magnesium-isotope ratios from marine skeletal carbonates. *Geochim. Cosmochim. Acta* **73**, 6134-6146.

Hopkinson L., Rutt K. and Cressey G. (2008) The transformation of nesquehonite to hydromagnesite in the system CaO-MgO-$H_2O$-$CO_2$: An experimental spectroscopic study. *J. Geol.* **116**, 387-400.

Immenhauser A., Buhl D., Richter D., Niedermayr A., Riechelmann D., Dietzel M., Schulte U. (2010) Magnesium-isotope fractionation during low-Mg calcite precipitation in a limestone cave – Field study and experiments. *Geochim. Cosmochim. Acta* **74**, 4346-4364.

Jasper P. and Silver S. (1977) Magnesium transport in microorganisms. In: *Microorganisms and Minerals* (Ed. Weinberg, E.D.), vol. 3. Marcel Dekker, Inc., pp. 7–47.

Lowenstam H. A. and Weiner S. (1989) *On biomineralization*, Oxford University Press, Oxford, New York.

Martinez R., Pokrovsky O.S., Schott J., Oelkers E.H. (2008) Surface charge and zeta-potential of metabolically active and dead cyanobacteria. *J. Colloid Interface Sci*. **323**, 317-325.

Martinez R. E., Gardes E., Pokrovsky O. S., Schott J. and Oelkers E. H. (2010) Do photosynthetic bacteria have a protective mechanism against carbonate precipitation at their surfaces? *Geochim. Cosmochim. Acta* **74**, 1329-1337.

Parkhurst D. L. and Appelo C. A. J. (1999) User's Guide to PHREEQC (Version 2) - *A Computer Program for Speciation, Batch- Reaction, One-Dimensional Transport, and Inverse Geochemical Calculations*. U.S. Geological Survey Water-Resources Investigations Report 99-4259, 310 pp.

Pearce C. R., Saldi G. D., Schott J., Burton K. W. and Oelkers E. H. (2009) Experimental quantification of kinetic Mg-isotope fractionation during magnesite precipitation. *Geochim. Cosmochim. Acta* **73**, 13, A1003.

Pentecost A. and Spiro B. (1990) Stable Carbon and Oxygen Isotope Composition of Calcites Associated with Modern Fresh-Water Cyanobacteria and Algae. *Geomicrobiol. J.* **8**, 17-26.

Planavsky N., Reid R. P., Lyons T. W., Myshrall K. L. and Visscher P. T. (2009) Formation and diagenesis of modern marine calcified cyanobacteria. *Geobiology* **7**, 566-576.

Pokrovsky O. S. and Kompantseva E. I. (2007) Experimental physicochemical modeling of interactions between phototrophic microorganisms (anoxiphotobacteria and cyanobacteria) with trace elements in aqueous solutions. *Geochem. Int*. **45**, 302-307.

Pokrovsky O. S., Martinez R. E., Golubev S. V., Kompantseva E. I. and Shirokova L. S. (2008) Adsorption of metals and protons on Gloeocapsa sp cyanobacteria: A surface speciation approach. *Appl. Geochem.* **23**, 2574-2588.

Power I. M., Wilson S. A., Thom J. M., Dipple G. M., Gabites J. E. and Southam G. (2009) The hydromagnesite playas of Atlin, British Columbia, Canada: A biogeochemical model for $CO_2$ sequestration. *Chem. Geol*. **260**, 286-300.

Power I. M., Wilson S. A., Thom J. M., Dipple G. M. and Southam G. (2007) Biologically induced mineralization of dypingite by cyanobacteria from an alkaline wetland near Atlin, British Columbia, Canada. *Geochem. T*. **8**, 16.

Raade G. (1970) Dypingite, a new hydrous basic carbonate of magnesium, from Norway. *Am. Miner.* **55,** 1457-1465.

Raven J. A. and Giordano M. (2009) Biomineralization by photosynthetic organisms: Evidence of co-evolution of the organisms and their environment? *Geobiology* **7**, 140-154.

Riding R. (2000) Microbial carbonates: the geological record of calcified bacterial-algal mats and biofilms. *Sedimentology* **47**, 179-214.

Teng F. Z., Wadhwa M. and Helz R. T. (2007) Investigation of magnesium isotope fractionation during basalt differentiation: Implications for a chondritic composition of the terrestrial mantle. *Earth Planet. Sci. Lett.* **261**, 84-92.

Thompson J. B. and Ferris F. G. (1990) Cyanobacterial Precipitation of Gypsum, Calcite, and Magnesite from Natural Alkaline Lake Water. *Geology* **18**, 995-998.

Young E. D. and Galy A. (2004) The isotope geochemistry and cosmochemistry of magnesium. *Rev. Mineral. Geochem.* **55**, 197-230.

**Table 1: Experimental conditions of all experiments performed in this study. All initial fluids contained 0.025-0.032 M $MgCl_2$ and 0.05 M $NaHCO_3$ except Abio-B which contained 0.05 M $MgCl_2$ and 0.01 M $NaHCO_3$. All abiotic experiments were conducted in the presence of 0.01 M $NaN_3$ to avoid possible microbial contamination. All experiments were performed under continuous light unless indicated. The Mg concentration range indicates total Mg concentration range measured at various during each experiment.**

| Experiment | Medium | Duration (days) | pH range | Mg concentration range ($10^{-3}$ mol/L) | DOC (mg/L) | Conditions |
|---|---|---|---|---|---|---|
| Bio-A | BG-11 | 30 | 8.2 - 10.4 | 25 - 4 | 50 | Stirring, bubbling |
| Bio-B | BG-11 | 27 | 8.3 - 10.0 | 26 – 13 | 60 | Stirring, bubbling |
| Bio-C | BG-11 | 42 | 8.3 - 10.0 | 31 – 7 | 9.5 | No stirring, no bubbling |
| Bio-D | BG-11 | 42 | 8.3 - 10.2 | 28 – 7 | 34 | Shaking, no bubbling |
| Bio-E | BG-11 | 45 | 8.6 – 9.4 | 29 – 17 | 30 | Stirring, no bubbling |
| Bio-F | BG-11 | 45 | 8.5 – 9.4 | 30 - 18 | 27 | No stirring, no bubbling |
| Bio-G | BG-11 | 143 | 8.3 – 10.0 | 28 – 8 | 5 | No stirring, no bubbling |
| Bio-I | BG-11 | 143 | 8.3 – 9.4 | 29 - 15 | 2 | Day/night cycle Shaking, no bubbling, Darkness |
| Abio-A | Sterile supernatant | 25 | 8.1 - 9.3 | 29 - 12 | 60 | Stirring, bubbling |
| Abio-B | Sterile supernatant | 67 | 8.7 – 9.4 | 47 - 16 | 61 | Stirring, bubbling |
| Abio-C | Sterile supernatant | 67 | 8.0 – 9.4 | 32 - 21 | 20 | Stirring, no bubbling |
| Abio-D1 | BG-11* | 73 | 8.6 – 9.5 | 32 - 14 | 30 | Stirring, bubbling |
| Abio-D2 | BG-11 | 73 | 8.7 – 9.3 | 32 - 13 | 31 | Stirring, bubbling |
| Abio-E | Sterile supernatant t | 20 | 8.0 – 9.3 | 32 – 19 | 50 | Stirring, bubbling |
| P-f | BG-11 | 44 | 8.2 - 10.65 | 0.003 - 0.006 | | Precipitation free |

* BG-11 with normal $PO_4$ content.

**Table 2: Ionic Activity Product (IAP) and degree of saturation with respect to hydromagnesite and nesquehonite of the fluid at its final steady-state condition of each experiment and apparent precipitation rates for biotic and abiotic experiments. Rates are reported in moles of precipitated mineral per liter per day. Uncertainty in precipitation rates is estimated to be 10-15%.**

| Experiment | $IAP_{Hydromagnesite}$ | $IAP_{Nesquehonite}$ | Number of values used for the average | $\Omega_{Hydromagnesite}$ | $\Omega_{Nesquehonite}$ | $dc_{Mg}/dt$ ($10^{-3}$ mol Mg $L^{-1}$ $day^{-1}$) | Elapsed time (days) | Mineralogy |
|---|---|---|---|---|---|---|---|---|
| Bio-A | 1.2E-34 | 9.0E-07 | 4 | 0.01 | 0.11 | -1.81 | 15 | Dypingite |
| Bio-B | | | | | | -1.13 | 11 | Nesque- |
| | 2.2E-32 | 5.6E-06 | 4 | 1.71 | 0.69 | | | honite |
| Bio-C | 9.0E-34 | 2.9E-06 | 4 | 0.07 | 0.36 | -0.68 | 40 | Dypingite |
| Bio-D | 5.3E-34 | 2.7E-06 | 4 | 0.04 | 0.33 | -0.55 | 40 | Dypingite |
| Bio-E | | | | | | -0.38 | 34 | Dypin- |
| | | | | | | | | gite+Nes |
| | 3.2E-33 | 6.0E-06 | 4 | 0.26 | 0.74 | | | quehonite |
| Bio-F | | | | | | -0.26 | 45 | Nesque- |
| | 1.0E-32 | 6.8E-06 | 4 | 0.82 | 0.84 | | | honite |
| Bio-G | | | | | | -0.31 | 40 | Nesque- |
| | 5.5E-33 | 3.5E-06 | 4 | 0.43 | 0.43 | | | honite |
| Bio-I | | | | | | -0.19 | 74 | Nesque- |
| | 6.1E-33 | 6.0E-06 | 4 | 0.48 | 0.75 | | | honite |
| Abio-A | 1.7E-34 | 3.2E-06 | 4 | 0.01 | 0.39 | -1.23 | 12 | Dypingite |
| Abio-B | | | | | | -1.58 | 14 | Nesque- |
| | 4.8E-33 | 6.7E-06 | 4 | 0.38 | 0.83 | | | honite |
| Abio-C | | | | | | -0.75 | 15 | Nesque- |
| | 3.0E-33 | 6.6E-06 | 4 | 0.24 | 0.82 | | | honite |
| Abio- | | | | | | -0.95 | 10 | Nesque- |
| D1 | 6.7E-33 | 7.1E-06 | 4 | 0.53 | 0.87 | | | honite |
| Abio- | | | | | | -1.06 | 12 | Dypingite |
| D2 | 9.9E-35 | 3.1E-06 | 5 | 0.01 | 0.38 | | | |
| Abio-E | | | | | | -1.21 | 11 | Nesque- |
| | 4.6E-33 | 6.7E-06 | 4 | 0.36 | 0.83 | | | honite |

**Table 3: Magnesium isotopic composition of liquid and solid samples, and fractionation factors, $\Delta^{25}Mg_{solid\text{-}liquid}$ and $\Delta^{26}Mg_{solid\text{-}liquid}$ in selected samples. Uncertainty is <0.07‰ for all measurements according to the standard deviation of replicate standards.**

| | Liquid samples | | | | | Solid samples | | | | | | Mineralogy (*) |
|---|---|---|---|---|---|---|---|---|---|---|---|---|
| Sample | Mg fraction in solution | $\delta^{25}Mg$ (‰) | 2σ | $\delta^{26}Mg$ (‰) | 2σ | $\delta^{25}Mg$ (‰) | 2σ | $\delta^{26}Mg$ (‰) | 2σ | $\Delta^{25}Mg_{solid\text{-}liquid}$ | $\Delta^{26}Mg_{solid\text{-}liquid}$ | |
| Bio-A-1 | 0.98 | -0.25 | 0.03 | -0.52 | 0.05 | -0.57 | 0.04 | -1.15 | 0.05 | -0.31 | -0.63 | N |
| Bio-A-3 | 0.97 | -0.29 | 0.03 | -0.55 | 0.03 | | | | | | | |
| Bio-A-4 | 0.87 | | | | | -0.38 | 0.01 | -0.76 | 0.02 | | | D |
| Bio-A-5 | 0.74 | -0.01 | 0.02 | -0.02 | 0.01 | | | | | | | |
| Bio-A-7 | 0.57 | 0.04 | 0.03 | 0.07 | 0.04 | | | | | | | |
| Bio-A-9 | 0.46 | 0.1 | 0.03 | 0.2 | 0.04 | -0.59 | 0.01 | -1.14 | 0.04 | -0.69 | -1.33 | D |
| Bio-A-10 | 0.22 | 0.3 | 0.01 | 0.6 | 0.02 | | | | | | | |
| Bio-A-12 | 0.16 | 0.36 | 0.03 | 0.71 | 0.06 | | | | | -0.80 | -1.55 | |
| Bio-A-13 | 0.17 | 0.36 | 0.03 | 0.69 | 0.03 | -0.44 | 0.01 | -0.84 | 0.03 | | | D |
| Bio-A-14 | 0.16 | 0.26 | 0.05 | 0.51 | 0.07 | | | | | | | |
| Bio-A-15 | 0.13 | 0.06 | 0.01 | 0.13 | 0.01 | -0.56 | 0.01 | -1.07 | 0.01 | -0.62 | -1.21 | D |
| Bio-B-1 | 1 | -0.36 | 0.04 | -0.69 | 0.02 | | | | | | | |
| Bio-B-5 | 0.65 | -0.25 | 0.06 | -0.43 | 0.04 | | | | | | | |
| Bio-B-11 | 0.49 | -0.07 | 0.01 | -0.13 | 0.03 | -0.68 | 0.03 | -1.33 | 0.05 | -0.61 | -1.19 | D |
| Bio-C-1 | 1 | -0.27 | 0.03 | -0.52 | 0.01 | | | | | | | |
| Bio-C-5 | 0.21 | 0.22 | 0.02 | 0.42 | 0.02 | -0.54 | 0.03 | -1.05 | 0.03 | -0.76 | -1.47 | D |
| Bio-D-1 | 1 | -0.34 | 0.02 | -0.66 | 0.01 | | | | | | | |
| Bio-D-3 | 0.26 | 0.18 | 0.02 | 0.33 | 0.02 | -0.46 | 0.02 | -0.9 | 0.02 | -0.63 | -1.23 | D |
| Abio-A-1 | 1 | -0.32 | 0.02 | -0.62 | 0.05 | | | | | | | |
| Abio-A-2 | 0.62 | -0.23 | 0.02 | -0.45 | 0.01 | | | | | | | |
| Abio-A-5 | 0.47 | -0.05 | 0.01 | -0.11 | 0.01 | -0.67 | 0.01 | -1.28 | 0.03 | -0.61 | -1.17 | D |
| Abio-A-10 | 0.34 | -0.01 | 0.01 | 0.01 | 0.02 | -0.64 | 0.02 | -1.21 | 0.03 | -0.64 | -1.22 | D |

(*) where N and D stands for Nesquehonite and Dypingite. (**)$\Delta^{x}Mg$ values for P-f experiment samples denote fractionation between initial $MgSO_4$ and the sample.

**Table 3(continued): Magnesium isotopic composition of liquid and solid samples, and fractionation factors, $\Delta^{25}Mg_{solid\text{-}liquid}$ and $\Delta^{26}Mg_{solid\text{-}liquid}$ in selected samples. Uncertainty is <0.07‰ for all measurements according to the standard deviation of replicate standards.**

| | | Liquid samples | | | | Solid samples | | | | | | Mineralogy (*) |
|---|---|---|---|---|---|---|---|---|---|---|---|---|
| Sample | Mg fraction in solution | $\delta^{25}Mg$ (‰) | 2σ | $\delta^{26}Mg$ (‰) | 2σ | $\delta^{25}Mg$ (‰) | 2σ | $\delta^{26}Mg$ (‰) | 2σ | $\Delta^{25}Mg_{solid\text{-}liquid}$ | $\Delta^{26}Mg_{solid\text{-}liquid}$ | |
| Abio-A-13 | 0.44 | 0.19 | 0.03 | 0.37 | 0.05 | -0.56 | 0.03 | -1.06 | 0.04 | -0.75 | -1.43 | D |
| $MgCl_2$ (initial solution) | | -0.27 | 0.02 | -0.53 | 0.02 | | | | | | | |
| $MgSO_4$ (BG-11) | | -0.47 | 0.03 | -0.91 | 0.01 | | | | | | | |
| P-f: Cells after 11 days | 0.9 | | | | | -0.36 | 0.03 | -0.71 | 0.02 | 0.11** | 0.18** | |
| P-f:Cells after 44 days | 0.9 | | | | | -0.46 | 0.02 | -0.87 | 0.02 | 0.01** | 0.04** | |

(*) where N and D stands for Nesquehonite and Dypingite. (**)$\Delta^{x}Mg$ values for P-f experiment samples denote fractionation between initial $MgSO_4$ and the sample.

**Figure 1: X-ray diffraction patterns of the solids recovered from (A) experiments Bio-A after 30 days and Abio-A after 27 days, and (B) experiments Bio-B after 23 days and Abio-C after 15 days compared to X-ray diffraction patterns of Dypingite and Nesquehonite reference patterns, respectively.**

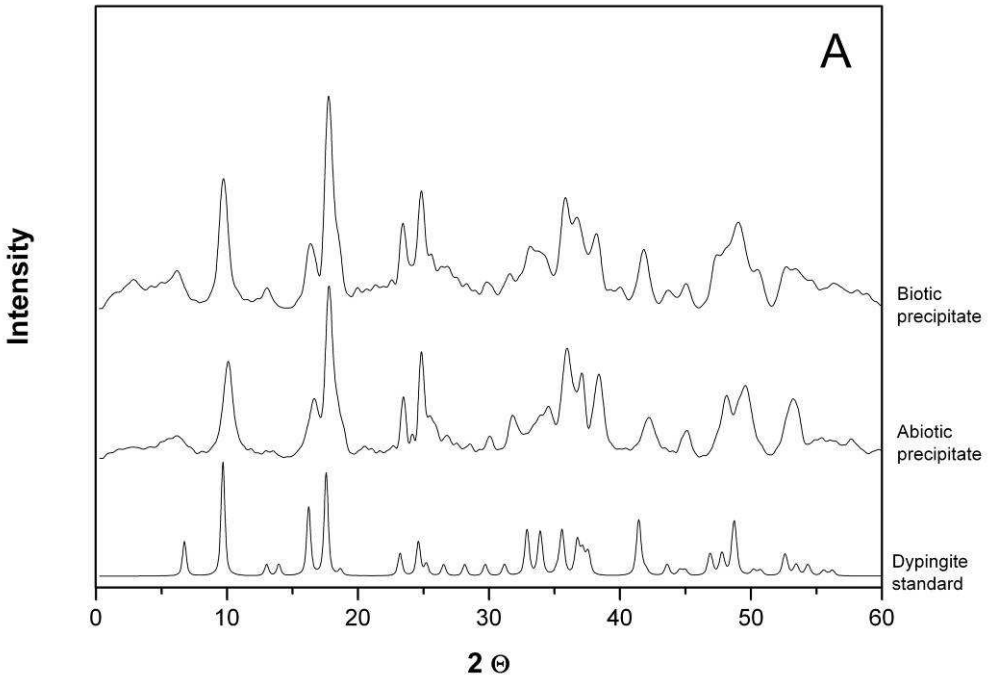


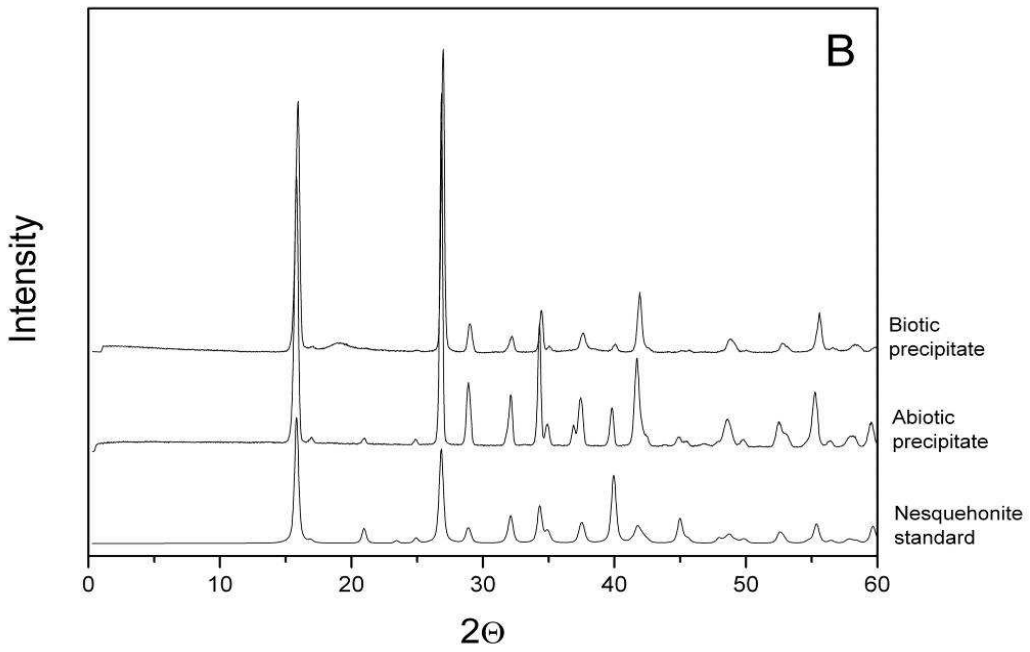

**Figure 2: SEM images of hydrous magnesium carbonate phases precipitated during this study: Nesquehonite needles collected from (A) experiment Bio-A after ~ 1 hour, (B); Dypingite rosettes collected from experiment Bio-A after 30 days, and (C) Abio-A after 27 days.**

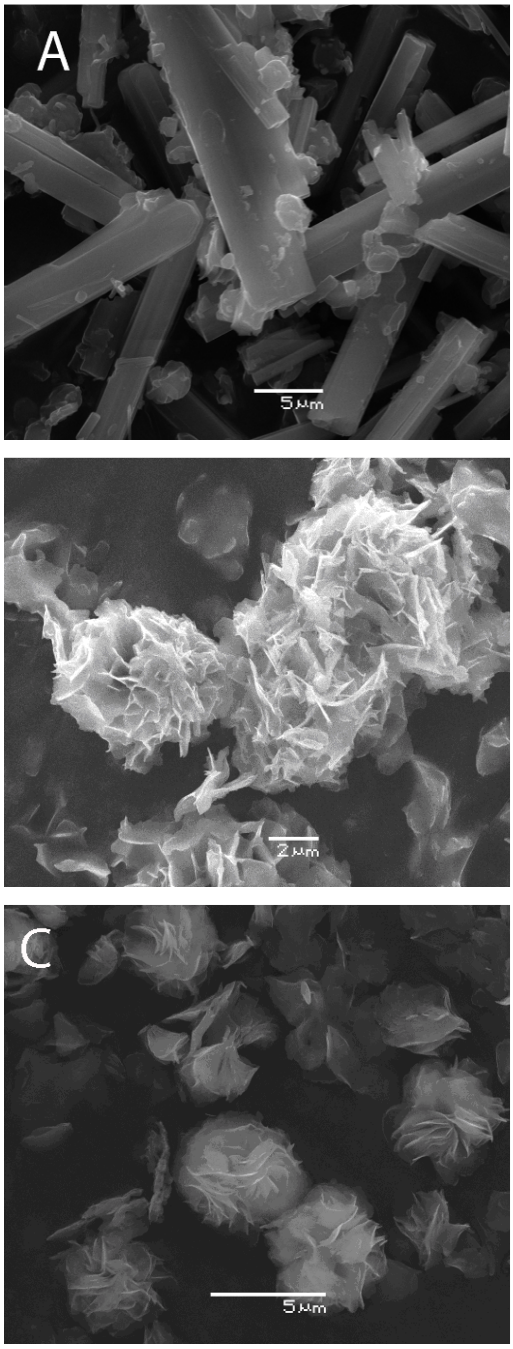

**Figure 3: TEM images of active *Gloeocapsa* sp. cyanobacteria and associated precipitates after 14 days in (A) BG-11 medium and (B-C) $MgCl_2$ – $NaHCO_3$ enriched BG-11 medium.**

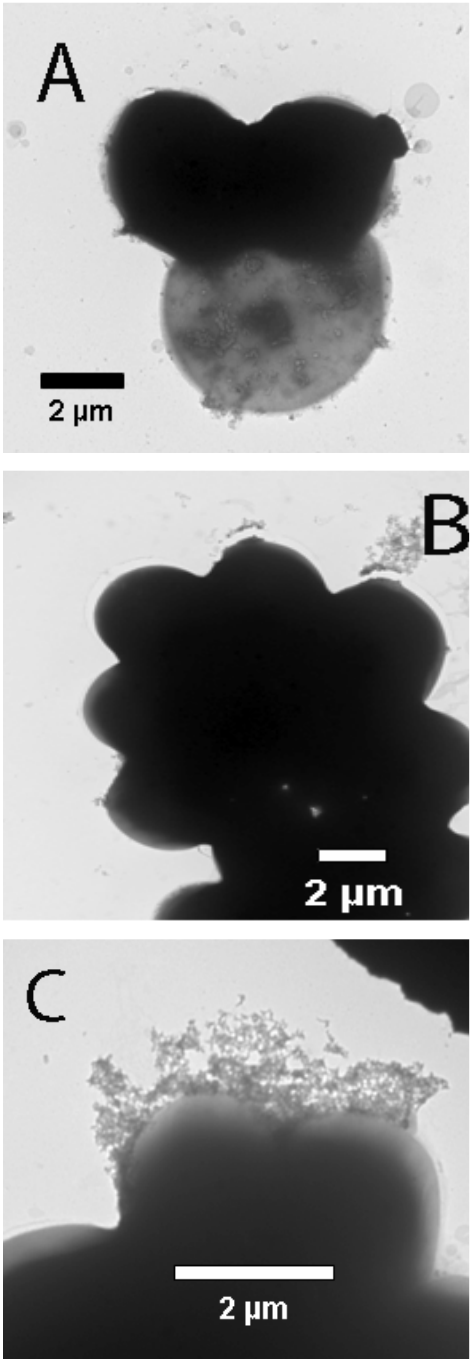

**Figure 4: Reactive fluid evolution during the experiments performed in this study. Temporal evolution of A) alkalinity, B) pH, C) Mg concentration ($C_{Mg}$), and D) biomass concentration during experiments Bio-A, Bio-B, Abio-A and Abio- C. Temporal evolution of E) Mg concentration and G) pH during experiments Bio-C, Bio-D, Bio-E, Bio-F, Bio-G and Bio-I Temporal evolution of F) Mg concentration and H) pH during experiments Abio-B, Abio-D1, Abio-D2 and Abio-E. The symbol size approximates the uncertainty of the analyses.**

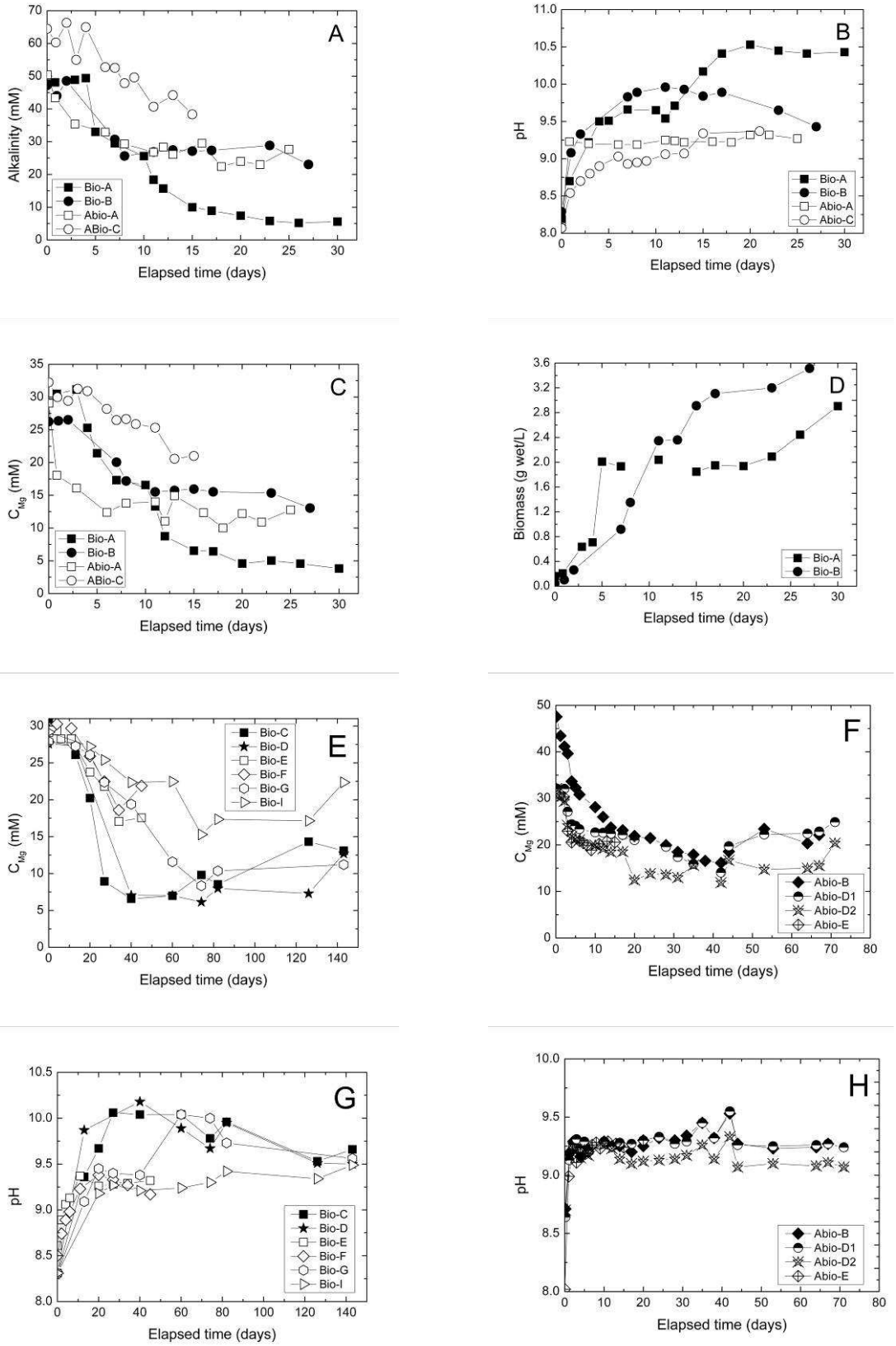

**Figure 5: Temporal evolution of saturation degree of nesquehonite ($\Omega_{nesquehonite}$) of the reactive fluids during experiments Bio-A and Abio-A.**

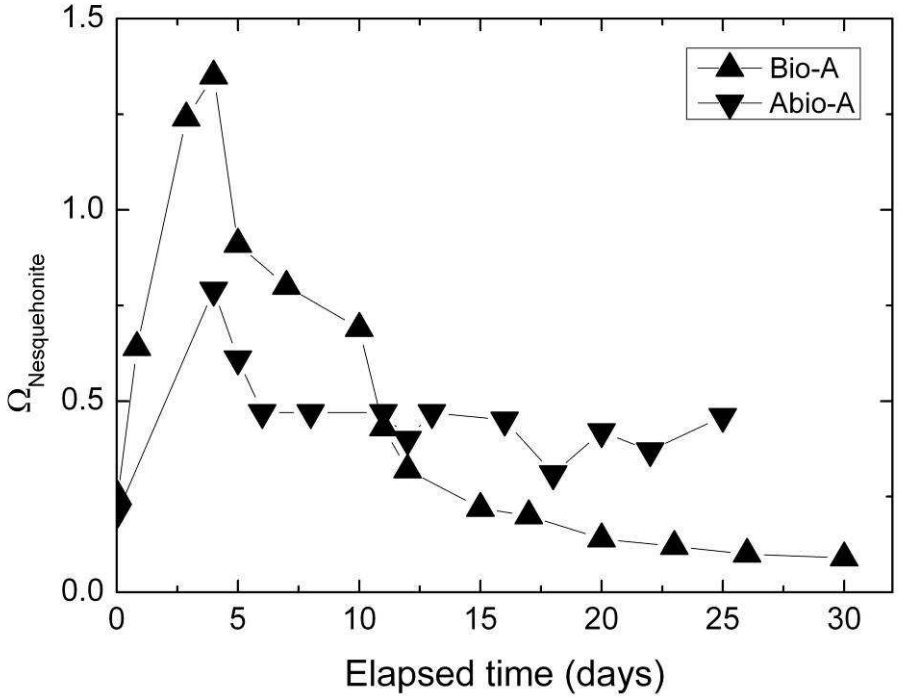

**Figure 6: Temporal evolution of $\delta^{26}$Mg values in the liquid and solid samples collected during experiments Bio-A and Abio-A. Size of the symbols incorporates the uncertainty (2σ) on $\delta^{26}$Mg.**

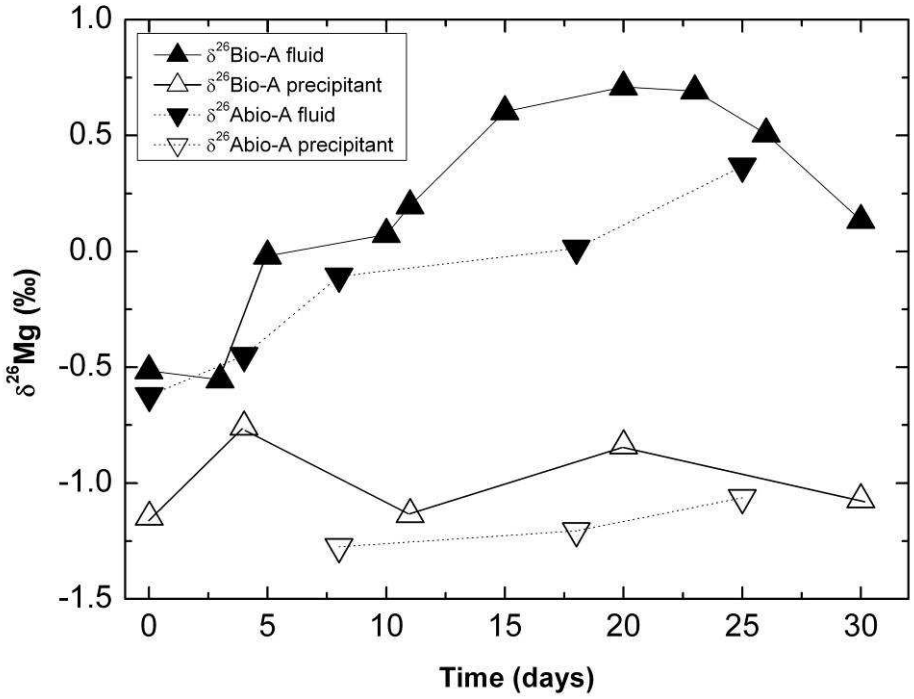

**Figure 7: $\delta^{26}$Mg values vs. Mg fraction remained in solution for (A) biotic experiment Bio-A, Bio-B, Bio-C, Bio-D and (B) abiotic experiment Abio-A. The solid lines in the figure correspond to trends predicted for closed system equilibrium using Eqn. (3) together with the mean measured $\Delta^{26}_{solid\text{-}liquid}$ value (-1.31±0.14‰) and the $\delta^{26}$Mg value of the $MgCl_2$ used to create the reactive fluids. Closed and open symbols correspond to liquid and solid samples respectively. Encircled symbols collected at the beginning of experiment Bio-A whcih may be affected by mineralogical changes or kinetic isotopic fractionation.**

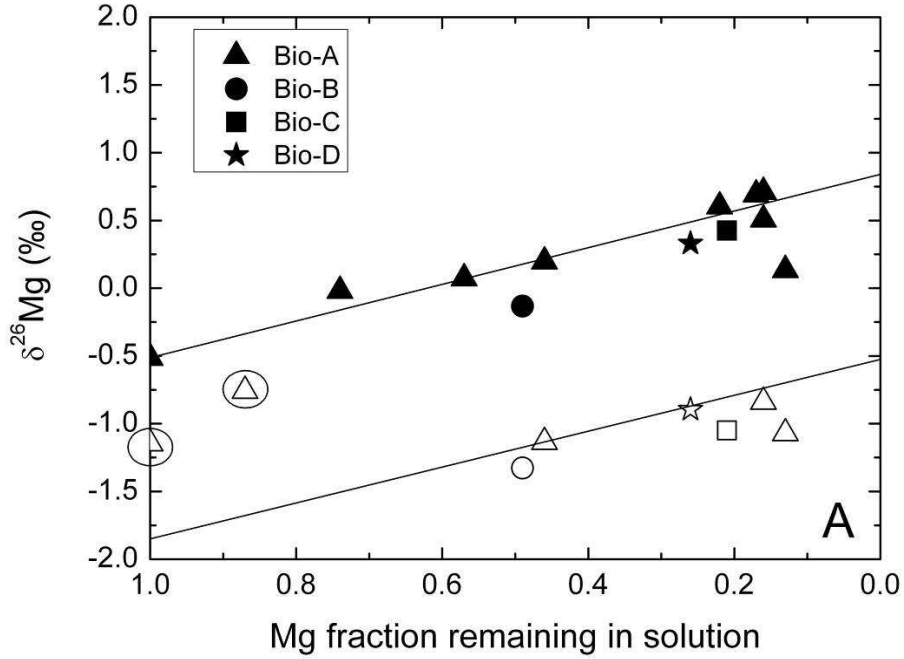


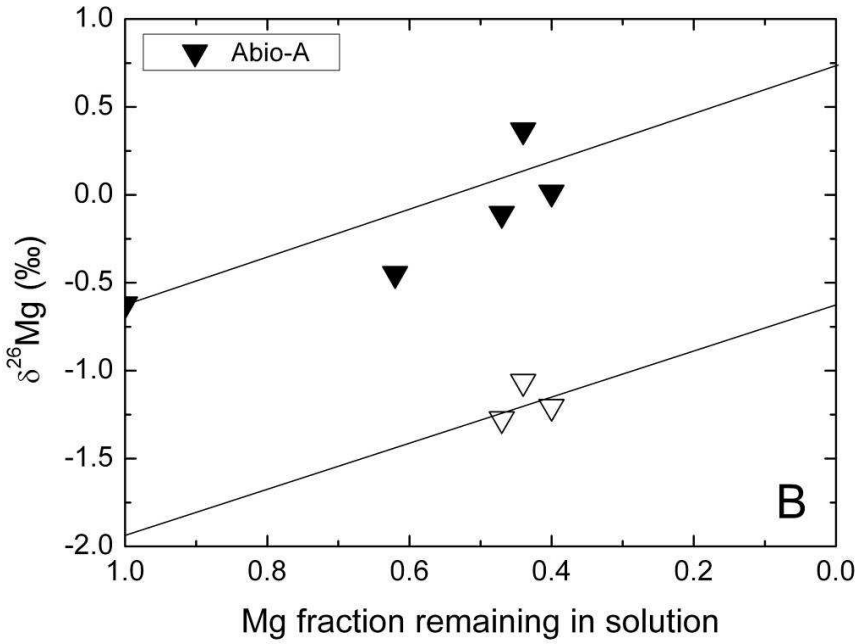

**Figure ESM 1: Correlation of $\Delta^{26}Mg_{solid\text{-}liquid}$ with (A) pH, (B) $IAP_{hydromagnesite}$, (C) aqueous Mg concentration, (D) alkalinity and (E) biomass concentration. Size of symbols corresponds to the uncertainty in the data. Encircled symbols were collected at the beginning of experiment Bio-A which may be affected by mineralogical changes or kinetic isotopic fractionation (see text).**

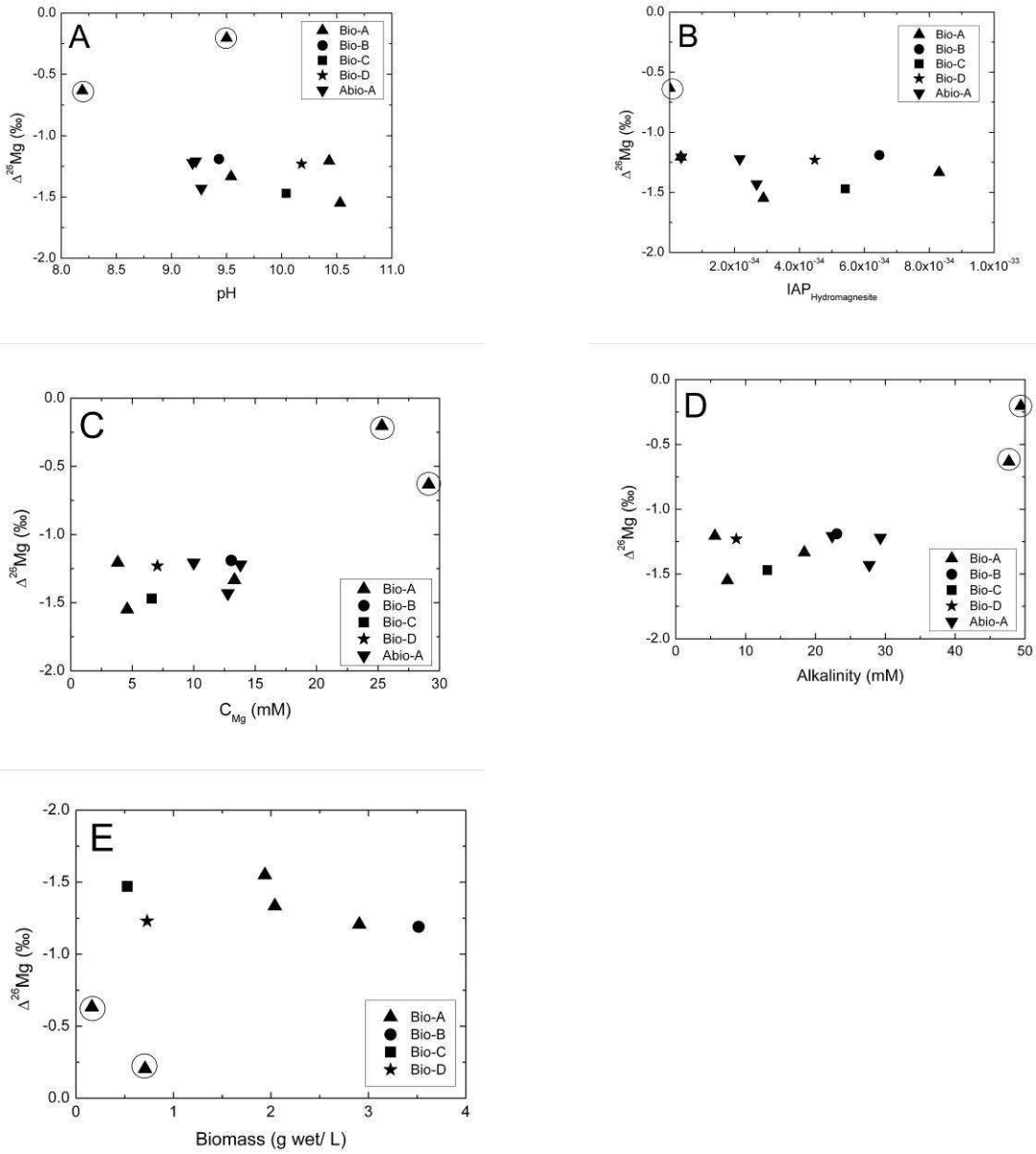

**Figure ESM-2: Correlation of $\Delta^{26}Mg_{solid\text{-}liquid}$ with the percent of aqueous Mg present as $MgCO_3^o$ in the fluid phase. Encircled symbols were collected at the beginning of experiment Bio-A and my be affected by mineralogical changes or kinetic isotopic fractionation (see text). Uncertainty in the calculation is estimated to be less than 5%.**

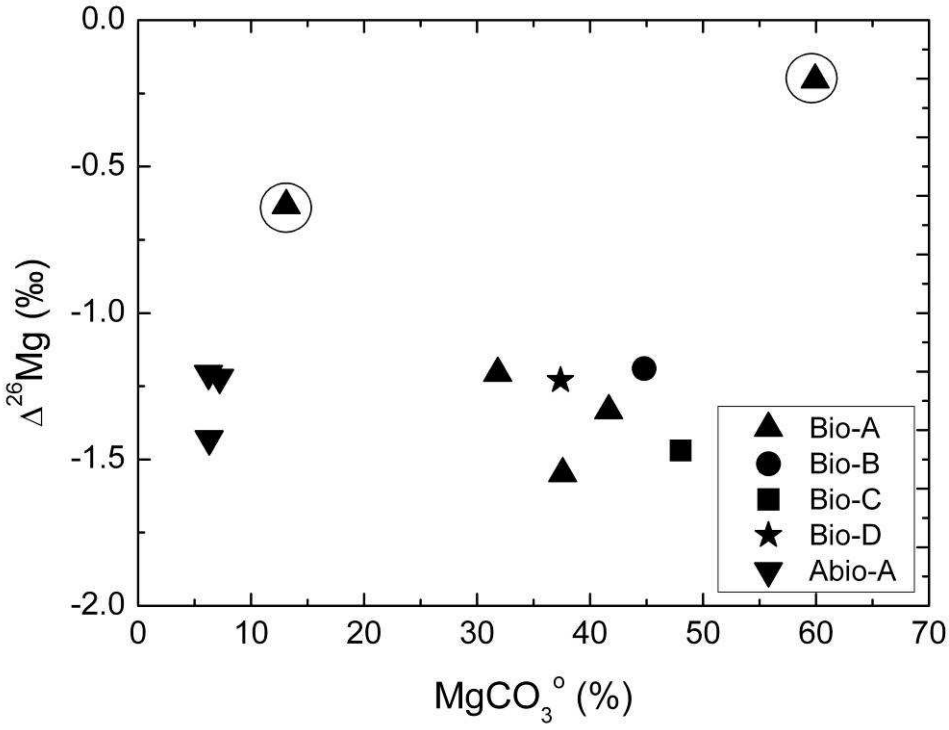

Appendix 2

# Appendix 3

# Summary of kinetic experiments with APB

| № | t, hrs | t, days | biomass, gwet/L | pH | Ca, mM/L | Alkalinity, mM/L | Ω calcite |
|---|---|---|---|---|---|---|---|
| 1 | 192 | 8 | 0,62 | 9,56 | 2,77 | 2,84 | 89,1 |
| | 288 | 12 | 0,88 | 9,42 | 3,03 | 2,53 | 74,1 |
| | 336 | 14 | 1,08 | 9,4 | 2,87 | 2,61 | 72,4 |
| | 432 | 18 | 1,24 | 9,26 | 2,59 | 2,76 | 61,7 |
| | 552 | 23 | 1,46 | 9,08 | 2,72 | 2,77 | 50,1 |
| | 624 | 26 | 1,46 | 9,01 | 2,74 | 3,36 | 54,9 |
| 2 | 192 | 8 | 0,68 | 9,1 | 5,81 | 2,44 | 70,8 |
| | 288 | 12 | 0,76 | 8,92 | 5,38 | 1,85 | 41,7 |
| | 336 | 14 | 0,92 | 8,87 | 6,04 | 1,85 | 41,7 |
| | 432 | 18 | 1,04 | 8,71 | 6,49 | 2,42 | 43,7 |
| | 552 | 23 | 1,12 | 8,61 | 7,30 | 2,53 | 41,7 |
| | 624 | 26 | 1,22 | 8,71 | 7,73 | 2,98 | 58,9 |
| 3 | 0 | 0 | 0,18 | 9 | 2,75 | 4,56 | 69,2 |
| | 72 | 3 | 0,56 | 9,73 | 1,93 | 3,21 | 89,3 |
| | 120 | 5 | 1 | 9,58 | 1,42 | 2,46 | 52,5 |
| | 168 | 7 | 0,92 | 9,44 | 1,31 | 2,55 | 44,7 |
| | 216 | 9 | 1,44 | 9,57 | 1,28 | 2,18 | 43,7 |
| | 264 | 11 | 1,7 | 9,31 | 1,04 | 2,14 | 27,5 |
| | 336 | 14 | 1,78 | 9,14 | 1,25 | 2,66 | 30,2 |
| | 408 | 17 | 1,92 | 9,07 | 1,47 | 2,66 | 30,9 |
| 4 | 0 | 0 | 0,14 | 8,83 | 4,83 | 4,53 | 79,4 |
| | 72 | 3 | 0,66 | 9,62 | 3,97 | 1,89 | 74,1 |
| | 120 | 5 | 1,02 | 9,91 | 3,48 | 1,95 | 85,1 |
| | 168 | 7 | 1,28 | 9,9 | 3,37 | 2,16 | 91,2 |
| | 216 | 9 | 1,88 | 9,96 | 2,86 | 1,7 | 69,2 |
| | 264 | 11 | 2,2 | 9,77 | 3,41 | 2,21 | 89,1 |
| | 336 | 14 | 2,38 | 9,82 | 3,45 | 1,87 | 77,6 |
| | 408 | 17 | 2,62 | 9,46 | 3,47 | 1,49 | 50,1 |
| 5 | 0 | 0 | 0,14 | 8,69 | 9,19 | 1,43 | 30,9 |
| | 72 | 3 | 0,68 | 9,55 | 7,62 | 1,75 | 81,3 |
| | 120 | 5 | 0,78 | 9,45 | 7,61 | 1,72 | 75,9 |
| | 168 | 7 | 1,12 | 9,39 | 6,93 | 1,83 | 75,9 |
| | 216 | 9 | 1,58 | 9,25 | 5,97 | 1,85 | 64,6 |
| | 264 | 11 | 1,86 | 9,43 | 6,18 | 2,21 | 89,1 |
| | 336 | 14 | 2,18 | 9,14 | 2,75 | 1,56 | 32,4 |
| | 408 | 17 | 2,7 | 9,1 | 7,46 | 1,89 | 61,6 |
| 6 | 0 | 0 | 0,12 | 8,58 | 13,11 | 0,7 | 15,1 |
| | 72 | 3 | 0,78 | 9,35 | 11,63 | 0,99 | 45,7 |
| | 120 | 5 | 1,5 | 9,55 | 10,34 | 0,89 | 43,6 |
| | 168 | 7 | 1,72 | 9,44 | 10,45 | 1,17 | 54,9 |
| | 216 | 9 | 2,04 | 9,63 | 19,43 | 1,63 | 91,2 |
| | 264 | 11 | 2,26 | 9,72 | 13,02 | 2,08 | 114,8 |
| | 336 | 14 | 2,5 | 9,94 | 11,04 | 1,42 | 77,6 |
| | 408 | 17 | 2,92 | 9,82 | 10,75 | 1,47 | 79,4 |
| 7 | 0 | 0 | 0,12 | 8,44 | 20,60 | 3,75 | 79,4 |
| | 72 | 3 | 0,52 | 9,26 | 21,14 | 1,52 | 75,9 |
| | 120 | 5 | 0,82 | 9,63 | 24,00 | 1,51 | 87,1 |
| | 168 | 7 | 1,08 | 9,79 | 19,20 | 1,71 | 97,7 |
| | 216 | 9 | 1,4 | 9,87 | 14,73 | 1,55 | 87,1 |
| | 264 | 11 | 1,42 | 9,79 | 19,80 | 1,56 | 89,1 |
| | 336 | 14 | 1,6 | 9,41 | 18,60 | 1,54 | 81,3 |
| | 408 | 17 | 2,76 | 9,45 | 18,82 | 1,03 | 54,9 |

(Continued)

| № | t, hrs | biomass, $g_{wet}$/L | pH | Ca, mM/L | DIC, mM/L | $\Omega_{calcite}$ |
|---|---|---|---|---|---|---|
| 11 | 2.5 | 2.13 | 8.33 | 9.78 | 10.49 | 123.00 |
| | 23.5 | 4.46 | 8.42 | 8.65 | 10.16 | 128.80 |
| | 114.5 | 14.51 | 8.78 | 5.14 | 5.33 | 100.00 |
| | 163 | 14.30 | 8.61 | 1.07 | 5.09 | 18.62 |
| | 216 | 14.67 | 8.57 | 0.89 | 4.86 | 14.13 |
| | 284 | 14.55 | 8.68 | 1.10 | 4.97 | 21.38 |
| 12 | 0.5 | 4.31 | 8.55 | 0.97 | 20.50 | 38.02 |
| | 44.5 | 9.63 | 8.57 | 0.70 | 18.93 | 26.92 |
| | 72.5 | 14.66 | 9.04 | 0.62 | 15.98 | 42.66 |
| | 141 | 16.94 | 9.30 | 0.18 | 12.67 | 15.14 |
| | 195.6 | 16.98 | 9.33 | 0.13 | 11.81 | 10.96 |
| | 242.6 | 16.74 | 9.27 | 0.11 | 12.49 | 8.92 |
| 13 | 4 | 8.07 | 8.92 | 0.94 | 24.60 | 66.07 |
| | 24 | 9.14 | 8.70 | 0.82 | 25.17 | 44.67 |
| | 75 | 15.00 | 8.91 | 0.70 | 18.30 | 43.65 |
| | 101 | 17.26 | 9.26 | 0.24 | 18.37 | 21.38 |
| | 119.5 | 17.46 | 9.03 | 0.10 | 19.41 | 7.41 |
| | 167 | 18.14 | 9.08 | 0.11 | 19.94 | 8.71 |
| 14 | 1 | 2.61 | 8.16 | 5.23 | 18.86 | 83.18 |
| | 43.5 | 4.01 | 8.11 | 4.44 | 17.98 | 63.10 |
| | 139 | 15.08 | 9.03 | 1.41 | 16.96 | 97.70 |
| | 187 | 15.02 | 8.79 | 0.53 | 16.54 | 26.92 |
| | 236.5 | 14.93 | 8.92 | 0.27 | 15.34 | 16.22 |
| | 307 | 15.36 | 8.95 | 0.40 | 15.42 | 24.55 |
| 15 | 1 | 5.58 | 8.38 | 9.46 | 21.41 | 229.00 |
| | 20 | 8.60 | 8.41 | 9.20 | 21.60 | 239.88 |
| | 94.5 | 15.55 | 8.43 | 4.67 | 14.37 | 104.72 |
| | 143.5 | 15.97 | 8.43 | 1.12 | 15.00 | 29.51 |
| | 187.5 | 16.26 | 8.47 | 1.10 | 14.88 | 30.90 |
| | 259.5 | 16.12 | 8.41 | 1.11 | 14.86 | 28.18 |
| 16 | 4 | 3.07 | 8.92 | 0.34 | 44.6 | 28.18 |
| | 24 | 4.14 | 8.70 | 0.32 | 45.17 | 21.38 |
| | 75 | 15.00 | 8.91 | 0.3 | 48.3 | 25.12 |
| | 101 | 17.26 | 9.26 | 0.14 | 48.37 | 15.14 |
| | 119.5 | 17.46 | 9.03 | 0.1 | 49.41 | 9.33 |
| | 167 | 18.14 | 9.08 | 0.11 | 49.94 | 10.72 |

*Bacteria S-17-65*

| № | t, hrs | biomass, $g_{wet}$/L | pH | Ca, mM/L | DIC, mM/L | $\Omega_{calcite}$ |
|---|---|---|---|---|---|---|
| 17 | 0.5 | 3.64 | 7.67 | 1.06 | 6.17 | 2.82 |
| | 43 | 3.84 | 7.66 | 0.86 | 6.85 | 2.45 |
| | 91.5 | 3.66 | 7.67 | 0.96 | 6.66 | 2.69 |
| | 163.5 | 5.61 | 7.96 | 0.85 | 6.99 | 4.89 |
| | 215.5 | 8.13 | 8.26 | 0.85 | 7.34 | 9.77 |
| | 263.3 | 16.43 | 8.92 | 0.99 | 9.35 | 44.67 |
| 18 | 4 | 5.13 | 8.01 | 1.16 | 5.00 | 5.49 |
| | 24 | 3.12 | 7.79 | 1.17 | 5.00 | 3.38 |
| | 75 | 7.75 | 8.39 | 1.18 | 5.95 | 14.79 |
| | 101 | 11.14 | 8.83 | 1.17 | 6.41 | 36.31 |
| | 119.5 | 13.19 | 8.90 | 1.21 | 7.07 | 44.67 |
| | 167 | 16.28 | 9.18 | 1.20 | 8.11 | 70.79 |

(Continued)

| № | t, hrs | biomass, $g_{wet}$/L | pH | Ca, mM/L | DIC, mM/L | $\Omega_{calcite}$ |
|---|---|---|---|---|---|---|
| 19 | 1 | 4.23 | 7.67 | 4.67 | 5.77 | 9.55 |
| | 42 | 4.84 | 7.93 | 4.42 | 5.35 | 15.49 |
| | 71.5 | 12.44 | 8.21 | 4.42 | 5.36 | 18.84 |
| | 167.5 | 20.31 | 9.24 | 3.36 | 4.21 | 123.03 |
| | 216 | 21.51 | 9.20 | 3.26 | 4.43 | 120.23 |
| | 308 | 21.63 | 9.30 | 3.23 | 4.04 | 125.89 |
| | 339 | 21.86 | 9.36 | 3.28 | 4.03 | 138.00 |
| 20 | 1.5 | 3.09 | 7.68 | 10.52 | 5.97 | 19.05 |
| | 48.5 | 7.01 | 8.18 | 10.29 | 5.83 | 54.95 |
| | 71.5 | 9.87 | 8.58 | 10.45 | 6.22 | 131.83 |
| | 115.5 | 16.13 | 9.05 | 7.40 | 5.34 | 199.50 |
| | 162.5 | 17.54 | 9.06 | 6.58 | 4.40 | 158.50 |
| | 187 | 19.29 | 9.14 | 6.20 | 4.01 | 158.50 |
| 21 | 0.5 | 6.85 | 7.53 | 10.79 | 4.12 | 9.55 |
| | 46 | 11.36 | 8.22 | 9.78 | 4.88 | 48.98 |
| | 139.5 | 19.22 | 8.72 | 7.94 | 3.84 | 91.20 |
| | 165 | 22.31 | 8.86 | 4.88 | 3.92 | 85.11 |
| | 190.5 | 20.09 | 8.99 | 4.45 | 3.61 | 93.33 |
| | 210.5 | 20.32 | 8.93 | 4.72 | 3.37 | 81.28 |
| 22 | 0.5 | 2.51 | 7.69 | 0.94 | 8.54 | 3.38 |
| | 46.5 | 5.33 | 8.17 | 1.01 | 9.79 | 11.75 |
| | 138.5 | 15.20 | 8.94 | 0.92 | 10.65 | 46.77 |
| | 194.5 | 16.43 | 9.23 | 0.94 | 11.38 | 69.18 |
| | 215.5 | 16.37 | 9.24 | 0.89 | 11.61 | 66.07 |
| | 306.5 | 16.18 | 9.04 | 1.03 | 11.53 | 61.66 |
| 23 | 0.5 | 2.14 | 7.89 | 5.56 | 10.45 | 30.90 |
| | 178 | 17.10 | 8.79 | 1.12 | 7.18 | 34.67 |
| 24 | 0.5 | 2.25 | 7.95 | 5.30 | 10.11 | 33.11 |
| | 744 | 16.80 | 9.11 | 1.33 | 6.78 | 64.56 |
| 25 | 1 | 1.85 | 7.84 | 5.28 | 10.72 | 26.92 |
| | 68 | 4.63 | 8.06 | 4.86 | 9.67 | 38.02 |
| | 91 | 6.48 | 8.23 | 4.84 | 8.86 | 50.12 |
| | 109 | 7.21 | 8.31 | 4.85 | 8.03 | 54.95 |
| | 133 | 10.57 | 8.64 | 4.84 | 8.18 | 104.70 |
| | 158 | 9.97 | 8.65 | 4.62 | 7.46 | 95.50 |
| | 230 | 17.38 | 8.96 | 2.03 | 7.88 | 83.18 |
| | 253 | 17.25 | 9.02 | 0.89 | 7.03 | 39.81 |
| | 277 | 16.38 | 8.96 | 0.99 | 7.74 | 42.66 |
| 26 | 2.5 | 2.81 | 8.04 | 9.69 | 9.10 | 58.89 |
| | 23.5 | 2.45 | 7.77 | 9.84 | 9.47 | 33.88 |
| | 114.5 | 9.44 | 8.47 | 10.24 | 9.80 | 154.88 |
| | 163 | 16.67 | 8.44 | 7.14 | 7.33 | 89.13 |
| | 216 | 18.42 | 8.80 | 3.42 | 7.26 | 95.50 |
| | 284 | 21.19 | 8.70 | 3.28 | 6.32 | 69.18 |
| 27 | 0.5 | 1.64 | 8.03 | 0.86 | 13.94 | 9.77 |
| | 44.5 | 1.80 | 7.92 | 0.83 | 13.93 | 7.41 |
| | 72.5 | 2.91 | 7.96 | 0.85 | 13.93 | 8.32 |
| | 141 | 6.05 | 8.31 | 0.88 | 13.70 | 17.37 |
| | 195.6 | 14.23 | 8.84 | 0.85 | 16.25 | 45.71 |
| | 242.6 | 16.87 | 8.92 | 0.85 | 18.03 | 53.70 |

(Continued)

| № | t, hrs | biomass, $g_{wet}$/L | pH | Ca, mM/L | DIC, mM/L | $\Omega_{calcite}$ |
|---|---|---|---|---|---|---|
| 28 | 1 | 3.19 | 7.71 | 4.56 | 14.69 | 22.91 |
| | 43.5 | 6.03 | 7.75 | 4.36 | 15.56 | 25.70 |
| | 139 | 20.01 | 8.70 | 2.99 | 16.99 | 125.89 |
| | 187 | 21.71 | 8.60 | 0.91 | 16.61 | 34.67 |
| | 236.5 | 20.61 | 8.55 | 0.86 | 15.65 | 28.84 |
| | 307 | 20.47 | 8.59 | 0.92 | 15.77 | 33.11 |
| 29 | 1 | 3.32 | 7.88 | 10.06 | 14.03 | 61.66 |
| | 20 | 2.84 | 7.74 | 9.97 | 13.91 | 44.66 |
| | 94.5 | 11.07 | 8.34 | 9.50 | 13.83 | 151.36 |
| | 143.5 | 17.55 | 8.35 | 5.36 | 12.42 | 91.20 |
| | 187.5 | 18.65 | 8.39 | 0.94 | 12.78 | 20.89 |
| | 259.5 | 17.94 | 8.18 | 0.73 | 12.90 | 10.72 |
| 30 | 4 | 1.79 | 8.01 | 1.21 | 4.77 | 5.50 |
| | 24 | 3.12 | 7.79 | 1.18 | 5.35 | 3.63 |
| | 75 | 7.75 | 8.39 | 1.17 | 4.49 | 11.75 |
| | 101 | 11.14 | 8.83 | 1.16 | 4.84 | 29.51 |
| | 119.5 | 13.19 | 8.90 | 1.12 | 4.49 | 30.20 |
| | 167 | 16.28 | 9.18 | 1.09 | 4.79 | 47.86 |

**B. Kinetic experiments with inactive bacteria ($NaN_3$ addition) in growth medium**

*Bacteria A-20s*

| № | t, hrs | biomass, $g_{wet}$/L | pH | Ca, mM/L | DIC, mM/L | $\Omega_{calcite}$ |
|---|---|---|---|---|---|---|
| 31 | 0.5 | 3.18 | 8.11 | 0.97 | 5.91 | 6.76 |
| | 43 | 3.40 | 8.22 | 0.92 | 5.40 | 7.59 |
| | 91.5 | 3.38 | 8.28 | 0.86 | 5.27 | 7.94 |
| | 163.5 | 3.60 | 8.16 | 0.86 | 5.52 | 6.31 |
| | 215.5 | 3.30 | 8.21 | 0.93 | 5.39 | 7.41 |
| | 263.3 | 3.56 | 8.11 | 0.89 | 5.37 | 5.75 |
| 32 | 1 | 3.81 | 8.40 | 5.51 | 5.56 | 52.48 |
| | 42 | 4.93 | 8.61 | 5.08 | 5.58 | 75.86 |
| | 71.5 | 5.92 | 8.84 | 5.04 | 5.82 | 117.49 |
| | 167.5 | 6.07 | 9.02 | 5.04 | 5.92 | 158.49 |
| | 216 | 5.53 | 9.15 | 5.07 | 5.52 | 181.97 |
| | 308 | 5.98 | 9.15 | 5.37 | 5.49 | 190.55 |
| 33 | 1.5 | 1.64 | 7.95 | 9.13 | 5.07 | 26.92 |
| | 48.5 | 1.65 | 7.70 | 9.03 | 5.05 | 15.14 |
| | 71.5 | 1.50 | 7.70 | 8.68 | 4.92 | 14.45 |
| | 115.5 | 1.29 | 7.71 | 9.45 | 4.96 | 15.85 |
| | 162.5 | 1.37 | 7.75 | 9.44 | 4.97 | 17.38 |
| | 187 | 1.52 | 7.70 | 9.34 | 4.99 | 15.49 |
| 34 | 0.5 | 8.89 | 8.08 | 10.11 | 4.77 | 36.31 |
| | 46 | 8.90 | 7.75 | 8.63 | 5.00 | 16.22 |
| | 139.5 | 8.52 | 7.65 | 9.08 | 5.00 | 13.48 |
| | 165 | 8.17 | 7.03 | 8.80 | 5.00 | 2.88 |
| | 190.5 | 7.91 | 7.31 | 10.28 | 5.07 | 6.61 |
| | 210.5 | 7.93 | 7.22 | 10.26 | 5.51 | 5.75 |
| 35 | 0.5 | 2.11 | 8.34 | 1.12 | 9.87 | 18.62 |
| | 744 | 2.45 | 8.11 | 1.10 | 9.97 | 11.48 |

(Continued)

| № | t, hrs | biomass, $g_{wet}$/L | pH | Ca, mM/L | DIC, mM/L | $\Omega_{calcite}$ |
|---|---|---|---|---|---|---|
| 36 | 0.5 | 2.55 | 8.20 | 0.89 | 10.06 | 11.48 |
| | 46.5 | 2.74 | 8.15 | 0.92 | 10.07 | 10.72 |
| | 138.5 | 3.15 | 8.28 | 0.88 | 10.28 | 13.45 |
| | 194.5 | 2.59 | 8.49 | 0.90 | 10.29 | 20.89 |
| | 215.5 | 3.30 | 8.24 | 0.88 | 10.10 | 12.30 |
| | 306.5 | 3.46 | 8.37 | 0.89 | 10.18 | 16.22 |
| 37 | 0.5 | 2.45 | 8.31 | 4.89 | 10.11 | 66.07 |
| | 178 | 2.54 | 8.45 | 4.94 | 10.07 | 89.13 |
| 38 | 1 | 2.53 | 7.96 | 5.03 | 9.91 | 31.62 |
| | 25 | 3.10 | 8.10 | 5.08 | 10.39 | 45.71 |
| | 90 | 2.98 | 8.45 | 5.58 | 10.66 | 102.33 |
| | 114 | 2.80 | 8.46 | 5.31 | 12.36 | 122.20 |
| | 139 | 3.21 | 8.61 | 5.43 | 11.76 | 144.50 |
| | 170 | 3.35 | 8.99 | 5.34 | 12.46 | 269.20 |
| | 187 | 2.78 | 8.60 | 5.46 | 10.46 | 131.80 |
| | 259 | 2.90 | 8.72 | 5.31 | 9.33 | 144.50 |
| 39 | 0.5 | 2.67 | 8.11 | 10.04 | 10.32 | 77.62 |
| | 744 | 3.13 | 8.24 | 10.11 | 10.11 | 100.00 |
| 40 | 2.5 | 1.81 | 8.25 | 9.87 | 9.26 | 93.33 |
| | 23.5 | 2.15 | 8.04 | 8.60 | 9.41 | 54.95 |
| | 114.5 | 2.28 | 8.12 | 9.35 | 9.60 | 70.79 |
| | 163 | 2.68 | 8.10 | 9.26 | 9.50 | 66.07 |
| | 216 | 2.74 | 8.22 | 8.74 | 9.60 | 83.18 |
| | 284 | 2.74 | 8.28 | 9.27 | 9.92 | 100.00 |
| 41 | 0.5 | 3.97 | 8.44 | 0.91 | 16.52 | 25.70 |
| | 44.5 | 4.52 | 8.31 | 0.97 | 16.72 | 21.88 |
| | 72.5 | 5.22 | 8.49 | 0.86 | 16.97 | 27.54 |
| | 141 | 5.63 | 8.71 | 0.88 | 17.70 | 40.74 |
| | 195.6 | 5.80 | 8.88 | 0.96 | 17.90 | 54.95 |
| | 242.6 | 6.11 | 8.85 | 0.97 | 17.98 | 54.95 |
| 42 | 4 | 8.24 | 8.92 | 0.90 | 21.94 | 60.26 |
| | 24 | 7.93 | 8.69 | 0.87 | 23.25 | 44.67 |
| | 75 | 7.51 | 8.73 | 0.92 | 22.40 | 48.98 |
| | 101 | 8.31 | 8.97 | 0.89 | 23.29 | 64.56 |
| | 119.5 | 8.15 | 8.81 | 0.88 | 22.80 | 52.48 |
| | 167 | 7.36 | 8.81 | 0.90 | 22.80 | 53.70 |
| 43 | 1 | 2.43 | 8.12 | 5.42 | 15.72 | 69.18 |
| | 43.5 | 1.87 | 8.00 | 5.12 | 15.83 | 51.29 |
| | 139 | 2.28 | 8.04 | 4.83 | 15.87 | 52.48 |
| | 187 | 2.36 | 7.93 | 4.74 | 15.58 | 40.74 |
| | 236.5 | 2.40 | 7.94 | 4.86 | 15.97 | 43.65 |
| | 307 | 1.30 | 7.95 | 5.25 | 15.77 | 46.77 |
| 44 | 1 | 4.76 | 8.23 | 9.86 | 15.43 | 138.10 |
| | 20 | 5.55 | 8.12 | 8.58 | 15.93 | 102.30 |
| | 94.5 | 5.90 | 8.33 | 9.04 | 16.11 | 162.18 |
| | 143.5 | 6.15 | 8.69 | 8.91 | 16.47 | 309.10 |
| | 187.5 | 6.66 | 8.78 | 9.08 | 17.21 | 371.50 |
| | 259.5 | 6.21 | 8.68 | 8.74 | 16.34 | 301.90 |

(Continued)

| № | t, hrs | biomass, $g_{wet}$/L | pH | Ca, mM/L | DIC, mM/L | $\Omega_{calcite}$ |
|---|---|---|---|---|---|---|
| 45 | 4 | 3.24 | 8.92 | 0.3 | 41.94 | 24.55 |
| | 24 | 2.93 | 8.69 | 0.27 | 43.25 | 17.38 |
| | 75 | 2.51 | 8.73 | 0.32 | 42.4 | 21.88 |
| | 101 | 4.31 | 8.97 | 0.29 | 43.29 | 25.12 |
| | 119.5 | 4.15 | 8.81 | 0.28 | 42.8 | 20.89 |
| | 167 | 2.36 | 8.81 | 0.3 | 42.8 | 22.38 |

*Bacteria S-17-65*

| № | t, hrs | biomass, $g_{wet}$/L | pH | Ca, mM/L | DIC, mM/L | $\Omega_{calcite}$ |
|---|---|---|---|---|---|---|
| 46 | 0.5 | 3.52 | 7.77 | 1.08 | 6.46 | 3.72 |
| | 43 | 3.49 | 7.64 | 0.76 | 6.77 | 2.04 |
| | 91.5 | 3.54 | 7.93 | 1.07 | 6.67 | 5.50 |
| | 163.5 | 3.29 | 7.73 | 0.81 | 6.60 | 2.63 |
| | 215.5 | 3.36 | 7.72 | 0.80 | 6.52 | 2.51 |
| | 263.3 | 3.31 | 7.73 | 0.96 | 6.06 | 2.88 |
| 47 | 4 | 2.97 | 8.08 | 1.15 | 4.91 | 6.31 |
| | 24 | 2.49 | 7.97 | 1.30 | 5.30 | 5.88 |
| | 75 | 2.02 | 7.98 | 1.30 | 5.31 | 6.03 |
| | 101 | 2.29 | 7.95 | 1.16 | 4.82 | 4.68 |
| | 119.5 | 2.25 | 7.85 | 1.20 | 4.00 | 3.24 |
| | 167 | 2.12 | 7.86 | 1.20 | 3.47 | 2.95 |
| 48 | 1 | 4.88 | 7.90 | 4.62 | 4.37 | 12.59 |
| | 42 | 4.86 | 7.60 | 4.62 | 4.71 | 6.76 |
| | 71.5 | 4.79 | 7.61 | 4.63 | 4.79 | 7.08 |
| | 167.5 | 3.36 | 7.91 | 4.63 | 4.96 | 14.45 |
| | 216 | 4.79 | 8.39 | 4.67 | 5.94 | 47.86 |
| | 308 | 4.41 | 9.14 | 4.70 | 7.09 | 204.20 |
| 49 | 1.5 | 2.69 | 7.73 | 10.10 | 4.36 | 15.13 |
| | 48.5 | 2.84 | 7.55 | 10.70 | 4.49 | 10.72 |
| | 71.5 | 2.97 | 7.63 | 9.73 | 4.46 | 12.02 |
| | 115.5 | 2.57 | 7.61 | 9.72 | 4.40 | 11.48 |
| | 162.5 | 2.49 | 7.53 | 10.26 | 4.39 | 9.77 |
| | 187 | 2.56 | 7.59 | 10.17 | 4.42 | 11.22 |
| 50 | 0.5 | 6.85 | 7.53 | 10.79 | 4.12 | 9.55 |
| | 46 | 6.71 | 7.40 | 10.62 | 3.99 | 6.61 |
| | 139.5 | 5.88 | 7.32 | 9.27 | 4.01 | 5.01 |
| | 165 | 5.98 | 7.34 | 10.55 | 4.06 | 5.89 |
| | 190.5 | 5.85 | 7.30 | 9.11 | 3.95 | 4.68 |
| | 210.5 | 5.78 | 7.35 | 10.92 | 4.13 | 6.31 |
| 51 | 0.5 | 2.47 | 7.66 | 0.92 | 7.96 | 2.95 |
| | 46.5 | 2.17 | 7.70 | 0.95 | 8.27 | 3.48 |
| | 138.5 | 2.14 | 7.72 | 0.88 | 7.59 | 3.16 |
| | 194.5 | 1.82 | 7.74 | 0.96 | 7.66 | 3.63 |
| | 215.5 | 1.57 | 7.72 | 0.98 | 7.89 | 3.55 |
| | 306.5 | 1.84 | 7.74 | 1.02 | 8.08 | 3.98 |
| 52 | 0.5 | 0.00 | 7.80 | 5.11 | 10.34 | 23.44 |
| | 178 | 0.00 | 7.56 | 5.09 | 10.12 | 13.18 |

(Continued)

| № | t, hrs | biomass, $g_{wet}$/L | pH | Ca, mM/L | DIC, mM/L | $\Omega_{calcite}$ |
|---|---|---|---|---|---|---|
| 53 | 1 | 1.85 | 7.87 | 4.83 | 7.90 | 20.89 |
| | 68 | 2.02 | 7.42 | 4.59 | 7.88 | 6.92 |
| | 91 | 2.04 | 7.52 | 4.75 | 7.96 | 9.12 |
| | 109 | 2.22 | 7.48 | 4.56 | 7.93 | 7.94 |
| | 133 | 2.42 | 7.60 | 4.81 | 8.17 | 11.48 |
| | 158 | 2.45 | 7.51 | 4.88 | 8.16 | 9.33 |
| | 230 | 3.26 | 7.87 | 5.14 | 8.25 | 22.39 |
| | 253 | 3.61 | 7.96 | 4.88 | 8.79 | 28.18 |
| | 277 | 2.74 | 7.64 | 5.05 | 8.42 | 13.49 |
| 54 | 2.5 | 2.32 | 7.99 | 9.59 | 7.70 | 44.67 |
| | 23.5 | 2.19 | 7.78 | 9.80 | 7.75 | 28.84 |
| | 114.5 | 2.20 | 7.77 | 10.33 | 7.76 | 28.84 |
| | 163 | 2.02 | 7.74 | 9.78 | 7.76 | 26.30 |
| | 216 | 2.35 | 7.82 | 10.23 | 7.49 | 31.62 |
| | 284 | 2.15 | 7.77 | 9.78 | 7.65 | 27.54 |
| 55 | 0.5 | 1.60 | 8.13 | 0.92 | 13.84 | 12.88 |
| | 44.5 | 1.47 | 8.02 | 0.83 | 13.77 | 9.12 |
| | 72.5 | 1.74 | 7.99 | 0.83 | 13.87 | 8.51 |
| | 141 | 1.60 | 8.01 | 0.83 | 13.72 | 8.91 |
| | 195.6 | 1.40 | 8.05 | 0.89 | 13.82 | 10.47 |
| | 242.6 | 1.29 | 7.97 | 0.93 | 13.87 | 9.12 |
| 56 | 1 | 3.11 | 7.81 | 4.55 | 14.04 | 28.18 |
| | 43.5 | 2.35 | 7.67 | 4.52 | 13.89 | 19.95 |
| | 139 | 3.26 | 7.76 | 4.54 | 14.16 | 25.12 |
| | 187 | 3.09 | 7.64 | 4.18 | 14.15 | 17.78 |
| | 236.5 | 2.91 | 7.64 | 4.38 | 14.42 | 18.86 |
| | 307 | 2.29 | 7.69 | 4.40 | 13.99 | 20.42 |
| 57 | 1 | 2.32 | 8.15 | 9.39 | 14.03 | 104.70 |
| | 20 | 3.24 | 7.93 | 10.20 | 14.09 | 69.18 |
| | 94.5 | 1.67 | 8.01 | 9.16 | 13.92 | 75.86 |
| | 143.5 | 1.84 | 8.14 | 10.44 | 14.00 | 109.60 |
| | 187.5 | 1.92 | 8.08 | 10.16 | 13.89 | 95.50 |
| | 259.5 | 2.64 | 7.99 | 10.23 | 13.96 | 79.43 |
| 58 | 4 | 1.79 | 8.08 | 1.15 | 4.77 | 6.17 |
| | 24 | 3.12 | 7.97 | 1.30 | 5.00 | 5.62 |
| | 75 | 7.75 | 7.98 | 1.30 | 5.00 | 5.75 |
| | 101 | 11.14 | 7.95 | 1.16 | 5.00 | 4.79 |
| | 119.5 | 13.19 | 7.85 | 1.20 | 5.07 | 3.98 |
| | 167 | 16.28 | 7.86 | 1.20 | 5.51 | 4.47 |

## C. Other abiotic experiments in growth medium

*Bacteria A-20s*

| № | Type of experiment | t, hrs | pH | Ca, mM/L | DIC, mM/L | $\Omega_{calcite}$ |
|---|---|---|---|---|---|---|
| 59 | without bacteria | 0 | 7.99 | 9.78 | 5.79 | 32.68 |
| | | 120 | 7.5 | 9.66 | 5.37 | 10.47 |
| | | 168 | 7.44 | 9.53 | 5.24 | 8.91 |
| | | 288 | 7.32 | 9.48 | 5.68 | 7.08 |
| | | 300 | 7.3 | 9.5 | 5.7 | 6.78 |

(Continued)

| № | Type of experiment | t, hrs | pH | Ca, mM/L | DIC, mM/L | $\Omega_{calcite}$ |
|---|---|---|---|---|---|---|
| 60 | without bacteria, with $NaN_3$ | 0 | 8.05 | 9.11 | 4.75 | 31.62 |
| | | 120 | 7.85 | 9.21 | 5 | 21.38 |
| | | 168 | 7.75 | 9.19 | 5.19 | 17.78 |
| | | 288 | 7.64 | 8.74 | 6.03 | 15.14 |
| | | 300 | 7.62 | 9.11 | 6.01 | 14.79 |
| 61 | with bacteria, autoclave | 0 | 8.1 | 9.81 | 5.81 | 44.67 |
| | | 120 | 7.86 | 9.99 | 5.76 | 26.3 |
| | | 168 | 7.81 | 10.11 | 5.02 | 20.89 |
| | | 288 | 7.65 | 10.14 | 5.83 | 16.59 |
| | | 300 | 7.62 | 10.11 | 5.74 | 15.48 |
| 62 | live bacteria, without ligh | 0.5 | 7.53 | 10.79 | 4.12 | 9.55 |
| | | 46 | 7.4 | 10.62 | 3.99 | 6.61 |
| | | 140 | 7.32 | 9.27 | 4.01 | 5.01 |
| | | 165 | 7.34 | 10.55 | 4.06 | 5.89 |
| | | 191 | 7.3 | 9.11 | 3.95 | 4.68 |
| | | 211 | 7.35 | 10.92 | 4.13 | 6.31 |
| 63 | without bacteria | 0.5 | 7.91 | 1.12 | 9.89 | 7.41 |
| | | 744 | 7.8 | 1.08 | 9.94 | 5.62 |
| 64 | without bacteria | 0.5 | 7.99 | 5.56 | 10.04 | 37.15 |
| | | 178 | 7.55 | 5.43 | 10.1 | 13.48 |
| 65 | without bacteria | 0.5 | 7.89 | 5.06 | 10.11 | 27.54 |
| | | 168 | 7.56 | 5.14 | 9.99 | 13.18 |
| 66 | without bacteria | 0.5 | 7.95 | 5.11 | 10.12 | 32.36 |
| | | 744 | 7.67 | 5.05 | 9.94 | 16.98 |
| 67 | without bacteria | 0.5 | 7.92 | 10.06 | 10.23 | 51.29 |
| | | 744 | 7.84 | 10.02 | 9.98 | 41.69 |
| 68 | without bacteria | 0.5 | 8.11 | 4.88 | 19.6 | 72.44 |
| | | 168 | 8.01 | 4.9 | 20.57 | 61.66 |

*Bacteria S-17-65*

| № | Type of experiment | t, hrs | pH | Ca, mM/L | DIC, mM/L | $\Omega_{calcite}$ |
|---|---|---|---|---|---|---|
| 69 | live bacteria without ligh | 0.5 | 7.53 | 10.79 | 4.12 | 9.54 |
| | | 46 | 7.40 | 10.62 | 3.99 | 6.61 |
| | | 139.5 | 7.32 | 9.27 | 4.01 | 5.01 |
| | | 165 | 7.34 | 10.55 | 4.06 | 5.89 |
| | | 190.5 | 7.30 | 9.11 | 3.95 | 4.68 |
| | | 210.5 | 7.35 | 10.92 | 4.13 | 6.31 |
| 70 | without bacteria | 0.5 | 7.67 | 5.14 | 9.89 | 16.98 |
| | | 168 | 7.55 | 5.23 | 9.87 | 12.88 |
| 71 | without bacteria | 0.5 | 7.67 | 9.67 | 10.23 | 28.18 |
| | | 168 | 7.56 | 9.78 | 10.11 | 21.88 |
| 72 | without bacteria | 0.5 | 7.62 | 5.12 | 9.98 | 15.14 |
| | | 178 | 7.55 | 5.10 | 9.90 | 12.59 |

(Continued)

**D. Kinetic experiments in inert electrolyte.**

*Bacteria A-20s*

| № | Type of experiment | t, hrs | biomass, $g_{wet}$/L | pH | Ca, mM/L | Alk, mM/L | $\Omega_{calcite}$ |
|---|---|---|---|---|---|---|---|
| 73 | live bacteria | 0 | 15.68 | 9.73 | 0.71 | 3.98 | 52.50 |
| | | 18.7 | 14.63 | 9.39 | 0.84 | 4.20 | 44.70 |
| | | 41.5 | 14.16 | 9.32 | 0.75 | 4.10 | 33.88 |
| | | 69 | 13.69 | 8.78 | 0.73 | 4.12 | 14.79 |
| | | 90.5 | 13.22 | 8.63 | 0.88 | 4.17 | 13.49 |
| | | 115 | 12.99 | 8.38 | 0.83 | 4.24 | 7.76 |
| | | 140.5 | 12.75 | 8.33 | 0.81 | 4.31 | 6.90 |
| | | 180.8 | 12.29 | 8.56 | 0.83 | 4.30 | 11.20 |
| | | 373 | 11.58 | 8.68 | 0.79 | 4.06 | 13.18 |
| 74 | live bacteria | 0 | 16.85 | 9.39 | 1.73 | 3.37 | 69.20 |
| | | 18.7 | 14.16 | 8.98 | 1.96 | 3.50 | 43.70 |
| | | 41.5 | 13.57 | 8.87 | 1.82 | 3.51 | 33.88 |
| | | 69 | 13.22 | 8.35 | 1.91 | 4.76 | 16.98 |
| | | 90.5 | 12.99 | 8.47 | 1.48 | 3.46 | 13.18 |
| | | 115 | 12.64 | 8.46 | 1.77 | 3.46 | 13.18 |
| | | 140.5 | 12.52 | 8.40 | 1.95 | 3.64 | 15.84 |
| | | 180.8 | 11.93 | 8.45 | 1.92 | 3.45 | 15.50 |
| | | 373 | 10.88 | 8.50 | 1.89 | 3.51 | 17.38 |
| 75 | live bacteria | 0 | 15.80 | 9.11 | 5.47 | 3.10 | 97.70 |
| | | 18.7 | 14.98 | 8.62 | 4.89 | 3.11 | 40.70 |
| | | 41.5 | 14.16 | 8.67 | 4.48 | 3.51 | 46.77 |
| | | 69 | 13.81 | 8.48 | 5.12 | 2.28 | 23.98 |
| | | 90.5 | 13.81 | 8.53 | 3.60 | 2.47 | 21.87 |
| | | 115 | 13.46 | 8.37 | 4.93 | 3.07 | 25.12 |
| | | 140.5 | 13.22 | 8.20 | 5.37 | 3.08 | 19.05 |
| | | 180.8 | 12.52 | 7.97 | 5.25 | 3.13 | 11.74 |
| | | 373 | 12.40 | 8.36 | 5.09 | 3.09 | 25.70 |
| 76 | live bacteria | 0 | 17.32 | 9.11 | 8.33 | 2.98 | 102.32 |
| | | 18.7 | 14.39 | 8.70 | 7.67 | 3.42 | 66.07 |
| | | 41.5 | 13.69 | 8.73 | 6.18 | 3.34 | 60.23 |
| | | 69 | 12.99 | 8.51 | 8.65 | 3.39 | 51.29 |
| | | 90.5 | 12.75 | 8.48 | 8.32 | 3.33 | 46.77 |
| | | 115 | 12.52 | 8.31 | 8.41 | 3.44 | 35.48 |
| | | 140.5 | 12.40 | 8.24 | 8.24 | 3.33 | 29.52 |
| | | 180.8 | 11.82 | 8.16 | 7.23 | 3.45 | 23.98 |
| | | 373 | 10.88 | 8.54 | 7.83 | 3.50 | 52.48 |
| 77 | live bacteria | 0 | 17.78 | 9.10 | 12.13 | 2.89 | 112.20 |
| | | 18.7 | 14.63 | 8.57 | 11.85 | 3.36 | 67.62 |
| | | 41.5 | 14.04 | 8.48 | 12.21 | 3.32 | 57.54 |
| | | 69 | 13.34 | 8.33 | 11.56 | 3.30 | 43.65 |
| | | 90.5 | 13.34 | 8.16 | 10.60 | 3.24 | 28.84 |
| | | 115 | 12.99 | 8.25 | 12.07 | 3.28 | 38.02 |
| | | 140.5 | 12.64 | 8.17 | 12.80 | 3.24 | 33.11 |
| | | 180.8 | 12.05 | 8.23 | 12.18 | 3.15 | 34.67 |
| | | 373 | 11.23 | 7.74 | 12.18 | 3.17 | 13.18 |

(Continued)

| № | Type of experiment | t, hrs | biomass, $g_{wet}$/L | pH | Ca, mM/L | Alk, mM/L | $\Omega_{calcite}$ |
|---|---|---|---|---|---|---|---|
| 78 | live bacteria | 0 | 15.44 | 9.06 | 16.78 | 2.74 | 134.90 |
| | | 18.7 | 14.51 | 8.24 | 15.30 | 2.87 | 37.15 |
| | | 41.5 | 14.04 | 8.02 | 16.43 | 2.97 | 26.30 |
| | | 69 | 13.46 | 8.34 | 15.62 | 2.85 | 44.67 |
| | | 90.5 | 13.22 | 8.11 | 14.17 | 2.87 | 28.18 |
| | | 115 | 12.87 | 7.93 | 16.01 | 2.88 | 20.89 |
| | | 140.5 | 12.75 | 7.79 | 15.41 | 2.93 | 15.48 |
| | | 180.8 | 11.82 | 8.15 | 15.06 | 2.80 | 30.20 |
| | | 373 | 11.00 | 7.93 | 16.34 | 2.93 | 21.88 |
| 79 | autoklaved bacteria | 0.5 | 5.15 | 8.64 | 2.97 | 4.66 | 41.68 |
| | | 22.75 | 4.22 | 7.57 | 2.90 | 4.50 | 4.26 |
| | | 40.25 | 4.12 | 7.38 | 2.92 | 4.51 | 2.82 |
| | | 69.75 | 5.38 | 7.35 | 2.97 | 4.50 | 2.63 |
| 80 | autoklaved bacteria | 0.5 | 5.37 | 8.41 | 9.49 | 4.89 | 64.56 |
| | | 22.75 | 4.48 | 7.53 | 9.04 | 4.80 | 10.00 |
| | | 40.25 | 4.22 | 6.98 | 9.16 | 5.00 | 3.02 |
| | | 69.75 | 5.59 | 7.14 | 9.21 | 4.99 | 4.36 |
| 81 | autoklaved bacteria | 0.5 | 5.00 | 8.10 | 18.88 | 5.01 | 54.95 |
| | | 22.75 | 3.58 | 7.39 | 17.82 | 5.00 | 12.02 |
| | | 40.25 | 3.35 | 7.08 | 18.33 | 4.88 | 6.03 |
| | | 69.75 | 4.00 | 7.06 | 17.89 | 4.99 | 5.75 |
| 82 | without bacteria | 0 | 0 | 8.65 | 3.11 | 4.66 | 43.65 |
| | | 21.5 | 0 | 8.54 | 3.08 | 4.65 | 35.48 |
| | | 48 | 0 | 8.23 | 2.69 | 4.67 | 17.38 |
| | | 73.25 | 0 | 8.31 | 2.91 | 4.67 | 21.88 |
| 83 | without bacteria | 0 | 0 | 8.73 | 9.58 | 4.78 | 107.15 |
| | | 21.5 | 0 | 7.68 | 9.90 | 4.08 | 12.88 |
| | | 48 | 0 | 7.55 | 9.25 | 3.99 | 8.91 |
| | | 73.25 | 0 | 7.53 | 8.46 | 4.04 | 8.13 |
| 84 | without bacteria | 0 | 0 | 8.29 | 19.83 | 4.63 | 74.13 |
| | | 21.5 | 0 | 7.82 | 19.21 | 4.56 | 28.84 |
| | | 48 | 0 | 8.06 | 19.78 | 4.31 | 45.71 |
| | | 73.25 | 0 | 7.55 | 18.85 | 3.98 | 14.12 |
| 85 | without bacteria | 0.5 | 0 | 7.67 | 5.11 | 9.98 | 17.37 |
| | | 744 | 0 | 7.26 | 4.98 | 9.88 | 6.76 |

*Bacteria S-17-65*

| No | Type of experiment | t, hrs | biomass, $g_{wet}$/L | pH | Ca, mM/L | Alk, mM/L | $\Omega_{calcite}$ |
|---|---|---|---|---|---|---|---|
| 86 | live bacteria | 0.5 | 2.90 | 8.63 | 5.69 | 10.65 | 131.80 |
| | | 24 | 3.27 | 8.80 | 5.04 | 10.64 | 158.50 |
| | | 47 | 3.20 | 8.71 | 5.06 | 10.70 | 138.00 |
| | | 94 | 3.18 | 8.77 | 5.01 | 10.65 | 151.40 |
| | | 214 | 3.23 | 8.76 | 4.86 | 10.50 | 144.54 |
| | | 234 | 2.96 | 8.74 | 4.83 | 10.71 | 141.25 |
| | | 263 | 3.21 | 8.76 | 4.86 | 10.55 | 144.54 |
| | | 330 | 3.10 | 8.75 | 4.99 | 10.42 | 144.54 |
| 87 | live bacteria | 0.5 | 2.89 | 8.58 | 5.33 | 10.18 | 112.20 |
| | | 744 | 2.19 | 7.55 | 5.30 | 10.20 | 13.80 |

(Continued)

| No | Type of experiment | t, hrs | biomass, $g_{wet}$/L | pH | Ca, mM/L | Alk, mM/L | $\Omega_{calcite}$ |
|---|---|---|---|---|---|---|---|
| 88 | live bacteria | 0.5 | 2.87 | 8.61 | 5.07 | 10.71 | 117.50 |
| | with $NaN_3$ | 24 | 2.82 | 8.55 | 5.13 | 10.56 | 107.20 |
| | | 47 | 2.19 | 8.65 | 5.24 | 10.71 | 128.80 |
| | | 94 | 2.47 | 8.71 | 5.21 | 10.55 | 141.30 |
| | | 214 | 2.23 | 8.70 | 4.81 | 10.50 | 128.80 |
| | | 234 | 2.32 | 8.69 | 5.22 | 10.76 | 138.10 |
| | | 263 | 2.45 | 8.70 | 5.22 | 10.65 | 138.10 |
| | | 330 | 2.47 | 8.63 | 5.07 | 10.62 | 114.50 |
| 89 | live bacteria | 360 | 7.21 | 8.22 | 3.00 | 4.39 | 18.2 |
| | | | 6.89 | 6.85 | 2.97 | 4.34 | 0 |
| 90 | live bacteria | 360 | 4.36 | 8.08 | 7.09 | 4.49 | 26.92 |
| | | | 3.78 | 6.96 | 6.38 | 4.34 | 1.62 |
| 91 | live bacteria | 360 | 4.12 | 7.88 | 14.61 | 4.19 | 26.3 |
| | | | 3.34 | 7.64 | 10.88 | 4.2 | 12.59 |

# Appendix 4

# Summary of kinetic experiments with *Gloeocapsa* sp.

| № | t, hrs | t, days | biomass, gwet/L | pH | Ca, mM/L | Alkalinity, mM/L | Ω calcite |
|---|---|---|---|---|---|---|---|
| 1 | 192 | 8 | 0,62 | 9,56 | 2,77 | 2,84 | 89,1 |
| | 288 | 12 | 0,88 | 9,42 | 3,03 | 2,53 | 74,1 |
| | 336 | 14 | 1,08 | 9,4 | 2,87 | 2,61 | 72,4 |
| | 432 | 18 | 1,24 | 9,26 | 2,59 | 2,76 | 61,7 |
| | 552 | 23 | 1,46 | 9,08 | 2,72 | 2,77 | 50,1 |
| | 624 | 26 | 1,46 | 9,01 | 2,74 | 3,36 | 54,9 |
| 2 | 192 | 8 | 0,68 | 9,1 | 5,81 | 2,44 | 70,8 |
| | 288 | 12 | 0,76 | 8,92 | 5,38 | 1,85 | 41,7 |
| | 336 | 14 | 0,92 | 8,87 | 6,04 | 1,85 | 41,7 |
| | 432 | 18 | 1,04 | 8,71 | 6,49 | 2,42 | 43,7 |
| | 552 | 23 | 1,12 | 8,61 | 7,30 | 2,53 | 41,7 |
| | 624 | 26 | 1,22 | 8,71 | 7,73 | 2,98 | 58,9 |
| 3 | 0 | 0 | 0,18 | 9 | 2,75 | 4,56 | 69,2 |
| | 72 | 3 | 0,56 | 9,73 | 1,93 | 3,21 | 89,3 |
| | 120 | 5 | 1 | 9,58 | 1,42 | 2,46 | 52,5 |
| | 168 | 7 | 0,92 | 9,44 | 1,31 | 2,55 | 44,7 |
| | 216 | 9 | 1,44 | 9,57 | 1,28 | 2,18 | 43,7 |
| | 264 | 11 | 1,7 | 9,31 | 1,04 | 2,14 | 27,5 |
| | 336 | 14 | 1,78 | 9,14 | 1,25 | 2,66 | 30,2 |
| | 408 | 17 | 1,92 | 9,07 | 1,47 | 2,66 | 30,9 |
| 4 | 0 | 0 | 0,14 | 8,83 | 4,83 | 4,53 | 79,4 |
| | 72 | 3 | 0,66 | 9,62 | 3,97 | 1,89 | 74,1 |
| | 120 | 5 | 1,02 | 9,91 | 3,48 | 1,95 | 85,1 |
| | 168 | 7 | 1,28 | 9,9 | 3,37 | 2,16 | 91,2 |
| | 216 | 9 | 1,88 | 9,96 | 2,86 | 1,7 | 69,2 |
| | 264 | 11 | 2,2 | 9,77 | 3,41 | 2,21 | 89,1 |
| | 336 | 14 | 2,38 | 9,82 | 3,45 | 1,87 | 77,6 |
| | 408 | 17 | 2,62 | 9,46 | 3,47 | 1,49 | 50,1 |
| 5 | 0 | 0 | 0,14 | 8,69 | 9,19 | 1,43 | 30,9 |
| | 72 | 3 | 0,68 | 9,55 | 7,62 | 1,75 | 81,3 |
| | 120 | 5 | 0,78 | 9,45 | 7,61 | 1,72 | 75,9 |
| | 168 | 7 | 1,12 | 9,39 | 6,93 | 1,83 | 75,9 |
| | 216 | 9 | 1,58 | 9,25 | 5,97 | 1,85 | 64,6 |
| | 264 | 11 | 1,86 | 9,43 | 6,18 | 2,21 | 89,1 |
| | 336 | 14 | 2,18 | 9,14 | 2,75 | 1,56 | 32,4 |
| | 408 | 17 | 2,7 | 9,1 | 7,46 | 1,89 | 61,6 |
| 6 | 0 | 0 | 0,12 | 8,58 | 13,11 | 0,7 | 15,1 |
| | 72 | 3 | 0,78 | 9,35 | 11,63 | 0,99 | 45,7 |
| | 120 | 5 | 1,5 | 9,55 | 10,34 | 0,89 | 43,6 |
| | 168 | 7 | 1,72 | 9,44 | 10,45 | 1,17 | 54,9 |
| | 216 | 9 | 2,04 | 9,63 | 19,43 | 1,63 | 91,2 |
| | 264 | 11 | 2,26 | 9,72 | 13,02 | 2,08 | 114,8 |
| | 336 | 14 | 2,5 | 9,94 | 11,04 | 1,42 | 77,6 |
| | 408 | 17 | 2,92 | 9,82 | 10,75 | 1,47 | 79,4 |
| 7 | 0 | 0 | 0,12 | 8,44 | 20,60 | 3,75 | 79,4 |
| | 72 | 3 | 0,52 | 9,26 | 21,14 | 1,52 | 75,9 |
| | 120 | 5 | 0,82 | 9,63 | 24,00 | 1,51 | 87,1 |
| | 168 | 7 | 1,08 | 9,79 | 19,20 | 1,71 | 97,7 |
| | 216 | 9 | 1,4 | 9,87 | 14,73 | 1,55 | 87,1 |
| | 264 | 11 | 1,42 | 9,79 | 19,80 | 1,56 | 89,1 |
| | 336 | 14 | 1,6 | 9,41 | 18,60 | 1,54 | 81,3 |
| | 408 | 17 | 2,76 | 9,45 | 18,82 | 1,03 | 54,9 |

| № | t, hrs | t, days | biomass, gwet/L | pH | Ca, mM/L | Alkalinity, mM/L | Ω calcite |
|---|---|---|---|---|---|---|---|
| 8 | 0 | 0 | 0,12 | 8,27 | 44,97 | 2,61 | 57,5 |
| | 72 | 3 | 0,4 | 9,29 | 36,17 | 2,8 | 154,9 |
| | 120 | 5 | 0,76 | 9,78 | 34,81 | 0,91 | 52,5 |
| | 168 | 7 | 0,9 | 9,42 | 39,77 | 1,21 | 69,2 |
| | 216 | 9 | 1,4 | 9,47 | 33,33 | 1,26 | 72,4 |
| | 264 | 11 | 1,54 | 9,72 | 25,77 | 0,93 | 52,5 |
| | 336 | 14 | 2,28 | 9,95 | 26,70 | 0,98 | 54,9 |
| | 408 | 17 | 1,98 | 9,56 | 38,24 | 0,94 | 53,7 |
| 9 | 0 | 0 | 0,15 | 9,37 | 1,00 | 10,00 | 75,8 |
| | 48 | 2 | | 9,7 | | | |
| | 72 | 3 | 0,66 | 10,35 | 0,11 | 7,70 | 12,0 |
| | 120 | 5 | 0,82 | 10,3 | 0,07 | 7,83 | 7,4 |
| | 216 | 9 | 1,22 | 9,74 | 0,09 | | |
| | 264 | 11 | 1,22 | 9,58 | | 8,00 | |
| | 356 | 15 | 1,22 | 9,49 | 0,09 | 7,95 | 6,7 |
| 10 | 0 | 0 | 0,15 | 8,79 | 5,00 | 10,00 | 147,9 |
| | 48 | 2 | | 8,89 | | | |
| | 72 | 3 | 0,64 | 9,92 | 0,31 | 2,63 | 19,9 |
| | 120 | 5 | 1,12 | 10,23 | 0,17 | 2,59 | 13,2 |
| | 216 | 9 | 1,62 | 9,49 | 0,22 | 2,53 | 9,8 |
| | 264 | 11 | 1,62 | 9,39 | 0,21 | | |
| | 356 | 15 | 1,74 | 9,19 | 0,24 | | |
| 11 | 0 | 0 | 0,15 | 8,17 | 10,00 | 10,00 | 81,3 |
| | 48 | 2 | | 8,46 | | | |
| | 72 | 3 | 0,52 | 9,47 | 2,30 | 0,45 | 12,6 |
| | 120 | 5 | 0,90 | 9,51 | 2,13 | 0,50 | 13,8 |
| 12 | 0 | 0 | 0,10 | 7,71 | 20,00 | 10,00 | 50,1 |
| | 48 | 2 | | 7,91 | | | |
| | 72 | 3 | 0,10 | 8,50 | 9,29 | 4,98 | 75,9 |
| | 120 | 5 | 0,62 | 9,25 | 8,83 | 0,37 | 14,5 |
| | 216 | 9 | 1,12 | 8,85 | 8,44 | 0,30 | 7,8 |
| | 264 | 11 | 1,32 | 8,83 | 9,11 | 0,31 | 8,1 |
| | 356 | 15 | 1,52 | 8,54 | 9,26 | | |
| 13 | 0 | 0 | | 7,42 | 20,00 | 10,00 | 26,9 |
| | 48 | 2 | | 7,9 | | | |
| | | | without | | | | |
| | 72 | 3 | bacteria | 8,23 | 9,12 | 0,93 | 8,9 |
| | 120 | 5 | | 7,98 | 9,13 | 0,81 | 4,7 |
| | 356 | 15 | | 7,89 | 9,04 | | |
| 14 | 0 | 0 | | 9,37 | 1,00 | 10,00 | 75,9 |
| | 48 | 2 | | 9,34 | | | |
| | 72 | 3 | 0,42 | 9,67 | 0,13 | 8,53 | 12,3 |
| | 120 | 5 | 0,82 | 9,97 | 0,08 | 9,55 | 8,9 |
| | 216 | 9 | 1,76 | 9,62 | 0,10 | 4,40 | 7,2 |
| | 264 | 11 | 1,88 | 9,73 | 0,09 | 12,30 | 8,9 |
| 15 | 0 | 0 | 0,15 | 8,51 | 5,00 | 10,00 | 93,3 |
| | 48 | 2 | | 8,93 | | | |
| | 72 | 3 | 0,46 | 9,01 | 0,48 | 2,43 | 10,0 |
| | 120 | 5 | 0,94 | 9,25 | 0,45 | 2,72 | 14,8 |
| | 216 | 9 | 2,3 | 9,62 | 0,42 | 3,52 | 25,1 |
| | 264 | 11 | 3,16 | 9,1 | 0,46 | 4,85 | 18,2 |

| № | t, hrs | t, days | biomass, gwet/L | pH | Ca, mM/L | Alkalinity, mM/L | Ω calcite |
|---|---|---|---|---|---|---|---|
| 16 | 0 | 0 | 0,15 | 7,75 | 10,00 | 10,00 | 34,7 |
| | 48 | 2 | | 9,02 | | | |
| | 72 | 3 | 0,8 | 8,71 | 1,83 | 10,40 | 58,9 |
| | 120 | 5 | 1,48 | 8,58 | 1,80 | 9,70 | 43,7 |
| 17 | 0 | 0 | 0,15 | 7,46 | 20,00 | 10,00 | 29,5 |
| | 48 | 2 | | 8,16 | | | |
| | 72 | 3 | 0,38 | 8,37 | 10,27 | 0,60 | 8,1 |
| | 120 | 5 | 0,84 | 8,34 | 10,86 | 0,59 | 7,8 |
| 18 | 0 | 0 | | 7,4 | 20,00 | 10,00 | 25,7 |
| | | | without | | | | |
| | 48 | 2 | bacteria | 7,74 | | | |
| | 72 | 3 | | 9,11 | | 0,95 | |
| | 120 | 5 | | 8,01 | 7,96 | 0,83 | 4,7 |
| 19 | 0 | 0 | 0,04 | 8,86 | 1,80 | 4,27 | 38,0 |
| | 24 | 1 | 0,08 | 8,93 | 0,85 | 2,93 | 16,9 |
| | 48 | 2 | 0,44 | 9,13 | 0,25 | 2,90 | 7,6 |
| | 72 | 3 | 0,5 | 9,92 | 0,12 | 2,72 | 7,9 |
| | 120 | 5 | 0,74 | 9,99 | 0,09 | 2,80 | 6,3 |
| | 144 | 6 | 0,86 | 10,59 | 0,12 | | |
| | 168 | 7 | 0,94 | 9,99 | 0,12 | | |
| | 192 | 8 | 1,12 | 10,09 | 0,11 | | |
| | 284 | 12 | 1,98 | 9,14 | 0,13 | | |
| 20 | 0 | 0 | 0,04 | 8,82 | 4,500 | 4,3 | 70,8 |
| | 24 | 1 | 0,08 | 8,45 | 1,176 | 1,03 | 3,4 |
| | 48 | 2 | 0,52 | 9,73 | 0,514 | 0,92 | 12,6 |
| | 72 | 3 | 0,5 | 10,31 | 0,453 | 0,87 | 13,8 |
| | 120 | 5 | 0,6 | 10,81 | 0,456 | 0,88 | 6,3 |
| | 144 | 6 | 0,62 | 10,97 | 0,460 | | |
| | 168 | 7 | 0,62 | 10,96 | 0,485 | | |
| | 192 | 8 | 0,68 | 10,48 | 0,486 | | |
| | 284 | 12 | 1,2 | 8,75 | 0,573 | | |
| 21 | 0 | 0 | 0,04 | 8,73 | 9,000 | 4,96 | 107,2 |
| | 24 | 1 | 0,16 | 8,14 | 3,216 | 1,57 | 6,0 |
| | 48 | 2 | 0,64 | 9,55 | 2,535 | 0,35 | 10,7 |
| | 72 | 3 | 0,6 | 9,59 | 2,564 | 0,32 | 9,8 |
| | 120 | 5 | 0,81 | 9,77 | 2,602 | 0,39 | 13,2 |
| | 144 | 6 | 0,8 | 10,14 | 2,704 | | |
| | 168 | 7 | 1,06 | 9,72 | 2,677 | 0,37 | 12,3 |
| | 192 | 8 | 0,86 | 9,54 | 2,692 | | |
| | 284 | 12 | 2,28 | 8,62 | | 0,77 | |
| 22 | 0 | 0 | | 8,6 | 9,000 | 4,47 | 79,4 |
| | | | without | | | | |
| | 24 | 1 | bacteria | 8,38 | 3,903 | 2,4 | 16,9 |
| | 48 | 2 | | 8,24 | 3,650 | 1,23 | 6,5 |
| | 72 | 3 | | | | | |
| | 284 | 12 | | 7,89 | 5,452 | 0,8 | 2,7 |

| № | t, hrs | t, days | biomass, gwet/L | pH | Ca, mM/L | Alkalinity, mM/L | Ω calcite |
|---|---|---|---|---|---|---|---|
| 23 | 0 | 0 | 0,17 | 8,64 | 1,52 | 4,43 | 23,4 |
| | 24 | 1 | 0,18 | 9,47 | 1,41 | 3,56 | 63,1 |
| | 44 | 2 | 0,28 | 9,66 | 0,67 | 3,59 | 39,8 |
| | 91 | 4 | 0,41 | 9,65 | 0,13 | 3,3 | 8,1 |
| | 115 | 5 | 0,48 | 9,76 | 0,19 | 3 | 12,3 |
| | 211 | 9 | 0,56 | 9,38 | 0,21 | 2,87 | 8,91 |
| | 259 | 11 | 0,62 | 9,4 | 0,22 | 2,76 | 9,33 |
| | 306 | 13 | 0,57 | 9,31 | 0,21 | 3,18 | 8,71 |
| | 378 | 16 | 0,52 | 9,33 | 0,27 | 3,01 | 10,9 |
| | 408 | 17 | 0,59 | 9,16 | 0,19 | 3,27 | 6,61 |
| | 427 | 18 | 0,55 | 9,43 | 0,2 | 3,32 | 7,94 |
| | 451 | 19 | 0,59 | 9,27 | 0,16 | 3,42 | 6,61 |
| | 479 | 20 | 0,55 | 9,19 | 0,18 | 3,27 | 6,64 |
| | 547 | 23 | 0,66 | 9,33 | 0,24 | 3,48 | 10,72 |
| | 811 | 34 | 0,63 | 9,51 | 0,2 | 3,4 | 10,96 |
| | 984 | 41 | 0,68 | 9,36 | 0,19 | 4 | 9,77 |
| | 1098 | 46 | 0,75 | 9,02 | 0,17 | 4,27 | 5,62 |
| | 1296 | 54 | 0,63 | 9,04 | 0,14 | 4,15 | 4,79 |
| | 1538 | 64 | 0,65 | 9,06 | 0,17 | 4,9 | 6,61 |
| | 1754 | 73 | 0,71 | 9,17 | 0,17 | 5,45 | 8,13 |
| | 2834 | 118 | 1,05 | 9,28 | | 7,36 | 6,46 |
| | 3276 | 136 | 1,08 | 9,3 | | 8,98 | 6,46 |
| 24 | 0 | 0 | 0,17 | 8,64 | 1,52 | 4,43 | 23,4 |
| | 24 | 1 | 0,12 | 8,5 | 1,48 | 4,73 | 18,2 |
| | 44 | 2 | 0,12 | 8,58 | 1,29 | 4,72 | 19,1 |
| | 91 | 4 | 0,08 | 8,62 | 1,1 | 4,91 | 18,2 |
| | 115 | 5 | 0,15 | 8,61 | 1,05 | 4,5 | 16,2 |
| | 211 | 9 | 0,12 | 8,37 | 0,95 | 4,45 | 9,1 |
| | 259 | 11 | 0,10 | 8,46 | 0,66 | 3,83 | 6,9 |
| | 306 | 13 | 0,13 | 8,44 | 0,67 | 3,76 | 6,6 |
| | 378 | 16 | 0,11 | 8,54 | 0,55 | 2,68 | 5 |
| | 408 | 17 | 0,09 | 8,65 | 0,51 | 3 | 6,5 |
| | 427 | 18 | 0,12 | 8,56 | 0,54 | 3,52 | 6,5 |
| | 451 | 19 | 0,10 | 8,55 | 0,39 | 3,25 | 4,4 |
| | 479 | 20 | 0,11 | 8,57 | 0,35 | 3,15 | 3,9 |
| | 547 | 23 | 0,10 | 8,65 | 0,48 | 2,82 | 5,8 |
| | 811 | 34 | 0,12 | 8,87 | 0,53 | 3,57 | 8,6 |
| | 984 | 41 | 0,15 | 8,84 | 0,42 | 3,64 | 8,9 |
| | 1098 | 46 | 0,12 | 8,63 | 0,28 | 3,54 | 3,9 |
| | 1296 | 54 | 0,12 | 8,65 | 0,38 | 3,77 | 5,9 |
| | 1538 | 64 | 0,10 | 8,64 | 0,46 | 3,77 | 6,9 |
| | 1754 | 73 | 0,11 | 8,75 | 0,37 | 3,94 | 7,1 |
| | 2834 | 118 | 0,16 | 8,77 | | 4,44 | 10 |
| | 3276 | 136 | 0,16 | 8,86 | | 3,8 | 2,8 |

| № | t, hrs | t, days | biomass, gwet/L | pH | Ca, mM/L | Alkalinity, mM/L | Ω calcite |
|---|---|---|---|---|---|---|---|
| 25 | 28 | 1,2 | 0,29 | 9,026 | 1,48 | 4,36 | 42,6 |
| | 44 | 1,8 | 0,35 | 8,79 | 0,58 | 3,12 | 9,8 |
| | 91 | 3,8 | 0,45 | 8,64 | 0,45 | 3,51 | 6,5 |
| | 115 | 4,8 | 0,43 | 8,69 | 0,39 | 3,5 | 6,2 |
| | 211 | 8,8 | 0,37 | 8,67 | 0,45 | 3,53 | 6,8 |
| | 259 | 10,8 | 0,42 | 8,62 | 0,34 | 3,5 | 4,7 |
| | 307 | 12,8 | 0,19 | 8,73 | 0,46 | 3,61 | 7,9 |
| | 379 | 15,8 | 0,24 | 8,66 | 0,4 | 3,58 | 6,0 |
| | 409 | 17,0 | 0,31 | 8,73 | 0,41 | 3,34 | 6,6 |
| | 452 | 18,8 | 0,30 | 8,68 | 0,31 | 3,39 | 4,7 |
| | 548 | 22,8 | 0,25 | 8,7 | 0,32 | 3,61 | 5,3 |
| 26 | 0 | 0 | 0,17 | 8,66 | 0,77 | 10,78 | 24,5 |
| | 24 | 1 | 0,17 | 9,31 | 0,72 | 9,74 | 51,3 |
| | 44 | 2 | 0,23 | 9,54 | 0,52 | 8,87 | 43,6 |
| | 91 | 4 | 0,38 | 9,63 | 0,11 | 8,83 | 10 |
| | 115 | 5 | 0,48 | 9,65 | 0,13 | 6,63 | 10,9 |
| | 211 | 9 | 0,47 | 9,68 | 0,13 | 8,17 | 11,7 |
| | 259 | 11 | 0,54 | 9,59 | 0,13 | 9,01 | 11,5 |
| | 306 | 13 | 0,41 | 9,58 | 0,18 | 9,33 | 15,8 |
| | 378 | 16 | 0,57 | 9,36 | 0,12 | 9,63 | 9,3 |
| | 408 | 17 | 0,56 | 9,67 | 0,11 | 9,41 | 10,5 |
| | 427 | 18 | 0,47 | 9,45 | 0,12 | 6,88 | 8,7 |
| | 451 | 19 | 0,49 | 9,46 | 0,10 | 9,56 | 8,3 |
| | 479 | 20 | 0,46 | 9,43 | 0,19 | 9,37 | 15,1 |
| | 547 | 23 | 0,58 | 9,49 | 0,15 | 9,73 | 12,9 |
| | 811 | 34 | 0,54 | 9,48 | 0,10 | 10,64 | 8,7 |
| | 984 | 41 | 0,72 | 9,75 | 0,11 | 11,16 | 11,2 |
| | 1098 | 46 | 0,56 | 9,5 | 0,14 | 10,76 | 12,3 |
| | 1296 | 54 | 0,44 | 9,46 | 0,09 | 9,35 | 7,4 |
| | 1538 | 64 | 0,44 | 9,51 | 0,08 | 12,72 | 7,4 |
| | 1754 | 73 | 0,45 | 9,57 | 0,14 | 13,75 | 13,8 |
| | 2834 | 118 | 1,02 | 9,45 | 0,07 | 17,14 | 6,8 |
| | 3276 | 136 | 0,82 | 9,51 | 0,09 | 17,53 | 9,1 |

| № | t, hrs | t, days | biomass, gwet/L | pH | Ca, mM/L | Alkalinity, mM/L | Ω calcite |
|---|---|---|---|---|---|---|---|
| 27 | 0 | 0 | 0,17 | 8,66 | 0,77 | 10,78 | 24,5 |
| | 24 | 1 | 0,13 | 8,7 | 0,73 | 10,73 | 25,1 |
| | 44 | 2 | 0,11 | 8,84 | 0,61 | 8,76 | 23,4 |
| | 91 | 4 | 0,09 | 8,86 | 0,35 | 8,97 | 14,1 |
| | 115 | 5 | 0,14 | 8,77 | 0,29 | 6,99 | 8,7 |
| | 211 | 9 | 0,10 | 8,99 | 0,17 | 8,52 | 8,1 |
| | 259 | 11 | 0,11 | 8,98 | 0,14 | 8,73 | 6,8 |
| | 306 | 13 | 0,12 | 9,03 | 0,15 | 8,84 | 7,8 |
| | 378 | 16 | 0,11 | 9,02 | 0,14 | 8,6 | 7,1 |
| | 408 | 17 | 0,12 | 9,69 | 0,14 | 7,54 | 12,6 |
| | 427 | 18 | 0,10 | 9,02 | 0,14 | 6,74 | 6,2 |
| | 451 | 19 | 0,10 | 8,99 | 0,13 | 8,4 | 6,3 |
| | 479 | 20 | 0,10 | 9,02 | 0,13 | 8,98 | 6,8 |
| | 547 | 23 | 0,10 | 9,1 | 0,14 | 9,25 | 8,1 |
| | 811 | 34 | 0,18 | 8,73 | 0,11 | 9,64 | 3,9 |
| | 984 | 41 | 0,15 | 9,3 | 0,09 | 9,83 | 6,6 |
| | 1098 | 46 | 0,11 | 9,08 | 0,15 | 9 | 8,3 |
| | 1296 | 54 | 0,15 | 9,05 | 0,15 | 8,88 | 7,9 |
| | 1538 | 64 | 0,08 | 9,05 | 0,14 | 10,06 | 7,9 |
| | 1754 | 73 | 0,13 | 9,18 | 0,08 | 11,2 | 5,5 |
| | 2834 | 118 | 0,13 | 9,18 | 0,12 | 13,34 | 8,9 |
| | 3276 | 136 | 0,15 | 9,28 | 0,12 | 11,62 | 9,3 |
| | 894 | 38 | 0,99 | 11,64 | 0 | | |
| | 1062 | 46 | 1,116 | 11,54 | 0 | | |
| | 1230 | 53 | 1,195 | 11,17 | 0 | | |
| | 1518 | 65 | 1,308 | 10,15 | 0 | | |
| 30 | 0 | 1 | 0,097 | 9,3 | 0,011 | | |
| | 28 | 2 | 0,114 | | 0,019 | | |
| | 49 | 3 | 0,113 | 10,08 | 0,011 | | |
| | 124,5 | 6 | 0,155 | 10,78 | 0,02 | | |
| | 217 | 10 | 0,216 | 10,98 | 0,009 | | |
| | 320 | 14 | 0,308 | 11,07 | 0,006 | | |
| | 388 | 17 | 0,416 | 11,19 | 0,001 | | |
| | 556 | 24 | 0,587 | 11,38 | 0 | | |
| | 652 | 28 | 0,739 | 11,37 | 0 | | |
| | 820 | 35 | 0,888 | 11,63 | 0,005 | | |
| | 894 | 38 | 0,979 | 11,58 | 0 | | |
| | 1062 | 46 | 1,119 | 11,49 | 0 | | |
| | 1230 | 53 | 1,2 | 11,30 | 0 | | |
| | 1518 | 65 | 1,324 | 9,96 | 0 | | |

| № | t, hrs | t, days | biomass, gwet/L | pH | Ca, mM/L |
|---|---|---|---|---|---|
| 31 | 0 | 1 | 0,074 | 9,15 | 0,53 |
| | 28 | 2 | 0,12 | 9,2 | 0,51 |
| | 49 | 3 | 0,114 | 9,58 | 0,49 |
| | 124,5 | 6 | 0,158 | 10,55 | 0,42 |
| | 217 | 10 | 0,21 | 10,72 | 0,41 |
| | 320 | 14 | 0,296 | 10,9 | 0,39 |
| | 388 | 17 | 0,346 | 10,95 | 0,43 |
| | 556 | 24 | 0,429 | 11,18 | 0,4 |
| | 652 | 28 | 0,616 | 11,21 | 0,38 |
| | 820 | 35 | 0,776 | 11,39 | 0,26 |
| | 894 | 38 | 0,84 | 11,41 | 0,3 |
| | 1062 | 46 | 0,987 | 11,29 | 0,32 |
| | 1230 | 53 | 1,037 | 10,69 | 0,39 |
| | 1518 | 65 | 1,159 | 9,82 | 0,42 |
| 32 | 0 | 1 | 0,074 | 9,18 | 0,55 |
| | 28 | 2 | 0,117 | | 0,48 |
| | 49 | 3 | 0,117 | 9,34 | 0,48 |
| | 124,5 | 6 | 0,177 | 10,49 | 0,41 |
| | 217 | 10 | 0,254 | 10,73 | 0,41 |
| | 320 | 14 | 0,308 | 10,91 | 0,4 |
| | 388 | 17 | 0,368 | 10,97 | 0,38 |
| | 556 | 24 | 0,503 | 11,11 | 0,41 |
| | 652 | 28 | 0,61 | 11,26 | 0,38 |
| | 820 | 35 | 0,754 | 11,32 | 0,27 |
| | 894 | 38 | 0,864 | 11,34 | 0,3 |
| | 1062 | 46 | 0,977 | 11,3 | 0,32 |
| | 1230 | 53 | 1,055 | 10,38 | 0,39 |
| | 1518 | 65 | 1,189 | 9,68 | 0,39 |
| 33 | 0 | 1 | 0,074 | 8,37 | 5,33 |
| | 28 | 2 | 0,113 | | 5,29 |
| | 49 | 3 | 0,18 | 8,16 | 5,25 |
| | 124,5 | 6 | 0,178 | 10,01 | 5,09 |
| | 217 | 10 | 0,267 | 10,3 | 5,07 |
| | 320 | 14 | 0,373 | 10,52 | 5,07 |
| | 388 | 17 | 0,409 | 10,55 | 4,88 |
| | 556 | 24 | 0,563 | 10,83 | 5,05 |
| | 652 | 28 | 0,613 | 10,98 | 5,09 |
| | 820 | 35 | 0,66 | 10,19 | 4,45 |
| | 894 | 38 | 0,753 | 9,87 | 4,5 |
| | 1062 | 46 | 0,857 | 8,9 | 4,95 |
| | 1230 | 53 | 0,996 | 9,16 | 4,89 |
| | 1518 | 65 | 1,055 | 8,72 | 4,87 |

| № | t, hrs | t, days | biomass, gwet/L | pH | Ca, mM/L | Alkalinity, mM/L | Ω calcite |
|---|---|---|---|---|---|---|---|
| 34 | 0 | 1 | 0,069 | 8,13 | 5,23 | | |
| | 28 | 2 | 0,116 | | 5,16 | | |
| | 49 | 3 | 0,114 | 8,82 | 4,63 | | |
| | 124,5 | 6 | 0,163 | 9,96 | 5,08 | | |
| | 217 | 10 | 0,215 | 10,26 | 5,07 | | |
| | 320 | 14 | 0,291 | 10,60 | 5,03 | | |
| | 388 | 17 | 0,376 | 10,47 | 4,80 | | |
| | 556 | 24 | 0,524 | 10,83 | 4,98 | | |
| | 652 | 28 | 0,590 | 10,94 | 4,98 | | |
| | 820 | 35 | 0,591 | 10,29 | 4,48 | | |
| | 894 | 38 | 0,718 | 9,76 | 4,51 | | |
| | 1062 | 46 | 0,855 | 8,89 | 4,78 | | |
| | 1230 | 53 | 0,976 | 9,05 | 4,93 | | |
| | 1518 | 65 | 1 019 | 8,80 | 4,83 | | |
| 35 | 0 | 0,0 | 1,66 | 9,07 | 3,35 | 4,19 | 83,2 |
| | 5 | 0,2 | 1,64 | 9,67 | 3,40 | 4,20 | 147,9 |
| | 19 | 0,8 | 1,74 | 9,99 | 3,37 | 3,98 | 165,9 |
| | 29 | 1,2 | 1,74 | 10,29 | 3,06 | 4,16 | 177,8 |
| | 43 | 1,8 | 1,88 | 10,55 | 3,40 | 4,42 | 194,9 |
| | 53 | 2,2 | 1,8 | 10,72 | 3,33 | 4,42 | 190,5 |
| | 70 | 2,9 | 1,96 | 10,71 | 3,28 | 4,41 | 190,5 |
| | 77 | 3,2 | 1,94 | 10,80 | 3,30 | 4,23 | 177,8 |
| | 94 | 3,9 | 1,94 | 10,66 | 3,33 | 4,20 | 186,2 |
| 36 | 0 | 0,01 | 1,66 | 8,96 | 2,95 | 4,27 | 66,1 |
| | 5 | 0,2 | 1,70 | 9,60 | 3,45 | 4,25 | 144,5 |
| | 19 | 0,8 | 1,80 | 9,97 | 3,37 | 4,95 | 194,9 |
| | 29 | 1,2 | 1,78 | 10,47 | 3,29 | 3,55 | 158,6 |
| | 43 | 1,8 | 1,96 | 10,63 | 2,83 | 3,29 | 138,0 |
| | 53 | 2,2 | 1,94 | 10,92 | 2,88 | 3,01 | 109,6 |
| | 70 | 2,9 | 2,00 | 10,66 | 2,76 | 3,17 | 128,8 |
| | 77 | 3,2 | 1,96 | 10,66 | 3,00 | 3,00 | 125,9 |
| | 94 | 3,9 | 1,94 | 10,66 | 2,59 | 2,93 | 117,5 |
| 37 | 0 | 0,01 | 1,60 | 8,90 | 5,11 | 4,18 | 93,3 |
| | 5 | 0,2 | 1,66 | 9,43 | 5,01 | 4,18 | 169,8 |
| | 19 | 0,8 | 1,70 | 9,81 | 5,04 | 3,14 | 151,4 |
| | 29 | 1,2 | 1,66 | 10,05 | 3,94 | 3,18 | 151,4 |
| | 43 | 1,8 | 1,66 | 10,35 | 4,34 | 2,68 | 123 |
| | 53 | 2,2 | 1,72 | 10,63 | 4,24 | 2,57 | 93,3 |
| | 70 | 2,9 | 1,74 | 10,44 | 4,14 | 2,63 | 117,5 |
| | 77 | 3,2 | 1,74 | 10,64 | 4,17 | 2,4 | 104,7 |
| | 94 | 3,9 | 1,68 | 10,43 | 4,04 | 2,43 | 107,2 |
| 38 | 0 | 0,01 | 1,50 | 8,85 | 6,27 | 4,00 | 85,1 |
| | 5 | 0,2 | 1,56 | 9,38 | 6,52 | 3,95 | 151,4 |
| | 19 | 0,8 | 1,60 | 9,57 | 5,76 | 4,62 | 144,5 |
| | 29 | 1,2 | 1,50 | 10,24 | 5,78 | 2,71 | 147,9 |
| | 43 | 1,8 | 1,68 | 10,52 | 6,19 | 2,58 | 131,8 |
| | 53 | 2,2 | 1,74 | 10,73 | 5,99 | 2,50 | 117,5 |
| | 70 | 2,9 | 1,80 | 10,38 | 5,74 | 2,36 | 125,9 |
| | 77 | 3,2 | 1,78 | 10,57 | 6,01 | 2,33 | 107,2 |
| | 94 | 3,9 | 1,76 | 10,25 | 5,49 | 2,08 | 114,8 |